Supramolecular approaches to graphene : generation of functional hybrid assemblies

Sébastien Haar

UNIVERSITÉ DE STRASBOURG

ÉCOLE DOCTORALE DES SCIENCES CHIMIQUES

UMR 7006 – Institut de Science et d'Ingénierie Supramoléculaires (I.S.I.S.)

THÈSE

présentée par :

Sébastien HAAR

soutenue le : **30 Septembre 2015**

pour obtenir le grade de : **Docteur de l'université de Strasbourg**

Discipline/ Spécialité : Chimie, Chimie-Physique

L'approche supramoléculaire appliquée au graphène: production d'assemblées hybrides fonctionnalisées

THÈSE dirigée par :

M. SAMORÌ Paolo	Professeur, Université de Strasbourg, France

RAPPORTEURS :

Mme KLYATSKAYA Svetlana	Docteur, Institut de Technologie de Karlsruhe, Karlsruhe, Allemagne
Mme DE LUCA Giovanna	Docteur, Université de Messina, Messina, Italie

---

AUTRES MEMBRES DU JURY :

M. BIANCO Alberto Strasbourg,	Directeur de Recherche, CNRS et Université de France – Examinateur interne

"Pense à la solution, pas au problème"

"La passion domine la raison, pour le meilleur et le pire."

***

"Think of the solution, not the problem"

"Passion rules reason for better or for worse"

Terry Goodkind

Résumé

Le graphène est un matériau bidimensionnel composé d'atomes de carbone qui sont arrangés en nid d'abeilles.[1] Il a été isolé expérimentalement pour la première fois en 2004 et le nombre de travaux le concernant ne cesse d'augmenter.[2-4] Ses excellentes propriétés électriques, thermiques, mécaniques et optiques le rendent incontournable pour des applications dans les domaines de l'électronique, des photoniques, des matériaux composites (membranes hybrides, encres conductrices et revêtements techniques), du stockage de gaz et d'énergie, des senseurs et enfin dans les bio-applications.[5-9] La fabrication du graphène à l'échelle industrielle est donc nécessaire afin de développer son énorme potentiel. Cependant, l'un des facteurs critiques qui limite l'utilisation de certains procédés de fabrication disponibles, est la production de graphène sans défauts et de taille contrôlée. Par conséquent, beaucoup d'efforts sont réalisés afin de synthétiser, à la fois des feuillets monocouches mais aussi des feuilles de graphène ayant 2 à 5 couches et ce par plus d'une vingtaine de procédés différents. L'exfoliation par voie liquide du graphène est actuellement très prometteuse.[10] Ceci est avantagé par le faible coût de production et par une qualité et quantité de feuillets supérieures aux autres techniques. L'exfoliation par voie liquide implique 3 étapes: dispersion du graphite dans un solvant, l'exfoliation, et la purification. Le choix du solvant est important, puisque seuls les solvants ayant une tension de surface proche de celle du graphène peuvent être capables de stabiliser les feuillets de graphène. L'exfoliation du graphite se produit lorsque les ultrasons cassent les interactions de van der Waals entre les feuillets et que le solvant est capable de stabiliser les feuillets qui se sont détachés. Afin d'augmenter le rendement d'exfoliation et/ou la qualité des feuillets, certains groupes de recherche utilisent des molécules organiques telles que des tensioactifs, des biomolécules, des super-acides ou des molécules fonctionnalisées.[11-13] Ces molécules agissent principalement comme des agents de

dispersion/stabilisation par physisorption de leurs fragments hydrophobes sur la surface de graphène durant l'exfoliation du graphite par sonication. L'exfoliation en phase liquide du graphite dans l'eau est plus difficile en raison de la nature hydrophobe des feuilles, mais l'addition de molécules telles que des tensioactifs ou des sels a montré une production de suspensions stables. Cependant, l'utilisation de l'eau comme milieu liquide pour l'exfoliation est généralement peu recommandée dans les domaines des appareils électroniques, encres conductrices et membranes. Par conséquent, l'utilisation de solvants organiques en tant que milieu liquide pour l'exfoliation doit être explorée. Dans la dernière décennie, l'effort exceptionnel dédié afin de relever ce défi, a mis en avant que certaines molécules organiques sont capables de dynamiser l'exfoliation du graphite avec des rendements toujours plus élevés. Mais, la question fondamentale, encore extrêmement important, afin de savoir ce qui fait qu'une molécule est un bon candidat pour promouvoir l'exfoliation de graphite reste ouverte. Ici, une compréhension fondamentale sur une approche supramoléculaire simple est présentée afin de préparer des dispersions homogènes de nano-feuillets de graphène non fonctionnalisés et non oxydés dans quatre solvants organiques. Afin d'explorer l'exfoliation en phase liquide du graphène en présence et en absence de molécules, nous avons étudié les systèmes suivants :

- La première étude porte sur la détermination des paramètres non explorés de l'exfoliation en phase liquide et de permettre un contrôle total de la fabrication de graphène.

- Ensuite nous avons exploré l'influence de l'ajout de molécules lors de l'exfoliation. Ces molécules ont été strictement sélectionnées grâce à leur affinité particulière avec les surfaces carbonées, c'est l'approche supramoléculaire. La taille de leur chaine alkyle linéaire ainsi que les groupes fonctionnels greffés sur ces chaines ont été analysés.

- Une molécule d'azobenzène comprenant deux anneaux phényles liés par un double pont N=N a aussi été utilisée afin promouvoir l'exfoliation du

graphène. Cette molécule permet aussi de doper directement le graphène et d'obtenir de nouvelles propriétés.

Dans le but de comprendre le procédé d'exfoliation et de déterminer l'influence de chaque paramètre sur l'exfoliation, nous avons décidé d'étudier dans un premier temps la fabrication de graphène sans l'addition d'agents dispersants/stabilisants. De plus, les paramètres tels que la puissance des ultrasons, la température du bain à sonication, la durée de sonication, les vitesses de centrifugation, la variation de la de source de graphite, les différentes masses de graphène et le volume des solvants ont été testés. Quatre solvants différents ont été sélectionnés pour l'exfoliation en phase liquide, i.e. N-methyl-2-pyrrolidinone (NMP), N,N-dimethylformamide (DMF), o-dichlorobenzène (*o*-DCB) and 1,3,5-trichlorobenzène (TCB) puisque leur tension de surface est proche de celle du graphène. Trois paramètres apparaissent plus importants que les autres: la puissance des ultrasons (600 watts et 1000 watts), la température du bain (20 et 50 °C) et le solvant. En effet, l'exfoliation du graphite à la température de 50 °C dans les quatre solvants à différentes puissances ne montre aucun changement en termes de quantité et de qualité de feuillets. Pour une température de 20 °C, NMP et DMF ne montrent pas de changement même lorsque la puissance varie. Mais l'exfoliation dans les solvants chlorés, i.e. *o*-DCB et TCB, montre une dépendance à la puissance. L'utilisation de 1000 watts permet de fabriquer des nano-feuillets qui font 16 nm en moyenne et sont majoritairement de forme ronde. Ces nano-feuillets sont trouvés sous la forme de mono et bi-feuillets et les mesures XPS confirment la qualité de ces feuillets. Ces nano-feuillets de graphène présentent des propriétés photoluminescentes ayant une efficacité de 2.4 % ce qui est très intéressant pour des matériaux purement carbonés.

Une fois que les bonnes conditions d'exfoliation ont été déterminées et maitrisées, nous avons mis en place une nouvelle approche qui est dite supramoléculaire. Cette approche est basée sur l'utilisation des interactions faibles, telles que l'interaction de van der Waal et la liaison hydrogène. Aussi, toute la science de l'auto-assemblage de surface peut être potentiellement appliquée, d'autant plus que le substrat utilisé dans ce domaine est principalement du graphite hautement ordonné (HOPG) qui peut être utilisé comme source de graphite pour l'exfoliation.

Les molécules organiques ayant une grande affinité avec la surface de graphène sont de parfaits candidats. Ces molécules doivent donc répondre à deux critères : 1) leur énergie d'adsorption sur le graphène doit être supérieure à l'adsorption des molécules de solvant; 2) elles doivent être bien solubles/miscibles dans les milieux organiques tels que $CHCl_3$. Nous nous sommes concentrés sur deux modules moléculaires simples qui sont 1-phenyloctane (NOTBZ) et l'acide arachidic, dont l'énergie d'adsorption calculée sur le graphène est beaucoup plus élevée que l'énergie d'adsorption du solvant (19.1 et 28.2 $kcal.mol^{-1}$, respectivement). NMP a été choisi puisque c'est le solvant qui montre la meilleure stabilité, une bonne qualité des feuillets de graphène et une haute concentration en graphène (-8.5 $kcal.mol^{-1}$ pour NMP). Afin de contrôler le nombre de molécules à ajouter, une formule simple a été développée. En considérant que la poudre de graphite initial forme un feuillet unique de graphène, nous avons calculé le nombre de molécules nécessaires à la formation de monocouches denses sur le graphène. L'auto-assemblage de ces molécules a été imagé par microscope à effet tunnel et l'analyse de ces images a permis la détermination de l'unité cellulaire sur la surface de graphite/graphene. Étant donné que le nombre de molécules calculées sera plus élevé que la surface réelle de graphite sous forme de poudre, nous avons utilisé 5, 10, 15, et 20% de molécules nécessaires pour couvrir la surface entière du graphène. L'ajout de ces molécules lors de l'exfoliation a permis d'augmenter la concentration de graphène. En effet, si on compare la concentration de graphène exfoliée dans NMP (~ $80\mu g.mL^{-1}$) avec celle de NOTBZ (~ $100\ \mu g.mL^{-1}$) et celle de l'acide arachidic (~ $130\ \mu g.mL^{-1}$), une hausse de 20 % et 50 % a été observée respectivement. En collaboration avec les groupes de Ovidiu Ersen et Cinzia Casiraghi, l'analyse de ses dispersions par TEM et par spectroscopie Raman confirme deux choses: premièrement, l'addition de molécule ayant des chaines alcanes n'affecte ni la qualité ni la structure du graphène et deuxièmement l'ajout de NOTBZ permet d'augmenter de 10 % le nombre de mono-feuillets tandis que l'acide arachidic augmente que légèrement le nombre de mono-feuillets. De plus les dispersions de graphène fabriquées avec notre procédé se sont révélées être une encre conductrice. Nous avons démontré que par la maîtrise d'une approche supramoléculaire, il est possible d'améliorer le rendement d'exfoliation du graphène et de produire des feuillets de graphène de haute qualité à partir de la poudre de graphite.

Puisque l'acide arachidic est capable d'améliorer l'exfoliation du graphène, nous nous sommes penchés sur l'influence les différentes fonctions quant à l'exfoliation. Une molécule ayant une chaine de 21 atomes de carbone a été décorée avec quatre fonctions, i.e. amine (NH_2), alcane (CH_3), alcool (OH) et acide carboxylique (COOH). Ces molécules possèdent une chaîne carbonée longue et auront tendance à s'adsorber sur la surface du graphène/graphite puis de former une monocouche auto-assemblée. Ces molécules, à l'exception de l'alcane, sont équipées de fonctions connues pour former des dimères via liaisons hydrogène dans la majorité des solvants organiques, ce qui conduit à la formation d'une structure supramoléculaire stable sur la surface de graphene/graphite. Le microscope à effet tunnel a été utilisé afin de prouver la formation de ses réseaux sur la surface de graphite. Puisque ces molécules montrent une grande affinité avec les surfaces carbonées, différents pourcentages pour chaque molécule ont été testés. L'acide carboxylique montre une augmentation de plus de 60 %, 30 % l'alcane et seulement 15 % pour l'alcool et l'amine en terme de concentration. L'analyse de ses dispersions par TEM et par spectroscopie Raman montre que l'exfoliation en présence de l'acide carboxylique permet de fabriquer majoritairement des feuillets allant 1 à 3 couches et de grande qualité. Par contre pour les autres molécules, peu de mono et bi-feuillets ont été observés. Ceci prouve que l'acide carboxylique est le meilleur candidat pour l'exfoliation en phase liquide.

Puisque certaines molécules organiques sont capables de tirer parti de l'exfoliation en phase liquide du graphite et d'augmenter la quantité et la qualité du graphène, nous avons étendu notre simple approche supramoléculaire à l'étude d'alcanes linéaires de différentes longueurs terminés par le groupe d'acide carboxylique (C6, C12, C18, C14 et C30). De plus quatre solvants ont été testés, i.e. NMP, *o*-DCB, DMF et TCB, afin d'atteindre le plein contrôle sur la production de graphène. En effet, ces molécules agissent comme des agents de dispersants/stabilisants du graphène pendant le processus d'exfoliation. L'efficacité de l'exfoliation en termes de concentration de graphène exfolié se trouve être proportionnelle à la longueur de la chaine de l'acide gras utilisé. Dans NMP et pour une longueur de chaîne C30, des valeurs de concentration proche de 240 $\mu g.mL^{-1}$ ont été mesurées, tandis que pour *o*-DCB et TCB, c'est une longueur de chaîne C24 qui donne les meilleures concentrations, 180 $\mu g.mL^{-1}$ et 150 $\mu g.mL^{-1}$. De plus, un pourcentage élevé de feuillets de graphène monocouche a

est révélé par microscopie électronique à transmission à haute résolution et analyse par spectroscopie Raman pour ces trois dispersions.

Puisque l'exfoliation en présence de NOTBZ molécules présente le meilleur pourcentage de mono-feuillets, nous nous sommes intéressés à l'exfoliation du graphite dans les quatre solvants, i.e. NMP, *o*-DCB, DMF et TCB, tout en contrôlant le nombre de NOTBZ molécules. Seul NMP et *o*-DCB ont montré des résultats intéressant ; en particulier la concentration en graphène exfolié a été trouvée être le plus élevé pour 15 % de NOTBZ, soit 250 $\mu g.mL^{-1}$ pour NMP et 190 $\mu g.mL^{-1}$ pour *o*-DCB. Plus surprenant encore, la concentration maximum en graphène dans tous les solvants a été trouvé pour 15 % de NOTBZ. De plus, un pourcentage élevé de graphène monocouche a été révélé par l'analyse HR-TEM et la spectroscopie Raman. En utilisant une nouvelle technique de dépôt mise au point dans notre laboratoire, des films de graphène homogènes ont été déposés sur des substrats de quartz. La résistance des feuillets a été mesurée entre 3000 à 1000 Ω/carré avec 75 % de transparence à 550 nm pour les dispersions dans *o*-DCB.

L'isomérisation *trans-cis* photo déclenchée des azobenzènes alkylés peut être utilisée pour promouvoir l'exfoliation du graphène dans des milieux liquides et de communiquer une réponse électrique réversible aux stimuli optiques dans les matériaux à base de graphène pour l'électronique. En particulier, nous avons préparé du graphène par sonication en phase liquide exfoliation du graphite, en présence de molécules photochromiques. L'irradiation *in situ* via de la lumière ultraviolette pendant le processus d'exfoliation déclenche l'isomérisation de *trans* à *cis* de molécules d'azobenzène, qui est accompagné par un grand changement de conformation dans les molécules photochromiques, entraînant finalement une augmentation significative du rendement d'exfoliation de graphène. Lorsque les molécules sont prises en sandwich entre des feuillets de graphène dans leur forme *trans* linéaire, la distance entre les couches est plus petite que lorsque les molécules adoptent la forme *cis* plus volumineuse. Nous avons démontré que lors de l'utilisation ces molécules photochromiques, il est possible d'améliorer le rendement d'exfoliation du graphite en graphène dans NMP. En particulier, l'exfoliation la plus efficace a été obtenue pour des molécules irradiées par la lumière UV dans

NMP à 40 °C, donnant une concentration de graphène exfolié de 110 µg mL^{-1}. Ceci correspond à une augmentation de près de 80% du rendement d'exfoliation par rapport aux échantillons préparés dans le pur NMP (63 µg mL^{-1}). Nous avons également démontré avec succès que les films minces hybrides sensibles à la lumière peuvent être formés lors du processus de co-déposition en une seule étape. La conductivité du matériau peut être modulée de manière réversible par l'utilisation de la photo-isomérisation *cis-trans* des molécules d'azobenzènes. Le système hybride présenté possède un grand potentiel dans des applications telles que la mémoire optique variable pour la programmation assistée par lumière ou des photo-capteurs à haute sensibilité par le choix des configurations de dispositifs appropriés.

Nous avons donc étudié le mécanisme de l'exfoliation en phase liquide, et plus particulièrement l'influence des différents paramètres. En ajustant la puissance, la température et en choisissant le solvant approprié, il est possible de contrôler la taille des feuillets de graphène et de fabriquer des nano-feuillets photo-luminescents ou du graphène. L'utilisation de l'approche supramoléculaire permet d'augmenter la quantité et la qualité des feuillets obtenus. La molécule qui semble être le meilleur candidat pour l'exfoliation est un acide carboxylique équipé d'une longue chaine alcane (C30 pour NMP et C24 pour *o*-DCB). Aussi l'ajout de NOTBZ montre des résultats intéressants surtout en nombre de mono-feuillets exfoliés. Notre approche supramoléculaire est simple mais efficace et elle permet de tirer parti de la production de graphène dans un milieu liquide tout en s'appuyant sur l'effet synergique de modules moléculaires simples et du solvant. Cette approche est adéquate et générale et permet de créer des encres de graphène stables et très concentrés. La fixation de certaines unités fonctionnelles à la fin des chaînes alcanes peut ouvrir la voie à la fabrication de matériaux nano-composites multifonctionnels à base de graphène.

Abstract

Graphene is a two-dimensional material composed of carbon atoms which are arranged in a honeycomb lattice.[1] Albeit this 2D system is known since a few decades, in 2004 groundbreaking experiments have been carried out on graphene providing unambiguous evidence for their extraordinary physical and chemical properties. This pioneering work has sparked works on graphene during the last decade.[2-4] Its excellent electrical, thermal, mechanical and optical properties make it an ideal building-block for applications in the fields of electronics, photonics, composite materials (hybrid membranes, conductive inks and coatings technology), storage of gas and energy, sensors and finally in bio-applications.[5-9] The fabrication of graphene on an industrial scale is therefore necessary to exploit its enormous potential. However, a critical factor which limits the use of certain manufacturing processes available is the production of graphene without defects and controlled size. Therefore, a great effort have been made to synthesize, both monolayer sheets but also sheets of graphene with 2-5 layers and those with more than twenty different processes. The exfoliation of graphene liquid process is currently very promising.[10] Since it combines cost effective production and a higher quality and quantity of sheets, compared to other techniques. Exfoliation in liquid media involves three steps: dispersion of graphite in a solvent, exfoliation, and purification. The choice of solvent is important, as only solvents having a surface tension similar to that of graphene may be able to stabilize the graphene sheets. Exfoliation of the graphite occurs when ultrasounds break the van der Waals interactions between the sheets and the solvent is capable of stabilizing sheets which are detached. To increase the yield of exfoliation and/or quality of the sheets, some research groups use organic molecules such as surfactants, biomolecules,

super acids or functionalized molecules.[11-13] These molecules function primarily as dispersants-stabilizing agent by physisorption their hydrophobic moieties on the graphene surface during exfoliation of the graphite by sonication. Exfoliation of the graphite in the liquid phase in water is more difficult because of the hydrophobic nature of the sheets, but the addition of molecules such as surfactants or salts showed a production of stable suspensions. However, the use of water as a liquid medium for exfoliation is generally not recommended for applications in electronics, conductive inks and membranes. Therefore, the use of organic solvents as the liquid medium for exfoliation must be explored.

In the last decade, the exceptional effort dedicated to this challenge, showed that some organic molecules are able to stimulate the exfoliation of graphite. It however remains open the fundamental question: what makes a molecule a good candidate to promote exfoliation of graphite? Here, a fundamental understanding of a simple supramolecular approach is presented in order to prepare homogeneous dispersions of non-functional and non-oxidized nanographene sheets in these four solvents. To explore the liquid phase exfoliation of graphene in the presence and the absence of molecules, we study the following systems:

- The first study focuses on determining the unexplored parameters of the liquid phase exfoliation and allowing total control during the production of graphene.

- Then we explored the influence of the addition of molecules during the exfoliation that have been strictly selected by their particular affinity with the carbon surfaces, the supramolecular approach. The size of the linear alkyl chain and the grafted functional groups on these chains were analyzed.

- An azobenzene molecule comprising two phenyl rings linked by a double bridge N = N has also been used to promote the exfoliation of graphene. This molecule also provides direct dope graphene and obtains new properties.

The technological exploitation of the extraordinary properties of graphene relies on the ability to achieve full control over the production of a high-quality material and its processing by up-scalable approaches in order to fabricate large-area films with single-layer or a few atomic-layer thickness, which might be integrated in working devices. A simple method is reported for producing homogenous dispersions of unfunctionalized and non-oxidized graphene nanosheets in *N*-methyl-2-pyrrolidone (NMP) by using simple molecular modules, which act as dispersion-stabilizing compounds during the liquid-phase exfoliation (LPE) process, leading to an increase in the concentration of graphene in dispersions. The LPE-processed graphene dispersion was shown to be a conductive ink. This approach opens up new avenues for the technological applications of this graphene ink as low-cost electrodes and conducting nanocomposite for electronics.

Since the arachidic acid is capable of improving exfoliation of graphene, we decided to explore the influence of the different functions grafted to an alkyl chain. Here we report on a fundamental study on the fabrication of unfunctionalized and non-oxidized graphene sheets dispersed in an organic solvent, namely NMP, by using a supramolecular approach. In particular, we focused our attention on the study of LPE of graphene in the presence of heneicosane linear alkanes terminated with different head groups. These molecules act as graphene dispersion-stabilizing agents during the exfoliation process. The efficiency of the exfoliation in terms of concentration of exfoliated graphene is found to depend on the functional head group, in particular in view of the strength of their dimerization through dipole-dipole interactions. Importantly, a high percentage of single-layer graphene flakes were

revealed by high-resolution transmission electron microscopy and Raman spectroscopy analyses.

As COOH function is showing the highest increase of concentration, we extended our interest to the importance of the length of the alkyl chain. In this thesis, a fundamental understanding on a straightforward supramolecular approach for producing homogenous dispersions of unfunctionalized and non-oxidized graphene nanosheets in four different solvents is attained, namely *NMP*, *N*,*N*-dimethylformamide, *ortho*-dichlorobenzene (*o*-DCB), and 1,2,4-trichlorobenzene (TCB). In particular, a comparative study on the liquid-phase exfoliation of graphene in the presence of linear alkanes of different lengths terminated by a carboxylic-acid head group is performed. These molecules act as graphene dispersion-stabilizing agents during the exfoliation process. The efficiency of the exfoliation in terms of concentration of exfoliated graphene is found to be proportional to the length of the employed fatty acid. Importantly, a high percentage of single-layer graphene flakes is revealed by high-resolution transmission electron microscopy and Raman spectroscopy analyses.

As *n*-octylbenzene (other name to 1-phenyloctane) molecules acted as graphene dispersing-stabilizing agents during the graphite LPE process, we wanted to explore the importance of the volume percentage in different solvents. In this way, we have demonstrated that by tuning the ratio between organic solvents such as NMP or *o*-DCB, and *n*-octylbenzene molecules, the concentration of exfoliated graphene can be enhanced by 230% as a result of the high affinity of the latter molecule for the basal plane of graphene. The LPE processed graphene dispersions were further deposited onto solid substrates by exploiting a new deposition technique called spin-controlled drop casting, which was shown to give uniform highly conductive and transparent graphene films.

Multifunctional materials can be engineered by combining multiple chemical components, each conferring a well-defined function to the ensemble. In this thesis, we show that the large conformational change associated with the *trans-cis* photochemical isomerization of alkyl-

substituted azobenzenes can be used to improve the efficiency liquid phase exfoliation of graphite, with the photochromic molecules acting as dispersion-stabilizing agents. We also demonstrate reversible photo-modulated current in two-terminal devices based on graphene-azobenzene composites. We assign this tunable electrical characteristics to the intercalation of the azobenzenes between adjacent graphene layers and the resulting increase in the interlayer distance upon (photo)switching from the linear *trans*-form to the bulky *cis*-form of the photochromes. These findings may pave the way towards the development of new optically controlled memories for light-assisted programming and high-sensitive photo-sensors.

Therefore, we examined the exfoliation mechanism in the liquid phase, especially the influence of different parameters. By adjusting the power, temperature and choosing the appropriate solvent, it is possible to control the size of graphene sheets and manufacture of photo-luminescent nanosheets or graphene. The use of the supramolecular approach allows increasing the quantity and quality of the sheets obtained. The molecule appears to be the best candidate for exfoliation is a carboxylic acid with a long chain alkane (C30 and C24 for NMP and o-DCB). Also adding NOTBZ shows interesting results especially number of exfoliated single sheets. Our supramolecular approach is simple but effective and it allows leveraging the production of graphene in a liquid medium while drawing on the synergistic effect of simple molecular modules and solvent. This approach is adequate and general and allows creating stable graphene inks and very concentrated. The attachment of certain functional units at the end of alkane chains may pave the way for the manufacture of multi-functional nano-composites based on graphene.

References

1. K. S. Novoselov, A. K. Geim, S. V. Morozov, D. Jiang, Y. Zhang, S. V. Dubonos, I. V. Grigorieva and A. A. Firsov, *Science*, 2004, **306**, 666-669.
2. A. K. Geim and K. S. Novoselov, *Nat Mater*, 2007, **6**, 183-191.
3. K. S. Novoselov, D. Jiang, F. Schedin, T. J. Booth, V. V. Khotkevich, S. V. Morozov and A. K. Geim, *P Natl Acad Sci USA*, 2005, **102**, 10451-10453.
4. K. S. Novoselov, A. K. Geim, S. V. Morozov, D. Jiang, M. I. Katsnelson, I. V. Grigorieva, S. V. Dubonos and A. A. Firsov, *Nature*, 2005, **438**, 197-200.
5. F. Torrisi, T. Hasan, W. P. Wu, Z. P. Sun, A. Lombardo, T. S. Kulmala, G. W. Hsieh, S. J. Jung, F. Bonaccorso, P. J. Paul, D. P. Chu and A. C. Ferrari, *Acs Nano*, 2012, **6**, 2992-30010.
6. F. Bonaccorso, Z. Sun, T. Hasan and A. C. Ferrari, *Nat Photonics*, 2010, **4**, 611-622.
7. K. S. Kim, Y. Zhao, H. Jang, S. Y. Lee, J. M. Kim, K. S. Kim, J. H. Ahn, P. Kim, J. Y. Choi and B. H. Hong, *Nature*, 2009, **457**, 706-710.
8. R. M. Westervelt, *Science*, 2008, **320**, 324-325.
9. M. D. Stoller, S. J. Park, Y. W. Zhu, J. H. An and R. S. Ruoff, *Nano Lett*, 2008, **8**, 3498-3502.
10. Y. Hernandez, V. Nicolosi, M. Lotya, F. M. Blighe, Z. Y. Sun, S. De, I. T. McGovern, B. Holland, M. Byrne, Y. K. Gun'ko, J. J. Boland, P. Niraj, G. Duesberg, S. Krishnamurthy, R. Goodhue, J. Hutchison, V. Scardaci, A. C. Ferrari and J. N. Coleman, *Nat Nanotechnol*, 2008, **3**, 563-568.
11. M. S. Kang, K. T. Kim, J. U. Lee and W. H. Jo, *J Mater Chem C*, 2013, **1**, 1870-1875.
12. J. Malig, A. W. I. Stephenson, P. Wagner, G. G. Wallace, D. L. Officer and D. M. Guldi, *Chem Commun*, 2012, **48**, 8745-8747.
13. J. Geng, B. S. Kong, S. B. Yang and H. T. Jung, *Chem Commun*, 2010, **46**, 5091-5093.

Contents

Symbols and Abbreviations

Abs	Absorbance
AFM	atomic force microscopy
AL	alkali lignin
BE	binding energy
CVD	chemical vapor deposition
CQD	carbon quantum dot
DLVO	Derjaguin and Landau, Verwey and Overbeek
DMF	N,N-dimethylformamide
DMSO	dimethylsulfoxyde
E_a	activation energy [Kj·mol^{-1}]
e-beam	electron beam
EDX	energy dispersive X-ray
eq.	equation
FET	field-effect transistor
FLG	few layers graphene
FTIR	Fourier transform infrared spectroscopy
FWHM	full width at half maximum
GD	graphite dots
GIC	graphene intercalate compound
GNP	graphene nanoparticle
GNR	graphene nanoribbon
GO	graphene oxide
GONP	graphene oxide nanoparticles
GQD	graphene quantum dot
GS	graphene silk
HMDS	hexamethyldisilazane
HOPG	highly oriented pyrolitic graphite
HOMO	highest occupied molecular orbitals
HR-TEM	high resolution transmission electron microscopy

I_{dark}	current in dark [A]
IE	ionization energy
I_{light}	current under illumination [A]
I_{off}	drain current in the off state [A]
I_{on}	drain current in the on state [A]
IR	infrared
ITO	indium tin oxide
k_B	Boltzmann constant
LED	light emitting diode
LPE	liquid-phase exfoliation
LUMO	lowest unoccupied molecular orbitals
MLG	mono layer graphene
MME	micro-mechanical exfoliation
N_A	Avogadro number
NMP	N-methyl-2-pyrrolidone
NMR	nuclear magnetic resonance
o-DCB	orthodichlorobenzene
OLED	organic light emitting diode
PMMA	poly(methylmethacrylate)
PS	photoelectron spectroscopy
PTFE	polytetrafluoroethylene
PL	photoluminescence
PY	pyrene
R_c	contact resistance [Ω cm]
RF	radio frequency
rGO	reduced graphene oxide
rpm	rotation per minute
R_s	sheet resistance [Ω sq]
SAM	self-assembled monolayer
SA	surface area
SE	secondary electrons
SEM	scanning electron microscope
SLG	single layer graphene
STM	scanning tunneling microscope
T	temperature [K or ˚C]
TEM	transmission electron microscopy
TFT	thin-film transistor
TGA	thermo gravimetric analysis
THF	tetrahydrofuran
UHV	ultra high vacuum
UV	ultraviolet

UV-Vis	ultraviolet-visible
VL	visible light
wt %	total weight %
W	Watt
XPS	X-ray photoemission spectroscopy
XRD	X-ray diffraction
γ	surface tension [$mJ.m^{-2}$]
λ	wavelength [nm]
σ	electrical conductivity [$S \cdot m^{-1}$]
2D	two dimensional
3D	three dimensional

Chapter 1 Introduction

1.1 Background

The scientific and technological progresses are the key for the development of new application areas ranging from materials to components and systems. Graphene and graphene based materials have the potential to impact many areas in view of its unique properties. However, what makes graphene really special, and gives it a disruptive value, is the assemblage of many properties in a single material. For instance its high transparency, conductivity and elasticity can find use in flexible electronics; its high mobility and ultimate thinness in efficient transistors for radio frequency applications, while transparency, impermeability and conductivity can be exploited for transparent protective coatings. Such combination of properties cannot be found in any other material or material systems. In fact researchers already list the survey of applications:

- Lower cost of display screens in mobile devices
- Lithium-ion batteries that recharge faster
- Ultracapacitors with better performance than batteries
- Components with higher strength to weight ratios
- Storing hydrogen for fuel cell powered cars
- Lower cost fuel cells
- Low cost water desalination

- Lightweight natural gas tanks
- More efficient dye sensitized solar cells
- Electrodes with very high surface area and very low electrical resistance
- Lower cost solar cells
- Transistors that operate at higher frequency
- Sensors to diagnose diseases
- Membranes for more efficient separation of gases
- Chemical sensors effective at detecting explosives

This long list of applications is even expected to growth more and more. In fact, by looking at the rapid development of graphene production and the diversification of these methods, it is reasonable to expect to see graphene in technological applications on the market with 10 years.

1.2 Objectives and approach

Since graphene re-discovery and the evidence of its amazing properties,[1] many efforts have been devoted for its production and isolation.[2-5] In fact, graphene was first isolated using a simple scotch-tape approach that is not suitable for larger production.[1, 6] Graphene can be prepared in bulk solution or as atomically thin films on a surface;[7, 8] it can be functionalized on the edges or basal plane and selectively patterned;[9] and small sections can be synthesized using chemical methods.[10] In this way, each fabrication method produces flakes, which have different characteristics. The key for graphene commercialization lies in its production method, which essentially determines its cost-effectiveness.[11] In terms of mass production of graphene, the main factors are the production cost, scalability, reproducibility, processability and the quality of the graphene products.[12] Considering the low cost and abundance of graphite flakes, the liquid-phase exfoliation (LPE) approaches of graphite to graphene seem to meet all the requirements. In fact solvent-processable graphene offers many advantages and can be produced by LPE of graphite into graphene and in particular by sonication assisted

liquid-phase exfoliation.[7] Very recently, some groups tried to improve this process by using *ad hoc* molecules during the LPE process.[13, 14] Despite an increasing number of reported molecules used for the LPE of graphite, the explanation which molecules are the best candidates for the LPE and the reason why they act as a stabilizing agent for graphene is still missing.

In this thesis we will discuss a successful approach for stabilizing graphene flakes in organic solvents by adding a certain type of molecular building blocks, which allows fabricating high quality of graphene sheets. More importantly by using our expertise in supramolecular chemistry, we explain in details the physical chemistry behind the LPE. In particular, we use our knowledge in molecular self-assembly of designed molecular systems on graphite surfaces in order to understand the different mechanisms behind LPE. Supramolecular chemistry relies on the use of non-covalent interactions to self-assemble, with a precision in the sub-nanometer scale, chemical entities forming materials with pre-programmed chemical and physical properties.[15] The main non-covalent interactions expected for surfactant-graphene interactions are electrostatic interactions, π-π interactions and van der Waals interactions.[16] Despite that hydrogen-bonding is one of most known non-covalent interactions, it will only be used as a intramolecular interaction for forming dimers of molecules. Electrostatic interactions are mainly used in the case of water based LPE of graphite, in particular by using ionic molecules. Also π-π interactions of different conjugated or non-conjugated molecules are widely used for LPE process in water, and more recently in organic solvents, like N-Methyl-2-pyrrolidone (NMP) that is commonly used. In this thesis we study the importance of van der Waals interactions between molecules and graphene surface. Typically molecules that self-assemble on graphite or graphene surface are designs with alkyl chains having different lengths. This class of molecules might be good candidate for molecules assisted LPE process.

1.3 Structure of the thesis

This thesis consists of 11 chapters and is organized as follow:

Chapter 1 provides a brief introduction about graphene and liquid-phase exfoliation.

Chapter 2 introduces in detail graphene and its properties. It also describes some applications of graphene in several technological areas. Different production methods of graphene are also presented.

Chapter 3 focuses on one production method, the liquid phase exfoliation in the presence and absence of surfactants in different types of solvents.

Chapter 4 describes the experimental techniques and methods used in the thesis.

Chapter 5 investigates different parameters of surfactants-free LPE process, which allows having a better control over the production in terms of quality, quantity and dimension.

Chapter 6 presents a simple method for producing homogenous dispersions of unfunctionalized and non-oxidized graphene sheets in NMP by using simple molecular modules, which act as dispersion-stabilizing compounds during the liquid-phase exfoliation (LPE) process, leading to an increase in the concentration of graphene in dispersions. As-prepared graphene dispersions were shown to be conductive ink.

Chapter 7 investigates the ability of long linear alkane decorated with four different functions to improve the exfoliation of graphene in terms of quantity and quality.

In Chapter 8, a fundamental understanding on a straightforward supramolecular approach for producing homogenous dispersions of unfunctionalized and non-oxidized graphene nanosheets in four different organic solvents is presented. In particular, a comparative study on the liquid-phase exfoliation of graphene in the presence of linear alkanes of different lengths terminated by a carboxylic-acid head group is performed.

Chapter 9 describes how a simple molecules, i.e. n-octylbenzene act as graphene dispersion-stabilizing agent during the graphite LPE process. It also describes a new developed technique called spin-controlled drop casting for the deposition of graphene dispersions on solid substrates.

Chapter 10 shows that the large conformational change associated with the trans-cis photochemical isomerization of alkyl-substituted azobenzenes can be used to improve the efficiency liquid phase exfoliation of graphite, with the photochromic molecules acting as dispersion-stabilizing agents.

Chapter 11 provides a summary of the thesis and a perspective into the future of graphene.

1.4 References

1. K. S. Novoselov, A. K. Geim, S. V. Morozov, D. Jiang, Y. Zhang, S. V. Dubonos, I. V. Grigorieva and A. A. Firsov, *Science*, 2004, **306**, 666-669.
2. W. A. de Heer, C. Berger, X. S. Wu, P. N. First, E. H. Conrad, X. B. Li, T. B. Li, M. Sprinkle, J. Hass, M. L. Sadowski, M. Potemski and G. Martinez, *Solid State Commun*, 2007, **143**, 92-100.
3. E. H. L. Falcao, R. G. Blair, J. J. Mack, L. M. Viculis, C. W. Kwon, M. Bendikov, R. B. Kaner, B. S. Dunn and F. Wudl, *Carbon*, 2007, **45**, 1367-1369.
4. A. K. Geim and K. S. Novoselov, *Nat Mater*, 2007, **6**, 183-191.
5. S. Stankovich, D. A. Dikin, R. D. Piner, K. A. Kohlhaas, A. Kleinhammes, Y. Jia, Y. Wu, S. T. Nguyen and R. S. Ruoff, *Carbon*, 2007, **45**, 1558-1565.
6. A. K. Geim, *Science*, 2009, **324**, 1530-1534.
7. Y. Hernandez, V. Nicolosi, M. Lotya, F. M. Blighe, Z. Y. Sun, S. De, I. T. McGovern, B. Holland, M. Byrne, Y. K. Gun'ko, J. J. Boland, P. Niraj, G. Duesberg, S. Krishnamurthy, R. Goodhue, J. Hutchison, V. Scardaci, A. C. Ferrari and J. N. Coleman, *Nat Nanotechnol*, 2008, **3**, 563-568.
8. S. Bae, H. Kim, Y. Lee, X. F. Xu, J. S. Park, Y. Zheng, J. Balakrishnan, T. Lei, H. R. Kim, Y. I. Song, Y. J. Kim, K. S. Kim, B. Ozyilmaz, J. H. Ahn, B. H. Hong and S. Iijima, *Nat Nanotechnol*, 2010, **5**, 574-578.
9. Z. W. Tang, H. Wu, J. R. Cort, G. W. Buchko, Y. Y. Zhang, Y. Y. Shao, I. A. Aksay, J. Liu and Y. H. Lin, *Small*, 2010, **6**, 1205-1209.
10. J. M. Cai, P. Ruffieux, R. Jaafar, M. Bieri, T. Braun, S. Blankenburg, M. Muoth, A. P. Seitsonen, M. Saleh, X. L. Feng, K. Mullen and R. Fasel, Nature, 2010, **466**, 470-473.
11. A. C. Ferrari, F. Bonaccorso, V. Fal'ko, K. S. Novoselov, S. Roche, P. Boggild, S. Borini, F. H. L. Koppens, V. Palermo, N. Pugno, J. A. Garrido, R. Sordan, A. Bianco, L. Ballerini, M. Prato, E. Lidorikis, J. Kivioja, C. Marinelli, T. Ryhanen, A. Morpurgo, J. N. Coleman, V. Nicolosi, L. Colombo, A. Fert, M. Garcia-Hernandez, A. Bachtold, G. F. Schneider, F. Guinea, C. Dekker, M. Barbone, Z. P. Sun, C. Galiotis, A. N. Grigorenko, G. Konstantatos, A. Kis, M. Katsnelson, L. Vandersypen, A. Loiseau, V. Morandi, D. Neumaier, E. Treossi, V. Pellegrini, M. Polini, A. Tredicucci, G. M. Williams, B. H. Hong, J. H. Ahn, J. M. Kim, H. Zirath, B. J. van Wees, H. van der Zant, L. Occhipinti, A. Di Matteo, I. A. Kinloch, T. Seyller, E. Quesnel, X. L. Feng, K. Teo, N. Rupesinghe, P. Hakonen, S. R. T. Neil, Q. Tannock, T. Lofwandera and J. Kinaret, Nanoscale, 2015, **7,** 4598-4810.
12. W. C. Ren and H. M. Cheng, Nat Nanotechnol, 2014, **9,** 726-730.
13. R. Hao, W. Qian, L. H. Zhang and Y. L. Hou, Chem Commun, 2008, **48**, 6576-6578.

14. M. Lotya, Y. Hernandez, P. J. King, R. J. Smith, V. Nicolosi, L. S. Karlsson, F. M. Blighe, S. De, Z. M. Wang, I. T. McGovern, G. S. Duesberg and J. N. Coleman, Journal of the American Chemical Society, 2009, **131**, 3611-3620.
15. J. M. Lehn, Supramolecular chemistry : concepts and perspectives, 1995.
16. M. W. Hosseini, Accounts Chem Res, 2005, **38**, 313-323

Chapter 2 Graphene: Theory and Background

2.1 Background

Graphite is a 3D material, which consists of many flat layers of hexagons composed of carbon atoms that are arranged in a honeycomb lattice with a distance between adjacent C atoms amounting to 0.142 nm and a layered structure where the distance between planes is 0.335 nm (see Figure 2.1). The term graphite was introduced in 1789 by Abraham Gottlob Werner as a writing stone. Graphene is obtained by isolation of single graphite layer that is composed of sp^2 hybridized carbon atoms. Historically, the word *graphene* comes from the Greek word *graphein*, which means to write, i.e. one of the earliest uses of this material.[1, 2] Graphene as a monolayer of graphite was studied theoretically for the first time in 1947 by P. R. Wallace and followed by J. W. McClure in 1956 and G. W. Semenoff in 1984.[3-5] Later Peierls, Landau, and later Mermin estimated that the isolation of graphene was thought to be not possible thermodynamically at room temperature as they expected that the 2D lattice melts due to thermal fluctuations and long range crystalline order would therefore be prevented.[6, 7]

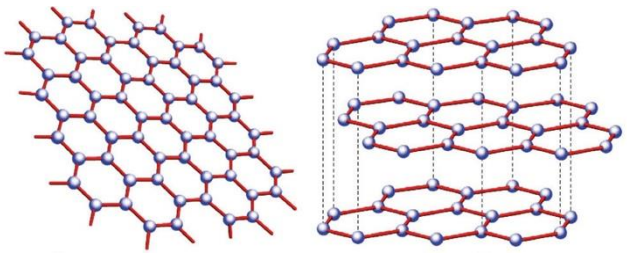

Figure 2.1. Single layer graphene and graphite.[2]

It is quite interesting that graphite is widely used as a substrate for Scanning Tunneling Microscopy (STM) studies and such investigations involves the pealing using scotch tape to expose fresh basal plane of graphene. Understandably, researchers used to throw away the Scotch tape with graphitic flakes on it. However, in 2004 A.K. Geim and K. Novoselov isolated the graphene by adhesive Scotch tape and characterized it successfully which enable them to be awarded the Nobel Prize in Physics in 2010.[8] They used a simple mechanical exfoliation method to produce single graphene sheet from graphite. Exfoliated graphene flakes were transferred onto silicon dioxide substrate. Their morphology was characterized by optical microscopy and Atomic Force Microscopy (AFM) and their electrical properties were measured.

However, it should be noted that graphene oxide (GO) and graphite intercalation compounds (GICs) have been already known since 1840s by German scientist Schafhaeutl who reported the insertion of acid or alkali metal between the carbon lamellae, i.e. intercalation, and exfoliation of graphite with sulfuric and nitric acids.[9] A lot of different intercalants and exfoliants have been used, including potassium, other alkali metals, fluoride salts of various types, transition metals (iron, nickel, and many others).[10] In fact the synthesis of GO has probably been obtained by the use of strong acids as intercalants.[11] In general, GO is synthesized by either the Brodie, Staudenmaier, or Hummers method, or some variation of these methods.[11-13] All three methods involve oxidation of graphite to various levels. Brodie and Staudenmaier used a combination of potassium chlorate ($KClO_3$) with nitric acid (HNO_3) to oxidize graphite, and the Hummers method involves treatment of graphite with potassium permanganate ($KMnO_4$) and sulfuric acid (H_2SO_4).[11-13] Boehm et al. found that the chemical reduction of dispersions of GO in dilute alkaline media with hydrazine, hydrogen sulfide, or iron (II) salts produced thin, lamellar carbon that contained only small amounts of hydrogen and oxygen and tried to prove that the thinnest lamella by transmission electron microscopy (TEM) (See Figure 2.2a-b). However exact identification of monolayer carbon at that time was a hard task due to the experimental error due to the thickness calibration standards.[14] Starting from 1970, epitaxial growth on metal substrates, on insulating carbides like SiC in 1975 and TiC, TaC in 1993 and on graphite in 2001 emerged as a new technique and ultrathin graphitic films and even monolayer pristine graphene were found.[15-18] However, before 2004, epitaxial growth was not the only way to produce pristine graphene, as a paper from the

Kurz's group had shown that a tape method (mechanical exfoliation) to get ultra-thin graphite films had been already used in 1990.[19] They used transparent tape to peel thin layers of graphite from highly ordered pyrolytic graphite (HOPG) and studied carrier dynamics of the sample.

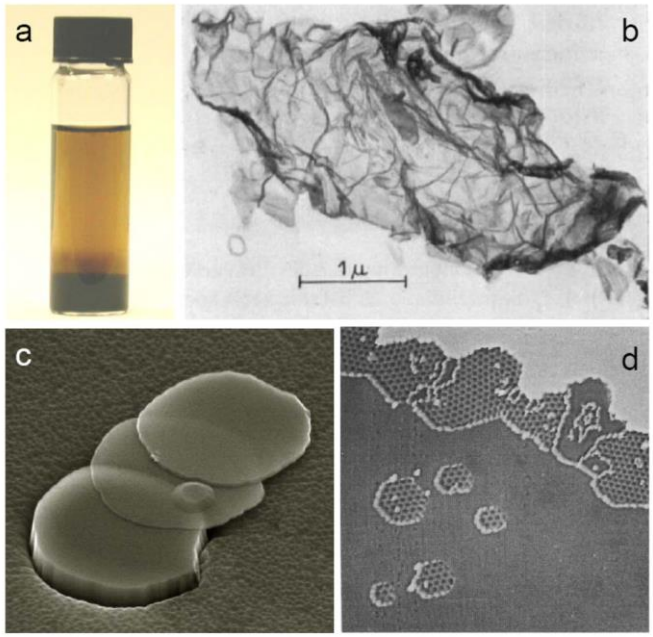

Figure 2.2. a) Graphite oxide suspension in water, b) TEM image of ultra-thin graphitic flakes from the early 1960s,[14] c) SEM image of thin graphite platelets by mechanical cleavage[20] and d) STM of graphene grown on Pt (image size is 100×100 nm^2).[21]

In 1995, visualization of a few -nm thick graphite was reported using AFM on top of HOPG and in 1999 using a Scanning Electron Microscope (SEM).[20, 22] (see Figure 2.2c) Production and visualization of ultra-thin graphite samples were not conducted alone and electrical properties were also analyzed for the samples with thickness down to 60 layers between 1997 and 2001.[23] Ultrathin epitaxial growth of graphite films composed of typically 3 graphene flakes from SiC in 2004 were reported by W. A. de Heer and coworkers.[24] In August 2004, Philip Kim's group described electronic properties of ultra-thin graphite platelets (down to ~35 layers), which were obtained by mechanical cleavage using a nanopencil.[25] But it is only in October 2004, that K. S. Novoselov and A. K. Geim carried out in depth and groundbreaking characterizations of monolayer graphene sheets.[8]

2.2 Properties of graphene

Graphene is defined as a single layer of carbon atoms arranged in a hexagonal honeycomb lattice (Figure 2.3a). A single carbon atom has four valence electrons with a ground-state electronic shell configuration of [He] $2s^2$ $2p^2$. In the case of graphene, the carbon-carbon chemical bonds are due to hybridized orbitals generated by the superposition of 2s with $2p_x$ and $2p_y$ orbitals (Figure 2.3b). The planar orbitals form the energetically stable and localized σ-bonds with three nearest-neighbor carbon atoms in the honeycomb lattice. They are also responsible for most of the binding energy and for the elastic properties of the graphene sheet. This carbon-carbon bond is very strong which gives rise to excellent strength, as well as chemical and structural stability. Its mechanical strength is higher than diamond and over 300 times greater than a steel film of the same thickness, but still light, flexible and stretchable up to 20% of its initial length.[26-28]

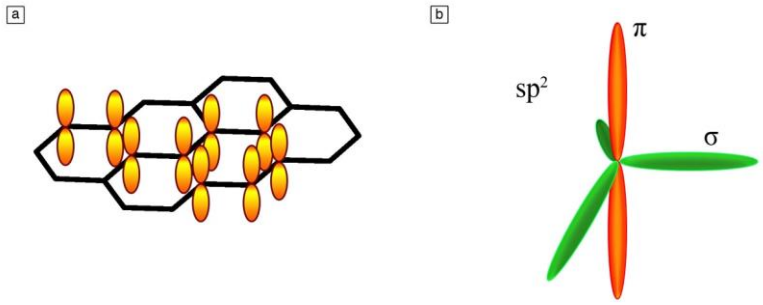

Figure 2.3. a) Schematic illustration of structural and electronic properties of graphene and b) sp2 hybridization illustrated in graphene.

The remaining free $2p_z$ orbitals present π symmetry orientation and the overlap of these orbital states between neighboring atoms plays a major role in the thermal and electronic properties of graphene. Graphene has a thermal conductance (>5000 W/m K) that is also higher than all the other carbon structures and theoretical surface area of 2600 m^2/g.[29, 30] Electrons move up to 100 times faster in graphene than in silicon and can flow through graphene more easily than even through copper.[31] In fact, graphene is a zero band gap semiconductor and charge carriers in graphene have very small effective mass so that carrier mobilities are as high as up to 200000 $cm^2V^{-1}s^{-1}$ at a carrier density of 1012 cm^{-2}.[32] The opacity of a single layer graphene is

2.3 % (Figure 2.4), therefore its optical transparency is 97.7 % observed in the visible range and decreases linearly as the number of layers increases. Consisting of a single layer of carbon atoms, graphene is the thinnest material and is completely impermeable even for He atoms.[33]

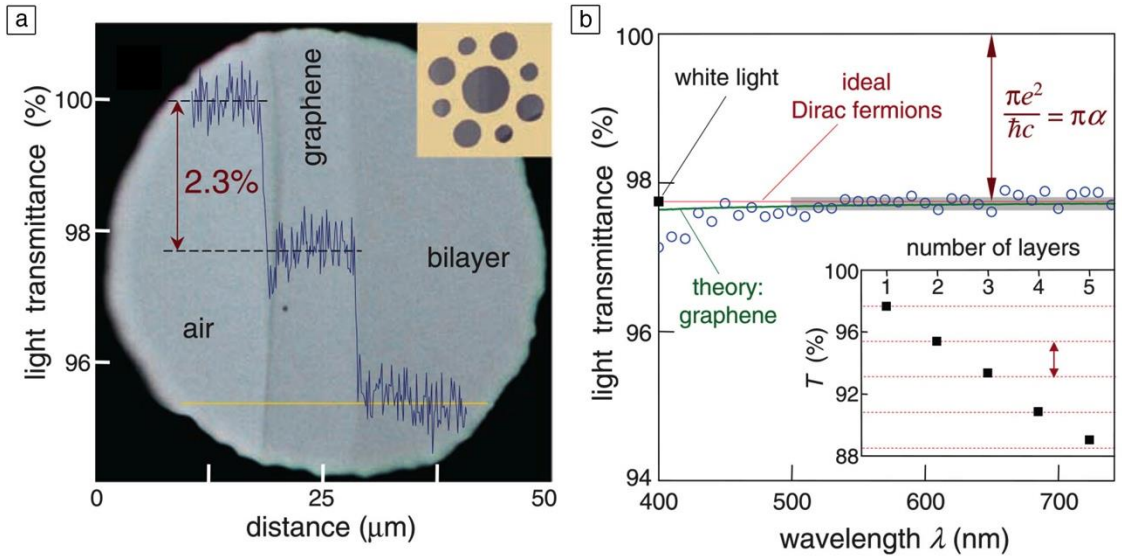

Figure 2.4. a) The transmittance of single or two-layer graphene prepared by mechanically exfoliated method, b) Transmittance spectrum of single-layer graphene.[34]

Adsorption and desorption of gases such as hydrogen and carbon monoxide is possible on graphene surface like on graphite.[35] Well design molecules can adsorb on graphene surface via weak interactions as van der Waals interaction or π-π stacking interaction through air, vacuum or liquid deposition. These non-covalent molecular building blocks make possible to tune or boost graphene properties.[36] Besides forming weak adsorbate on graphene surface, graphite can be also oxidized to graphene oxide (GO) that is the functionalized form graphene with functional groups like epoxy and carboxyl.[37] Further chemical or thermal reduction of so-called graphene oxide yields to reduced - graphene oxide (rGO).

2.3 Potential application of graphene

These exceptional properties enable graphene to meet challenges within diverse areas (Figure 2.5). Four main areas were prioritized in the following sections.

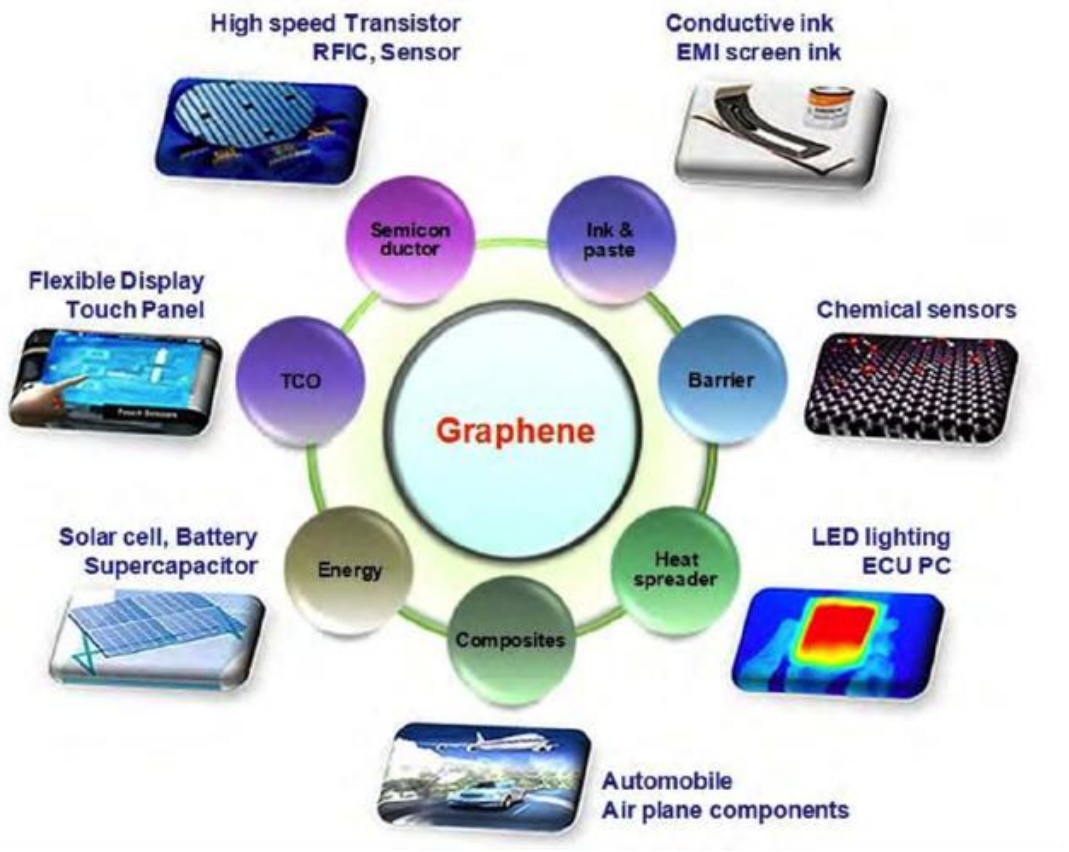

Figure 2.5. Overview of applications of graphene in different sectors ranging from conductive ink to chemical sensors, light emitting devices, composites, energy, touch panels and high frequency electronics.[38]

2.3.1 Energy

Graphene-based systems for energy production (photovoltaic, fuel cells, and solar cells), energy storage (supercapacitors and batteries) and hydrogen storage are suggested to bring disruptive solutions to the current industrial challenges.

Increasing energy storing capacity in smaller volumes is the key-driving factor in the battery research. Commercially available cathodes for lithium-ion batteries have a relatively low conductivity, which can be tuned by the addition of graphite or carbon black. Graphene with its layered structure can be used as conductive filler but also as novel sandwich-type nanocomposite structures. By designing new systems having a higher conductivity it would be possible to overcome the main limiting factor, which is the low specific power density. For example, a lithium-ion battery fabricated from on a graphene ink anode and a lithium iron phosphate cathode exhibits a high battery performance in terms of specific capacity with 165 mA h g^{-1}, and an estimated energy density around 190 W h kg^{-1}. Also a stable operation for over 80 charges–discharge cycles is proven.[39] More recently, other examples of new graphene based batteries have been published.[40-41]

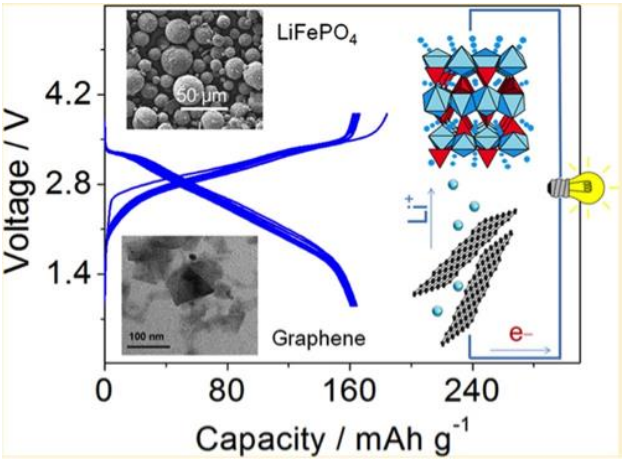

Figure 2.6. Schematic overview an advanced lithium-ion battery based on a graphene anode and a lithium iron phosphate cathode.[39]

Supercapacitors combine the high-energy storage capacity of batteries and the high power possibility of capacitors. They store electrical energy directly in form of electronic charge within electrochemical double layer capacitor, compared to batteries storing electrical energy in form of chemical bonds.[42] The conversion of chemical energy to electrical energy is a time consuming process and therefore by circumventing this conversion, a supercapacitor can charge up as well as deliver electricity at a very high rate. For his high electrical conductivity,

accessible and defined pore structures and high stability temperature graphene based materials is one of the best candidates. Recent works have shown the possibility to develop graphene-based supercapacitors with even higher performance.[43-44]

Taking the advantage of its unique properties, i.e. highly optical transparence, highly electrical conduction, and mechanical flexibility, graphene and its derivatives have been investigated in the field of solar cells. In particular, it has been shown that graphene can be used as electrodes, (transparent anodes,[45-47] non-transparent anodes,[48] transparent cathodes,[49, 50]) and counter electrodes,[51, 52]. But graphene can also be used as active layer or in other terms as light harvesting material.[53, 54] In 2013, Wang and his co-workers demonstrated graphene based solar cells with notable performance of up to 15.6 % conversion efficiency (Figure 2.7.).[55]

Figure 2.7. Cover page of solution-processable perovskite-based solar cells showing remarkable performance of up to 15.6 % conversion efficiency.[55]

2.3.2 Electronics

One of the most promising areas for graphene applications is flexible electronics. In fact, electronic products like E-paper, organic light-emitting diodes (OLEDs), piezoelectric devices

or touch screen displays require more than 90 % transmittance and a low sheet resistance. Research in foldable electronic circuits for paper substrates by using graphene nanoflakes is increasing (see Figure 2.8.)[56] Also flexible mobile phones application is showing new concepts. Light-emitting diodes (LEDs) made by stacking metallic graphene, and other well-chosen 2D materials can be designed.[57]

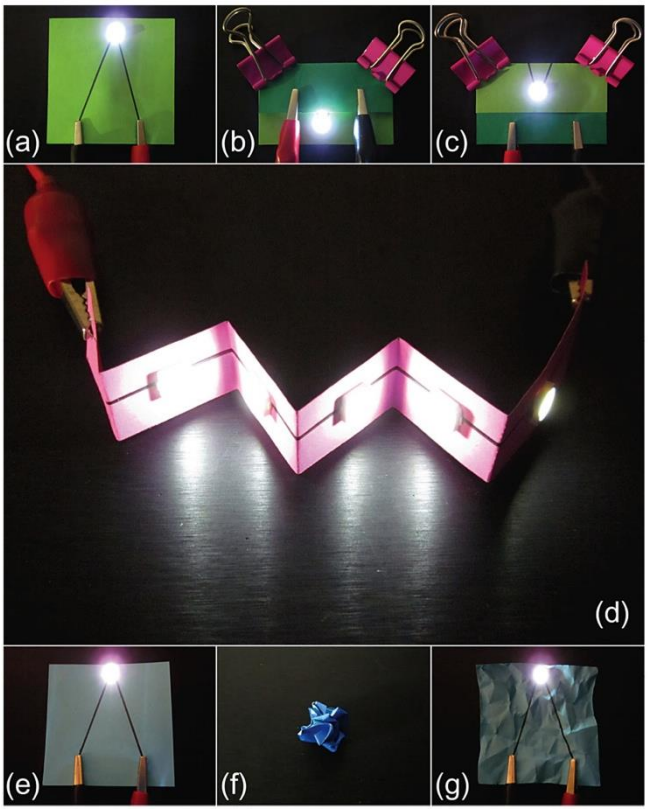

Figure 2.8. Photographs of applications. a, b, c) Operation of a LED chip with graphene circuits on a paper substrate under −180° folding and 180° folding, d) array of LED chips on a three-dimensional circuit board including negative and positive angle folding and e, f, g) operation of a LED chip on the paper-based circuit board before and after crumpling.[56]

Realization of printable radio frequency identification (RFID) antenna by low temperature processing of graphene ink was demonstrated. The required low resistance is achieved by applying at the same time compression and winding of graphene laminate. This result in an increase of the conductivity of graphene laminates by more than 50 times compared to that of as-deposited one.[58] Graphene is in its general state non-piezoelectric but it has been shown

that piezoelectric effects could be tuned into non-piezoelectric graphene by taking advantage of the selective surface adsorption of atoms.[59] Graphene thermal conductivity was proven to be the highest of known materials and is dominated by phonons near the room temperature. It has been confirmed that graphene heat spreaders can lower the hot-spot temperature during device operation which results in enhanced performance and reliability of the devices.[60, 61]

High frequency transistors have been accepted from the very beginning as one of the most promising fields of applications for graphene having the potential to significant outperform all transistors in terms of speed. Charge carrier mobility, large saturation velocity and 2D nature of graphene may open new prospects for up-scalable devices. Graphene transistors have the potential to break the frequency limits of well-established materials within the near future. These make possible to dream about novel fields of applications not conceivable with state-of-the-art technologies ranging from ultrafast data-communication to spectroscopy.[62-65]

2.3.3 Sensors

The rapidly increasing use of sensors and the demand for cheaper and better devices with less power consumption is governed by the emergence of new sensor materials. Graphene has potential for sensor development within a very wide range of applications, including industrial monitoring, surveillance, security, interactive electronics, communication, lab-on-chip, point-of-care, environmental monitoring, transportation and automation. Electrochemical sensors (H_2O, H_2O_2, glucose, nucleic acids, protein markers, chemical and biomolecules),[66-70] electronic sensor (mechanisms, gases, chemical and biomolecules),[71-77] and optical sensors (fluorescence, UV-Vis, IR)[78-80] are widely studied. For example, a lot of efforts are made on pressure sensors for pressure sensitive displays [81] and on graphene bio-sensors fabricated for detection of cancer risk biomarker.[82]

2.3.4 Coating and Composites

Coating plays an important role for the development of surface quality and provides protection for substrates. For example, transparent conductive coating deposed on copper substrate via the combination of plasma chemical vapor deposition (CVD) and roll-to-roll process could impact touch panel application.[83] Graphene is an effective barrier toward oxidation and corrosion of a substrate. The potential of graphene based materials as anti-corrosion and anti-oxidation coating on different substrates with different coating methods has been reported.[84-86] Also the unique structure of graphene-based materials can find a place in absorbent applications. For example, a hydrophobic and oleophilic sponge was fabricated by coating graphene on melamine via dip coating (Figure 2.9.) exhibiting absorption capacities up to 165 times of its weight, high selectivity, recyclability, lightweight, good robustness, and inertness to corrosive environments.[84]

Polymer composites have become an important part as the incorporation of graphene-based materials into polymer can enhanced several properties at the same time such as electrical properties and mechanical properties. There has been considerable effort for the incorporation of graphene into polymer matrices. So far, the research results have shown large increases in Young's modulus, tensile stress, electrical conductivity, and thermal conductivity.[87-92] For example, scientists used CVD to create 2-inch-by-2-inch sheets of graphene, contained in a polymer composite. (See Figure 2.9) Layering graphene between polymer matrices is forming new materials which are showing high mechanical properties and electrical conductivities.[93]

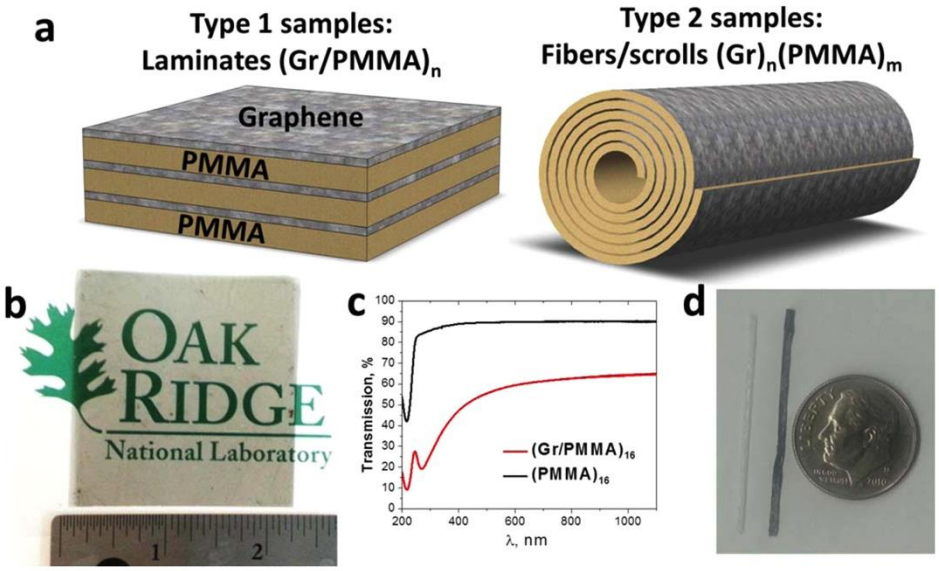

Figure 2.9. a) Scheme of laminates and fibers/scrolls. b) $(Gr/PMMA)_{16}$ laminate. c) UV/ vis spectra of $(Gr/PMMA)_{16}$ and $(PMMA)_{16}$ laminates. d) Photograph of $(PMMA)_1$ fiber (left) and $(Gr)6/(PMMA)_1$ fiber (right).[93]

Despite considerable amount of works reported on polymer-graphene composites in the literature, the use of graphene for reinforcing ceramics and glass matrices is relatively limited. In a recent study graphene nanoplatelets (GNP) and graphene oxide nanoplatelets (GONP) were used to reinforce silica. It was also reported that the new composite has a better machinability compared to pure silica.[94] Incorporation of graphene nanoparticles in cement paste showed interesting modifications in microstructural, morphological, electrical and thermal properties of the paste.[95] Also very recently, silk directly spun by spiders produced after the exposure of spiders to dispersions of graphene (See Figure 2.10a-b) were found to improve mechanical properties.[96]

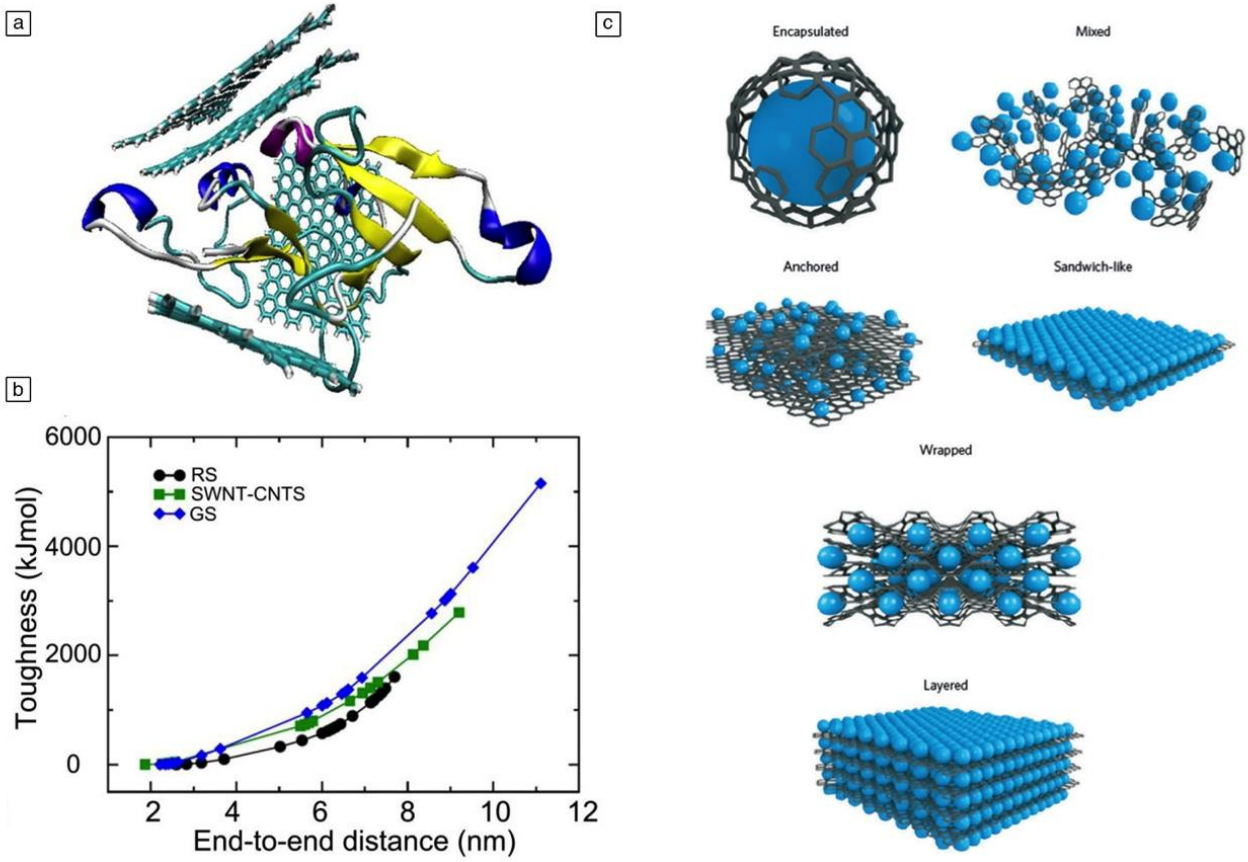

Figure 2.10. a) Arrangement of graphene around MASP2 fiber protein, b) corresponding dissipated energy (here called toughness)[96] and c) Schematic diagram of the different structures of graphene composite materials.[97]

Also graphene-nanoparticle composites are able to offer numerous unique and advantageous properties for various applications depending on the particular characteristics possessed by the nanoparticles used to form the composites. Various metal (Au, Ag and Pt)[98-100] and metal oxide nanoparticles (FeO_4, TiO_2, SnO_2, MnO_2, and more)[101-105] are widely studied, either in graphene-encapsulated nanoparticles and graphene decorated with nanoparticles (See Figure 2.10c).

2.4 Synthesis of graphene

Over 20 methods have been proposed and exploited in the last decade for the production of graphene and they give graphene with different dimension, shape, thickness, number of defects and quality. In this case, the targeted final application is fully depended of the production methods. In this way each production method should be promote in order to cover the maximum of applications (See Table 2.1).

Method	Crystallites Size, μm	Sample Size, mm	μ	Applications
Micromechanical Cleavage	1,000	1	2×10^5 $cm^2/V\cdot s$ $10^6 cm^2/V\cdot s$ (@T=4K) 2×10^4 $cm^2/V\cdot s$ @RT	Fundamental research and proof of principle devices
LPE of graphite	0.01-1	0.1-1 (∞ as overlapping flakes)	100 $cm^2/V\cdot s$ (for a layer of overlapping flakes) @RT	Inks, coatings, paints, batteries, supercaps, solar cells, fuel cells, composites, sensors, TCs, photonics, flexible electronics and optoelectronics, bio-applications
LPE of GO	>1	>1 (∞ as overlapping flakes)	1 $cm^2/V\cdot s$ (for a layer of overlapping flakes) @RT	Inks, coatings, paints, batteries, supercap, solar cells, fuel cells, composites sensors, TCs, photonics, flexible electronics and optoelectronics, bio-applications
Growth on SiC	100	100 (6'')	6×10^6 $cm^2/V\cdot s$ @T=4K	RF transistors other electronic devices
CVD	50,000	1,000	6.5×10^4 $cm^2/V\cdot s$ @T=1.7K 3×10^4 $cm^2/V\cdot s$ @RT	Photonics, nanoelectronics, TCs, sensors, bio-applications,flexible electronics

Table 2.1. State of the art of the main production approaches and foreseen applications.[38]

Two distinct strategies have been undertaken for graphene production, i.e. the bottom-up and the top-down approaches as summarized in Figure 2.11.

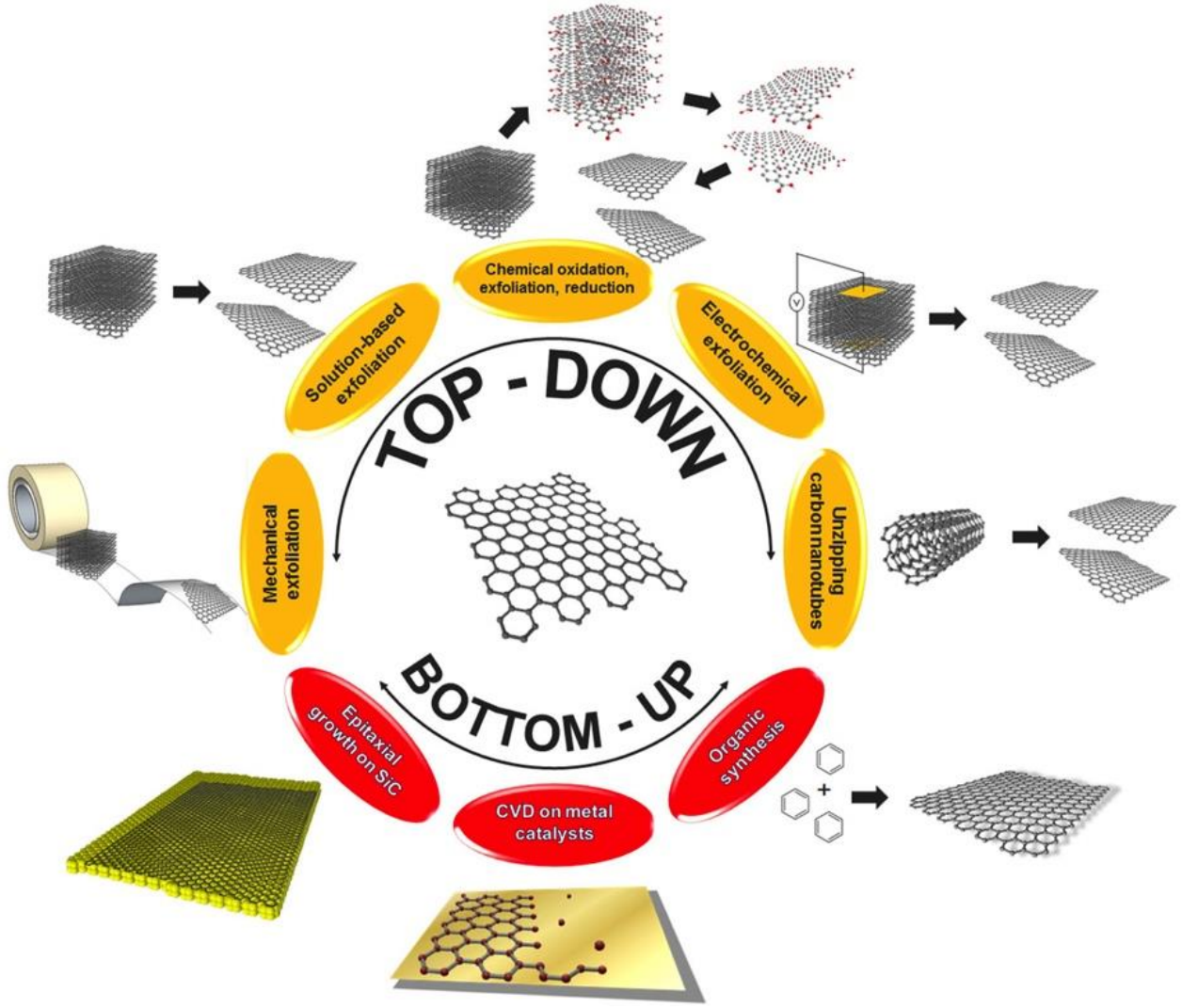

Figure 2.11. Overview of the main graphene production techniques.[106]

2.4.1 Bottom-up approaches

The large choice of chemical species and preparation methods makes the bottom-up fabrication an important candidate. Since graphene can built from discrete atomic or small

molecular entities, the fabrication can be done with atomic-level precision using synthetic chemical techniques that have been developed over the past century.

2.4.1.1 Chemical vapor deposition

Chemical vapor deposition made it possible to grow large area and uniform graphene films from solid, liquid or gaseous precursors. There are many different kinds of CVD process: thermal, plasma enhanced, cold or hot wall, reactive, *etc.* Depending on the precursor, materials quality, specific equipment and conditions for CVD, the final graphene film can vary in terms of performance.[107] Basically, the procedure involves a high-temperature decomposition step of a carbon source in the presence of a transition-metal catalyst on which carbon atoms will deposit and rearrange into carbon structures (Figure 2.12.). The carbon source is usually a gaseous species such as methane, ethane, or propane, although the use of a solid source has also been demonstrated.[108, 109]

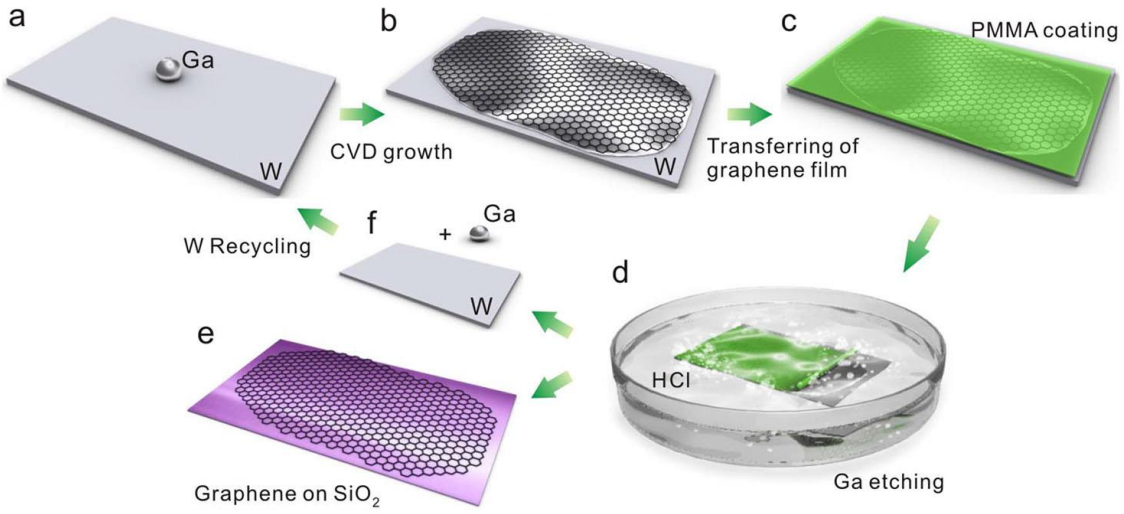

Figure 2.12. Schematic illustration of graphene growth over liquid Ga supported on a W substrate. a) A droplet of Ga is placed on a W support foil, b) CVD growth of graphene on the liquid Ga surface, c) the as-grown graphene is coated with a PMMA layer by a spin-coating process, d) graphene coated with PMMA is gradually separated from the W foil driven by H_2 bubbles produced at the interface between the graphene and the Ga–W substrate, e) graphene transferred onto a SiO_2/Si substrate and f) the W foil can be reused as Ga-support.[110]

2.4.1.2 Synthesis of SiC

Graphene growth has been achieved on SiC substrates by heat treatment at high temperatures under ultrahigh vacuum (UHV) conditions.[111] During the process, Si atoms sublimate to leave an exposed layer of carbon atoms that will rearrange to form epitaxial graphene.[112] Precise control of the sublimation temperatures may lead to the formation of very thin graphitic layers, occasionally of single sheets. The properties of graphene grown on SiC are different than those of mechanically exfoliated graphene. This is mainly due to the presence of substrate-induced corrugations and irregular orientations of the graphene layers, which alter the electronic properties.[113]

2.4.1.3 Molecular self-assembly

The synthesis of small "graphene molecules" represents a very interesting route because it allows the preparation of graphene sheets with well-defined shape and controlled edge structures from organic molecules with diverse functionalities available as the elementary building blocks with tunable properties. Recently, it has been proved that self-assembled monolayers of aromatic molecules on copper substrates can be converted into high-quality single-layer graphene using low-energy electron irradiation and subsequent annealing.[114] By using this approach it is also possible to fabricate nitrogen-doped graphene, which is among the most promising metal-free catalysts for replacing platinum.[115] Also Müllen and co-worker demonstrated the first synthesis of graphene nanoribbons of 30 nm in length and the largest graphene molecule consisting of 222 carbons with a size of 3.2 nm among others.[116]

2.4.2 Top-down approaches

Exfoliation of bulk graphite is the most commonly used method for mass production of graphene sheets. Depending on the strategy used, there are considerable differences in yield, efficiency, cost, accompanying pollution, ease of production and scalability of the manufacturing process, and in the morphology, structure and properties of the products such as thickness, lateral size, surface chemistry, solubility, defect and impurity contents, and electrical and thermal conductivities. Among all top-down techniques, only five methods will be discussed.

2.4.2.1 Mechanical exfoliation

One of the most important method is the micromechanical cleavage of highly oriented pyrolitic graphite (HOPG), which was the first method used to isolate a single layer graphene.[8] This method involves repetitively peeling off layers of graphene from HOPG with the help of an adhesive tape to give single graphene layers that can be transferred onto an appropriate surface through a wet or dry transfer technique. (See Figure 2.13) Also named as "Scotch-tape method", this method is extremely simple, enables the isolation of single layer graphene with a dimension up to 1 mm in size and causes minimal modification to the graphene sheet.[117] Although micromechanical exfoliation is not a good candidate for mass production, it is still the method of choice for fundamental studies, as the majority of new device concepts were obtained by using this technique.

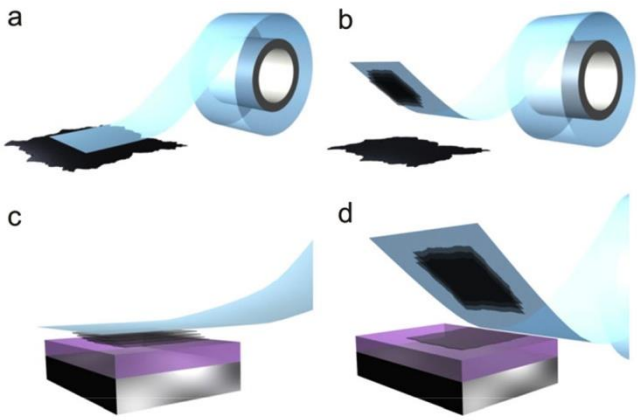

Figure 2.13. a-d) Step by step formation of graphene via Scotch-tape method.[21]

2.4.2.2 Liquid-phase exfoliation of graphite

Graphite can be successfully exfoliated in liquid environments by exploiting shear force to extract individual layers.[118] After exfoliation, the solvent-graphene interaction needs to balance the inter-sheet attractive forces. Several approaches to prepare dispersed graphene flakes in a liquid phase have been reported, including blender, mixer, ultrasounds, temperature and ball milling. In this thesis, we will focus our attention on ultrasound assisted graphite exfoliation and it will be discussed in Chapter 3.

A ball-milling treatment can be employed to exfoliate graphite through interactions with commercially available melamine under solid conditions. This procedure allows the fast production of relatively large quantities of material with a low presence of defects. The milling treatment can be modulated in order to achieve graphene flakes with different sizes. Once prepared, the graphene samples can be redispersed in organic solvents or water forming stable dispersions that can be used for multiple usages.[119]

In 2014, Coleman and co-workers showed that high-shear mixing of graphite in suitable stabilizing liquids results in large-scale exfoliation to give dispersions of graphene as shown in Figure 2.14. They have developed a simple model that shows exfoliation to occur once the local shear rate exceeds 10^4 s^{-1} (Figure 2.14). By fully characterizing the scaling behavior of the graphene production rate, they show that exfoliation can be achieved in liquid volumes from hundreds of milliliters up to hundreds of liters and beyond.

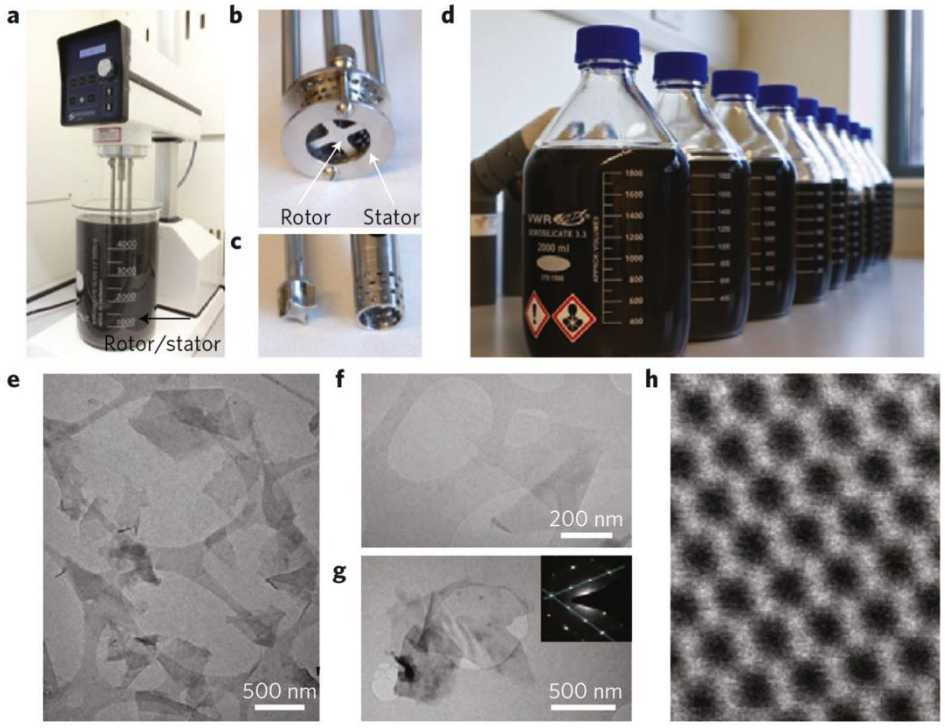

Figure. 2.14. Production of graphene by shear mixing. a) A Silverson model L5M high-shear mixer with mixing head in a 5 L beaker of graphene dispersion. Close-up view of b) a D = 32 mm mixing head and c) a D = 16 mm mixing head with rotor (left) separated from stator. d) Graphene–NMP dispersions produced by shear exfoliation. e) Wide-field TEM image of SEG nanosheets after centrifugation. TEM images of f) individual nanosheets and g) a multilayer and monolayer as evidenced by its electron diffraction pattern. h) HRTEM of a monolayer.[120]

2.4.2.3 Oxidation-reduction of graphene oxide

In general, graphene oxide is synthesized by either Brodie, Staudenmaier, or Hummers method, or some variation of these methods.[11, 13, 14] All these methods involve oxidation of graphite to various levels. Brodie and Staudenmaier used a combination of potassium chlorate ($KClO_3$) with nitric acid (HNO_3) to oxidize graphite, and the Hummers method involves treatment of graphite with potassium permanganate ($KMnO_4$) and sulfuric acid (H_2SO_4). (See Figure 2.15) GO flakes can be produced via sonication, stirring, thermal expansion and of graphene oxide. Liquid-phase exfoliation of graphite oxide is now one of the most widely used methods for preparation of graphene. One of the aces of GO is certainly is easily

processible in liquid media such as water.[121] Moreover all the different functional groups that are exposed on GO, including hydroxyl, epoxy, carbonyl and carboxyl groups, can be used to covalently and non-covalently attach functional units, thereby changing its physical and chemical properties.[122, 123]

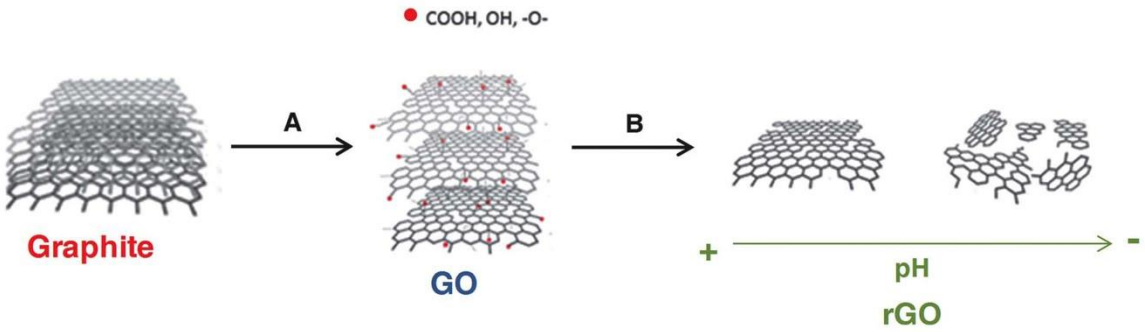

Figure 2.15. Representation of the processes occurring during the experiment. (A) Hummers oxidation of graphite: (i) $NaNO_3$, H_2SO_4, $KMnO_4$, 0 °C, (ii) H_2O_2. (B) Hydrothermal reduction at 180 °C and different pH values in the 3–11 interval. As a function of the pH, drastic changes in the morphologies and sizes of the obtained carbon forms can be observed.[124]

2.4.2.4 Electrochemical exfoliation of graphite

In 2008, Liu et al. developed an electrochemical exfoliation method to obtain graphene sheets from graphite in ionic liquid and water. These treated graphene sheets can be individually dispersed in DMF, DMSO or NMP without the need of further deoxidization.[125] Electrochemical approaches to the fabrication of graphene typically involve the use of a electrolyte and an electrical current to run structural deformation of a graphite-working electrode. When a positive potential is applied, the graphite electrode is oxidized and the intercalation of negatively charged ions from the solution into the graphitic layers starts. This step is then followed by the application of a negative potential that facilitates the exfoliation process (See Figure 2.16.)

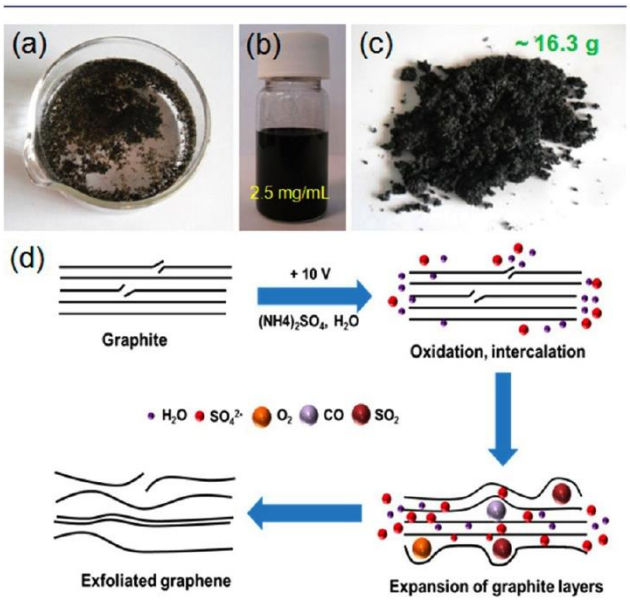

Figure 2.16. Photograph of a) graphite flakes after electrochemical exfoliation, b) dispersed Exfoliated Graphene (EG) in DMF solution (concentration~2.5 mg mL^{-1}), c) EG powders on a bulk scale (~110.3 g) and d) Schematic illustration of the mechanism of electrochemical exfoliation.[126]

For example, the exfoliation of graphite into graphene sheets has been achieved by using sulfuric acid and poly(styrenesulfonate) as electrolytes among others.[127] Electrochemical routes allow the production of milligram and gram scale quantities of few-layer graphene materials having different degrees of quality and purity related to the conditions employed, for example the operating voltage of the exfoliation procedure. Being a relatively new technique, much effort is necessary before mastering all the parameters.

2.4.2.5 LPE of intercalated graphite

Graphite intercalation compounds (GIC) are formed by insertion of atomic or molecular species between graphene layers. This technique was introduced by Schafhaeutl in 1840.[9] This method begins with the intercalation of different compounds in graphite. The second step is the expansion of graphite via a rapid increase in the vapor pressure of the volatile intercalated substance under microwave or thermal treatment. Hundreds of GICs with donor (alkali, alkali earth metals, lanthanides, metal alloys or ternary compounds, etc.) or acceptor intercalates (i.e.

halogens, halogen mixtures, metal chlorides, acidic oxides, etc.) have been reported.[128] This makes GICs promising to produce graphene via LPE. However, although the exfoliation process is often called spontaneous, due to the absence of ultrasonication, it requires mechanical energy, often provided by stirring. The role of the solvent and intercalates is crucial to achieve large quantities of graphene. Also the majority of recipes are limited by using either poisonous chemical agents or dangerous chemical reactions.[129, 130]

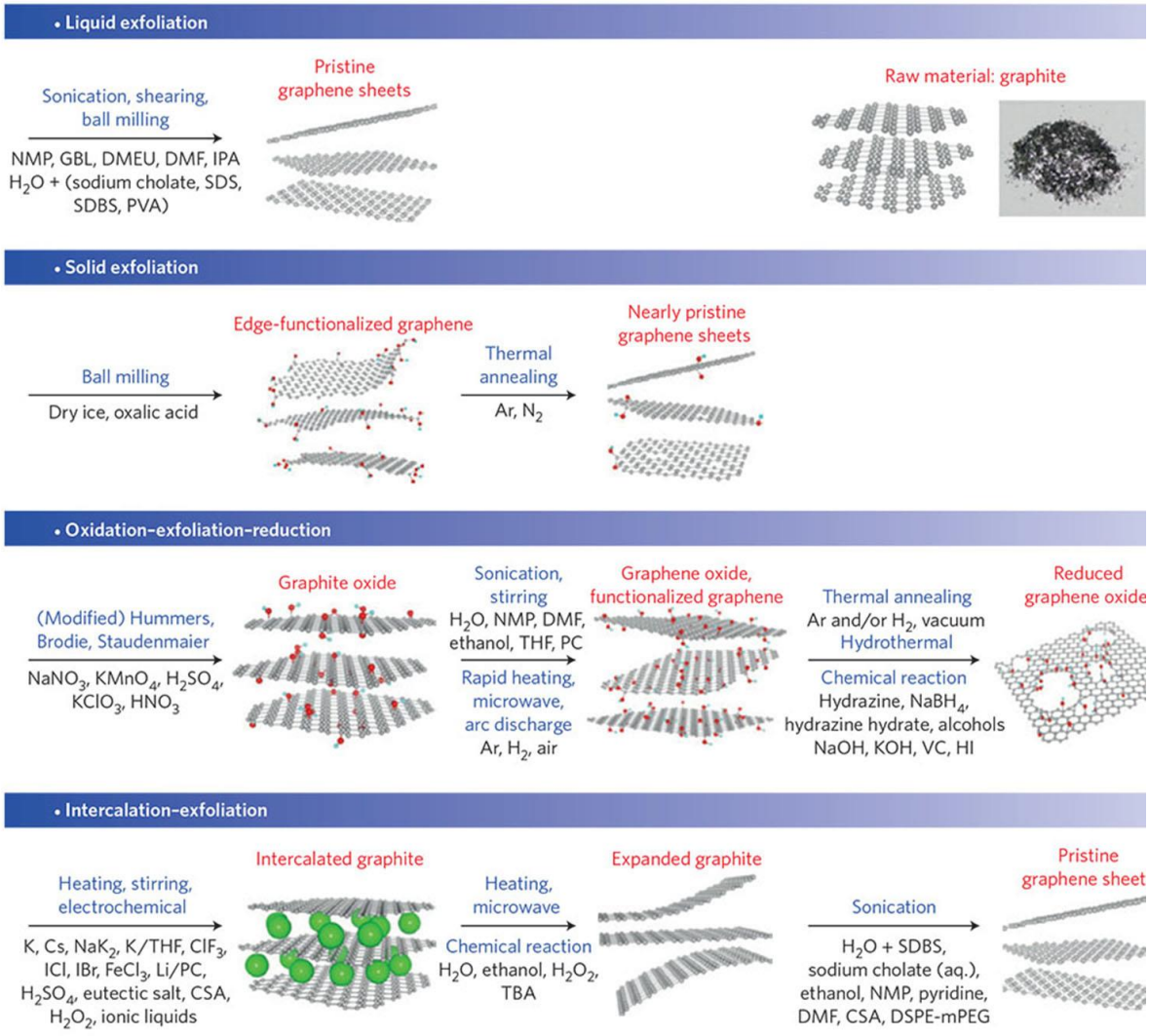

Figure 2.17. Main mass production methods of graphene.[131]

2.5 Conclusions

In this chapter, a background on graphene was presented in addition to a brief explanation about its different fundamental properties. Furthermore, basic description of the several potential applications in various field were explained. Finally, the main production methods for graphene fabrication were developed highlighting the importance of choosing the right approach to produce graphene for targeted applications.

2.6 References

1. H. P. Boehm, R. Setton and E. Stumpp, *Carbon*, 1986, **24**, 241-245.
2. A. K. Geim and K. S. Novoselov, *Nat Mater*, 2007, **6**, 183-191.
3. J. W. McClure, *Physical Review* 1956, **104**, 666-671.
4. G. W. Semenoff, *Physical Review Letters.*, 1984, **53**, 2449-2452.
5. P. R. Wallace, *Physical Review*, 1947, **71**, 622-634.
6. N. D. Mermin, *Physical Review*, 1968, **176**, 250-254.
7. R. E. Peirls, *Helv. Phys. Acta.*, 1934, **7**, 81-83.
8. K. S. Novoselov, A. K. Geim, S. V. Morozov, D. Jiang, Y. Zhang, S. V. Dubonos, I. V. Grigorieva and A. A. Firsov, *Science*, 2004, **306**, 666-669.
9. C. Schafhaeutl, *Philosophical Magazine Series 3.*, 1840, **16**, 70-590.
10. M. Inagaki, *J Mater Res*, 1989, **4**, 1560-1568.
11. B. C. Brodie *Philosophical Transactions of the Royal Society of London*, 1859, **149**, 249-259.
12. L. Staudenmaier, *Berichte der deutschen chemischen Gesellschaft* 1898, **31**, 1481-1487.
13. W. S. Hummers and R. E. Offeman, *Journal of the American Chemical Society*, 1958, **80**, 1339-1339.
14. H. P. Boehm, A. Clauss, G. O. Fischer and U. Hofmann, *Zeitschrift für anorganische und allgemeine Chemie*, 1962, **316**, 119-127.
15. A. M. Affoune, B. L. V. Prasad, H. Sato, T. Enoki, Y. Kaburagi and Y. Hishiyama, *Chemical Physics Letters*, 2001, **348**, 17-20.
16. J. M. Blakely, J. S. Kim and H. C. Potter, *Journal of Applied Physics* 1970, **41**, 2693-2697.
17. A. Nagashima, K. Nuka, K. Satoh, H. Itoh, T. Ichinokawa, C. Oshima and S. Otani, *Surface Science*, 1993, **2**, 287–288.
18. A. J. Van Bommel, J. E. Crombeen and A. Van Tooren, *Surface Science*, 1975, **48**, 463-472.
19. K. Seibert, G. C. Cho, W. Kütt, H. Kurz, D. H. Reitze, J. I. Dadap, H. Ahn, M. C. Downer and A. M. Malvezzi, *Physical Review B*, 1990, **42**, 2842-2851.
20. L. Xuekun, Y. Minfeng, H. Hui and S. R. Rodney, *Nanotechnology*, 1999, **10**, 269-27

21. A. K. Geim, *Physica Scripta*, 2012, **2012**, 014003.
22. T. W. Ebbesen and H. Hiura, *Advanced Materials*, 1995, **7**, 582-5810.
23. Y. Ohashi, T. Koizumi, T. Yoshikawa, T. Hironaka and K. Shiiki, *TANSO*, 1997, **180**, 235-238.
24. C. Berger, Z. Song, T. Li, X. Li, A. Y. Ogbazghi, R. Feng, Z. Dai, A. N. Marchenkov, E. H. Conrad, P. N. First and W. A. de Heer, *The Journal of Physical Chemistry B*, 2004, **108**, 19912-199110.
25. Y. B. Zhang, J. P. Small, M. E. S. Amori and P. Kim, *Phys Rev Lett*, 2005, **94**, 176803.
26. Z. H. Ni, T. Yu, Y. H. Lu, Y. Y. Wang, Y. P. Feng and Z. X. Shen, *Acs Nano*, 2008, **2**, 2301-2305.
27. Z. H. Ni, H. M. Wang, Y. Ma, J. Kasim, Y. H. Wu and Z. X. Shen, *Acs Nano*, 2008, **2**, 1033-1039.
28. C. Lee, X. D. Wei, J. W. Kysar and J. Hone, *Science*, 2008, **321**, 385-388.
29. S. S. Chen, Q. Z. Wu, C. Mishra, J. Y. Kang, H. J. Zhang, K. J. Cho, W. W. Cai, A. A. Balandin and R. S. Ruoff, *Nat Mater*, 2012, **11**, 203-207.
30. S. Stankovich, D. A. Dikin, R. D. Piner, K. A. Kohlhaas, A. Kleinhammes, Y. Jia, Y. Wu, S. T. Nguyen and R. S. Ruoff, *Carbon*, 2007, **45**, 1558-1565.
31. J. H. Chen, C. Jang, S. D. Xiao, M. Ishigami and M. S. Fuhrer, *Nat Nanotechnol*, 2008, **3**, 206-209.
32. X. Du, I. Skachko, A. Barker and E. Y. Andrei, *Nat Nanotechnol*, 2008, **3**, 491-495.
33. J. S. Bunch, S. S. Verbridge, J. S. Alden, A. M. van der Zande, J. M. Parpia, H. G. Craighead and P. L. McEuen, *Nano Lett*, 2008, **8**, 2458-2462.
34. R. R. Nair, P. Blake, A. N. Grigorenko, K. S. Novoselov, T. J. Booth, T. Stauber, N. M. R. Peres and A. K. Geim, *Science*, 2008, **320**, 1308-1308.
35. E. Kayhan, R. M. Prasad, A. Gurlo, O. Yilmazoglu, J. Engstler, E. Ionescu, S. Yoon, A. Weidenkaff and J. J. Schneider, *Chem-Eur J*, 2012, **18**, 14996-15003.
36. J. M. MacLeod and F. Rosei, *Small*, 2014, **10**, 1038-1049.
37. D. C. Marcano, D. V. Kosynkin, J. M. Berlin, A. Sinitskii, Z. Z. Sun, A. Slesarev, L. B. Alemany, W. Lu and J. M. Tour, *Acs Nano*, 2010, **4**, 4806-4814.
38. A. C. Ferrari, F. Bonaccorso, V. Fal'ko, K. S. Novoselov, S. Roche, P. Boggild, S. Borini, F. H. L. Koppens, V. Palermo, N. Pugno, J. A. Garrido, R. Sordan, A. Bianco, L. Ballerini, M. Prato, E. Lidorikis, J. Kivioja, C. Marinelli, T. Ryhanen, A. Morpurgo, J. N. Coleman, V. Nicolosi, L. Colombo, A. Fert, M. Garcia-Hernandez, A. Bachtold, G. F. Schneider, F. Guinea, C. Dekker, M. Barbone, Z. P. Sun, C. Galiotis, A. N. Grigorenko, G. Konstantatos, A. Kis, M. Katsnelson, L. Vandersypen, A. Loiseau, V. Morandi, D. Neumaier, E. Treossi, V. Pellegrini, M. Polini, A. Tredicucci, G. M. Williams, B. H. Hong, J. H. Ahn, J. M. Kim, H. Zirath, B. J. van Wees, H. van der Zant, L. Occhipinti, A. Di Matteo, I. A. Kinloch, T. Seyller, E. Quesnel, X. L. Feng, K. Teo, N. Rupesinghe, P. Hakonen, S. R. T. Neil, Q. Tannock, T. Lofwandera and J. Kinaret, *Nanoscale*, 2015, **7**, 4598-4810.
39. J. Hassoun, F. Bonaccorso, M. Agostini, M. Angelucci, M. G. Betti, R. Cingolani, M. Gemmi, C. Mariani, S. Panero, V. Pellegrini and B. Scrosati, *Nano Lett*, 2014, **14**, 4901-49010.
40. K. H. Park, D. Lee, J. Kim, J. Song, Y. M. Lee, H. T. Kim and J. K. Park, *Nano Lett*, 2014, **14**, 4306-4313.
41. E. Yoo, J. Kim, E. Hosono, H. Zhou, T. Kudo and I. Honma, *Nano Lett*, 2008, **8**, 2277-2282.

42. P. Simon and Y. Gogotsi, *Nat Mater*, 2008, **7**, 845-854.
43. P. G. Campbell, M. D. Merrill, B. C. Wood, E. Montalvo, M. A. Worsley, T. F. Baumann and J. Biener, *J Mater Chem A*, 2014, **2**, 17764-17770.
44. D. S. Yu, K. Goh, H. Wang, L. Wei, W. C. Jiang, Q. Zhang, L. M. Dai and Y. Chen, *Nat Nanotechnol*, 2014, **9**, 555-562.
45. S. Bae, H. Kim, Y. Lee, X. F. Xu, J. S. Park, Y. Zheng, J. Balakrishnan, T. Lei, H. R. Kim, Y. I. Song, Y. J. Kim, K. S. Kim, B. Ozyilmaz, J. H. Ahn, B. H. Hong and S. Iijima, *Nat Nanotechnol*, 2010, **5**, 574-578.
46. L. G. De Arco, Y. Zhang, C. W. Schlenker, K. Ryu, M. E. Thompson and C. W. Zhou, *Acs Nano*, 2010, **4**, 2865-2873.
47. C. L. Hsu, C. T. Lin, J. H. Huang, C. W. Chu, K. H. Wei and L. J. Li, *Acs Nano*, 2012, **6**, 5031-5039.
48. J. Liang, H. Bi, D. Y. Wan and F. Q. Huang, *Adv Funct Mater*, 2012, **22**, 1267-1271.
49. H. Park, S. Chang, J. Jean, J. J. Cheng, P. T. Araujo, M. S. Wang, M. G. Bawendi, M. S. Dresselhaus, V. Bulovic, J. Kong and S. Gradecak, *Nano Lett*, 2013, **13**, 233-239.
50. D. Zhang, F. X. Xie, P. Lin and W. C. H. Choy, *Acs Nano*, 2013, **7**, 1740-1747.
51. L. Kavan, J. H. Yum and M. Gratzel, *Acs Nano*, 2011, **5**, 165-172.
52. L. Kavan, J. H. Yum, M. K. Nazeeruddin and M. Gratzel, *Acs Nano*, 2011, **5**, 9171-9178.
53. X. Yan, X. Cui, B. S. Li and L. S. Li, *Nano Lett*, 2010, **10**, 1869-1873.
54. V. Gupta, N. Chaudhary, R. Srivastava, G. D. Sharma, R. Bhardwaj and S. Chand, *Journal of the American Chemical Society*, 2011, **133**, 9960-9963.
55. J. T. Wang, J. M. Ball, E. M. Barea, A. Abate, J. A. Alexander-Webber, J. Huang, M. Saliba, I. Mora-Sero, J. Bisquert, H. J. Snaith and R. J. Nicholas, *Nano Lett*, 2014, **14**, 724-730.
56. W. J. Hyun, O. O. Park and B. D. Chin, *Advanced Materials*, 2013, **25**, 4729-4734.
57. F. Withers, O. Del Pozo-Zamudio, A. Mishchenko, A. P. Rooney, A. Gholinia, K. Watanabe, T. Taniguchi, S. J. Haigh, A. K. Geim, A. I. Tartakovskii and K. S. Novoselov, *Nat Mater*, 2015, **14**, 301-3010.
58. X. J. Huang, T. Leng, X. Zhang, J. C. Chen, K. H. Chang, A. K. Geim, K. S. Novoselov and Z. R. Hu, *Appl Phys Lett*, 2015, **106**, 203105.
59. M. T. Ong and E. J. Reed, *Acs Nano*, 2012, **6**, 1387-1394.
60. A. A. Balandin, S. Ghosh, W. Z. Bao, I. Calizo, D. Teweldebrhan, F. Miao and C. N. Lau, *Nano Lett*, 2008, **8**, 902-907.
61. S. Ghosh, I. Calizo, D. Teweldebrhan, E. P. Pokatilov, D. L. Nika, A. A. Balandin, W. Bao, F. Miao and C. N. Lau, *Appl Phys Lett*, 2008, **92**, 151911.
62. L. Liao, J. W. Bai, R. Cheng, Y. C. Lin, S. Jiang, Y. Q. Qu, Y. Huang and X. F. Duan, *Nano Lett*, 2010, **10**, 3952-39510.
63. L. Liao, Y. C. Lin, M. Q. Bao, R. Cheng, J. W. Bai, Y. A. Liu, Y. Q. Qu, K. L. Wang, Y. Huang and X. F. Duan, *Nature*, 2010, **467**, 305-308.
64. S. J. Han, K. A. Jenkins, A. V. Garcia, A. D. Franklin, A. A. Bol and W. Haensch, *Nano Lett*, 2011, **11**, 3690-3693.
65. A. Mishchenko, J. S. Tu, Y. Cao, R. V. Gorbachev, J. R. Wallbank, M. T. Greenaway, V. E. Morozov, S. V. Morozov, M. J. Zhu, S. L. Wong, F. Withers, C. R. Woods, Y. J. Kim, K. Watanabe, T. Taniguchi, E. E. Vdovin, O. Makarovsky, T. M. Fromhold, V. I. Fal'ko, A. K. Geim, L. Eaves and K. S. Novoselov, *Nat Nanotechnol*, 2014, **9**, 808-813.

66. R. S. Dey and C. R. Raj, *J Phys Chem C*, 2010, **114**, 21427-21433.
67. X. H. Kang, J. Wang, H. Wu, J. Liu, I. A. Aksay and Y. H. Lin, *Talanta*, 2010, **81**, 754-759.
68. H. F. Xu, H. Dai and G. N. Chen, *Talanta*, 2010, **81**, 334-338.
69. H. S. Yin, Y. L. Zhou, Q. A. Ma, S. Y. Ai, Q. P. Chen and L. S. Zhu, *Talanta*, 2010, **82**, 1193-1199.
70. G. H. Zeng, Y. B. Xing, J. A. Gao, Z. Q. Wang and X. Zhang, *Langmuir*, 2010, **26**, 15022-150210.
71. F. Schedin, A. K. Geim, S. V. Morozov, E. W. Hill, P. Blake, M. I. Katsnelson and K. S. Novoselov, *Nat Mater*, 2007, **6**, 652-655.
72. T. O. Wehling, K. S. Novoselov, S. V. Morozov, E. E. Vdovin, M. I. Katsnelson, A. K. Geim and A. I. Lichtenstein, *Nano Lett*, 2008, **8**, 173-177.
73. G. H. Lu, L. E. Ocola and J. H. Chen, *Nanotechnology*, 2009, **20**, 445502.
74. S. Mao, G. H. Lu, K. H. Yu, Z. Bo and J. H. Chen, *Advanced Materials*, 2010, **22**, 3521–35210.
75. T. Zhang, Z. G. Cheng, Y. B. Wang, Z. J. Li, C. X. Wang, Y. B. Li and Y. Fang, *Nano Lett*, 2010, **10**, 4738-4741.
76. Y. X. Huang, X. C. Dong, Y. X. Liu, L. J. Li and P. Chen, *J Mater Chem*, 2011, **21**, 12358-12362.
77. H. G. Sudibya, Q. Y. He, H. Zhang and P. Chen, *Acs Nano*, 2011, **5**, 1990-1994.
78. Y. X. Xu, L. Zhao, H. Bai, W. J. Hong, C. Li and G. Q. Shi, *Journal of the American Chemical Society*, 2009, **131**, 13490-13497.
79. Y. J. Song, K. G. Qu, C. Zhao, J. S. Ren and X. G. Qu, *Advanced Materials*, 2010, **22**, 2206-2210
80. Z. W. Tang, H. Wu, J. R. Cort, G. W. Buchko, Y. Y. Zhang, Y. Y. Shao, I. A. Aksay, J. Liu and Y. H. Lin, *Small*, 2010, **6**, 1205-1209.
81. H. Tian, Y. Shu, X. F. Wang, M. A. Mohammad, Z. Bie, Q. Y. Xie, C. Li, W. T. Mi, Y. Yang and T. L. Ren, *Sci Rep-Uk*, 2015, **5**, 8603.
82. Z. Tehrani, G. Burwell, M. A. M. Azmi, A. Castaing, R. Rickman, J. Almarashi, P. Dunstan, A. M. Beigi, S. H. Doak and O. J. Guy, *2d Mater*, 2014, **1**, 025004.
83. T. Yamada, M. Ishihara and M. Hasegawa, *Thin Solid Films*, 2013, **532**, 89-93.
84. S. S. Chen, L. Brown, M. Levendorf, W. W. Cai, S. Y. Ju, J. Edgeworth, X. S. Li, C. W. Magnuson, A. Velamakanni, R. D. Piner, J. Y. Kang, J. Park and R. S. Ruoff, *Acs Nano*, 2011, **5**, 1321-1327.
85. L. Nilsson, M. Andersen, R. Balog, E. Laegsgaard, P. Hofmann, F. Besenbacher, B. Hammer, I. Stensgaard and L. Hornekaer, *Acs Nano*, 2012, **6**, 10258-102610.
86. D. Prasai, J. C. Tuberquia, R. R. Harl, G. K. Jennings and K. I. Bolotin, *Acs Nano*, 2012, **6**, 1102-1108.
87. F. He, S. Lau, H. L. Chan and J. T. Fan, *Advanced Materials*, 2009, **21**, 710-715.
88. C. C. Teng, C. C. M. Ma, C. H. Lu, S. Y. Yang, S. H. Lee, M. C. Hsiao, M. Y. Yen, K. C. Chiou and T. M. Lee, *Carbon*, 2011, **49**, 5107-51110.
89. S. Vadukumpully, C. Basheer, C. S. Jeng and S. Valiyaveettil, *J Chromatogr A*, 2011, **1218**, 3581-3587.
90. J. U. Lee, D. Yoon and H. Cheong, *Nano Lett*, 2012, **12**, 4444-4448.
91. R. J. Young, I. A. Kinloch, L. Gong and K. S. Novoselov, *Composites Science And Technology,*, 2012, **72**, 1459.

92. M. El Gemayel, S. Haar, F. Liscio, A. Schlierf, G. Melinte, S. Milita, O. Ersen, A. Ciesielski, V. Palermo and P. Samori, *Advanced Materials*, 2014, **26**, 4814–4819
93. I. Vlassiouk, G. Polizos, R. Cooper, I. Ivanov, J. K. Keum, F. Paulauskas, P. Datskos and S. Smirnov, *Acs Appl Mater Inter*, 2015, **7**, 10702-10709.
94. H. Porwal, P. Tatarko, S. Grasso, C. Hu, A. R. Boccaccini, I. Dlouh and M. J. Reece, *Sci. Technol. Adv. Mater.*, 2013, **14**, 55007.
95. A. Sedaghat, M. K. Ram, A. Zayed, R. Kamal and N. Shanahan, *Open Journal of Composite Materials*, 2013, **4**, 12-21.
96. E. Lepore, F. Bonaccorso, M. Bruna, F. Bosia, S. Taioli, G. Garberoglio, A. C. Ferrari and N. M. Pugno, *Condensed Materials*, 2015, **in press**.
97. K. Chen, Q. H. Shu and M. Schmittel, *Chem Soc Rev*, 2015, **44**, 136-160.
98. R. Muszynski, B. Seger and P. V. Kamat, *J Phys Chem C*, 2008, **112**, 5263-52610.
99. J. D. Qiu, G. C. Wang, R. P. Liang, X. H. Xia and H. W. Yu, *J Phys Chem C*, 2011, **115**, 15639-15645.
100. H. W. Tien, Y. L. Huang, S. Y. Yang, J. Y. Wang and C. C. M. Ma, *Carbon*, 2011, **49**, 1550-1560.
101. Y. Y. Liang, H. L. Wang, H. S. Casalongue, Z. Chen and H. J. Dai, *Nano Res*, 2010, **3**, 701-705.
102. Y. M. He, W. J. Chen, X. D. Li, Z. X. Zhang, J. C. Fu, C. H. Zhao and E. Q. Xie, *Acs Nano*, 2013, **7**, 174-182.
103. J. Lin, Z. W. Peng, C. S. Xiang, G. D. Ruan, Z. Yan, D. Natelson and J. M. Tour, *Acs Nano*, 2013, **7**, 6001-60010.
104. L. L. Peng, X. Peng, B. R. Liu, C. Z. Wu, Y. Xie and G. H. Yu, *Nano Lett*, 2013, **13**, 2151-2157.
105. J. Lin, A. R. O. Raji, K. W. Nan, Z. W. Peng, Z. Yan, E. L. G. Samuel, D. Natelson and J. M. Tour, *Adv Funct Mater*, 2014, **24**, 2044-2048.
106. A. Ambrosi, C. K. Chua, A. Bonanni and M. Pumera, *Chem Rev*, 2014, **114**, 7150-7188.
107. K. S. Novoselov, V. I. Fal'ko, L. Colombo, P. R. Gellert, M. G. Schwab and K. Kim, *Nature*, 2012, **490**, 192-200.
108. Z. Z. Sun, Z. Yan, J. Yao, E. Beitler, Y. Zhu and J. M. Tour, *Nature*, 2010, **468**, 549-552.
109. J. K. Wassei, M. Mecklenburg, J. A. Torres, J. D. Fowler, B. C. Regan, R. B. Kaner and B. H. Weiller, *Small*, 2012, **8**, 1415-1422.
110. W. J. Yu, Y. Liu, H. L. Zhou, A. X. Yin, Z. Li, Y. Huang and X. F. Duan, *Nat Nanotechnol*, 2013, **8**, 952-958.
111. C. Berger, Z. M. Song, T. B. Li, X. B. Li, A. Y. Ogbazghi, R. Feng, Z. T. Dai, A. N. Marchenkov, E. H. Conrad, P. N. First and W. A. de Heer, *J Phys Chem B*, 2004, **108**, 19912-199110.
112. C. Berger, Z. M. Song, X. B. Li, X. S. Wu, N. Brown, C. Naud, D. Mayou, T. B. Li, J. Hass, A. N. Marchenkov, E. H. Conrad, P. N. First and W. A. de Heer, *Science*, 2006, **312**, 1191-11910.
113. W. A. de Heer, C. Berger, X. S. Wu, P. N. First, E. H. Conrad, X. B. Li, T. B. Li, M. Sprinkle, J. Hass, M. L. Sadowski, M. Potemski and G. Martinez, *Solid State Commun*, 2007, **143**, 92-100.

114. D. G. Matei, N. E. Weber, S. Kurasch, S. Wundrack, M. Woszczyna, M. Grothe, T. Weimann, F. Ahlers, R. Stosch, U. Kaiser and A. Turchanin, *Advanced Materials*, 2013, **25**, 4146-4151.
115. K. Parvez, S. B. Yang, Y. Hernandez, A. Winter, A. Turchanin, X. L. Feng and K. Mullen, *Acs Nano*, 2012, **6**, 9541-9550.
116. J. M. Cai, P. Ruffieux, R. Jaafar, M. Bieri, T. Braun, S. Blankenburg, M. Muoth, A. P. Seitsonen, M. Saleh, X. L. Feng, K. Mullen and R. Fasel, *Nature*, 2010, **466**, 470-473.
117. A. K. Geim, *Science*, 2009, **324**, 1530-1534.
118. Y. Hernandez, V. Nicolosi, M. Lotya, F. M. Blighe, Z. Y. Sun, S. De, I. T. McGovern, B. Holland, M. Byrne, Y. K. Gun'ko, J. J. Boland, P. Niraj, G. Duesberg, S. Krishnamurthy, R. Goodhue, J. Hutchison, V. Scardaci, A. C. Ferrari and J. N. Coleman, *Nat Nanotechnol*, 2008, **3**, 563-568.
119. V. Leon, A. M. Rodriguez, P. Prieto, M. Prato and E. Vazquez, *Acs Nano*, 2014, **8**, 563-571.
120. K. R. Paton, E. Varrla, C. Backes, R. J. Smith, U. Khan, A. O'Neill, C. Boland, M. Lotya, O. M. Istrate, P. King, T. Higgins, S. Barwich, P. May, P. Puczkarski, I. Ahmed, M. Moebius, H. Pettersson, E. Long, J. Coelho, S. E. O'Brien, E. K. McGuire, B. M. Sanchez, G. S. Duesberg, N. McEvoy, T. J. Pennycook, C. Downing, A. Crossley, V. Nicolosi and J. N. Coleman, *Nat Mater*, 2014, **13**, 624-630.
121. E. Treossi, M. Melucci, A. Liscio, M. Gazzano, P. Samori and V. Palermo, *Journal of the American Chemical Society*, 2009, **131**, 15576-15577.
122. J. N. Coleman, M. Lotya, A. O'Neill, S. D. Bergin, P. J. King, U. Khan, K. Young, A. Gaucher, S. De, R. J. Smith, I. V. Shvets, S. K. Arora, G. Stanton, H. Y. Kim, K. Lee, G. T. Kim, G. S. Duesberg, T. Hallam, J. J. Boland, J. J. Wang, J. F. Donegan, J. C. Grunlan, G. Moriarty, A. Shmeliov, R. J. Nicholls, J. M. Perkins, E. M. Grieveson, K. Theuwissen, D. W. McComb, P. D. Nellist and V. Nicolosi, *Science*, 2011, **331**, 568-571.
123. V. Nicolosi, M. Chhowalla, M. G. Kanatzidis, M. S. Strano and J. N. Coleman, *Science*, 2013, **340**, 1420-1424.
124. C. Bosch-Navarro, E. Coronado, C. Marti-Gastaldo, J. F. Sanchez-Royo and M. G. Gomez, *Nanoscale*, 2012, **4**, 3977-3982.
125. N. Liu, F. Luo, H. X. Wu, Y. H. Liu, C. Zhang and J. Chen, *Adv Funct Mater*, 2008, **18**, 1518-1525.
126. K. Parvez, Z. S. Wu, R. J. Li, X. J. Liu, R. Graf, X. L. Feng and K. Mullen, *Journal of the American Chemical Society*, 2014, **136**, 6083-6091.
127. A. M. Abdelkader, A. J. Cooper, R. A. W. Dryfe and I. A. Kinloch, *Nanoscale*, 2015, **7**, 6944-69510.
128. W. J. Zhao, P. H. Tan, J. Liu and A. C. Ferrari, *Journal of the American Chemical Society*, 2011, **133**, 5941-59410.
129. E. H. L. Falcao, R. G. Blair, J. J. Mack, L. M. Viculis, C. W. Kwon, M. Bendikov, R. B. Kaner, B. S. Dunn and F. Wudl, *Carbon*, 2007, **45**, 1367-1369.
130. W. T. Gu, W. Zhang, X. M. Li, H. W. Zhu, J. Q. Wei, Z. Li, Q. K. Shu, C. Wang, K. L. Wang, W. C. Shen, F. Y. Kang and D. H. Wu, *J Mater Chem*, 2009, **19**, 3367-3369.
131. W. C. Ren and H. M. Cheng, *Nat Nanotechnol*, 2014, **9**, 726-730.

Chapter 3 Liquid-Phase Exfoliation of Graphite

3.1 Background

In the last decade graphene has emerged as an exciting new material, with potential to impact many areas of science and technology. It can be produced using *top-down* or *bottom-up* approaches.[1] There is no such a thing as the best method to produce graphene; the method has to be chosen in view of the application that is targeted. Different types of production provide graphene with different lateral size, number of defects, etc., thereby varying its properties. Several approaches to prepare dispersed graphene flakes in a liquid phase have been reported including oxidation-reduction of graphene oxide, surfactant free liquid-phase exfoliation (LPE) using organic solvents, surfactant assisted LPE, ball milling and electrochemical exfoliation followed by dispersion in organic solvents.[2] Out of all these techniques, ultrasound assisted LPE of graphite adopted in this thesis is a good method, which results in graphene dispersions for applications in conductive inks, opto-electronics, composites, coatings and paints.[3]

3.2 Liquid-phase exfoliation of graphite

The LPE process typically involves three steps: 1) dispersion of graphite in a solvent, 2) exfoliation, and 3) purification. Graphene can be produced *via* chemical wet dispersion

followed by ultrasonication, in aqueous and non-aqueous solvents. Exfoliation through sonication is controlled by hydrodynamic shear-forces, associated with cavitation (this process is detailed in Chapter 4). After the exfoliation, the solvent-graphene interactions compensate the loss in inter-sheet attractive forces. Solvents dispersing graphene need to minimize the interfacial tension [mN m^{-1}] between the liquid and graphene flakes. If the interfacial tension is high, the flakes tend to adhere to each other and the cohesion between them is high, hindering their dispersion in liquid. In this way, liquids with surface tension $\gamma \sim 40$ mN m^{-1} are the best solvents for the dispersion of graphene, since they minimize the interfacial tension between solvent and graphene.

3.2.1 Organic solvents

After efficaciously dispersing carbon nanotubes by sonication, Coleman's group reported the fabrication of graphene by the ultrasound assisted liquid-phase exfoliation of graphite.[4] In their work, graphite powder was dispersed in specific organic solvents, such as N,N-dimethylformamide (DMF, $\gamma \sim 37.1$ mN m^{-1}), benzyl benzoate ($\gamma \sim 45.95$ mN m^{-1}), gamma-butyrolactone (GBL, $\gamma \sim 45.95$ mN m^{-1}), 1,3-Dimethyl-2-Imidazolidinone (DMEU, $\gamma \sim 42.5$ mN m^{-1}) and N-methylpyrrolidone (NMP, $\gamma \sim 40$ mN m^{-1}) to name only a few, followed by sonication and centrifugation. Concentrations up to ~ 0.01 mg mL^{-1} were prepared showing a high quality of unoxidized monolayer graphene at yields of 1 wt %. Also the process could potentially be improved to give yields of up to 12 wt % of the starting graphite mass with sediment recycling. The number fraction of monolayer graphene can be estimated as 28% (Figure 3.1d). They started to increase graphene concentration and tried to keep at the same time the graphene quality. In this aim, sonication time and centrifugation speed were boosted for LPE in NMP in order to increase the concentration up to >1 mg mL^{-1}.[5]

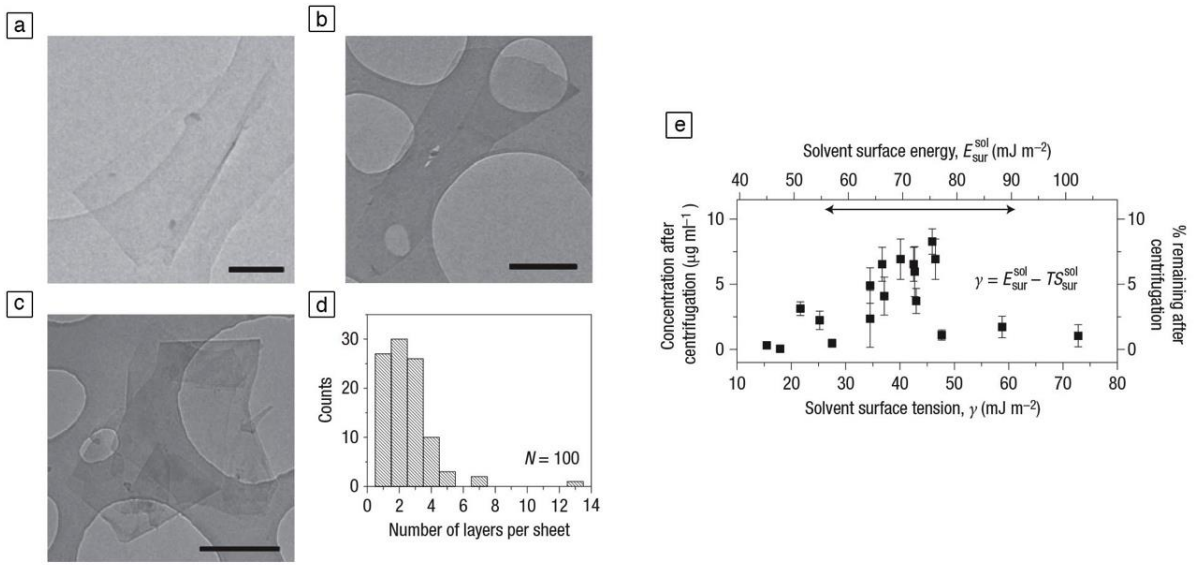

Figure 3.1. Bright-field TEM images of monolayer graphene flakes deposited from the following solvents: a) GBL, b) DMEU and c) NMP. d) Histogram of the number of visual observations of flakes as a function of the number of monolayers per flake for NMP dispersions and e) Graphite concentration measured after centrifugation for a range of solvents plotted versus solvent surface tension.[4]

Graphite powder was suspended by applying 1 hour of sonication in a series of perfluorinated aromatic solvents to afford moderately dark-gray colloidal dispersions (Figure 3.2).[6] To demonstrate the existence of a colloid in these dispersions, the Tyndall effect is often used. It consists of light scattering by particles in suspensions or a colloid. Depending on the solvent, the concentrations of the dispersions after settling were varied between 0.05 and 0.1 mg mL^{-1}. Pentafluorobenzonitrile provided the highest colloidal concentration (0.1 mg mL^{-1}) with octafluorotoluene and pentafluoropyridine equally exhibiting the poorest function (0.05 mg mL^{-1}). Hexafluorobenzene displayed an intermediate efficacy within this series, for example, 0.07 – 0.08 mg mL^{-1}.

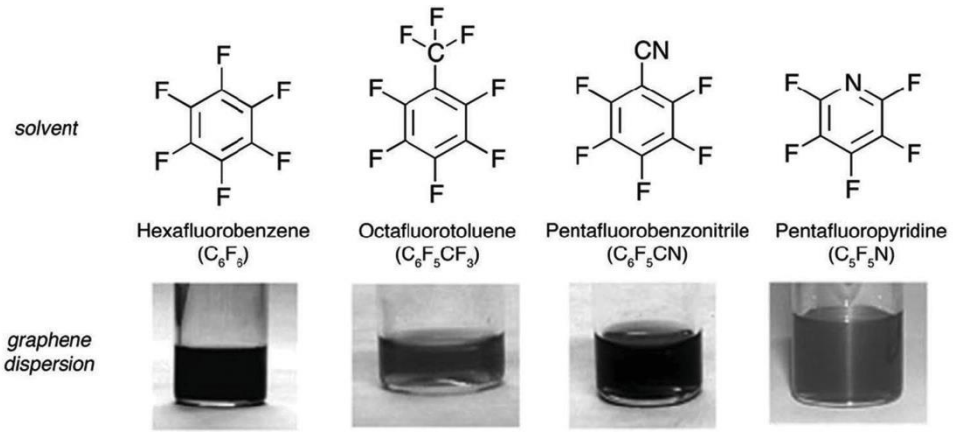

Figure 3.2. Colloidal dispersions obtained after liquid-phase exfoliation of graphite using perfluorinated aromatic solvents[3]

Recently Schuhmann and co-workers showed the graphite exfoliation yielding few-layer graphene (FLG) using number of new solvents.[7] They show that graphene can be exfoliated and dispersed at higher concentrations in four dispersing agents, namely 3,30-iminobis-(N,N-dimethylpropylamine) (DMPA), N-[3-(dimethylamino)propyl] methacryl-amide (DMAPMA), 2-(tert-butylamino)ethyl methacrylate (BAEMA) and 2-(dimethylamino)-ethyl methacrylate (MAEMA) than in any previously used solvents or surfactants. Starting with pre-exfoliated graphite in isopropanol obtained after 12 h of bath ultrasonication greatly promoted the exfoliation reaching a graphene concentration of up to ~ 1.4 mg mL^{-1} which can be further enhanced to 3.5 mg mL^{-1} in a yield of ~ 41% upon redispersing the graphite sediments by means of 15 min of mild ultrasonication.

3.2.2 Ionic liquids

Noteworthy, in 2011 Mariani and co-workers demonstrated that graphene could be obtained by sonication of graphite powder in ionic liquid, namely 1-hexyl-3-methyl-imidazolium hexafluorophosphate (HMIH).[8] Unfortunately, while the graphene concentration was estimated as being as high as 83 mg mL^{-1}, the AFM analysis showed the presence of 2 nm thick graphite-like flakes, highlighting a low exfoliation yield. Novel ionic liquids were

designed and synthesized to contain aromatic groups on the imidazolium cation that non-covalently interact with graphene surfaces.[9] Table 2.2. shows the different ionic liquids tested. IL-1 and IL-4 did successfully disperse graphene, and notably, IL-4 yielded an unusually high graphene concentration of 5.8 mg mL^{-1}. These results indicate a much stronger interaction of graphene with IL-4 than with IL-1.

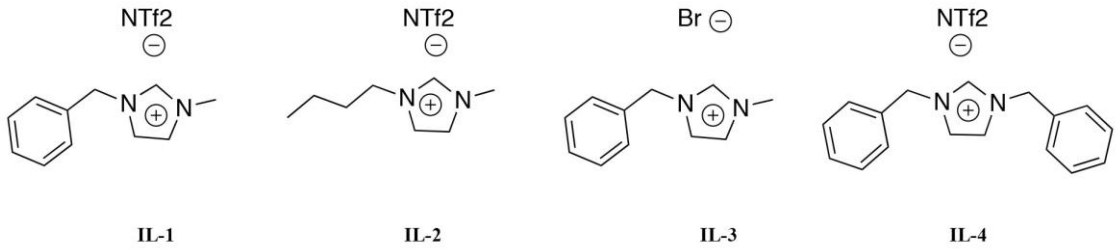

Table 2.2 List of ionic liquids tested for dispersion of graphene.[9]

3.2.3 Aqueous dispersions

Exfoliation of graphite towards graphene in water is very challenging, as graphene sheets exhibit hydrophobic properties. Nevertheless, in 2014 Ricardo and co-workers report an ultrasound exfoliation of graphite in a weakly basic solution to produce multi-layer graphene dispersion.[10] A unique feature of this process is that no surfactant was added to stabilize the exfoliated graphene in water. The concentration of the graphene dispersion prepared by this approach can be up to 0.02 mg mL^{-1} and dispersions were stable at room temperature for several months. But the surface tension of water ($\gamma \sim 72.8$ mN m^{-1}) is unsuitable considering the above-mentioned optimized surface tension. This limits the direct exfoliation and dispersion processes, and thus additional materials are required, such as molecules.

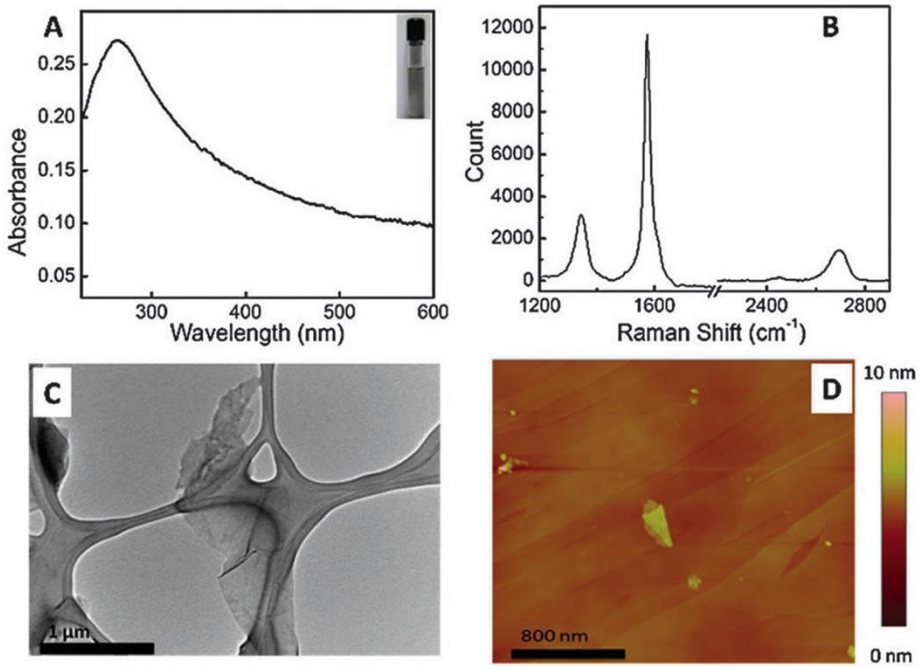

Figure 3.3. a) UV-Vis spectrum of exfoliated graphene in a NaOH solution (pH = 11). Inset: photographic image of the exfoliated graphene, b) Raman spectrum of exfoliated graphene, c) TEM micrograph of a graphene flake and d) AFM image of a graphene flake on an HOPG substrate.[10]

3.3 Surfactants assisted exfoliation

The use of small molecules can promote the exfoliation of graphite into graphene. The high adsorption energy on graphene surface of these molecules has to be higher than the one of solvents. The procedure of molecules assisted LPE is similar to the surfactant-free LPE and include the same three steps. New solvents in addition to well-chosen molecules might boost the exfoliation in terms of graphene flakes concentration, quality and size. Different types of molecules can be chosen, including ionic and non-ionic molecules with different stabilization mechanisms. Ionic molecules can provide both electrostatic and steric repulsion, between graphene flakes covered by molecules, and prevent them from aggregation. In the case of non-ionic molecules, the presence of nonelectrical steric barrier between the graphene flakes covered by molecules stabilizes the graphene flakes in the solution.

3.3.1 Aqueous dispersions

Water is a preferable choice because of its non-toxicity which opens perspective for the formation of biocompatible graphene based materials for biomedical applications. Exfoliation and dispersion of graphene in water is challenging because of its unsuitable surface tension and the hydrophobic nature of the sheets. The use of molecules appears to be the only way to satisfy the conditions for exfoliation.

3.3.1.1 Pyrenes

Various groups have used pyrene derivatives to stabilize carbon nanotube and graphene dispersions. Adsorption of these compounds onto the graphene surface occurs through π–π interactions between the planar π-conjugated surfaces, by reducing the surface free energy of the dispersion. In these interactions both aromatic planar surfaces share the electrons of π-orbitals through a non-covalent bond.

He and co-workers reported the exfoliation of graphite into graphene by sonication in an aqueous solution of two pyrene molecules that had been functionalized with different water-soluble groups, i.e. 1-pyrenemethylamine hydrochloride (Py-NH2) and 1,3,6,8-pyrene-tetrasulfonic acid (Py-SO3).[11] The sizes of the graphene flakes are in the micrometer range and the thickness of a single-layer graphene-Py-NH2 ranges from 0.7 to 1.1 nm with an average of 0.9 ± 0.3 nm.

By using a similar approach to those using pyrene derivatives, Palermo and co-workers went one step further into the thermodynamics of liquid-phase exfoliation of graphite.[12] They studied four pyrene derivatives with varying number of polar functionalization for their efficiency as exfoliation agents in the preparation of stable, aqueous graphene suspensions with liquid phase exfoliation. They found that the four studied derivatives exfoliate graphite, yielding stable suspensions in water. Figure 3.4a is clearly showing the effect of pH on the exfoliation yield. The total concentration of suspended graphene depends significantly on the polar functionalization present on the pyrene core (Figure 3.4b). The exfoliation efficiency is highest at neutral pH and decreases in strongly basic or acidic conditions (Figure 3.4c). Also

the adsorption of the molecules from solution to bulk graphite is simply inversely proportional to the number of polar sulfonic groups present.

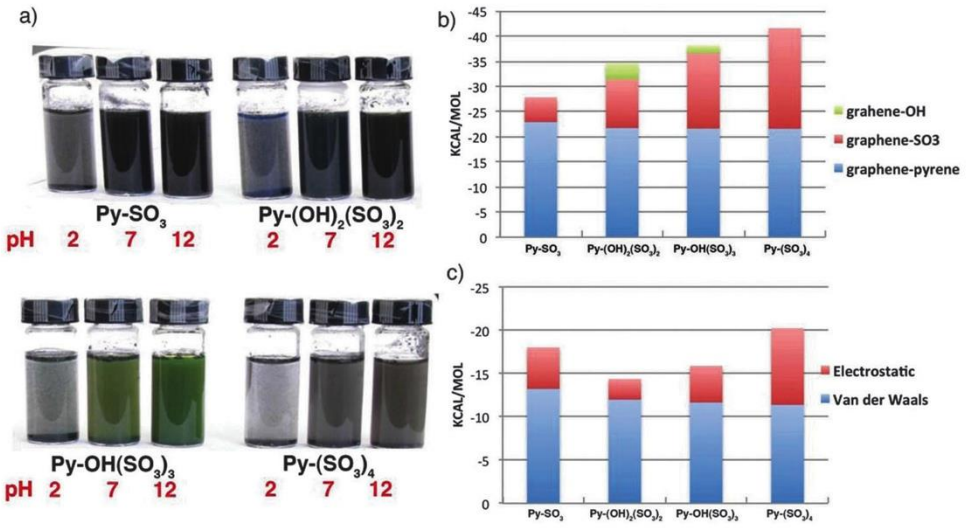

Figure 3.4. a) Image of the solutions obtained on sonicating graphite with the different pyrenes at pH = 2, 7 and 10, b) contribution of the different components of pyrenes to the interaction energy of the molecules with graphene, c) electrostatic and van der Waals contributions of the pyrene core of adsorbed molecules with the surrounding aqueous medium.[3]

3.3.1.2 Other surface stabilizers

Several alternative surfactants, also called surface stabilizers, have been used to promote the exfoliation of graphite in aqueous solutions, including 7,7,8,8-tetracyanoquinodimethane (TCNQ),[13] coronene tetra- carboxylic acids (CTCA),[14] perylene-based bolaamphiphiles,[15] or pyrene-based hydrophilic dendrones,[16] to name a few.

In particular, it has been demonstrated that stable dispersions of graphene can be prepared in sodium cholate/water systems.[17] Concentrations up to 0.3 mg mL^{-1} were found through this low-cost and scalable process. The dispersed concentration increases sublinearly with sonication time, while high-quality dispersions are obtained for centrifugation rates between 500 and 2000 rpm.

More recently, Jiang et al reported the use of urea, a cheap and environmentally friendly reagent, as a stabilizer for highly efficient aqueous exfoliation of natural graphite to prepare high-quality graphene sheets.[18] Exfoliated graphene with concentration of up to 0.15 mg mL^{-1}

is achieved in water with the presence of urea, which outperforms the exfoliation in DMF under similar conditions.

Also Khademhosseini and co-workers propose a facile, green, and inexpensive approach for preparing stable aqueous graphene dispersions, which involves the exfoliation and fragmentation of graphite into graphene through sonication in bovine serum albumin (BSA) aqueous solution, as shown in Figure 3.5a.[19] Figure 3.5b is showing that the final exfoliation yield of graphene is depending of the starting amount of BSA molecules added for exfoliation. TEM images showed that most graphene sheets had a maximum lateral dimension from tens of nm to a few μm, as shown in Figure 3.5c. In addition, the AFM images of the graphene sheets revealed that they had a thickness of 10.7 ± 4.6 nm, suggesting the presence of single-layered to few-layered graphene flakes in the aqueous dispersion (See Figure 3.5e).

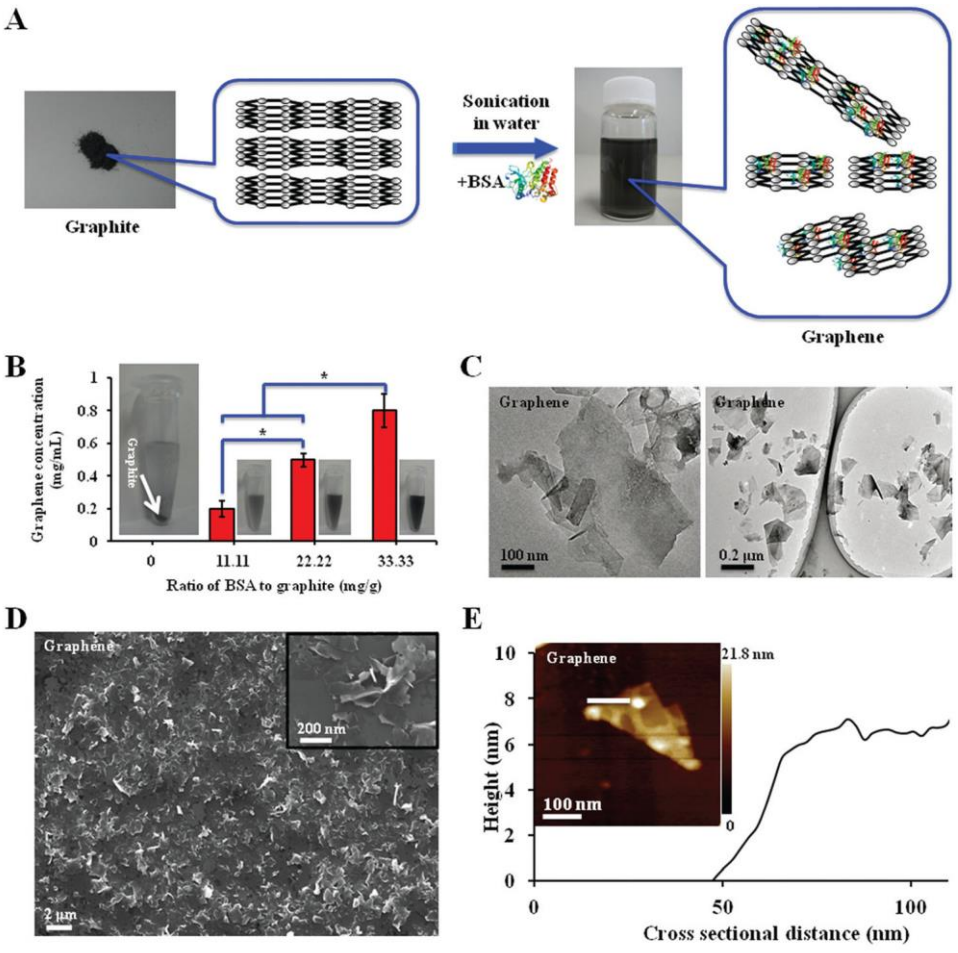

Figure 3.5. a) Pictures and schematic representation of the fabrication of aqueous graphene dispersion from graphite, b) different concentrations of graphene dispersion as a function of BSA concentration in the medium (*p < 0.05) and representative pictures are shown to the right of the corresponding bars, c) TEM images of graphene, d) SEM images of graphene and e) AFM image and corresponding height profile of graphene.[19]

Carbon quantum dots (CQDs) were used as stabilizers and exfoliation agents to exfoliate graphite to graphene in an aqueous medium (Figure 3.6.).[21] The functions of CQDs are to reduce the surface tension of water to match that of graphite and to make weak interactions with the graphite surface. The concentration of exfoliated graphene was found 0.4 mg mL^{-1} based on measuring the membrane mass difference before filtration of exfoliated graphene at a constant volume.

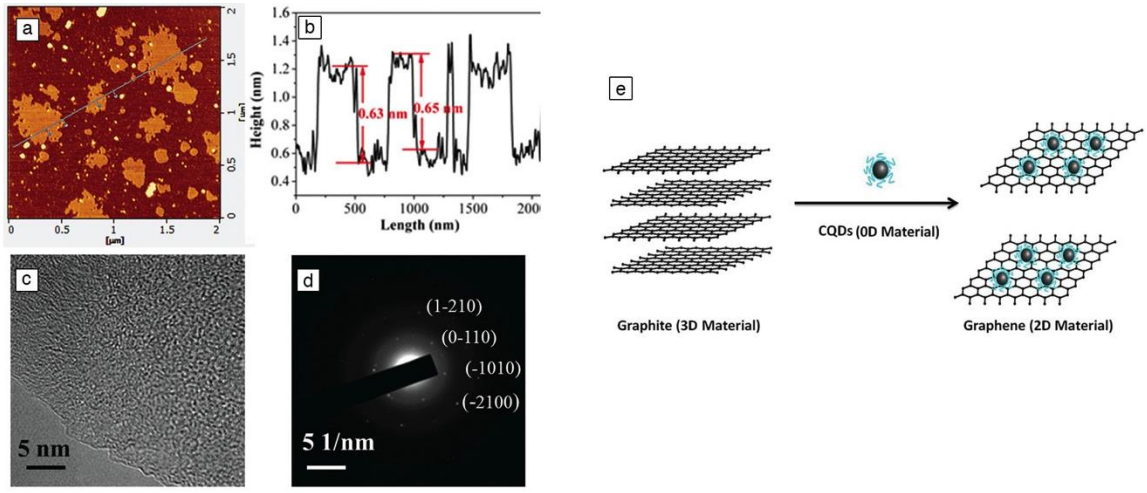

Figure 3.6. a) AFM image and b) the corresponding height profiles of the exfoliated graphenes, c) TEM image and d) the corresponding SAED pattern of the exfoliated graphene, e) Schematic of the transformation of exfoliating graphite (3D material) with the aid of CQDs (0D material) into graphene (2D material).[21]

3.3.2 Organic dispersions

The use of water as an exfoliation medium is not recommended for the exploitation of graphene in electronic devices such as field-effect transistors (FETs) because the presence of

residual water molecules at the interface with dielectrics can improve the charge-trapping phenomena. Therefore, the use of organic solvents as exfoliating media has to be explored. Despite the increasing interest in the field, the knowledge gathered about the molecules-assisted LPE of graphite in organic solvents is still relatively poor.

Graphene flakes directly exfoliated from graphite using sonication and cetyltrimethylammonium bromide (CTAB) as a stabilizer have been demonstrated by Valiyaveettil and co-workers.[22] Mild ultrasonication of HOPG, in presence of a cationic surfactant CTAB and acetic acid yielded graphene nanoflakes, which formed a stable colloidal suspension in organic solvent such as DMF. The yield of this approach was found to be ~ 10%.

Another method for preparing graphene has been developed by making use of three porphyrin derivatives and tetrabutylammonium hydroxide (TBA) for exfoliation of graphite in NMP, as shown in Figure 3.7.[23] As shown in Figure 3.7b, only porphyrin-**3** exfoliate graphite. The π–π interactions between graphene and porphyrin-**3** were identified by using UV-visible spectroscopy (Figure 3.7c). The graphene sheets prepared by this method have undisturbed sp^2 carbon networks. Graphene prepared in NMP with the aid of the porphyrin-3 and TBA, has a concentration of ~ 0.05 mg mL^{-1}.

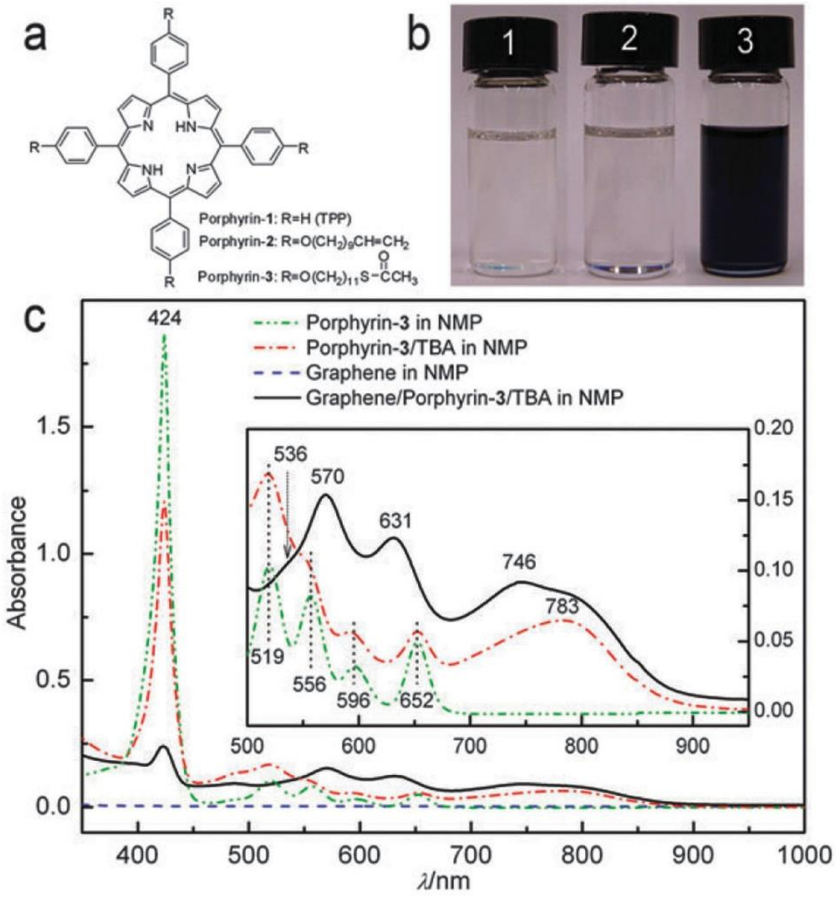

Figure 3.7. a) Porphyrin structures used for preparing graphene, b) optical images of (1) solvent NMP, (2) a graphene dispersion in NMP, (3) a graphene dispersion in a porphyrin-3/TBA solution in NMP and c) UV-visible spectra of graphene dispersions.[23]

Jo and co-workers demonstrate the formation of a stable dispersion of pristine graphene in ethanol by exfoliating graphite flakes into individual graphene layers using a non-ionic polymer surfactant under sonication.[24] Oligothiophene-terminated poly(ethylene glycol) (5TN-PEG) was synthesized and used as a non-ionic and amphiphilic surfactant for exfoliating graphite into graphene (see Figure 3.8a). Figure 3.8b is showing that ethanol is a better solvent in this case than tetrahydrofuran (THF). A high-quality graphene film was fabricated from the exfoliated graphene solution by the vacuum filtration method. In Figure 3.8d, TEM and SEM reveal that the size of exfoliated graphene flakes is larger than 1 μm.

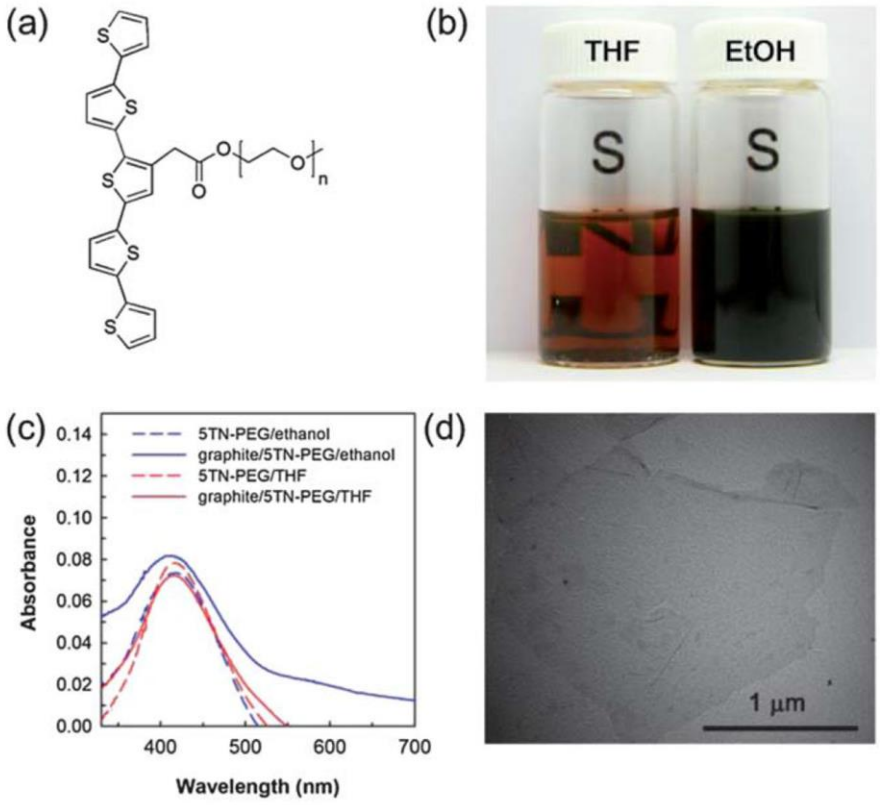

Figure 3.8. a) Chemical structure of 5TN-PEG, b) comparison of graphite–5TN-PEG in THF and ethanol, c) UV-vis absorption spectra of 5TN-PEG–ethanol (dashed blue) and graphite–5TN-PEG–ethanol (solid blue), 5TN-PEG–THF (dashed red), and graphite–5TN-PEG–THF (solid red) and d) TEM image of exfoliated graphene.[24]

3.4 Characterization methods

Typically, for graphene prepared by LPE process, the first parameter to analyze is the exfoliation yield, which can be defined as:

- the yield by weight, Y_W [%]
- the yield by single layer of graphene (SLG) percentage, Y_M [%]
- the yield by SLG weight, Y_{WM} [%]

The yield by weight, Y_W [%], is the ratio between the weight of dispersed graphitic material and that of the starting graphite flakes.[4] Y_W is calculated through the concentration *c* in [g L^{-1}]

of dispersed graphitic material. This concentration can be determined via UV-Vis absorption spectroscopy, exploiting the Beer-Lambert Law: $A=\alpha cl$.[25] Another method is to filtrate 1 mL of dispersions on μ-porous filter.

Y_M is the ratio between the number of SLG and the total number of graphitic flakes present in the dispersions.[4] In this case TEM and AFM are needed. AFM can be used to determine layer numbers of graphene flakes.[26, 27] It is based on measuring the thickness of the flakes by comparison with a substrate of known thickness. Although it can be very precise and reliable, AFM is a low throughput technique for counting layers, and any surface roughness of the substrate can be misleading. Then, one of the most unambiguous methods to determine the number of layers in graphitic flakes is TEM, in particular through the analysis of electron diffraction patterns and by counted both by analyzing the edges of the flakes.[28] Also Raman spectroscopy is providing information about the determination of exfoliation yield and to confirm the results obtained with TEM and/or AFM.[29]

Y_{WM} is defined as the ratio between the total mass of dispersed SLG and the total mass of all dispersed flakes.[4] This yield determination is difficult and is time consuming, as recycling of sediment and HR-TEM are needed.

Techniques such as Fourier transform infrared spectroscopy (*FTIR*) and X-ray photoelectron spectroscopy (*XPS*) can also be used to study the quality of graphene, with XPS providing the composition of graphene samples. Thermal gravimetric analysis (*TGA*) is typically used to determine the content of defects or amount of functional groups of the graphene samples.

3.5 Non-covalent interactions with graphene

3.5.1 Background

Alfred Werner introduced the principles of supramolecular chemistry in 1893 with the idea of coordination chemistry and by Emil Fisher in 1894 with the lock and key concept. However, the concept of supramolecular chemistry was introduced in 1979 by Jean-Marie Lehn as: "*the*

chemistry of molecular assemblies and of the intermolecular bond".[30] Supramolecular chemistry[31, 32] is a highly interdisciplinary field of science covering the chemical, physical and biological features of the chemical species. The latter are held together and organized by means of intermolecular (non-covalent) interactions. Supramolecular species are characterized both by spatial arrangement of their components, to attain tunable architectures or superstructures, and by the nature of the intermolecular bonds that hold together these components. Such structures possess well-defined structural, conformational, thermodynamic, kinetic and dynamical properties. Supramolecular chemistry relies on the use of non-covalent interactions such as: metal ion coordination, electrostatic forces, hydrogen bonding,[33] van der Waals interactions (Figure 3.9.).[34] In terms of energy, the van der Waals interactions are the lowest (ca. 0,5-2 kcal mol^{-1}), and H-bonding are middle interactions (ca. 1-40 kcal mol^{-1}), electrostatic interactions may be strong (ca. 50 kcal mol^{-1}) and coordination bond are the strangest (ca. 40-70 kcal mol^{-1})[35] (See Figure 3.9. bottom).

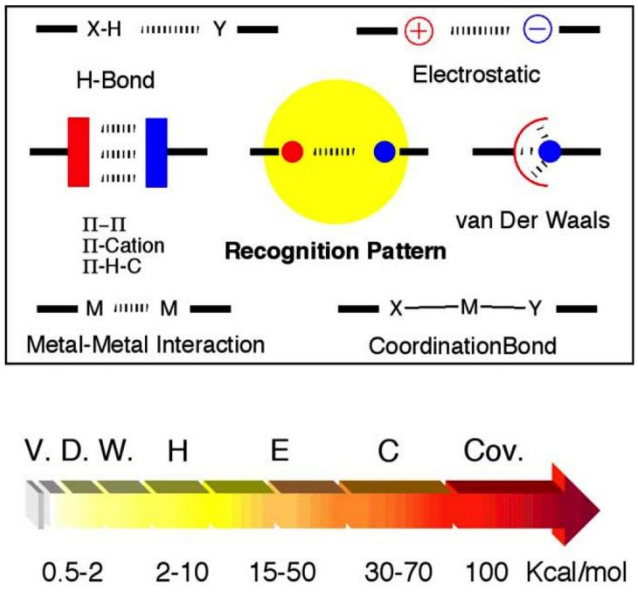

Figure 3.9. Schematic representation of toolbox of reversible intermolecular interactions (top) and their energy (bottom).[35]

3.5.2 Molecule-graphene interactions

3.5.2.1 Π-interactions

Aromatic compounds with extended π-systems such as pyrene, perylene, graphene quantum dots or porphyrins are the most suitable candidates to interact with the graphene surface by π-stacking. Also known as aromatic stacking, π-stacking is a noncovalent attractive force between two aromatic rings.[36] The electrons of the aromatic rings are localized on both sides of the ring, so that there is a small partial negative charge on the face, and a small partial positive charge on hydrogens on the edge, which gives the possibility of electrostatic interactions. Basically, pairs of phenyl ring centroids that are separated by a favored distance of between 4.5 Å to 7 Å allow justifying the denomination of aromatic-aromatic interactions as shown in Figure 3.10a. Side chain aromatic rings tend to stack with edge to face at an angle of 60-90° in about 2 out of 3 interactions (Figure 3.10b); when they stack face to face, the rings are offset so that the partial charges may interact. The binding energy is of the order of 1-2 kcal mol^{-1}.[36] Graphene can be considered as a large and indefinite aromatic system. In this way, a large number of molecules have the potential to interact through these π-π interactions during the liquid-phase exfoliation of graphite into graphene.

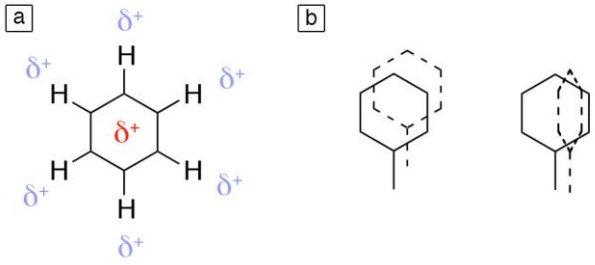

Figure 3.10. Schematic representation a) delocalization of partial charges in benzene and b) face to face and face to edge interactions between two benzenes.

3.5.2.2 Electrostatic interactions

Electrostatic interactions have been exploited to non-covalently bind ionic molecules like polymers, surfactants, metal ions, GDs, or macromolecules devoid of aromatic moieties to graphene sheets. Electrostatic interactions can be described as the electric force between two charged objects.[37] Ionic surfactants were first introduced to assist the exfoliation process and as the first example, Valiyaveettil et al. used a cation surfactant named cetyltrimethylammonium bromide (CTAB).[22] For these ionic surfactants, graphite flakes were first exfoliated by sonication-derived cavitation and shear force, and the exfoliated graphene sheets were then adhered by charged surfactant molecules (See Figure 3.11). It has been recently demonstrated that graphene flakes dispersed in a solvent are charged. This allows researchers to consider the mechanism of stabilization of the surfactant-coated graphene and in particular the Derjaguin and Landau, Verwey and Overbeek (DLVO) theory for stabilization of charged colloids.[38] The theory clarifies the aggregation of aqueous dispersions quantitatively and describes the force between charged surfaces interacting through a liquid environment. It combines the effects of the van der Waals attraction and the electrostatic repulsion due to the so-called double layer of counter ions.

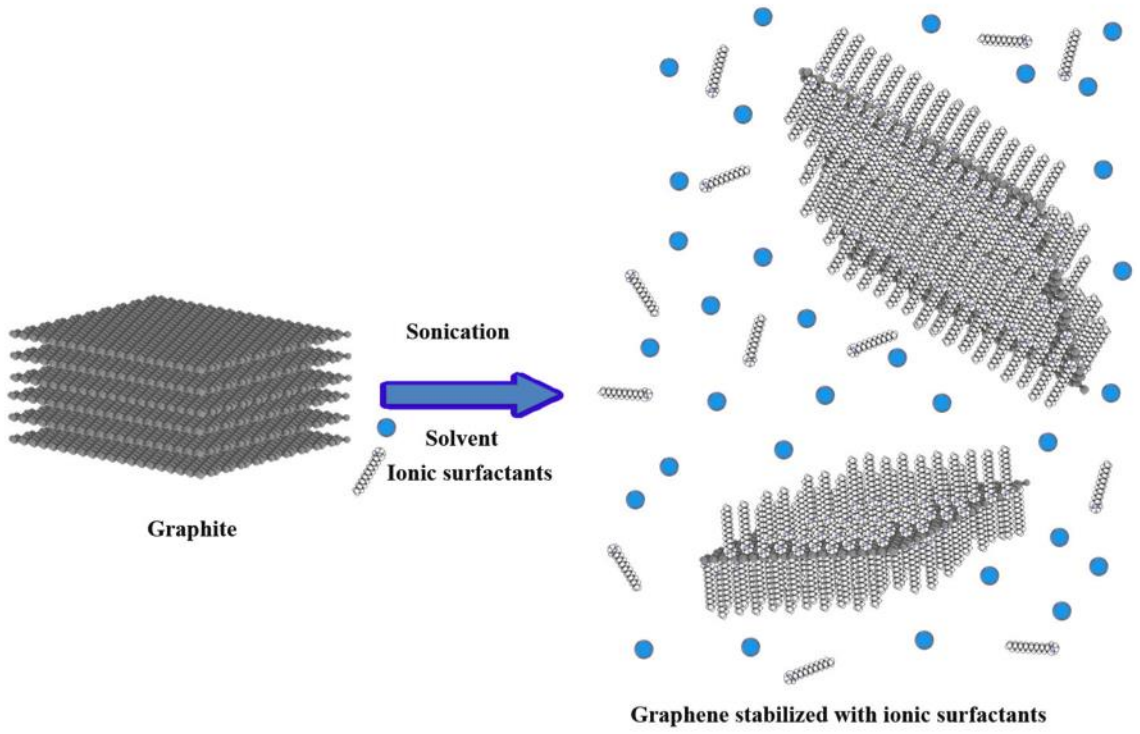

Figure 3.11. Schematic representation of DLVO stabilization process.

3.5.2.3 Van der Waals interactions

For non-ionic surfactants, the graphene sheets adhered by the surfactant molecules were merely charged, and the double layer electrostatic force becomes much lower. When the hydrophobic tails (hydrocarbon chain) of the surfactant molecules from two coated graphene sheets interact, the steric repulsion force plays a more important role. Steric force was used to explain the lack of adhesion or aggregation of uncharged lipids, and it was proved to be dominating over the electrostatic force and Van der Waals force in a short distance.[39] Van der Waals interaction comes from the polarization of an electronic cloud close to a nucleus, resulting in a weak electrostatic attraction. These van der Waals interactions are non-directional and unspecific. They can be divided into the dispersion interactions[39] and the exchange repulsion. The dispersion interaction is an attractive component that results from the interactions between fluctuating multipoles in adjacent molecules. The exchange repulsion defines molecular shape and equilibrates dispersive forces. So the van der Waals interactions

result a general attractive interaction for polarizable species with interaction energy proportional to the surface area of contact. Van der Waals forces come into play at first instance in the adsorption of molecules on atomically flat surfaces. Alkanes have been reported to have a stronger adsorption on HOPG if compared to aromatics having the same number of carbon atoms. For example, the hexane has a desorption barrier of 17 kcal mol^{-1} on HOPG[40] and 13 kcal mol^{-1} on Au(111);[41] conversely the desorption barrier of benzene is 11.5 kcal mol^{-1} on HOPG.[42] When exploiting van der Waals interactions, especially the dispersive forces, stabilization of the 2D self-assembly can be achieved by equipping the molecules of interest with long aliphatic chains. These molecules have the potential to be used as surface-stabilizing agent during the LPE of graphite into graphene.

3.6 Conclusion

In this chapter, a background on the liquid phase exfoliation was presented in addition to a brief explanation of molecular assisted exfoliation of graphene in different solvents. Furthermore, basic principle on supramolecular chemistry were explained, and in particular the different interactions used for graphene stabilization in a liquid medium during exfoliation process.

3.7 References

1. K. S. Novoselov, V. I. Fal'ko, L. Colombo, P. R. Gellert, M. G. Schwab and K. Kim, *Nature*, 2012, **490**, 192-200.
2. M. Yi and Z. G. Shen, *J Mater Chem A*, 2015, **3**, 11700-11715.
3. A. Ciesielski and P. Samori, *Chem Soc Rev*, 2014, **43**, 381-398.
4. Y. Hernandez, V. Nicolosi, M. Lotya, F. M. Blighe, Z. Y. Sun, S. De, I. T. McGovern, B. Holland, M. Byrne, Y. K. Gun'ko, J. J. Boland, P. Niraj, G. Duesberg, S. Krishnamurthy, R. Goodhue, J. Hutchison, V. Scardaci, A. C. Ferrari and J. N. Coleman, *Nat Nanotechnol*, 2008, **3**, 563-568.
5. J. N. Coleman, *Accounts Chem Res*, 2013, **46**, 14-22.
6. A. B. Bourlinos, V. Georgakilas, R. Zboril, T. A. Steriotis and A. K. Stubos, *Small*, 2009, **5**, 1841-1845.
7. Z. Y. Sun, X. Huang, F. Liu, X. N. Yang, C. Rosler, R. A. Fischer, M. Muhler and W. Schuhmann, *Chem Commun*, 2014, **50**, 10382-10385.
8. D. Nuvoli, L. Valentini, V. Alzari, S. Scognamillo, S. B. Bon, M. Piccinini, J. Illescas and A. Mariani, *J Mater Chem*, 2011, **21**, 3428-3431.
9. R. Bari, G. Tamas, F. Irin, A. J. A. Aquino, M. J. Green and E. L. Quitevis, *Colloid Surface A*, 2014, **463**, 63-69.
10. K. B. Ricardo, A. Sendecki and H. T. Liu, *Chem Commun*, 2014, **50**, 2751-2754.
11. M. Zhang, R. R. Parajuli, D. Mastrogiovanni, B. Dai, P. Lo, W. Cheung, R. Brukh, P. L. Chiu, T. Zhou, Z. F. Liu, E. Garfunkel and H. X. He, *Small*, 2010, **6**, 1100-1107.
12. A. Schlierf, H. F. Yang, E. Gebremedhn, E. Treossi, L. Ortolani, L. P. Chen, A. Minoia, V. Morandi, P. Samori, C. Casiraghi, D. Beljonne and V. Palermo, *Nanoscale*, 2013, **5**, 4205-42110.
13. R. Hao, W. Qian, L. H. Zhang and Y. L. Hou, *Chem Commun*, 2008, **48**, 6576-6578.
14. A. Ghosh, K. V. Rao, S. J. George and C. N. R. Rao, *Chem-Eur J*, 2010, **16**, 2700-2704.
15. J. M. Englert, J. Rohrl, C. D. Schmidt, R. Graupner, M. Hundhausen, F. Hauke and A. Hirsch, *Adv Mater*, 2009, **21**, 4265-4269.
16. D. W. Lee, T. Kim and M. Lee, *Chem Commun*, 2011, **47**, 8259-8261.
17. M. Lotya, P. J. King, U. Khan, S. De and J. N. Coleman, *Acs Nano*, 2010, **4**, 3155-3162.
18. P. He, C. Zhou, S. Y. Tian, J. Sun, S. W. Yang, G. Q. Ding, X. M. Xie and M. H. Jiang, *Chem Commun*, 2015, **51**, 4651-4654.
19. S. Ahadian, M. Estili, V. J. Surya, J. Ramon-Azcon, X. B. Liang, H. Shiku, M. Ramalingam, T. Matsue, Y. Sakka, H. Bae, K. Nakajima, Y. Kawazoe and A. Khademhosseini, *Nanoscale*, 2015, **7**, 6436-6443.
20. W. S. Liu, R. Zhou, D. Zhou, G. G. Ding, J. M. Soah, C. Y. Yue and X. H. Lu, *Carbon*, 2015, **83**, 188-197.
21. M. Xu, W. Zhang, Z. Yang, F. Yu, Y. Ma, N. Hu, D. He, Q. Liang, Y. Su and Y. Zhang, *Nanoscale*, 2015, **7**, 10527-10534.
22. S. Vadukumpully, J. Paul and S. Valiyaveettil, *Carbon*, 2009, **47**, 3288-3294.
23. J. Geng, B. S. Kong, S. B. Yang and H. T. Jung, *Chem Commun*, 2010, **46**, 5091-5093.
24. M. S. Kang, K. T. Kim, J. U. Lee and W. H. Jo, *J Mater Chem C*, 2013, **1**, 1870-1875.

25. M. Lotya, Y. Hernandez, P. J. King, R. J. Smith, V. Nicolosi, L. S. Karlsson, F. M. Blighe, S. De, Z. Wang, I. T. McGovern, G. S. Duesberg and J. N. Coleman, *J Am Chem Soc*, 2009, **131**, 3611-3620.
26. C. Valles, C. Drummond, H. Saadaoui, C. A. Furtado, M. He, O. Roubeau, L. Ortolani, M. Monthioux and A. Penicaud, *J Am Chem Soc*, 2008, **130**, 15802-15804.
27. F. Bonaccorso, A. Lombardo, T. Hasan, Z. P. Sun, L. Colombo and A. C. Ferrari, *Mater Today*, 2012, **15**, 564-589.
28. A. C. Ferrari and D. M. Basko, *Nat Nanotechnol*, 2013, **8**, 235-2410.
29. F. Torrisi, T. Hasan, W. P. Wu, Z. P. Sun, A. Lombardo, T. S. Kulmala, G. W. Hsieh, S. J. Jung, F. Bonaccorso, P. J. Paul, D. P. Chu and A. C. Ferrari, *Acs Nano*, 2012, **6**, 2992-30010.
30. J. M. Lehn, *Supramolecular chemistry : concepts and perspectives*, 1995.
31. J. M. Lehn, *Pure Appl Chem*, 1979, **51**, 979-997.
32. T. F. A. de Greef and E. W. Meijer, *Nature*, 2008, **453**, 171-173.
33. A. Ciesielski, G. Schaeffer, A. Petitjean, J. M. Lehn and P. Samori, *Angew Chem Int Edit*, 2009, **48**, 2039-2043.
34. J. D. van der Waals, *Nobel lecture*, 1910.
35. M. W. Hosseini, *Accounts Chem Res*, 2005, **38**, 313-323.
36. S. K. Burley and G. A. Petsko, *Science*, 1985, **229**, 23-28.
37. J. M. MacLeod and F. Rosei, *Small*, 2014, **10**, 1038-1049.
38. M. Lotya, Y. Hernandez, P. J. King, R. J. Smith, V. Nicolosi, L. S. Karlsson, F. M. Blighe, S. De, Z. M. Wang, I. T. McGovern, G. S. Duesberg and J. N. Coleman, *J Am Chem Soc*, 2009, **131**, 3611-3620.
39. J. Israelachvili, *Intermolecular & Surfaces Forces* 1992.
40. A. J. Gellman and K. R. Paserba, *J Phys Chem B*, 2002, **106**, 13231-13241.
41. S. M. Wetterer, D. J. Lavrich, T. Cummings, S. L. Bernasek and G. Scoles, *J Phys Chem B*, 1998, **102**, 9266-9275.
42. R. Zacharia, H. Ulbricht and T. Hertel, *Phys Rev B*, 2004, **69**, 155406

Chapter 4 Experimental Techniques

4.1 Liquid-phase exfoliation process

4.1.1 Introduction

Since the first successful exfoliation of graphite into graphene in an organic solvent such as NMP in 2008, improvements in concentrations of graphene dispersions have been achieved.[1] The two out of many important parameters is the type and time of sonication, which allows the exfoliation of graphite. The uses of ultrasonication have become increasingly important in analytical chemistry since 10 years, in particular for carbon nanotubes, graphene and other 2D materials. To reach a total control of LPE, a fundamental comprehension of the ultrasonication and all involved parameters is mandatory.

4.1.2 Sonication

4.1.2.1 Cavitation

Ultrasounds can be transmitted through any physical environment by waves. These waves can compress and stretch the molecular spacing of the environment through which it crosses. When the negative pressure is powerful enough, the distance between the liquid molecules surpasses the minimum distance required to hold the liquid together, and then the liquid breaks down (See Figure 4.1). Those voids are the called cavitation bubbles.[2-4] The cavitation

bubbles process is dictated from two main ways.[2] First, bubbles formed at relatively low ultrasonic intensities (1 – 3 Wcm^{-2}) oscillate for many cycles: stable cavitation. The second, bubbles are made using sound intensities exceeding of 10 Wcm^{-2}: transient cavitation. Transient bubbles expand through a few acoustic cycles and collapse brutally on compression. The second process is considered to be the main source of the chemical and mechanical effects of ultrasonic energy. Ultrasonication is exceptional, since no other method can produce such effects.[5, 6]

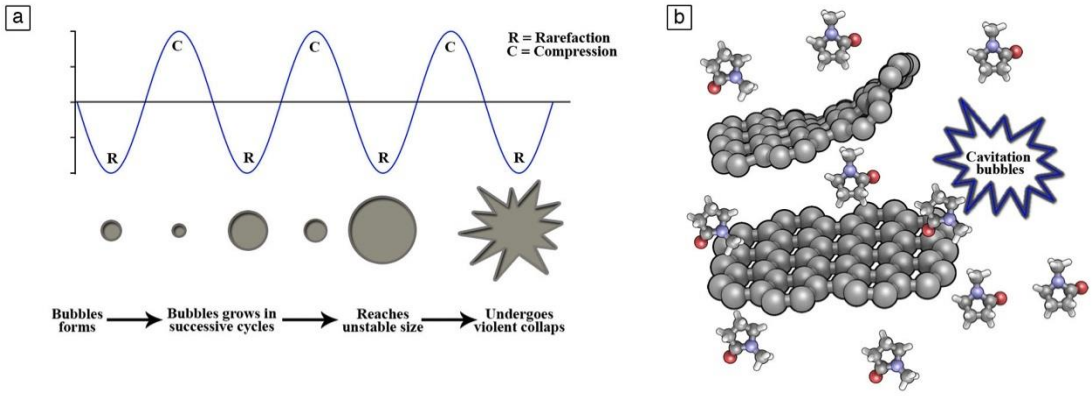

Figure 4.1. Schematic overview of a) transient cavitation mechanism and b) the graphite exfoliation process to form few-layer graphene.

4.1.2.2 Temperature

First, high temperatures improve to cut strong solute–matrix interactions like Van der Waals forces, hydrogen bonding and dipole attractions. Then, cavitation can be easily obtain at lower temperatures.[9] As the temperature of the solvent rises, its vapor pressure does increase also and so more solvent vapor fills the cavitation bubbles. Hence a compromise between temperature and cavitation must be attained. If the temperature is not controlled some undesired effects could occur. The most obvious is the degradation of compounds of interest, but also the volatilization of low volatile can occur.[10] In addition, as the temperature is increased, the physical characteristics of the liquid media change in such a way that the ultrasonic transmission can be affected and no cavitation is achieved. This phenomenon is

known as decoupling.[3, 4] It is not easy to control the temperature when ultrasonication is applied with an ultrasonic probe.

4.1.2.3 Dead zones

After a certain time, the ultrasonic intensity quickly falls both radially and axially from the ultrasonic probe. This is why, the space between the probe and the wall of the bath has to be minimum and constant, as shown in Figure 4.2. Keeping dead zones to a minimum certifies a maximum contact between the sample and the cavitation zones, and also among the sample particles, which helps to diminish their size by collisions.[10] The final result will be an increment in desired effects, such as, for example, a decrease in the solid–liquid exfoliation efficiency.

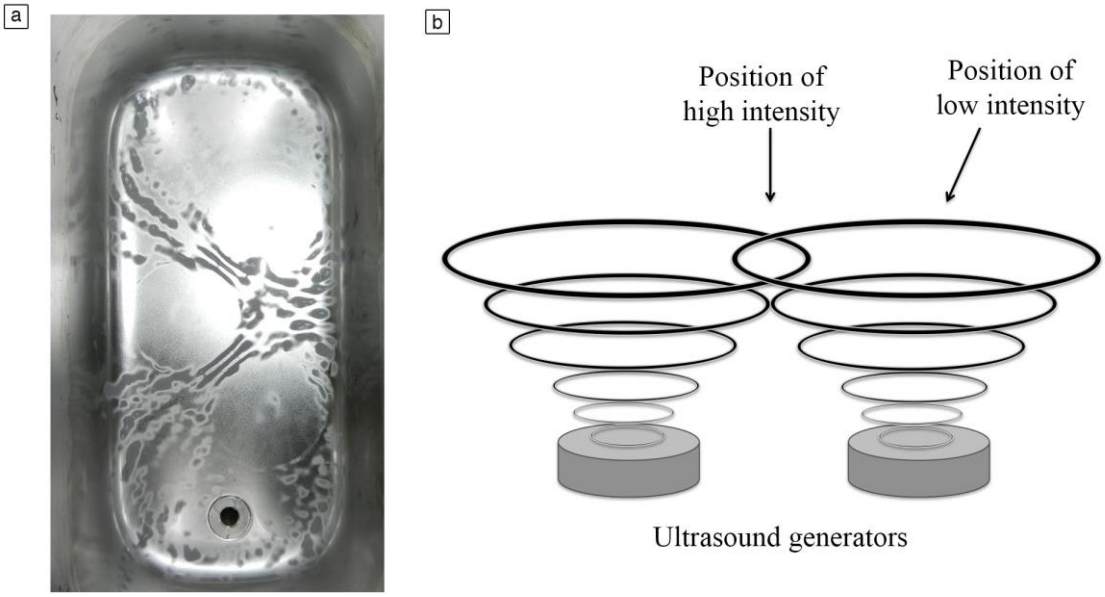

Figure 4.2. a) Photograph of our ultrasonic bath been used for 1 year and b) Schematic overview of two ultrasound generators working in the same time

4.1.2.4 Time

The ultrasonication duration is typically a parameter that is specific to each experiment. In the case of graphene, each group uses its own exfoliation time, i.e. from 20 minutes to several hundreds of hours. High concentration of graphene dispersions can be obtained by using drastically longer sonication times (~ 500 h^{-2} mg mL^{-1}).[11] Such a time consuming approach needs high energy; in addition, as previously observed for nanotubes, with the increasing sonication time, the size of the flakes is severely reduced[12] being a serious parameter for several applications. Very long sonication of graphite can also affect the quality of graphene.

4.1.2.5 Setup

There is no standard model and each facility is different. In the graphene majority of groups focused their research on the Ultrasonic Baths, Bioruptors and the Ultrasonic Probes. In Chapters 5, 6, 7, 8 and 9, ultrasonic baths connected to a thermal controller were preferred to prepare graphene dispersions. And in Chapter 10, an ultrasonic probe was used for exfoliation, because it was necessary to establish a system for which the UV irradiation was possible. Figure 4.3 shows the 3 different set-ups.

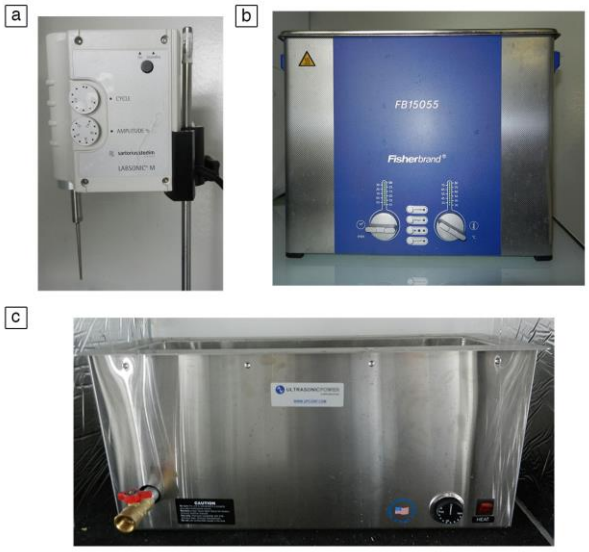

Figure 4.3. Photograph of the different setups used for graphite exfoliation: a) probe sonication, b) constant intensity bath sonication and c) advanced ultrasonic bath with frequency and intensity controller.

4.1.3 Graphite

In order to explore and understand the liquid-phase exfoliation process, the first important parameter that should be well select is the graphite. Graphite is one of two naturally occurring crystalline forms of the sixth element on earth: carbon. Graphite can be found in different sources, i.e. crystalline flake graphite, highly ordered pyrolitic graphite, lump graphite or amorphous graphite. Natural crystalline graphite flakes exist in different forms with flakes of different size and different thickness, pre-treated and having high or low quality. It is a 3D material and has a layer structure in which the atoms are arranged in a hexagonal pattern within each layer and the layers are stacked in the AB sequence, as shown in Figure 1.b. For our work, we explored different graphite sources for exfoliation, in particular crystalline flake of graphite and HOPG. As HOPG didn't give any results in terms of concentration and quality of graphene flakes, we focused our attention on natural crystalline graphite flakes. In order to test different flakes sizes, a milling system was used to separate flakes by size: 5 mm, 3 mm, 1 mm, 0.5 mm (see Figure 4.4). But the best result in terms of concentration, size and quality was found with the mixture of all sizes. Also graphite flakes with a carbon content of 98 % were better than 96 %, 94 % and 93 %.

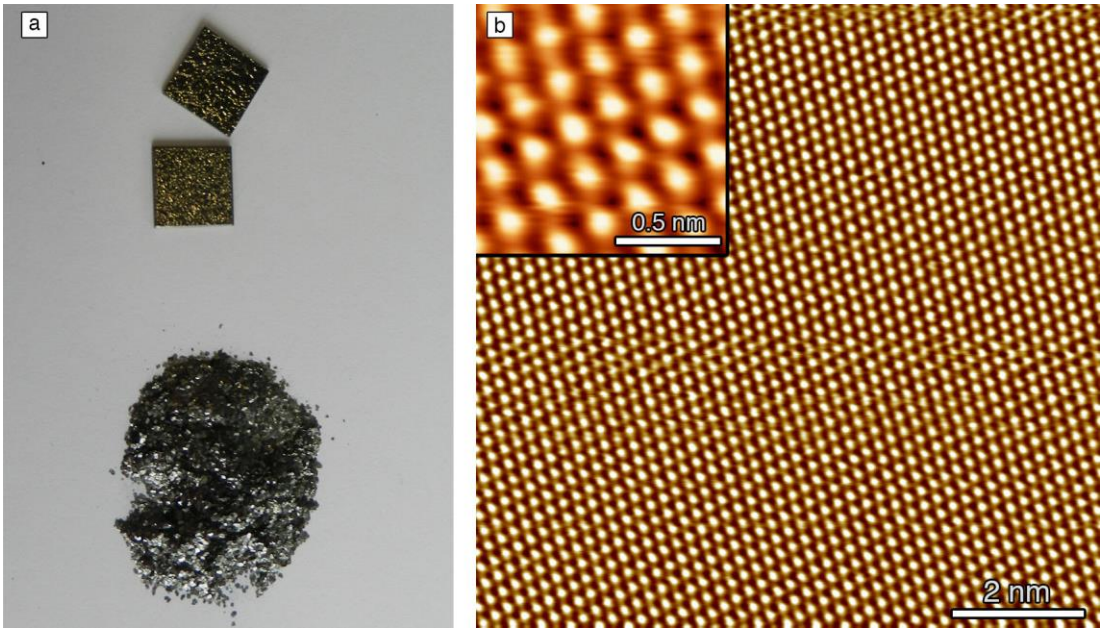

Figure 4.4. a) Photographs of HOPG and graphite flakes and b) STM images of HOPG surface.

4.2 Thin film preparation from LPE graphene

Liquid-phase exfoliation of graphite results in graphene flakes, which are suspended in a solution and can be considered as conductive inks. Many applications require the deposition of graphene on specific substrates, like optoelectronic devices, transparent and/or flexible electrodes or coatings. Several methods have been developed to fabricate graphene thin film from inks based on solution-processed graphene, including spin coating, drop casting, spray coating, inkjet printing, doctor blade, filtration, dip coating and layer-by-layer using Langmuir-Blodgett technique. In fact, these methods have been extended in advanced technique for the graphene area. Among these methods, only the one used during the thesis will be presented.

4.2.1 Drop casting

In the drop casting method, a few µL of dispersion are deposed in the middle of the substrate and depending of the wettability between the substrate and the solvent, the drop can cover the entire surface and sometime heating of the sample is necessary to speed-up the evaporation process. (See Figure 4.5a) This method is very simple and all the materials will remain on the substrate. Typically, the film thickness is proportional to the concentration of the dispersions. However, the film thickness is hard to control and exhibits a poor uniformity.

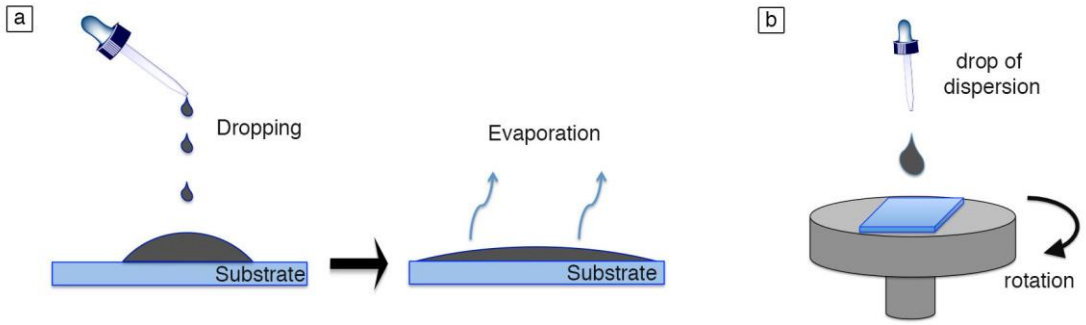

Figure 4.5. Schematic representation of a) drop casting technique and b) spin coating technique.

4.2.2 Spin coating

In a spin coating method, a few drops of dispersions are deposed in the center of a substrate, which is then spun at a specified rotational speed during a certain time. In this case, the dispersion will be spread on the substrate and cover it to form a thin film by centrifugal force, as shown in Figure 4.5b. This method has a good uniformity and reproducibility. The thickness of the films is controlled by the rotation speed and the concentration of graphene dispersion.

4.2.3 Spray coating

In a spray coating method, substrate is hit by a vaporized solution flux of graphene dispersions and droplets merge on the hot substrate into a full wet film before fast drying, as shown in Figure 4.6. This method permits to form adjustable thickness layer and to cover large area, but is independence on substrate topology. The thickness and morphology of the films is controlled by many parameters, like air pressure, solution viscosity, solvent properties, gun tip geometry, distance between nozzle and substrate, *etc*...

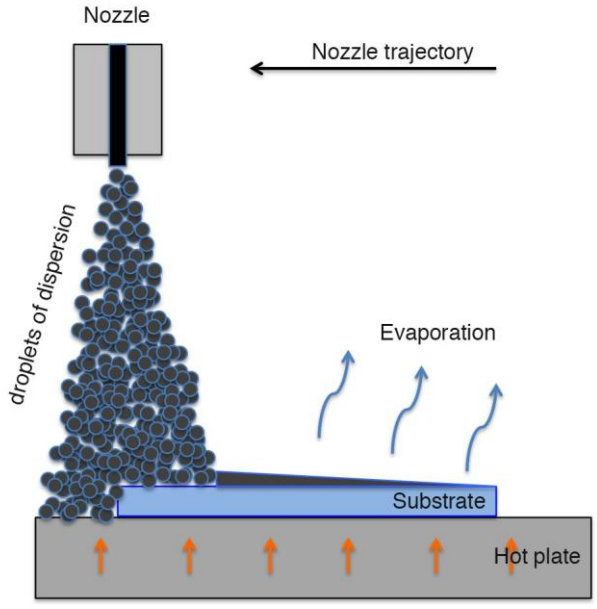

Figure 4.6. Schematic representation of the spray coating technique.

4.3 Experimental characterization techniques

4.3.1 Scanning tunneling microscopy

STM, made it possible to visualize and manipulate single molecules, therefore study a variety of physicochemical properties and processes of nanostructured materials, as shown in Figure4.7. The main working principle of STM is based on the concept of quantum tunneling.[24, 25] STM can operate under various environmental conditions including ultra-high vacuum (UHV), gas stream, air and liquid, thus making it possible to investigate structure and reactivity in 2D with a single molecules resolution.[26] STM at the solid-liquid interface has provided detailed insight into the molecule-substrate and molecule-molecule interactions responsible for the ordering of molecules on the atomically flat surface. In most of the studies performed at the solid-liquid interface the STM tip is immersed in an almost saturated solution in a poorly volatile and apolar solvent (1-phenyloctane, 1,2,5-trichlorobenzene, tetradecane…). In order to obtain good resolution during STM imaging, substrates featuring an atomic flatness over several hundred squared nanometers area are required. A typical conductive substrate used for STM investigations is Highly Oriented Pyrolitic Graphite (HOPG), which is a layered substrate that can be freshly prepared by simple cleaving its surface with an adhesive tape. STM measurements were performed using a Veeco multimode Nanoscope III, at the interface between a highly oriented pyrolitic graphite substrate and a supernatant solution. Scanning tunneling microscopy analyses were carried out at the interface between a highly oriented pyrolitic graphite substrate and a supernatant solution by means of a Veeco multimode Nanoscope III set-up. Solutions of long linear alkane decorated with four different functions were applied to the basal plane of the surface. First the substrates were glued to a magnetic disk and an electric contact was made with silver paint (Aldrich Chemicals). Tips were mechanically cut from a Pt/Ir wire (90/10, diameter 0.25 mm). The raw STM data were processed through the application of background flattening and the drift was corrected using the underlying graphite lattice as a reference. Before starting our measurements, the graphite lattice was visualized by lowering the bias voltage down to 20 mV and raising the current up to 65 pA. This allows confirming the good quality of the tip and the flatness substrate.

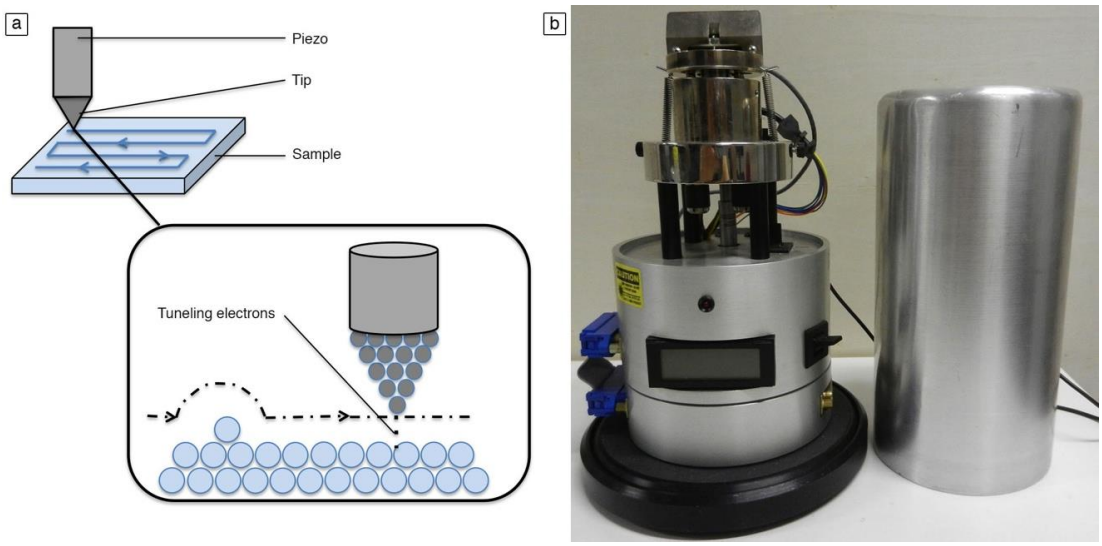

Figure 4.7. a) Schematic overview of STM working principle, b) Photograph of our STM set-up.

4.3.2 Transmission electron microscopy

The transmission electron microscope (TEM) is used to characterize the microstructure of materials with very high spatial resolution. Information about the morphology, crystal structure and defects, crystal phases and composition, and magnetic microstructure can also be obtained by a combination of electron-optical imaging, electron diffraction, and small probe capabilities.[27] The transmission electron microscope uses a high-energy electron beam transmitted through a very thin sample to image and analyze the microstructure of materials with atomic scale resolution. The electrons are accelerated at several hundred kV, giving wavelengths much smaller than that of light (200 kV electrons). Thus, TEMs can reveal the finest details of internal structure, in some cases as small as individual atoms. The thickness, lateral size and the number of layers of graphene flakes were determined by High-Resolution Transmission Electron Microscopy using a JEOL 2100 F microscope, a FEI Tecnai 20 TEM and a Philips CM120 Transmission Electron Microscope operating at 100kV with a LaB6 cathode. Areas of structures of interest are recorded at a magnification of 120x on a Pelletier cooled scan CCD camera.

4.3.3 Scanning electron microscopy

The scanning electron microscope (SEM) is a powerful and frequently used instrument to study surface topography, composition, crystallography and properties on a local scale (see Figure 4.8.). Besides surface topographic studies the SEM can also be used for determining the chemical composition of a material, its fluorescent properties, formation of magnetic domains and so on. SEM was used to characterize graphene and graphene hybrids structures, in particular to analyze the surface coverage of graphene on different treated substrates and the morphology. A normal scanning electron microscope operates at a high vacuum. The basic principle is that a beam of electrons is generated by a suitable source, typically a tungsten filament or a field emission gun.[28] The electron beam is accelerated through a high voltage, e.g. 1 to 30 kV, and passed through a system of apertures and electromagnetic lenses to produce a thin beam of electrons, and then the beam scans the surface of the specimen by means of scan coils. Electrons are emitted from the specimen by the action of the scanning beam and collected by a suitably positioned detector. The SEM can be operated in many different modes where each mode is based on a specific type or signal. The choice of operating mode depends on the properties of the sample and on what features one wants to investigate. We mainly used secondary electrons and backscattered electrons. SEM images were registered using FEI Quanta 250 FEG on different systems deposed on Al or Si substrate.

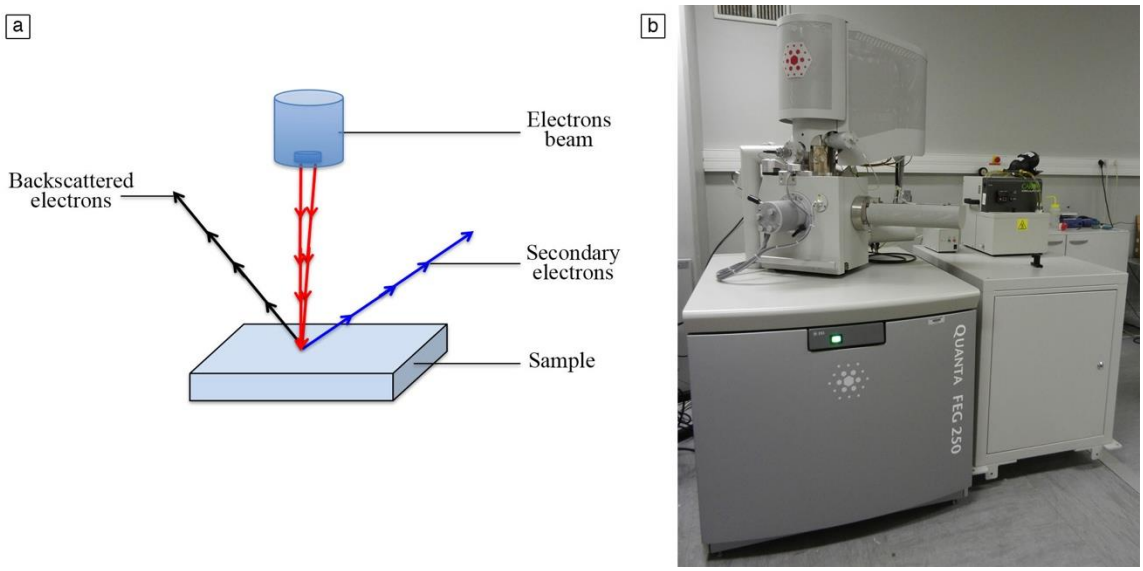

Figure 4.8. a) Schematic overview of SEM working principle, b) Photograph of our SEM set-up

4.3.4 Ultraviolet-visible absorption spectroscopy

Ultraviolet-visible absorption spectroscopy has been extensively used for characterization of materials due to the versatility, simplicity, speed, and inexpensive nature of this technique, in particular for graphene dispersions and graphene thin film characterization. Ultraviolet-visible spectroscopy (UV = 200-400 nm, visible = 400-800 nm) corresponds to electronic excitations between the energy levels that correspond to the molecular orbitals of the systems. In particular, transitions involving π orbitals and lone pairs (n = non-bonding) are important and so UV-Vis spectroscopy is of most use for identifying conjugated systems which tend to have stronger absorptions. Ultraviolet-visible absorption spectra of thin films and solutions were recorded on JASCO V670 and JASCO V650 (in a dark room) spectrophotometers. All dispersions were also transferred on 10 mm path length quartz cuvette and analyzed by UV-vis-IR absorption spectroscopy equipped with a Peltier thermostated cell holder at 20 ± 0.05°C.

4.3.5 X-ray photoelectron spectroscopy

X-ray photoelectron spectroscopy is a technique for analyzing the surface chemistry of a material. (See Figure 4.9) XPS can measure the elemental composition, empirical formula, chemical state and electronic state of the elements within a material. For our study, XPS were used to analyze the presence of molecules, impurities and defects. XPS allows quantification of the amount of oxygen present, and identification and quantification of the C-C and C-O bonding. When an atom or molecule absorbs an X-ray photon, an electron can be ejected. The kinetic energy (KE) of the electron depends upon the photon energy (hν) and the binding energy (BE) of the electron, i.e. the energy required removing the electron from the surface. By measuring the kinetic energy of the emitted electrons, it is possible to determine which elements are near a material's surface, their chemical states and the binding energy of the electron. XPS analyses were carried out on a Thermo Scientific K-Alpha X-ray photoelectron spectrometer with a basic chamber pressure of ~10^{-9} mbar and an Al anode as the X-ray source (X-ray radiation of 1486 eV). Spot sizes of 400 µm were used and pass energies of 200.00 eV for survey scans and 50.00 eV for high-resolution scans were used.

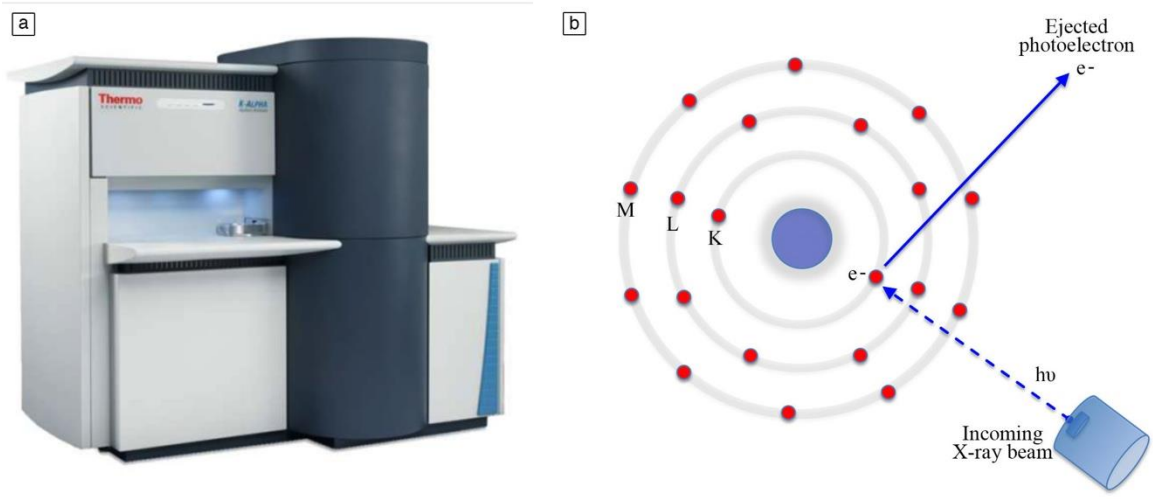

Figure 4.9. a) Photograph of our STM set-up, b) Schematic overview of STM working principle

4.3.6 Thermo gravimetric analysis

Thermogravimetric Analysis measures weight changes in a material as a function of temperature or time under a controlled atmosphere. Its principal uses include measurement of a material's thermal stability and composition. TGA were used to characterize the amount of molecules that are trapped or adsorbed into graphene layers. Also TGA can provide information about physical phenomena: second-order phase transition, including vaporization, sublimation, absorption, adsorption and desorption. Likewise, TGA can provide information about chemical phenomena including chemisorption, desolvation (especially dehydration), decomposition, and solid-gas reactions, e.g., oxidation or reduction. In particular, a TGA/DSC 2 STAR^e System coupled with μ-balance from Mettler Toledo allows measuring our sample deposed in Aluminia crucibles. Also, some thermogravimetric analyses were performed on a Perkin Elmer Pyris 6TGA and samples were heated to 800 °C at 20 °C/min in N2 atmosphere.

4.3.7 Raman Spectroscopy

Raman spectroscopy is a vibrational technique that is extremely sensitive to geometric structure and bonding within molecules. Raman spectroscopy measures the vibrational motions of the molecule and in particular the light scattering.[29] Even small differences in geometric structure lead to significant differences in the observed Raman spectrum of a molecule. This extreme sensibility to geometric structure made it the perfect tool for the study of the different allotropes of carbon, i.e. diamond, graphite, fullerene, nanotubes. In the graphene field, Raman spectroscopy is used to determine the number and orientation of layers, the quality and types of edge, and the effects of perturbations, such as electric and magnetic fields, strain, doping, disorder and functional groups. Raman measurements were carried out with a Renishaw 1000 at 532nm and 632.8nm and a 100X objective, with an incident power of ≈1 mW. Also some micro Raman measurements were carried out with a Renishaw spectrometer in confocal mode and backscattering geometry with excitation energy of 488 nm, 514.5 nm and 633 nm. A 100X objective with a NA of 0.95 was used for the characterization.

4.4 References

1. Y. Hernandez, V. Nicolosi, M. Lotya, F. M. Blighe, Z. Y. Sun, S. De, I. T. McGovern, B. Holland, M. Byrne, Y. K. Gun'ko, J. J. Boland, P. Niraj, G. Duesberg, S. Krishnamurthy, R. Goodhue, J. Hutchison, V. Scardaci, A. C. Ferrari and J. N. Coleman, *Nat Nanotechnol*, 2008, **3**, 563-568.
2. T. J. Mason and J. P. Lorimer, *Sonochemistry: Theory, Application and uses of Ultrasound in Chemistry*, Wiley-Interscience, New-York, 1989.
3. T. J. Mason, *Practical Sonochemistry: User's Guide to Applications in Chemistry and Chemical Engineering*, Ellis Horwood Ltd, New-York, 1992.
4. T. J. Mason, *Sonochemistry, Oxford Chemistry Primers*, Oxford, UK, 2000.
5. G. Wibetoe, D. T. Takuwa, W. Lund and G. Sawula, *Fresen J Anal Chem*, 1999, **363**, 46-54.
6. J. L. Capelo-Martinez, P. Ximenez-Embun, Y. Madrid and C. Camara, *Trac-Trend Anal Chem*, 2004, **23**, 331-340.
7. R. Rial-Otero, E. M. Gaspar, I. Moura and J. L. Capelo, *Talanta*, 2007, **71**, 1906-1914.
8. E. C. Lima, F. Barbosa, F. J. Krug, M. M. Silva and M. G. R. Vale, *J Anal Atom Spectrom*, 2000, **15**, 995-1000.
9. K. S. Suslick, R. E. Cline and D. A. Hammerton, *Journal of American Chemical Society*, 1986, **108**, 5641.
10. J. L. Capelo, M. M. Galesio, G. M. Felisberto, C. Vaz and J. C. Pessoa, *Talanta*, 2005, **66**, 1272-1280.
11. U. Khan, A. O'Neill, M. Lotya, S. De and J. N. Coleman, *Small*, 2010, **6**, 864-871.
12. F. Hennrich, R. Krupke, K. Arnold, J. A. R. Stutz, S. Lebedkin, T. Koch, T. Schimmel and M. M. Kappes, *J Phys Chem B*, 2007, **111**, 1932-1937.
13. G. E. Bacon, *acta crystallographica*, 1951, **4**, 558-561.
14. J. D. Bernal, *Proceedings of the Royal Society*, 1924, **106**, 749-752.
15. X. B. Chen, F. Y. Tian, C. Persson, W. H. Duan and N. X. Chen, *Sci. Rep.*, 2013, **3**, 3646
16. Z. Liu, J. Z. Liu, Y. Cheng, Z. H. Li, L. Wang and Q. S. Zheng, *Phys Rev B*, 2012, **85**, 205418
17. M. C. Schabel and J. L. Martins, *Phys Rev B*, 1992, **46**, 7185-7188.
18. J. N. Israelachvili, *Intermolecular and surface forces.*, revised 3rd edn., Academic press, 2011.
19. H. M. Solomon, B. A. Burgess, G. L. Kennedy and R. E. Staples, *Drug Chem. Toxicol.*, 1995, **18**, 271-293.
20. T. Svedberg and K. O. Pedersen, Oxford, 1940.
21. M. K. Brakke, *Arch. Biochem. Biophys.*, 1953, **45**, 275–290.
22. L. Gong, I. A. Kinloch, R. J. Young, I. Riaz, R. Jalil and K. S. Novoselov, *Adv Mater*, 2010, **22**, 2694-2697.
23. U. Khan, A. O'Neill, H. Porwal, P. May, K. Nawaz and J. N. Coleman, *Carbon*, 2012, **50**, 470-475.
24. G. Binnig, H. Rohrer, C. Gerber and E. Weibel, *Phys. Rev. Lett.* , 1982, **49**, 57.
25. H. Rohrer, *PNAS*, 1987, **84**, 46610.

26. J. Tersoff and D. R. Hamann, *Phys. Rev. B*, 1985, **31**, 805.
27. A. C. Ferrari, J. C. Meyer, V. Scardaci, C. Casiraghi, M. Lazzeri, F. Mauri, S. Piscanec, D. Jiang, K. S. Novoselov, S. Roth and A. K. Geim, *Phys Rev Lett*, 2006, **97**.
28. W. C. Nixon, *Philosophical Transactions of the Royal Society of London, Series B, Biological Sciences*, 1971, **261**, 45.
29. A. C. Ferrari and D. M. Basko, *Nat Nanotechnol*, 2013, **8**, 235-2410.

Chapter 5 Tuning the size of graphene

5.1 Introduction

In the last decade, graphene has emerged as an exciting new material, with potential to impact many areas of science and technology since its first experimental isolation in 2004.[1] However, the zero band gap of graphene strongly limits its direct applications in photonics and opto-electronic. To open and tune this band gap, different tactics, like surface functionalization, or size confinement of graphene into nanoribbon and quantum dots have been developed to tune the band gap.[2] A quantum dot (QD) is a nanometers-sized object, where excitons are confined in all three special dimensions. In extension, graphene fragments that are small enough to cause quantum size effect and excitons confinement are considered as QDs. Typically GQDs are defined as the graphene sheets with dimensions below 100 nm, in single-, double- and few- layers and the shape can be defined, i.e. circular, triangular, hexagonal or even randomly distributed; depending mainly on their fabrication method. GQDs became attractive for a wide range of applications due to their biocompatibility,[3] chemical inertness,[4] low toxicity,[5] ultrafine dimensions [6] and for their luminescence [7, 8]. GQDs can be produced by size reduction processes of graphene sheets (*top-down* approach) [3, 9] or by synthesis of well-defined structures of graphene-like molecules (*bottom-up* approach) [10]. Typical top-down approaches for GQDs productions are based on hydrothermal [11, 12] and solvothermal synthesis [13, 14], electrochemical exfoliation [8, 15] and physical routes like microwaves irradiation [16], nanolithography [17, 18], and other advanced techniques [7, 19]. Bottom-up methods for GQDs fabrications are stepwise organic synthesis, pyrolysis or carbonization of organic precursors [30].

Not all these production methods are economical synthetic routes and lead most of the time to graphene flakes or GQDs with defects. For the fabrication of GQDs using top-down method, it is important to start from defect- and oxide-free graphene flakes that can be obtained by liquid phase exfoliation (LPE) in organic solvents (*top-down* approach) such as N-Methyl-2-pyrrolidone (NMP) that was first demonstrated in 2008 to be a successful solvent [31]. Since then, improvements in concentrations of graphene dispersions have been achieved by varying many factors in the exfoliation process, including the choice of an appropriate solvent or a dramatic increase of the sonication time. For example, concentrations as high as 83 mg mL^{-1} were obtained in ionic liquid [32]. Moreover, the use of new surfactants [33], can boost not only the concentration but also the quality of the graphene flakes. Multiple sonication of such restacked films, gave dispersed concentrations of up to 60 mg mL^{-1} but only 25 mg/ml remained dispersed indefinitely [34]. Increasing the sonication time to more than 400 hours is a way to tune the concentration of graphene flakes in the solvent up to 0.3 mg mL^{-1}. Such a time consuming approach requires high energy and results in a reduction of the sheet size, introduction of defects at the edges and sometimes on the basal plane; therefore affecting the quality of graphene being a critical parameter for several applications [35-37]. Recently, GQDs has been produced via one step wet chemical reaction through acid treatment of carbon fibers [48]. Alternatively, it was demonstrated that GQDs could be synthesized by LPE using graphite nanoparticles (GNPs) with a diameter of 4-6 nm [11]. Also graphite intercalation compounds approach was used to synthetized GQDs [39]. However the challenge remains the development of novel strategies to produce GQDs with a controlled and a low oxidation degree in large quantities for industrial applications. Different sources of starting material have been tried, like GNPs, carbon fibers or coal but they are all exhibiting a high oxidation degree [11, 38, 40]

5.2 Scope

Therefore, here we present the synthesis of GQDs starting from LPE of graphite powder. We investigate the influence of the power and the temperature of the ultrasonic bath on the exfoliation process carried out in different solvents. Particularly, we demonstrate how by

optimizing these parameters, GQDs can be obtained using this simple technique without involving any chemical reaction.

5.3 Experimental

5.3.1 Materials

Graphite powder (product 332461, batch number 08722AH), *ortho*-dichlorobenzene (o-DCB) (product number 240664), 1,2,4-trichlorobenzene (TCB) (product number 256412) and N-methyl-2-pyrrolidone (NMP) (product number 332461) have been purchased from Sigma Aldrich and used as received.

5.3.2 Preparation of graphene

Graphene dispersions were prepared by adding 1 wt% of graphite powder in 10 mL of o-DCB, TCB and NMP followed by 6 hours of ultrasonication at two different temperatures, i.e. 20°C and 50°C, and two different sonication powers, i.e. 600 W and 1000 W. A Hygea Ultrasonic Meter from Ultrawave was used to verify the power levels and uniformity. In order to have a uniform exfoliation for all dispersions, a mechanical stirring of all the samples was utilized (30 rpm). Sonication of graphite powder led to grey liquid consisting of a homogeneous phase and large numbers of macroscopic aggregates. As previously reported, these aggregates can be removed by centrifugation (Eppendorf 5804, rotor F-34-6-38, 30 min at 5000 rpm followed by 15 min at 8000 rpm and 15 min at 10000 rpm), yielding homogeneous dispersions

5.3.3 Characterizations

To quantify the concentration after centrifugation, a mixture of graphene dispersion and chloroform ($CHCl_3$) was first heated up to 50 °C for 30 min and then passed through polytetrafluoroethylene (PTFE) membrane filters (pore size 100 nm). The remaining solvent molecules were washed away several times with diethyl ether and $CHCl_3$. Careful measurements of the filtered mass were performed on a microbalance (Sartorius MSA2.75) to give the concentration of graphene. In the case of the dispersions prepared at 20 °C in chlorinated solvents, while all the material is passing through the 100 nm pore size, the dispersions were placed in an oven (100°C) under vacuum for 3 days to evaporate all the solvent. 5 µl of graphene dispersion were deposed on a 10 nm thick carbon film coated on a 400 Cu mesh grid. After 1 min of adsorption, the drop of material is drained away and replaced by another 5µl drop of dispersion. After reproducing 3 times the same procedure, TEM grids were dried under vacuum.

Fluorescence spectroscopy was performed on a Spex Fluorolog spectrofluorimeter (JY Horiba). Emission spectra were excited at wavelengths as indicated in Figure 5 using a slit size of 2 nm (emission was collected through 5 nm slits). The corrected emission signal was divided by the intensity of the lamp at the respective irradiation wavelength, as to compensate for the different output efficiencies at different wavelengths of the Xenon arc lamp.

5.4 Results and discussion

5.4.1 Liquid-phase exfoliation

In order to fully control the LPE of graphene, we tested two important parameters: temperature of exfoliation (at 20 and 50°C) and ultrasound power (600 and 1000 Watt) by keeping the exfoliation time at 6 hours for all experiences. For this study, we selected three solvents: NMP, orthodichlorobenzene (o-DCB) and Trichlorobenzene (TCB). The concentration of the graphene dispersions was measured by filtration (See Methods). Figure 1a shows the variation of the concentration of graphene obtained after the exfoliation process

carried out at 20°C and at 50°C in three different organic solvents using two different sonication powers. First, the exfoliation was performed at two different temperatures, i.e. 20°C and 50°C at a constant power of 600 W. In order to keep the temperature constant, an automatic thermal cooler was used via a cooling coil in a closed circuit. For graphene dispersions prepared in NMP, no significant change in terms of concentration were observed, i.e. 80 $\mu g.mL^{-1}$ at 20°C and 78 $\mu g.mL^{-1}$ at 50°C. Similarly, there was no change in the concentration of graphene if exfoliated in TCB at these temperature. The obtained values were 65 $\mu g.mL^{-1}$ at 20°C and 60 $\mu g.mL^{-1}$ at 50°C. As for dispersions in o-DCB, the concentration was slightly decreasing with the temperature, from 100 to 80 $\mu g.mL^{-1}$.

By increasing the power to 1000 W, two different types of colored dispersions were observed i.e. dark black and yellow in the case of chlorinated solvents, i.e. o-DCB and TCB depending on the temperature used. Figure 5.1b shows pictures of the supernatant taken after centrifugation of the solutions in o-DCB at 1000 W at 50°C (left side image) and at 20°C (right side image). At 20°C the dispersions in chlorinated solvents were yellowish and exhibited a very poor concentration of 20 $\mu g.mL^{-1}$ for TCB and 25 $\mu g.mL^{-1}$ for o-DCB. These values are much lower than the ones obtained for the same solvents at 20°C at 600 W. If the temperature is increased to 50°C, higher concentrations, up to 98 $\mu g.mL^{-1}$ for o-DCB and 63 $\mu g.mL^{-1}$ for TCB were obtained at 1000 W and were comparable to the ones obtained at the same temperature using 600 W. However, for the case of NMP, dark dispersions of a concentration of around 80 $\mu g.mL^{-1}$ were obtained regardless of the temperature and the power used.

These results indicate that the temperature strongly influence the exfoliation for high power sonication. Interestingly, the changes of the power had a great impact on the exfoliation yield when o-DCB and TCB were used as liquid media. In view of the results of exfoliation and in order to gain a better understanding of the origin of this yellowish solution we decided to deeply investigate graphene obtained in the DCB at 20°C.

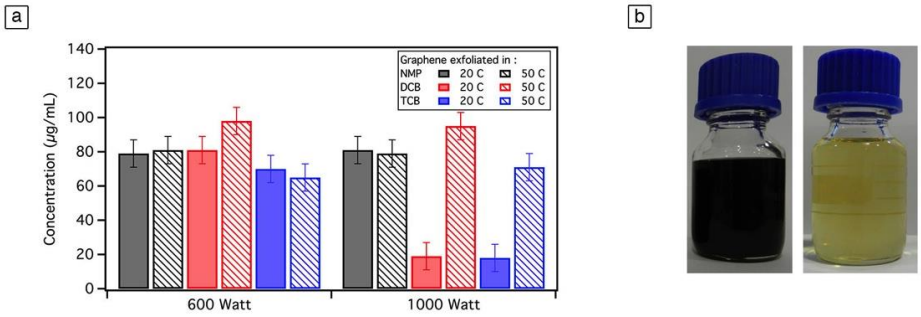

Figure 5.1. a) Average concentrations of dispersions exfoliated in o-DCB, TCB and NMP at two different temperatures (average of 15 exfoliations for each parameter). Full and patterned bars correspond to the exfoliation at 20°C and 50°C, respectively. B) Images showing the supernatant taken after centrifugation and corresponding to 50°C (left side) and 20°C (right side) at 1000 Watt in o-DCB.

5.4.2 High resolution transmission electron microscopy

We focused our attention on the characterization of the dispersions prepared at 20°C in o-DCB in order to investigate the change of the color observed. Figure 5.2a and b show TEM images of graphene prepared at 1000 watt in o-DCB. Their diameters are mainly distributed in the range of 10 to 20 nm with a maximum diameter at 16.7 nm (see Figure 5.2c). This well-defined graphene nanosheets are known as GQDs. Here we note that the contrast between GQDs and the carbon coated TEM grids is very low; therefore, the determination of the number of layers by HR-TEM was difficult. The obtained GQDs have in most cases a rather isotropic shape (as depicted in both Figures 5.2a and b) and an average surface area ~224 nm^2 (see Figure 5.2d). Furthermore, we investigated the morphology and height distribution by AFM. The phase image in Figure 5.2d shows a spherical like shape of these dots. GQDs dispersions were deposed on ozone cleaned silicon substrate. Their height was mostly distributed in the range of 0.6 to 1.2 nm and it was around 1.03 nm on average (see Figure 5.2e for the height distribution and Figure 5.2g for the topography image) suggesting that the GQDs consist of 1-3 layers. Typically, graphene flakes on silicon have usually a thickness of 0.9 nm for the first layer and lower 0.4 nm on mica [51]

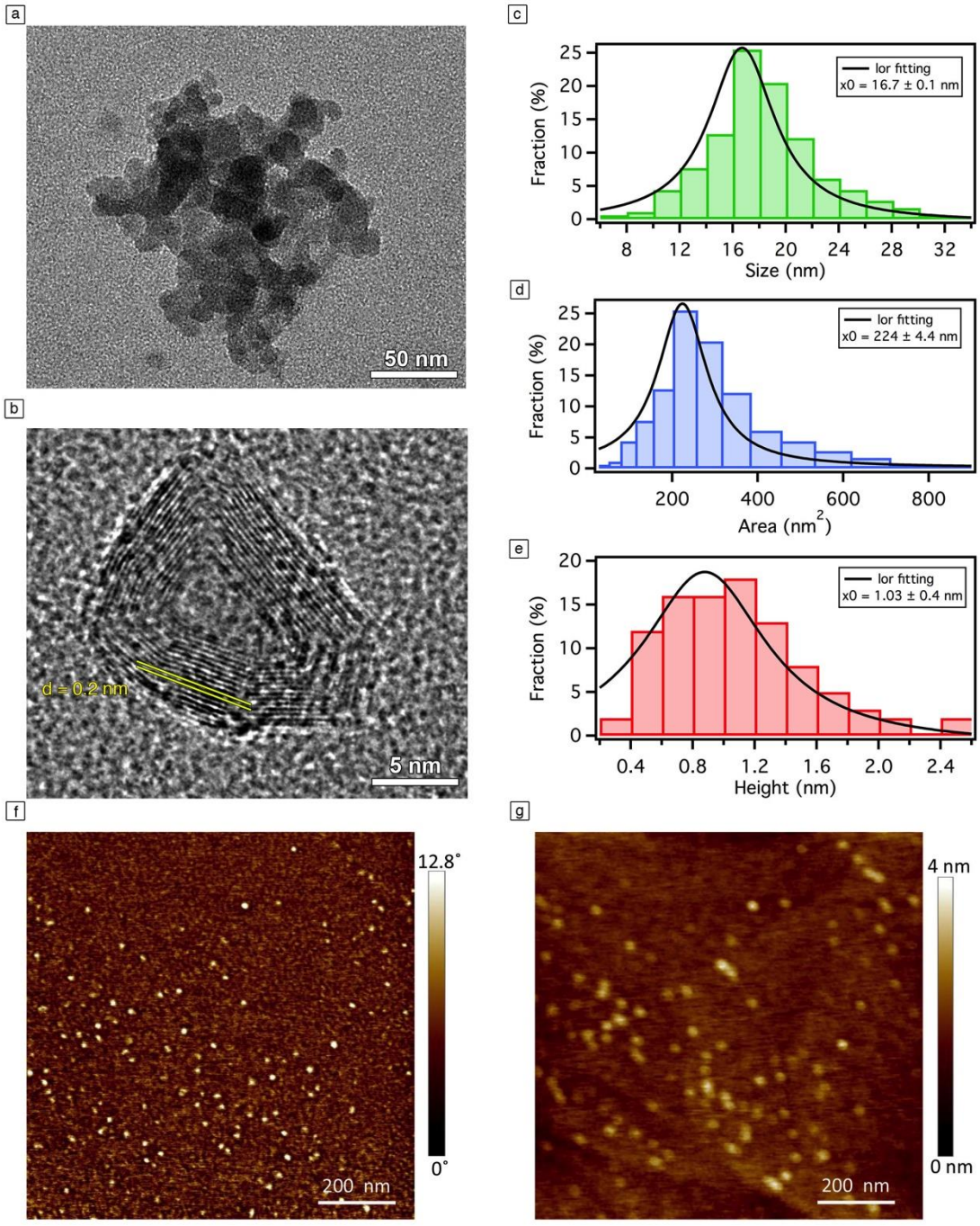

Figure 5.2. a) TEM, b) HRTEM images c) Diameter distribution, d) surface area distribution, e) height distributions, f) AFM phase image and g) AFM height image of GQDs prepared at 20°C with 1000 watt.

By lowering the power to 600 watt, the size of graphene sheets increased even more as demonstrated in the TEM image in Figure 5.2a. Their lateral sizes are distributed in the range

of 100 to 650 nm with a maximum average around 195 nm (see Figure 5.3b). These graphene sheets exhibit a surface area distributed between 10^{-3} to 10^{-1} μm^2 with a maximum average around 1.9 x 10^{-2} μm^2 (see Figure 5.3c). In this case, the majority of graphene are 1-2 layers thick. HR-TEM was used to determine the number of layers by analyzing the edges of graphene flakes (see TEM image in Figure 4.3d and statistics in Figure 5.3e). These results are in good agreement with previous studies [3, 43, 52].

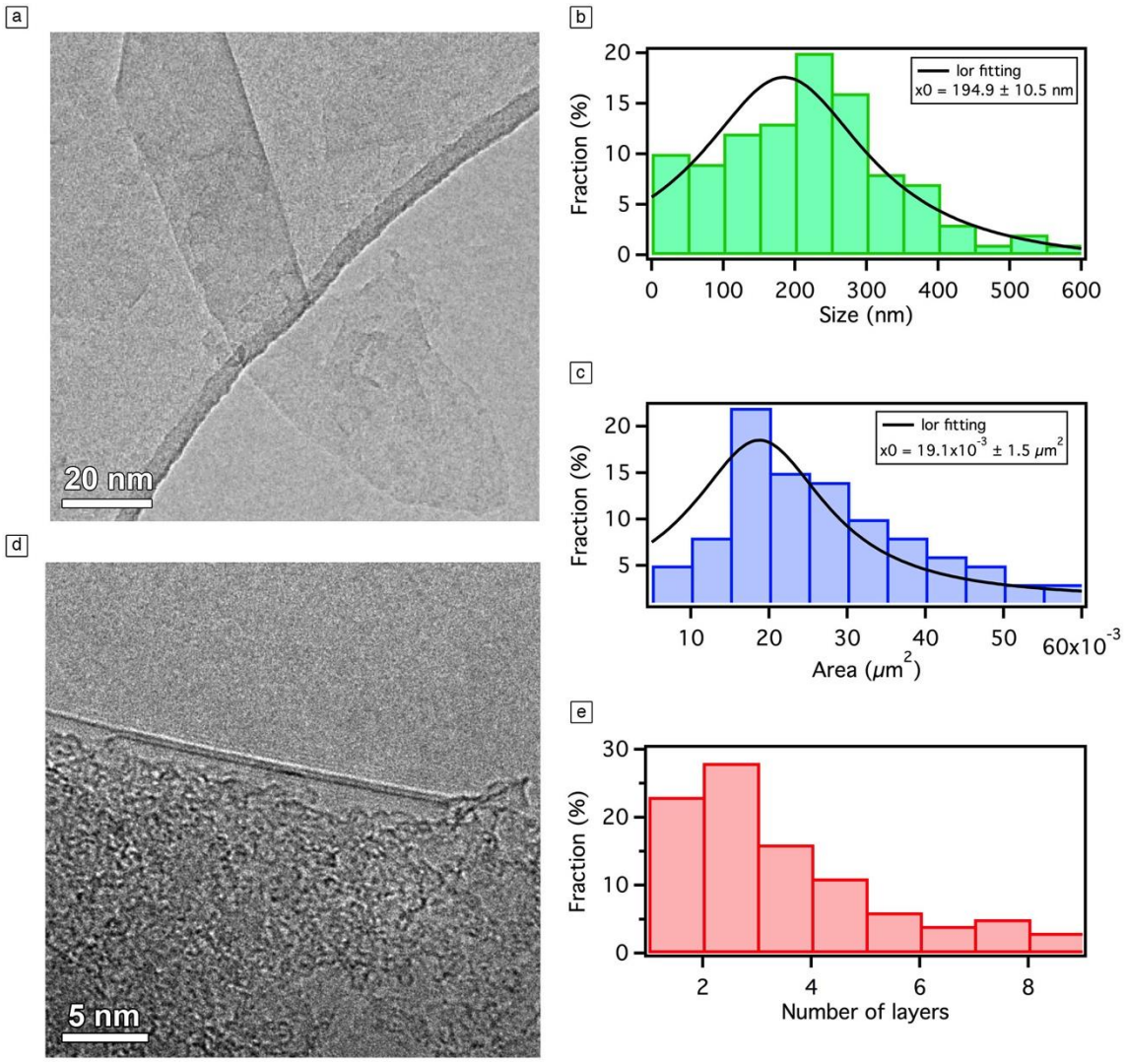

Figure 5.3. a) TEM, b) lateral size, c) surface area d) HRTEM and e) number of layers of graphene prepared at 20°C with 600 watt.

5.4.3 Raman spectroscopy

Figure 5.4a plots the Raman spectrum measured at 532nm excitation wavelength, of representative GQDs deposited on Si/SiO_2 substrate. The G peak corresponds to the E_{2g} phonon at the Brillouin zone centre [33]. The D peak is due to the breathing modes of sp^2 rings and requires a defect for its activation by double resonance [33-35]. The 2D peak is the second order of the D peak. This is a single peak in single layer graphene (SLG), whereas it splits in few-layer graphene (FLG), reflecting the evolution of the electronic band structure. The 2D peak is always detected, even when no D peak is present, since no defects are required for the activation of two phonons with the same momentum, one backscattered from the other. Double resonance can also happen as intra-valley process, *i.e.* connecting two points belonging to the same cone around K or K'. This process gives rise to the D' peak.

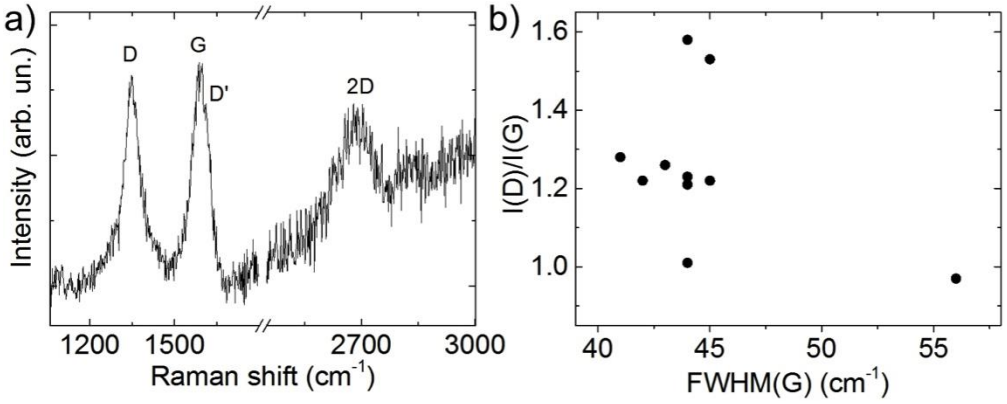

Figure 5.4. a) Raman spectrum at 532nm for representative GQDs. b) Distribution of I(D)/I(G) as a function of FWHM(G).

Statistical analysis, based on 20 measurements for each excitation wavelength (532 and 633nm), give an average position of the 2D peak, Pos(2D), ~2694cm^{-1}, while Pos(G) is peaked at 1585cm^{-1}. These two peaks, however, are very broad. Indeed, FWHM(2D) is ~92 cm^{-1} while FWHM(G) is 45 cm^{-1}, both larger with respect to LPE graphene flakes, where in average FWHM(2D) is <70cm^{-1} and FWHM(G)<25cm^{-1}. This broadening of the G and 2D bands can be attributed to both the size- and edge effect. Indeed, in finite-size domains there is the relaxation of momentum conservation rule. Moreover, as the lateral size of the flakes

shrinks, the fractions of edge carbon atoms, which act as defects by breaking the translational symmetry of the lattice [7, 36], increase. Furthermore, as reported by XPS analysis, the GQDs have oxygen-containing functional groups such as C-O and COOH. The higher electronegativity of oxygen with respect to carbon results in hole doping of the GQDs, resulting in stiffening of Pos(G), as well as charge inhomogeneity between edge and basal plane [37]. The latter could be responsible for the broad G band (FWHM(G)=45cm^{-1}) of our GQDs. Our GQDs show also high I(D)/I(G) ratio, 1.20 in average, see Figure 5.4b). However, this is attributed to the edges of the as-prepared GQDs rather than to the presence of a large amount of structural defects within the GQDs themselves. This observation is supported by the lack of a clear correlation between I(D)/I(G) and FWHM(G) (see Figure 5.4b), an indication that the major contribution to the D peak comes from the sample edges. In fact, combining I(D)/I(G) with FWHM(G) allows us to discriminate between disorder localized at the edges and disorder in the bulk. In the latter case, a higher I(D)/I(G) would correspond to higher FWHM(G).

5.4.4 X-ray photoelectron characterization

X-ray photoemission spectroscopy (XPS) measurements were carried out to probe the composition of GQDs and graphene sheets. In Figure 5.5a, the XPS shows the C1s spectra with a C-C peak at 284.7 eV, C-O peak at 285.8 eV and a COOH peak at 288.7 eV. When the power is increasing, the size of the graphene flakes is decreasing. We observed a slight increase of the COOH peak and the C-O peak (see Figure 5.5b) with the size, which might be due to an increase of the number of defects. The reductions in size enhance the contribution of the oxygen-containing functional groups that are mostly located at the edges. This is in good agreement with the values obtained for GQD exfoliated, as an increase of COOH peak is also observed at 288.8 eV coming from the edges oxidation during cutting process [38]. Also the C:O atomic ratios for graphene and GQDs are 19.2 and 13.7 respectively.

For the two studied solutions, i.e of graphene exfoliated in *o*-DCB at two different sonication powers and at a constant temperature of 20˚C, we found that the Ionization Energy (IE) of the

graphene or GQDs films is influenced by their size which is in turn affected by the sonication power used (see Figure 5.5c). IE values vary from 5.1 eV for Graphene to 5.65 eV for GQDs. Tuning the electronic properties is an attractive target for many technological applications. The dependence of the IE on the size is in line with theoretical calculation performed on nanographenes with various sizes [38]. Particularly, the value measured for our GQDs is in the same range as the one calculated for a similar structure (*i.e.* GQD) featuring 42 carbon atoms in the main core [38]. Here we note that the IE values of drop-casted films of graphene or GQDs (determined by ambient photoelectron spectroscopy) vary from the theoretical calculation simulated for one molecule [38].

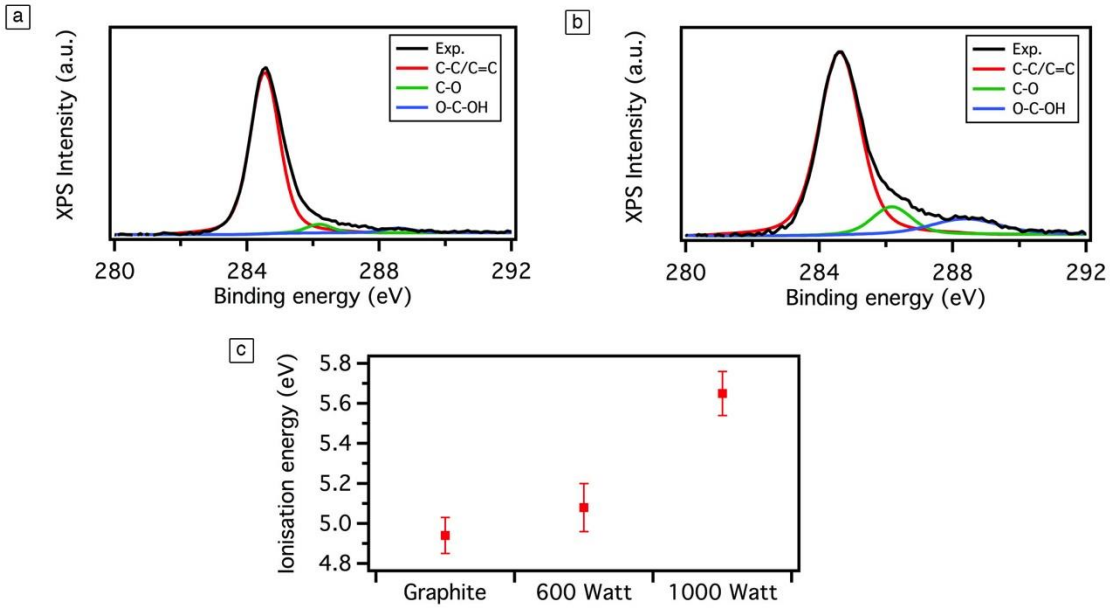

Figure 5.5. a) C1s XPS spectra of graphene at 600 Watt, b) C1s XPS spectra of graphene at 1000 Watt and c) UPS spectra of graphene exfoliated at different temperatures and different powers.

5.4.5 Photophysical properties

All dispersions were also characterized by UV–vis absorption spectroscopy. The spectra displayed in Figure 5.6a are as expected, featureless in the visible region for the dispersions exfoliated at 20ºC. The result reveals that the power of the ultrasonic bath affects the absorption properties of graphene exfoliated in o-DCB. It indicates a clear trend with the size and interestingly it shows an absorption shoulder between 350 and 400 nm for the high sonication power sample that is comparable to previously reported results of nanographene and graphene nanoribbon in o-DCB. The sample sonicated at 600 W showed a more graphene like absorption envelope. A Lambert – Beer behavior was observed for all samples (Figure 5.6b), with extracted values of the regression from the linear fitting amounting to 0.98 for all samples.

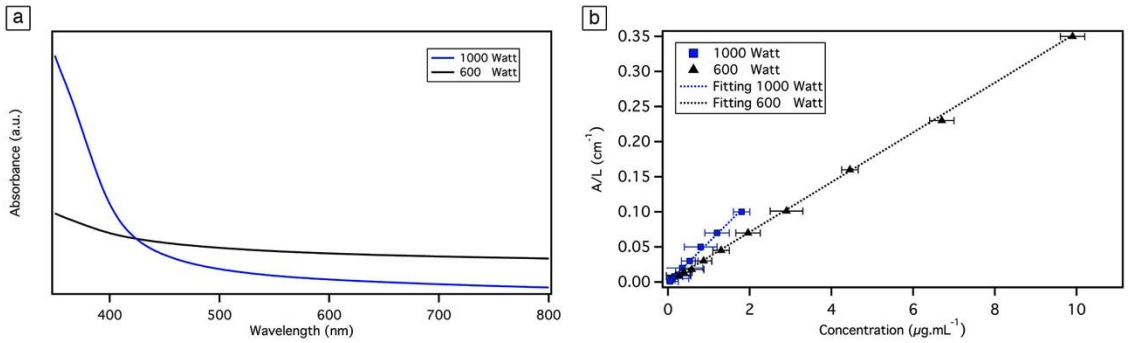

Figure 5.6. a) UV-Vis spectra of graphene dispersions exfoliated at different powers and b) Optical absorbance (at λ=660 nm) divided by cell length (A/l) as a function of concentration for graphene in *o*-DCB, showing Lambert – Beer behavior. Red dashed line is the fitting.

The emission properties of the dispersions exfoliated at low temperatures were compared to graphene dispersion exfoliated at high temperature. All dispersions show an excitation wavelength dependent emission profile, where short wavelength excitation generated a stronger emission response. The dependence of excitation wavelength can be explained by a distribution of graphene sizes and the variation in emission strength on excitation can be explained by the fact that smaller polyaromatic hydrocarbons in general are more fluorescent

(and mostly absorb at shorter wavelengths) than larger ones. In Figure 5.7, graphene is exfoliated at different power but same temperature.

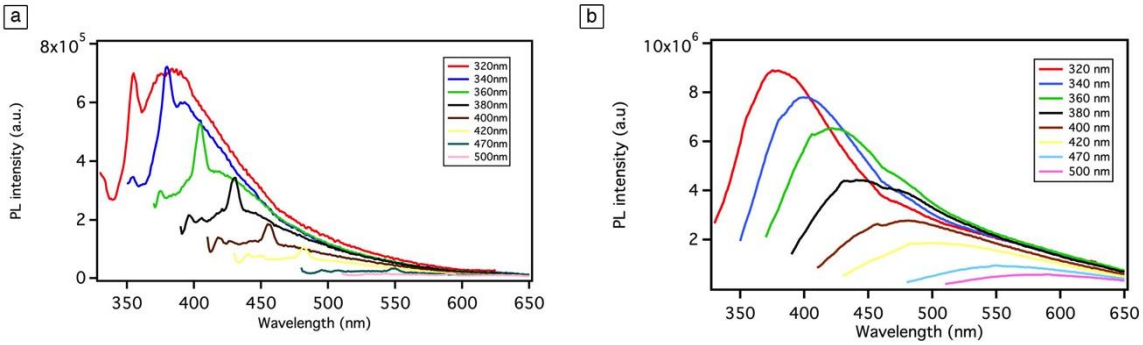

Figure 5.7. Photoluminescence spectra of dispersions of graphene exfoliated in DCB at a) 600 watt and b) 1000 watt. A Raman scattering peak at 3000 cm^{-1} from the excitation wavelength is visible in some of the spectra.

The difference of intensity in the emission is nearly one order of magnitude even though the concentration of graphene is larger for the dispersion sonicated at low power (see Figure 5.1 for concentration differences), this most likely is a consequence of the smaller flake size in the dispersions exfoliated at high power and in figure 5.7, photoluminescence spectra of the two different dispersions exited at 320 nm are plotted showing a clear decrease in terms of intensity when the size of graphene sheets is increasing. It should be noted that even though we know the size distribution of the graphene exfoliated at different temperatures and intensities, we do not know which sizes in that distribution that emits light. It might be so that only the smallest sizes in each size distribution actually emits light, and the differences in intensities seen reflects a difference in concentration of these emitting species. (See figure 5.8)

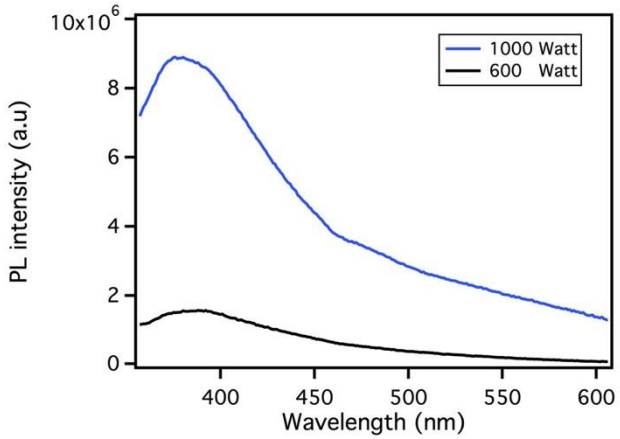

Figure 5.8. Photoluminescence spectra of all dispersions exited at 320 nm.

5.5 Conclusion

In conclusion, we developed a system that allows us to control the liquid-phase exfoliation process. By simply choosing the right parameters, graphene quantum dots can be produced. Moreover, we found that the solvent chosen for the exfoliation plays a key role. *o*-DCB and TCB seems to exfoliate and stabilize better the small sheets. By using chlorinated solvents for exfoliation, we are able to form graphene with variable width from GQDs to nanosheets with luminescent properties. In fact, TEM reveals that the size of GQDs is around 16.7 nm and AFM shows that the height was mostly distributed in the range of 0.6 to 1.2 nm suggesting mono and few-layers sheets. Furthermore, our GQDs exhibiting photoluminescence could have promising applications in opto-electronic devices.

5.6 References

1. K. S. Novoselov, A. K. Geim, S. V. Morozov, D. Jiang, Y. Zhang, S. V. Dubonos, I. V. Grigorieva and A. A. Firsov, *Science*, 2004, **306**, 666-669.
2. S. Kim, S. W. Hwang, M. K. Kim, D. Y. Shin, D. H. Shin, C. O. Kim, S. B. Yang, J. H. Park, E. Hwang, S. H. Choi, G. Ko, S. Sim, C. Sone, H. J. Choi, S. Bae and B. H. Hong, *Acs Nano*, 2012, **6**, 8203-8208.
3. F. Liu, M. H. Jang, H. D. Ha, J. H. Kim, Y. H. Cho and T. S. Seo, *Adv Mater*, 2013, **25**, 3657-3662.
4. L. L. Li, G. H. Wu, G. H. Yang, J. Peng, J. W. Zhao and J. J. Zhu, *Nanoscale*, 2013, **5**, 4015-4039.
5. S. J. Zhu, J. H. Zhang, C. Y. Qiao, S. J. Tang, Y. F. Li, W. J. Yuan, B. Li, L. Tian, F. Liu, R. Hu, H. N. Gao, H. T. Wei, H. Zhang, H. C. Sun and B. Yang, *Chem Commun*, 2011, **47**, 6858-6860.
6. S. Y. Lim, W. Shen and Z. Q. Gao, *Chem Soc Rev*, 2015, **44**, 362-381.
7. X. T. Zheng, A. Ananthanarayanan, K. Q. Luo and P. Chen, *Small*, 2015, **11**, 1620-16310.
8. M. Bacon, S. J. Bradley and T. Nann, *Part Part Syst Char*, 2014, **31**, 415-428.
9. S. J. Zhuo, M. W. Shao and S. T. Lee, *Acs Nano*, 2012, **6**, 1059-1064.
10. Y. Li, Y. Hu, Y. Zhao, G. Shi, L. Deng, Y. Hou and L. Qu, *Adv Mater*, 2011, **23**, 776-780.
11. Y. Q. Dong, J. W. Shao, C. Q. Chen, H. Li, R. X. Wang, Y. W. Chi, X. M. Lin and G. N. Chen, *Carbon*, 2012, **50**, 4738-4743.
12. J. Lu, P. S. E. Yeo, C. K. Gan, P. Wu and K. P. Loh, *Nat Nanotechnol*, 2011, **6**, 247-252.
13. S. H. Jin, D. H. Kim, G. H. Jun, S. H. Hong and S. Jeon, *Acs Nano*, 2013, **7**, 1239-1245.
14. D. Pan, J. Zhang, Z. Li and M. Wu, *Adv Mater*, 2010, **22**, 734-738.
15. S. J. Zhu, J. H. Zhang, X. Liu, B. Li, X. F. Wang, S. J. Tang, Q. N. Meng, Y. F. Li, C. Shi, R. Hu and B. Yang, *Rsc Adv*, 2012, **2**, 2717-2720.
16. J. Zong, Y. H. Zhu, X. L. Yang, J. H. Shen and C. Z. Li, *Chem Commun*, 2011, **47**, 764-7610.
17. X. Y. Tan, Y. C. Li, X. H. Li, S. X. Zhou, L. Z. Fan and S. H. Yang, *Chem Commun*, 2015, **51**, 2544-25410.
18. L. B. Tang, R. B. Ji, X. K. Cao, J. Y. Lin, H. X. Jiang, X. M. Li, K. S. Teng, C. M. Luk, S. J. Zeng, J. H. Hao and S. P. Lau, *Acs Nano*, 2012, **6**, 5102-5110.
19. J. Lee, K. Kim, W. I. Park, B. H. Kim, J. H. Park, T. H. Kim, S. Bong, C. H. Kim, G. Chae, M. Jun, Y. Hwang, Y. S. Jung and S. Jeon, *Nano Lett*, 2012, **12**, 6078-6083.
20. L. A. Ponomarenko, F. Schedin, M. I. Katsnelson, R. Yang, E. W. Hill, K. S. Novoselov and A. K. Geim, *Science*, 2008, **320**, 356-358.
21. N. Mohanty, D. Moore, Z. Xu, T. S. Sreeprasad, A. Nagaraja, A. A. Rodriguez and V. Berry, *Nat Commun*, 2012, **3**, 844-852.

22. S. K. Lai, C. M. Luk, L. Tang, K. S. Teng and S. P. Lau, *Nanoscale*, 2015, **7**, 5338-5343.
23. Y. Hernandez, V. Nicolosi, M. Lotya, F. M. Blighe, Z. Y. Sun, S. De, I. T. McGovern, B. Holland, M. Byrne, Y. K. Gun'ko, J. J. Boland, P. Niraj, G. Duesberg, S. Krishnamurthy, R. Goodhue, J. Hutchison, V. Scardaci, A. C. Ferrari and J. N. Coleman, *Nat Nanotechnol*, 2008, **3**, 563-568.
24. D. Nuvoli, L. Valentini, V. Alzari, S. Scognamillo, S. B. Bon, M. Piccinini, J. Illescas and A. Mariani, *J Mater Chem*, 2011, **21**, 3428-3431.
25. S. Haar, A. Ciesielski, J. Clough, H. Yang, R. Mazzaro, F. Richard, S. Conti, N. Merstorf, M. Cecchini, V. Morandi, C. Casiraghi and P. Samori, *Small*, 2015, **11**, 1691-1702.
26. J. N. Coleman, *Accounts Chem Res*, 2013, **46**, 14-22.
27. K. Kouroupis-Agalou, A. Liscio, E. Treossi, L. Ortolani, V. Morandi, N. M. Pugno and V. Palermo, *Nanoscale*, 2014, **6**, 5926-5933.
28. R. Durge, R. V. Kshirsagar and P. Tambe, *Procedia Engineering*, 2014, **97**, 1457-1465.
29. T. Skaltsas, X. X. Ke, C. Bittencourt and N. Tagmatarchis, *J Phys Chem C*, 2013, **117**, 23272-23278.
30. J. Peng, W. Gao, B. K. Gupta, Z. Liu, R. Romero-Aburto, L. H. Ge, L. Song, L. B. Alemany, X. B. Zhan, G. H. Gao, S. A. Vithayathil, B. A. Kaipparettu, A. A. Marti, T. Hayashi, J. J. Zhu and P. M. Ajayan, *Nano Lett*, 2012, **12**, 844-849.
31. S. H. Song, M.-H. Jang, J. Chung, S. H. Jin, B. H. Kim, S.-H. Hur, S. Yoo, Y.-H. Cho and S. Jeon, *Advanced Optical Materials*, 2014, **2**, 1016-1023.
32. R. Ye, C. Xiang, J. Lin, Z. Peng, K. Huang, Z. Yan, N. P. Cook, E. L. Samuel, C. C. Hwang, G. Ruan, G. Ceriotti, A. R. Raji, A. A. Marti and J. M. Tour, *Nat Commun*, 2013, **4**, 2943-2949.
33. F. Bonaccorso, A. Lombardo, T. Hasan, Z. P. Sun, L. Colombo and A. C. Ferrari, *Mater Today*, 2012, **15**, 564-589.
34. A. Ciesielski, S. Haar, M. El Gemayel, H. Yang, J. Clough, G. Melinte, M. Gobbi, E. Orgiu, M. V. Nardi, G. Ligorio, V. Palermo, N. Koch, O. Ersen, C. Casiraghi and P. Samori, *Angew Chem Int Ed Engl*, 2014, **53**, 10355-10361.
35. A. C. Ferrari and D. M. Basko, *Nat Nanotechnol*, 2013, **8**, 235-2410.
36. A. C. Ferrari, J. C. Meyer, V. Scardaci, C. Casiraghi, M. Lazzeri, F. Mauri, S. Piscanec, D. Jiang, K. S. Novoselov, S. Roth and A. K. Geim, *Phys Rev Lett*, 2006, **97**, 187401
37. A. C. Ferrari and J. Robertson, *Phys Rev B*, 2000, **61**, 14095-14107.
38. F. Torrisi, T. Hasan, W. P. Wu, Z. P. Sun, A. Lombardo, T. S. Kulmala, G. W. Hsieh, S. J. Jung, F. Bonaccorso, P. J. Paul, D. P. Chu and A. C. Ferrari, *Acs Nano*, 2012, **6**, 2992-30010.
39. L. Liu, S. M. Ryu, M. R. Tomasik, E. Stolyarova, N. Jung, M. S. Hybertsen, M. L. Steigerwald, L. E. Brus and G. W. Flynn, *Nano Lett*, 2008, **8**, 1965-1970.
40. Y. Z. Tan, B. Yang, K. Parvez, A. Narita, S. Osella, D. Beljonne, X. Feng and K. Mullen, *Nat Commun*, 2013, **4**, 2646-2653.

Chapter 6 Harnessing LPE using aliphatic compounds

6.1 Introduction

It was shown that the exfoliation of graphite in a liquid media could be assisted by using organic molecules such as surfactants,[1, 2] functionalized pyrenes,[3-6] diazaperopyrenium dications[7] and biomolecules.[8, 9] The organic molecules mainly act as a stabilizer via physisorption of their hydrophobic moieties on the graphene surfaces once graphite is exfoliated by sonication. The exfoliation of graphene in water is particularly challenging due to the hydrophobic nature of the sheets, but surfactants can solve this problem and help exfoliated sheets to remain suspended. However, the use of water as a media is not recommended for the exploitation of graphene in electronic devices because the presence of residual water molecules at the interface with dielectrics can enhance charge trapping phenomena.[10] Thus, the use of organic solvents as an exfoliating media has to be explored. It was recently shown that the exfoliation in an organic media could be promoted by adding a further organic molecule acting as dispersion-stabilizing agent during the exfoliation process.[2] In particular, only two examples were reported so far on the use on non-charged small organic molecules. Graphene dispersions were prepared in NMP with the aid of nonionic porphyrin molecules.[1] Organic molecules such as e.g. 1,2-distearoyl-sn glycero-3-phosphoethanolamine-N-[methoxy (polyethyleneglycol)-5000] (DSPE-mPEG) were also used to stabilize graphene sheets at the end of the exfoliation process to inhibit the re-stacking of graphene sheets.[6] It has been also shown recently, that polymeric systems can have an impact on exfoliation yield.[2, 3]

6.2 Scope

Here we show that the concentration of defect-free, few layer thick (with about 30% single-layers) graphene dispersions in NMP can be increased by addition of simple alkane molecules in the LPE process. The chosen dispersion-stabilizing compound needs to meet primarily two criteria: (*i*) its adsorption energy on graphene has to be larger than the adsorption of solvent molecule; (*ii*) it needs to be very well soluble/miscible in/with organic media such as $CHCl_3$.

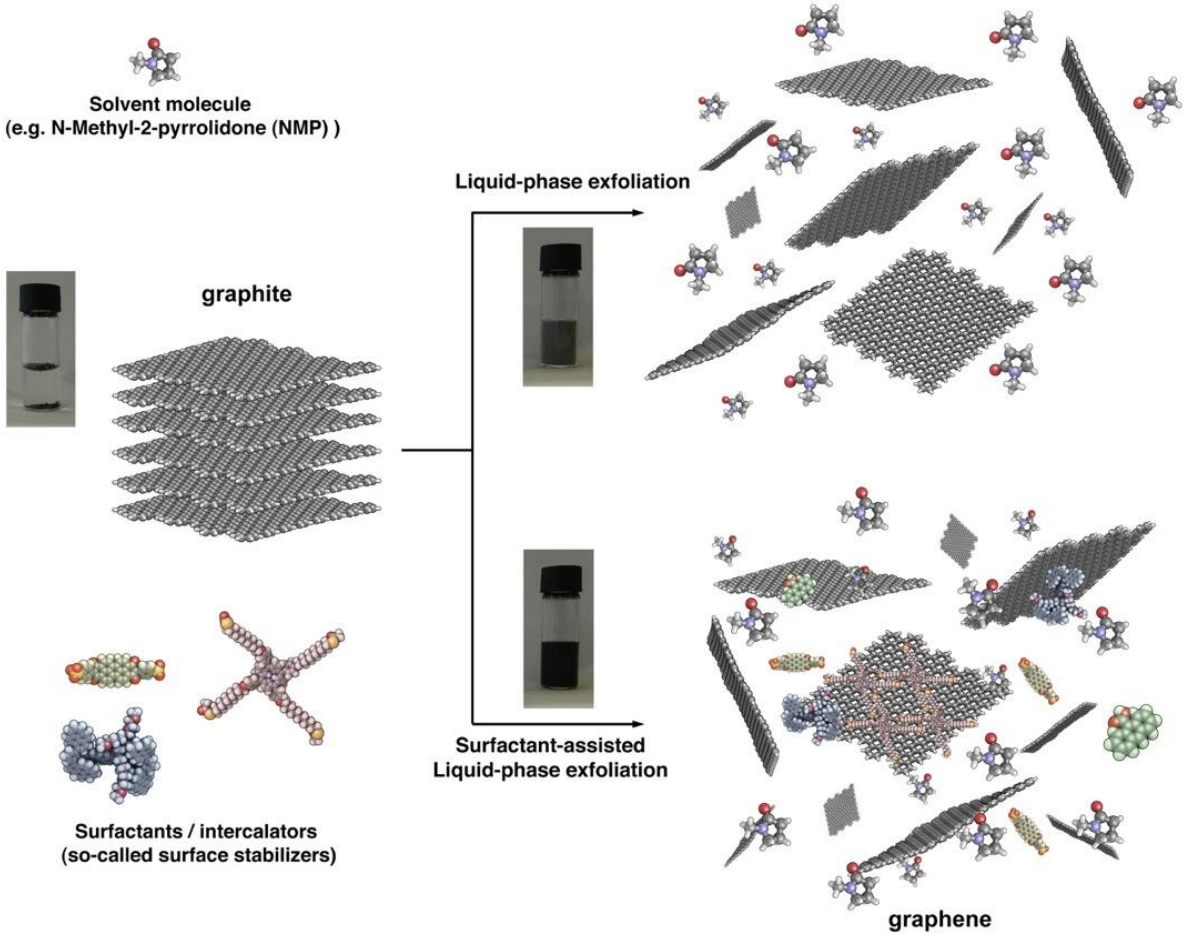

Scheme 6.1. Schematic representation of the liquid-phase exfoliation process of graphite in the absence (top-right) and presence (bottom-right) of surfactant molecules.

We focused our attention on two simple molecular modules, i.e. 1-phenyloctane and arachidic acid, whose calculated adsorption energy on graphene (-19.1 and -28.2 kcal mol^{-1}, respectively) is much higher than the adsorption energy of NMP (-8.5 kcal mol^{-1}), thus

fulfilling with criterion (*i*). Additionally, to qualitatively test the affinities of both molecules for graphene surface we performed scanning tunneling microscopy (STM)[13-15] experiments at the solid-liquid interface, using highly oriented pyrolitic graphite (HOPG) as a substrate. Self-assembly of molecular building blocks capable of undergoing controlled self-assembly from solution at surfaces and interfaces relies on a subtle balance between molecule–molecule, molecule–substrate, molecule–solvent, and solvent–substrate interactions leading to the targeted 2D patterns.[16] In fact, alkanes and in particular carboxylic acids are one of the first molecules visualized with the sub-molecular resolution at the solid-liquid interface by STM.[17] Because of its simple structure, capability to form highly ordered architectures on graphite surface, as well as its low-cost we decided to focus our attention on its C_{20} derivative, i.e. arachidic acid. Noteworthy, it is well accepted in the STM community that 1-phenyloctane (typically used as a solvent in STM experiments) by itself doesn't form ordered monolayers (at room temperature) at the solution-HOPG interface. Although its adsorption energy on graphene is as high as -19.1 kcal mol^{-1}, the dynamic nature of adsorption/desorption process of this small molecule on HOPG occurs on a time scale, which is much faster than the scanning speed of STM tip, hindering its visualization by STM. (See Scheme 6.1)

6.3 Experimental

6.3.1 Materials

Arachidic acid, 1-phenyloctane and N-Methyl-2-Pyrrolidinone (spectrophotometric grade, 99%) were purchased from Sigma-Aldrich, and used as received, i.e. without purification. Graphite powder was purchased from Aldrich (Aldrich product 332461, batch number 08722AH).

	Volume of NMP (mL)	Mass of graphite (mg)	Mass of molecules 100% SA (mg)	Mass of molecules 20% SA (mg)
Graphene exfoliated with arachidic acid	9.71	100	108	21.6
Graphene exfoliated with 1-phenyloctane	9.71	100	14.03	2.81

Graphene exfoliated without additives compounds	9.71	100	/	/

Table 6.1. Masses of graphite, solvent and organic molecules used in LPE process.

6.3.2 Device

In order to obtain graphene dispersions, graphite flakes were sonicated for 6 hours at 40 ± 2°C (100 W) in the chosen solvents, keeping the graphite weight percent constant, i.e. 1 wt%. Since the ratio between graphite powder and the solvent was kept constant, different masses of graphite flakes have been used. Sonication of graphite powder led to grey liquid consisting of a homogeneous phase and large numbers of macroscopic aggregates. As previously reported, these aggregates can be removed by centrifugation (Eppendorf 5804, rotor F-34-6-38, 60 min at 10 000 rpm), yielding a homogeneous dark dispersion.

6.3.3 Characterizations

Centrifugation of graphene dispersions was perform by using Eppendorf 5804, rotor F-34-6-38, 1h at 10000 rpm.

SEM images were recorded by using Strata 400 Dual Beam. After drop-casting graphene dispersions on patterned n++ - Si/SiO2 the samples where annealed at 80° C. In order to avoid charging of Si/SiO2 substrate during imaging with SEM, thin layer of platinum was spattered.

NMR experiments measurement of self-diffusion coefficients were performed on a BRUKER 600 MHz spectrometer - Avance III, equipped with a high strength z gradient probe DOTY Scientific, developing a pulse field gradient of 50 G/cm/A. The gradient coil is cooled by air flow and the sample was thermostated at 298 K. Diffusion NMR data were acquired using a Stimulated Echo pulse sequence with bipolar z gradients. Limited Eddy current Delay was fixed to 5 ms. The gradient strength varied linearly between 6 and 304 G.cm-1 in 30-40 experiments. The diffusion time and the duration of the sinusoidal gradients were optimized

for each sample. Typically the diffusion time was set between 6 and 8 ms, and the half-gradient delay between 0.6 and 1 ms. The gradient recovery delay was set to 1ms.

The viscosities of solutions were measured using a falling ball micro-viscometer Anton Paar, at 298 K (thermostat Peltier effect). The samples were prepared in CDCl3 with a constant concentration of 4.5 mM of non-deuterated DMSO and/or NMP and 0.5 mM of arachidic acid for each measurements and the experiment were repeated at least two times.

The extraction of the sheet resistance from two-terminals devices was performed starting from n^{++} - Si/SiO_2 substrates exposing pre-patterned interdigitated gold electrodes pairs (IPMS Fraunhofer). The same substrates were successively used in order to apply a gate voltage and study the current modulation with varying the bias on a third electrode. Before the deposition of graphene, the substrates were treated with ozone (5 min irradiation followed by 25 min of incubation). Subsequently they were transferred to the glove-box (nitrogen atmosphere) and they were treated with either HMDS or OTS. In the former case, HMDS was deposited by spin-coating 100 μL at 1500 rpm for 60 s and then annealed at 120°C for 1 hour. Whereas in the latter case, the substrates were immersed for 15 h in OTS solution (10 mM in toluene) then thoroughly rinsed with toluene and heated at 60˚C for one hour. Then, 200 μL of graphene dispersion were drop-casted (in air) onto the treated substrates followed by a gentle annealing in a vacuum oven at 45˚C for 3 days.

The sheet resistance was calculated by considering the following relationship:

$$R_{TOT} = \rho \frac{L}{tW_{eff}} \qquad (1)$$

where R_{TOT} is the ration between V and I(V), L is the electrode gap, *t* is the material thickness and W_{eff} is the effective width of the material covering the inter-electrodic region as estimated through an optical microscope. Assuming that in the case of graphene *t* is negligible the previous formula becomes:

$$R_s = \rho \frac{L}{W_{eff}} \qquad (2)$$

The field-effect mobility values we reported in the main text were extracted from the linear regime in I_D-V_{GS} curves by means of the following relationship:

$$\mu_{lin} = \frac{\partial I_D}{\partial V_{GS}} \frac{L}{W_{eff}} \frac{1}{C_{i_{[SiO_2]}}} \frac{1}{|V_{DS}|} \tag{3}$$

where V_{DS} and V_{GS} are the source-drain and source-gate voltage, respectively, $C_{i[SiO2]}$ is the capacitance of the silicon dioxide (thickness: 230 nm) which amounts to 1.5 10^{-8} F/cm^2. In our case the parameters' extraction was done at V_{DS} = 0.6 V (electron mobility) or -0.6 V (hole mobility).

The linear conductance, $g_{D,lin}$, can be written as:

$$g_{D,lin} = \frac{\partial I_D}{\partial V_{DS}} = \mu C_{ins} \frac{W_{eff}}{L} (V_{GS} - V_{TH}) \approx \mu C_{ins} \frac{W_{eff}}{L} V_{GS} \tag{4}$$

under the assumption that the neutrality point could be seen as the transistor threshold voltage and it is close to zero, ($\| V_{GS} \| >> \| V_{TH} \|$).

6.4 Results and discussion

6.4.1 Scanning tunneling microscopy and coverage calculations

The self-assembly of arachidic acid in 2D has been investigated by applying 4 µL drop of a (100 ± 2) µM solution on the freshly cleaved HOPG surface. Given that the solvent used for STM experiments has to be apolar (dielectric constant (ε) = 2-4), STM measurements cannot be performed by using NMP as a liquid medium (ε = 31), thus 1-phenyloctane was chosen as a solvent. The STM current image in Figure 1 shows a monocrystalline lamellar structure. In this 2D crystal, arachidic acid molecules are physisorbed flat on the surface forming H-

bonded dimers, which are interdigitated between adjacent lamellae, as shown in Figure 5.1.1. Conversely, the 1-phenyloctane molecules have not been found to pack on HOPG. In light of this observation the calculated adsorption energy of arachidic acid on graphene is twice the one the monomeric specie, thus amounting to –26.4 kcal mol-1. The unit cell, containing two molecules, exhibits the following parameters: a = (0.84 ± 0.10) nm, b = (2.52 ± 0.10) nm, and α = (88 ± 2)°, leading to an area A = (2.12 ± 0.25) nm2, in agreement with previous reports.[18, 19]

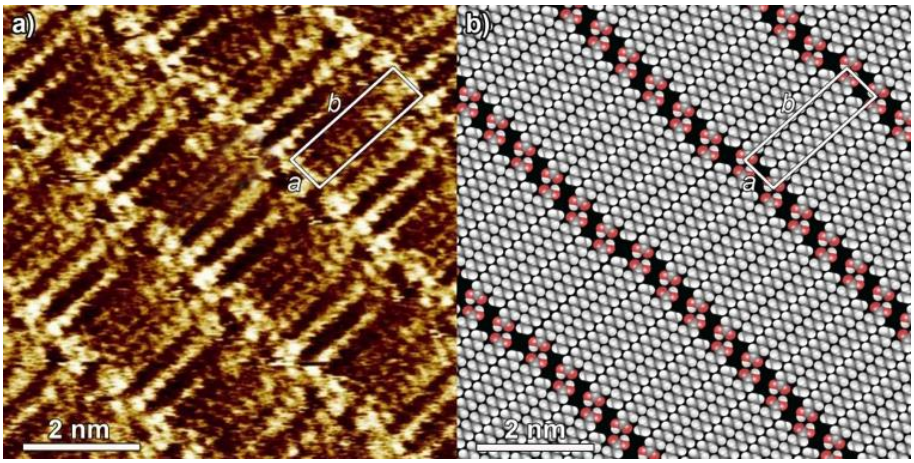

Figure 6.2. a) STM current image of arachidic acid monolayer at the HOPG-solution interface; b) molecular packing motif. Tunneling parameters: average tunneling current (It) = 20 pA, tip bias voltage (Vt) = 350 mV.

Proposed molecular packing motif of arachidic acid on graphene surface has been shown in Figure 6.2. As described in the main text, 1-phenyloctane (typically used as a solvent in STM experiments) does not form any ordered monolayers at the HOPG surface. Nevertheless, theoretical assumption of 1-phenyloctane packing motif on graphene (Figure 6.3) has been used for calculation the coverage areas.

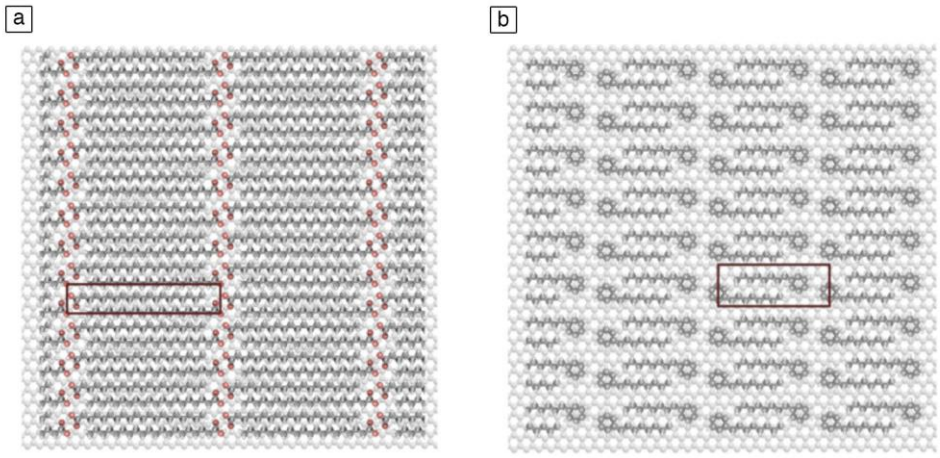

Figure 6.3. a) Proposed molecular packing motif of arachidic acid on graphene surface as observed with scanning tunneling microscopy at the solid-liquid interface. The red cell parameters, a = (0.98 ± 0.10) nm, b = (2.52 ± 0.10) nm, and α = (90 ± 2)°, lead to an area A = (2.46 ± 0.05) nm2, where each cell contains 2 molecules, therefore the area occupied by single molecule equals to A = (1.23 ± 0.05) nm2. b) Theoretical molecular packing motif of 1-phenyloctane on graphene surface. The area occupied by single molecule equals to A = (5.92 ± 0.9) nm^2.

The areas A occupied by single dispersion-stabilizing molecules ($A_{DS.}$), as well as area of graphene unit cell ($G_{unit\ cell}$ = (0.052 ± 0.004) nm2.) determined by STM can be used for calculating the mass (and number) of dispersion-stabilizing molecules needed to cover accessible graphene area (MDS.). Noteworthy, in our calculations graphite powder has been considered as a single (rectangular) graphene sheet ($S_{graphene}$).

$$M_{DS.} = \left(\frac{\left(\frac{S_{graphene}}{A_{DS.}} \right)}{N_A} \right) \times Mw_{DS.} \qquad (5)$$

Where

$$S_{graphene} = G_{unit\ cell} \times \left(\frac{M_{graphite\ powder} \times N_A}{M_{C\ atom}} \right) \qquad (6)$$

6.4.2 DOSY NMR

Although the formation of spatially extended, ordered and stable self-assembled monolayer on graphene sheets during the sonication process is unlikely, the presence of the alkane molecules leads to an increased yield of exfoliation. As expected from different adsorption energies of phenyloctane and arachidic acid on graphene sheets, the latter exfoliates the graphene more efficiently, highlighting the importance of the molecular length in the structure of dispersion-stabilizing agents. In this regard, in order to explore the propensity of arachidic acid molecules to undergo dimerization in NMP, 2D 1H NMR (DOSY) experiments have been carried out (see Table 6.2). Surprisingly, diffusion coefficients provided evidence for the existence of monomeric species of arachidic acid in NMP. Although the majority of molecules exist as monomeric species in solution, it is likely that they undergo dimerization through H-bonding when the dimensionality is reduced from the 3D of a solution to the 2D on the graphene surface. This is in line with previous STM observations of H-bonded patterns obtained by dissolving molecules in similarly polar media like dimethylsulfoxide and further diluted with other solvents to form ordered monolayers at the solid-liquid interface, ultimately proving the key templating effect of the substrate. Statistical analysis of the flake thickness revealed that the use of dispersion-stabilizing molecules increases the amount of produced graphene flakes, i.e. increases the exfoliation yield, but also rises the percentage of mono- and bilayer graphene flakes produced in LPE process. An average value of the determined diffusion coefficient (D) and viscosity (η) values were used for determination of the preferential form.

	D measured	η measured	D_{mono} calculated	D_{dim} calculated
Arachidic acid in $CDCl_3$	7.45×10^{-10}	800×10^{-4}	1.08×10^{-9}	10.58×10^{-10}
Arachidic acid and NMP in $CDCl_3$	3.17×10^{-10}	1.702×10^{-3}	3.36×10^{-10}	2.05×10^{-10}
Arachidic acid and DMSO in $CDCl_3$	3.92×10^{-10}	1.231×10^{-3}	4.65×10^{-10}	2.84×10^{-10}

The diffusion coefficient of dispersion-stabilizing molecules in solution depends on the effective size and shape (dimer or monomer) in the given conditions (i.e., solvent,

temperature). The size of the molecules can be determined by using the diffusion coefficient. In the case of a spherical particle in a homogeneous solution, the hydrodynamic radius r can be calculated by using the Stokes-Einstein equation. However, in our case, the molecules are in the dimer or monomer form that can be described by the prolate ellipsoid model (Prolate: a,b,b):

$$D = \frac{k_B \times T}{6\pi\eta_0}\left(\frac{4\pi N_A}{3M\bar{\upsilon}}\right)^{1/3} \times \frac{\left(\frac{\bar{\upsilon}}{\upsilon_s}\right)^{1/3}}{P} \qquad (7)$$

Where N_A is Avogadro's number, M is the molar mass, $\bar{\upsilon}$ the partial specific volume, k_B, is Boltzmann's constant, T the absolute temperature, η_0 the viscosity of water at 20.0" C and P is defined as Perrin function (named in recognition of F. Perrin).

$$P = \frac{\left(1-\frac{b^2}{a^2}\right)^{1/2}}{\left(\frac{b}{a}\right)^{2/3} \times ln\left(\frac{1+\left(1-\frac{b^2}{a^2}\right)^{1/2}}{\frac{b}{a}}\right)} \qquad (8)$$

The diffusion coefficients of arachidic acid in the presence of NMP or DMSO were determined by diffusion NMR spectroscopy in $CDCl_3$. In order to estimate the preferred form of the molecule, the obtained diffusion coefficients were compared with the diffusion coefficient calculated with the equation (7).

6.4.3 Liquid-phase exfoliation

To test the capability of the two molecules to increase the graphene exfoliation yields we prepared dispersions by adding graphite powder in NMP (1 wt%) by bath sonication (6 h), in

presence of the dispersion-stabilizing compounds, and compared it with the blank experiments, i.e. graphene dispersion prepared in absence of additional molecules. By considering the initial graphite powder as a single graphene sheet, we calculated the number of molecules needed to form densely packed monolayers on graphene. Given that the calculated quantity of the molecules will be higher than the real surface of graphite in the form of powder, we have used only 20% of molecules needed to cover the entire graphene surface. Sonication of all samples, i.e. two samples containing organic molecules and the one in their absence, led to grey liquids consisting of a homogeneous phase and large numbers of macroscopic aggregates. As previously reported, these aggregates can be removed by centrifugation, yielding a homogeneous dark dispersion.

To quantify the concentration after centrifugation, a mixture of graphene dispersion and CHCl3 was heated at 50°C and passed, through polytetrafluoroethylene (PTFE) membrane filters (pore size 100 nm). The remaining NMP solvent molecules were washed away with diethyl ether. The presence of adsorbed molecules on graphene sheets may affect the mass measurements and ultimately the exfoliation yields. Thus, we found that the heating process is necessary, in order to nearly completely remove, i.e. desorb, the dispersion-stabilizing compounds from graphene. Careful measurements of the filtered mass gave the concentration of dispersed phases after centrifugation (see Figure 6.4).

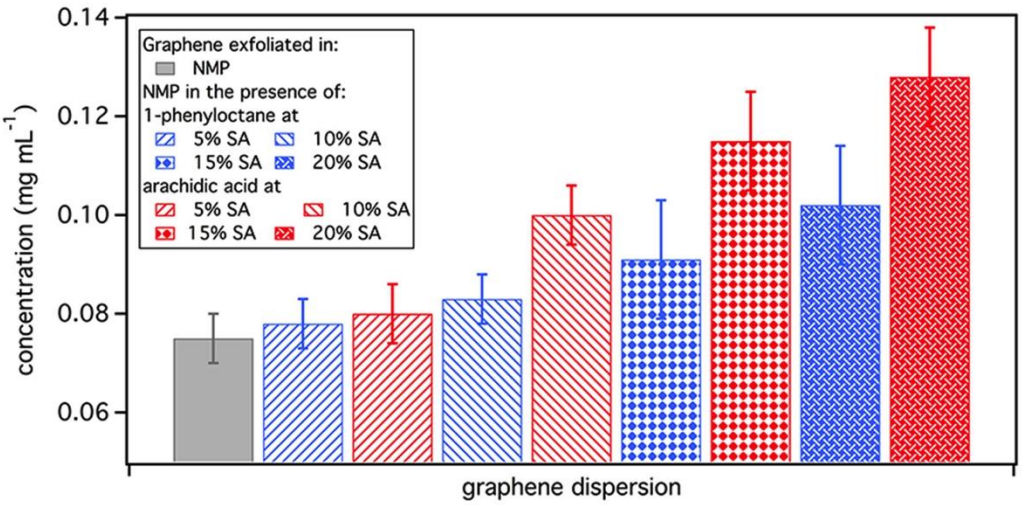

Figure 6.4. Average concentration of three dispersions after the filtration process. The error bars correspond to the different values obtained in 10 independent experiments.

6.4.4 UV-Vis-IR spectroscopy

Graphene dispersions were characterized by UV–Vis–IR absorption spectroscopy. As expected, the spectra are featureless in the visible – IR region. Each of these three dispersions, i.e. graphene, graphene with 1-phenyloctane and graphene with arachidic acid (all in NMP) was diluted a number of times and the absorption spectra recorded (Figure 6.5 and 6.6).

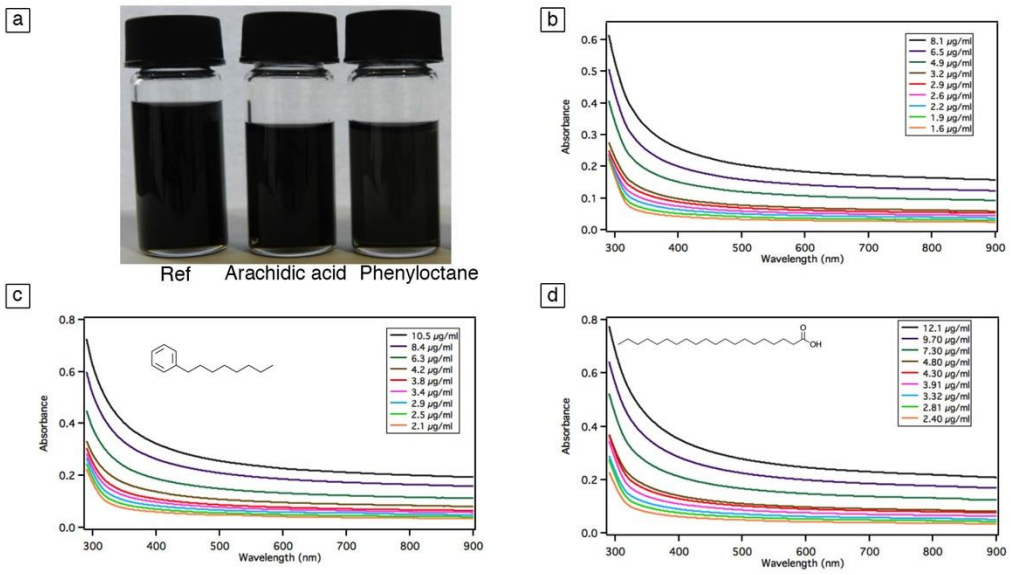

Figure 6.5. a) Images of graphene dispersions, b) UV–Vis spectra of graphene dispersion in NMP at different concentrations, c) UV–Vis spectra of graphene/1-phenyloctane dispersion in NMP at different concentrations, d) UV–Vis spectra of graphene/arachidic acid dispersion in NMP at different concentrations.

In order to quantify the concentration after centrifugation, a mixture of graphite dispersion (1 mL) and chloroform (20 mL) was heated at 50°C and passed, through polytetrafluoroethylene (PTFE) membrane filters (100 nm). The remaining NMP solvent molecules were washed away with diethyl ether (20 mL). The presence of adsorbed dispersion-stabilizing molecules

on graphene sheets may affect the mass measurements and ultimately the exfoliation yields. Therefore, we found that the heating process is necessary, in order to remove, i.e. desorb, the organic compounds from graphene. Among the two compounds, i.e. 1-phenyloctane and arachidic acid, only the former absorbs light (270-275 nm) in the UV-vis range.

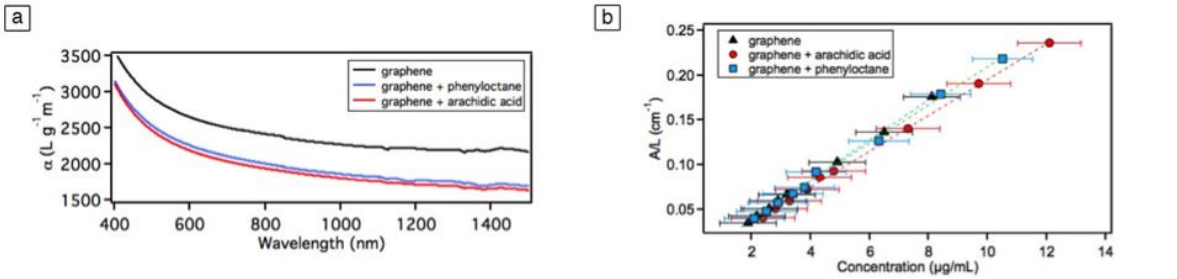

Figure 6.6. a) Absorption spectra for graphene flakes dispersed in NMP, in the presence and absence of dispersion-stabilizing compounds; b) Optical absorbance (at λ = 660 nm) divided by cell length (A/l) as a function of concentration for graphene in the three samples, showing Lambert – Beer behavior. The x-axis error bars are due to the uncertainty in measuring the mass of graphene/graphite in solution.

As shown in Figure 6.7, filtration-washing process of graphene dispersions allows removing molecules from dispersions as proven by the analysis of re-sonicated graphene dispersion after removal of 1-phenyloctane, which is mandatory for the determination of concentration of graphene-dispersions. Note that all the dilutions were treated equally, i.e. even if the dispersion-stabilizing compounds were not added into graphene dispersions

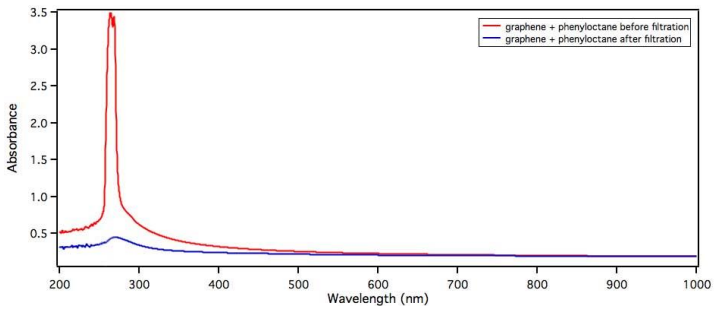

Figure 6.7. UV–Vis spectra of graphene/1-phenyloctane dispersions in NMP before and after heating-filtration-washing cycle.

6.4.5 Thermogravimetric analysis

The presence of dispersion-stabilizing compounds and residual solvent at a significant amount (i.e. ~ 15% of NMP, and ~ 7% of dispersion-stabilizing compounds) in the graphene products indicates their adsorption on the surface of graphene flakes after filtration. After heating and washing in chloroform/diethyl ether, remaining solvent and organic molecules were completely removed (Figure 6.8.)

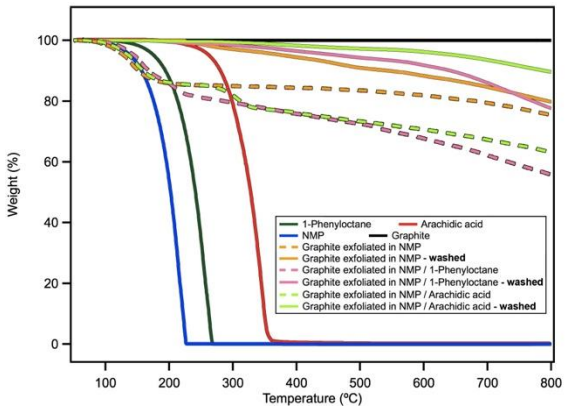

Figure 6.8. TGA curves for graphite, dispersion-stabilizing compounds, solvent and graphite exfoliated in NMP in the presence of dispersion-stabilizing compounds with and without washing.

6.4.6 X-ray Spectroscopy

Survey spectra were collected in the carbon and nitrogen region (see Figure 6.9) for all samples in order to obtain the residual NMP content after samples preparation. The results indicate that NMP can be almost completely removed, leaving less than 2% residual traces of

nitrogen in the case of graphene/NMP and graphene/1-phenyloctane samples, and 8% in the graphene/arachidic acid drop-cast film.

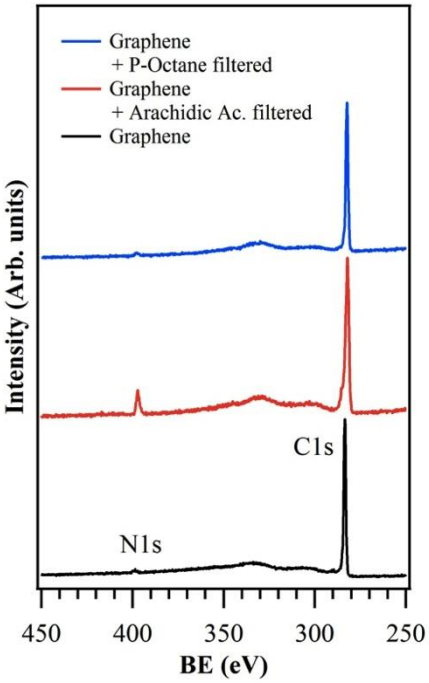

Figure 6.9. XPS spectra of the N1s, C1s region.

The variance with respect to the TG analyses, can be related to the higher surface sensitivity of XPS compared to TGA. The NMP residual trace amounts are summarized in Table 6.3.

Sample	XPS				
	C (%)	N (%) from NMP	C (%) from NMP	C (%) from solvent	C (%) graphenic
Graphene	98.3	1.7	8.5	0.0	91.5
Graphene + Arachidic Ac. filtered	91.9	8.1	40.5	10.5	49.0
Graphene + Arachidic Ac. filtered	98.3	1.7	8.5	0.0	91.5

Table 6.3. Surface composition from XPS

The spectra in Figure 6.10 reveal the presence of graphene by the peak at 284.5 eV BE, showing the typical asymmetric Doniach-Sunjic profile of graphene, in agreement with literature. The residual contribution (green and blue lines) stemming from NMP is apparent in all spectra. In Figure 6.10b the amount of residual NMP is 40.5% and also some traces of arachidic acid are still detectable after filtration.

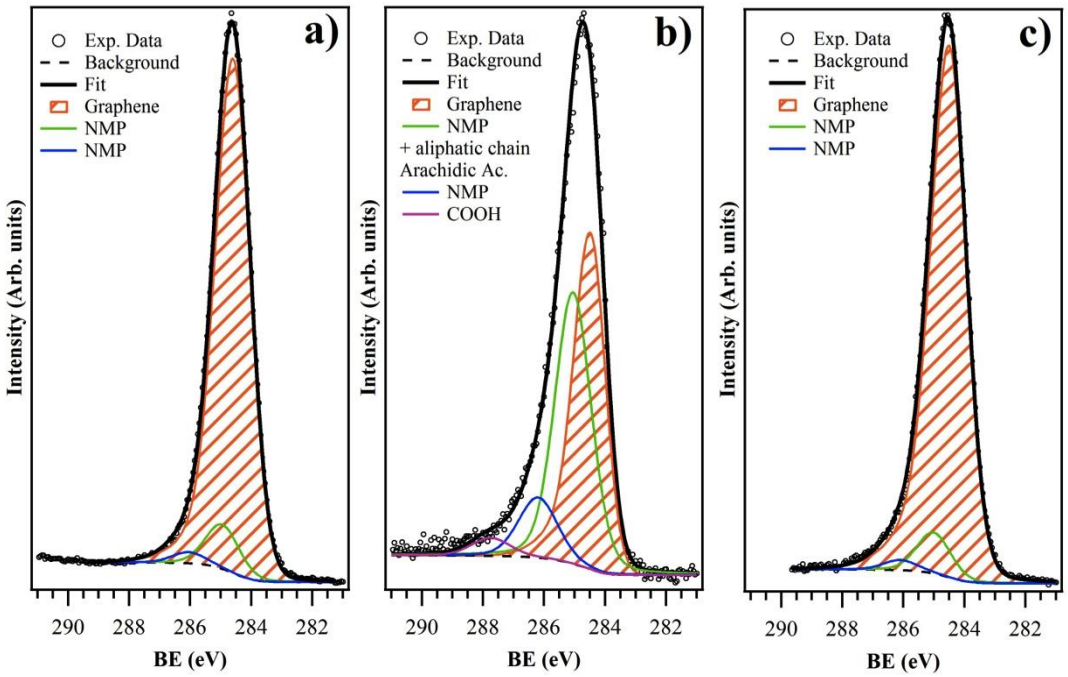

Figure 6.10. High-resolution C1s spectra for graphene a), graphene + arachidic acid b), and graphene + 1-phenyloctane c). Experimental data are shown as black dots, the total fit curves as thick black lines, and the individual deconvolved components as solid colored lines (red, green, blue, violet); the filled area highlights the graphene component.

6.4.7 High resolution TEM

Graphene dispersions were also investigated by means of High Resolution Transmission Electron Microscopy (HR-TEM). In a number of cases we observed folded monolayer graphene sheets as seen in Figure 6.11a with a size below 1 µm, as typically observed in LPE processed graphene. The average lateral size of the monolayer graphene (MLG) sheets was nearly identical in all dispersions and amounts to 0.051±0.012 µm^2. The number of layers per

sheet was determined by analyzing the flake edges using HR-TEM. Statistical analysis of the flake thickness is displayed in the histogram in Figure 6.11b.

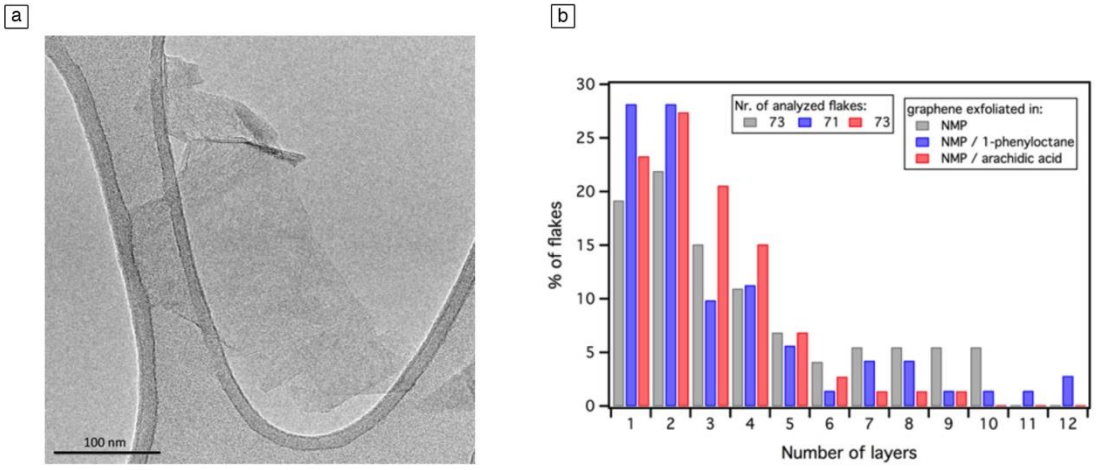

Figure 6.11. a) Representative TEM image of graphene deposited from NMP dispersion showing folded graphene sheet, b) Histogram of the number of flakes observed as a function of number of layers per flake from NMP dispersions.

Since the first successful exfoliation of graphene in an organic solvent such as NMP in 2008, improvements in concentrations of graphene dispersions were achieved, e.g. through the addition of dispersion-stabilizing compounds such as nonionic porphyrins, obtaining concentrations as high as ca. 0.05 mg mL^{-1}, or by using drastically longer sonication times (ca. 500 h – 1.2 mg mL^{-1}). The latter approach is time consuming and requires high-energy consumption; in addition, it is known that with the increasing sonication time, the size of the flakes are severely reduced, being a critical parameter for several applications. Therefore, a comparative study like the one presented here it is extremely important in order to gain a deep understanding on the role of surface-stabilizing molecules in the graphene exfoliation process, which potentially can result in shortening and simplifying the LPE process. Noteworthy, we found that graphene dispersions prepared in the presence of arachidic acid molecules (0.12 mg mL^{-1}) are more concentrated if compared to samples prepared just in NMP (0.08 mg mL^{-1}), therefore corresponding to a 50% increase in the yield of exfoliation.

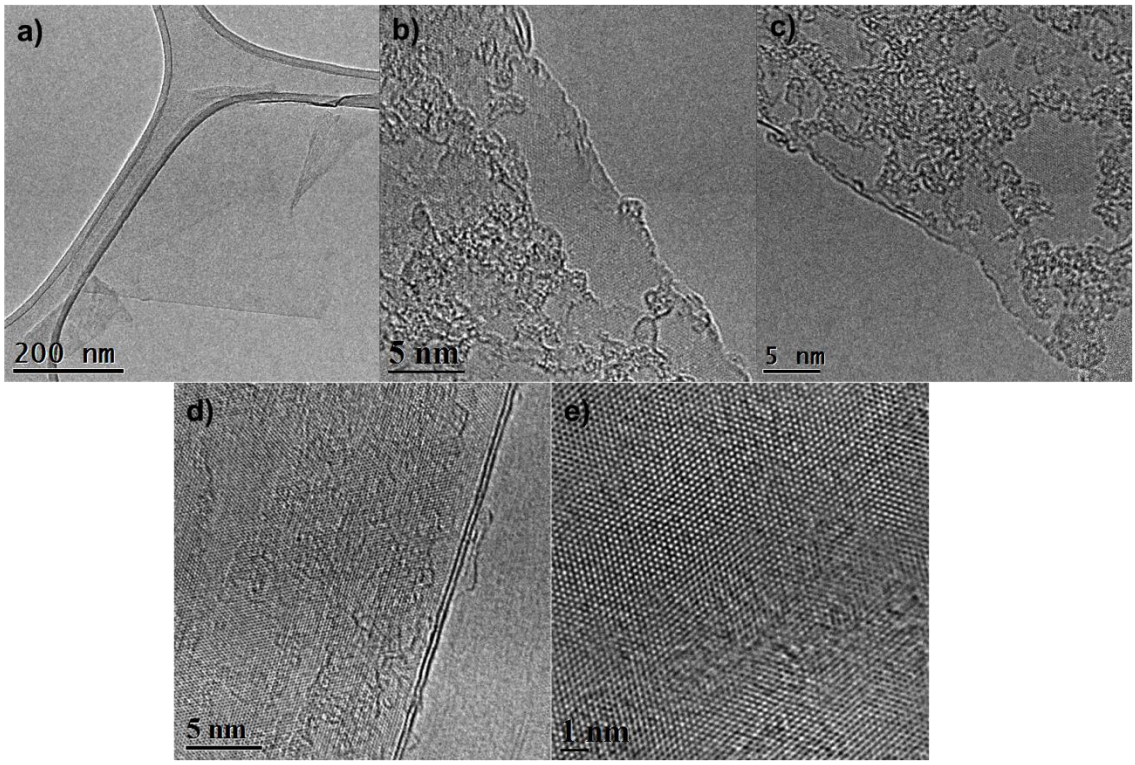

Figure 6.12. a) TEM image of a monolayer graphene flake; example HR-TEM images taken on the edges of monolayer (b,c) and bi-layer (d) graphene flakes; e) HR-TEM image taken in the center of a bi-layer graphene flake.

6.4.8 Raman spectroscopy

We then focused our attention on comparing the quality of three graphene dispersions by the means of Raman spectroscopy, which is a powerful tool for the investigation of graphene.[20,21] We performed micro Raman measurements by casting the suspensions on a silicon substrate, heated at 60ºC to facilitate NMP evaporation. In order to avoid damage and heating induced effects, which can desorb or damage the molecules,[6] the laser power was kept well below 1 mW. Note that the Raman spectrum of graphene produced by LPE is very different from the one of graphene produced by micro-mechanical exfoliation (MME).[22] This is expected since during sonication, the material is strongly interacting with the solvent and it is subjected to strong mechanical stress due to the collapse of bubbles and voids in the liquid, which

ultimately break the flakes into smaller pieces: overall the process may produce considerable changes in the Raman peaks, which could be related to structural changes, but also doping, solvent residuals, and re-stacking.

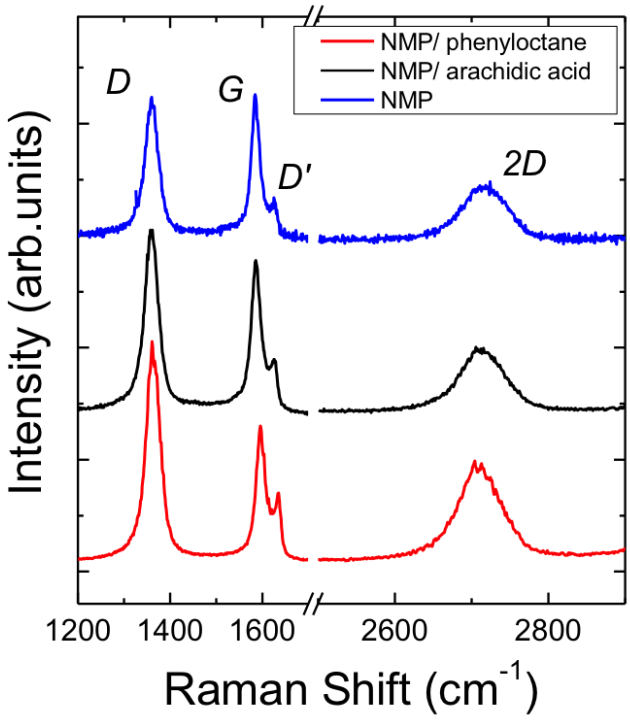

Figure 6.13. Typical Raman spectrum of graphene produced in NMP, NMP/arachidic acid and NMP/ phenyloctane. The single peak shape of the 2D peak indicates that the flake is a single-layer.

Figure 6.13. shows the typical Raman spectra obtained from the NMP/aliphatic dispersions as compared to NMP-based dispersions. The first order Raman spectrum of LPE graphene is characterized by the G and D peak, at about 1580 and 1350 cm^{-1}, respectively. While the D peak is usually not visible in the Raman spectrum of MME graphene, this features is always observed in LPE graphene and it is attributed to its edges,[2, 23] which acts as "defects" in the Raman scattering process.[6] Noteworthy, the D peak intensity increases with decreasing size of the flakes[3] (typically smaller than the size of the laser beam) and it also depends on the excitation energy.[24] Therefore comparisons between different Raman spectra of LPE graphene

should be done with care, and statistical analysis of intensities of both G and D peaks should be performed. For example in our case, although the D peak in Figure 6.13. looks very strong, as compared to the G peak intensity, by performing statistical analysis (Figure 6.14) is possible to observe that for the NMP dispersions prepared in the presence of additional molecules, the intensity ratio between D and G peak intensity, I(D)/I(G), can change considerably from flake to flake (between 1 and 2.4). The average I(D)/I(G) obtained for NMP dispersions is 1.6, showing that the dispersions are of comparable quality. This will be further confirmed by electrical measurements.

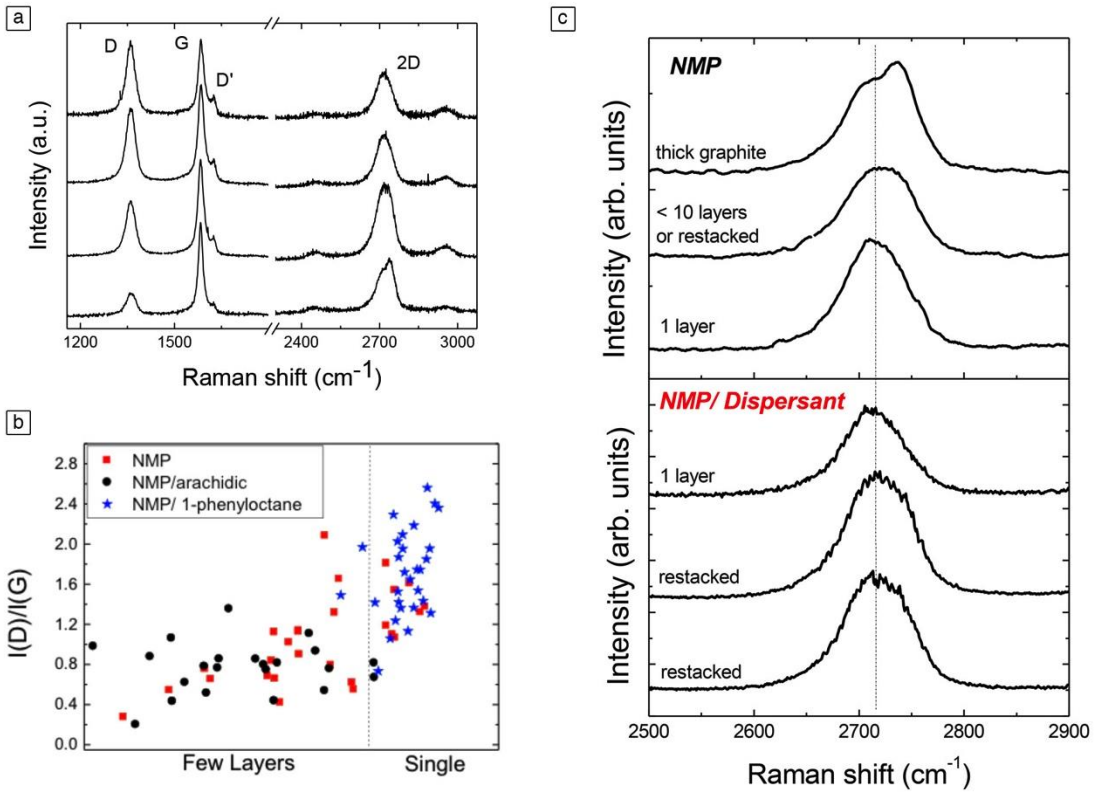

Figure 6.14. a) Raman spectra (measured at 2.41 eV) of the flakes obtained from the graphene/NMP dispersion b) ID/IG ratio analysis of three graphene dispersions, and c) Typical 2D peaks observed in graphene/NMP dispersion

The second order Raman spectrum is very important because it allows qualitative identification of the thickness of the flakes through the 2D peak shape:[21] in the case of MME graphene, a single layer has a single and intense peak, while few layers are composed by at

least 2 broad components for AB stacking. However, in the case of graphene-based dispersions, the 2D peak can also assume complex lineshapes due to re-aggregation and folding. This can also affect the 2D peak intensity, making the Raman spectrum very different from the one of MME graphene.[2] Therefore, one can only distinguish between three cases: single-layers, AB thick flakes (i.e. graphite residuals) and thin flakes (with or without AB stacking). Thus, we compared the Raman spectra measured on 30-40 flakes of the dispersions obtained with and without the dispersing agent. While the first order Raman spectra did not show strong differences, we observed a different 2D peak shape distribution between the dispersions: thick AB stacked flakes have been rarely observed in the NMP/dispersing agent (either arachidic acid or phenyloctane), as compared to the NMP dispersion (see Figure 6.14.). This provides unambiguous proof that the dispersing agent plays a key role in the exfoliation mechanism (i.e. in breaking the multilayered pieces of graphite), thereby increasing the overall yield. Furthermore, Raman spectroscopy shows that the addition of dispersion-stabilizing compounds does not affect the quality and structure of graphene, as compared to the use of NMP alone since there are no major changes in the first order Raman spectrum (Figure 6.13.). From the analysis on the 2D peak shape one can qualitatively estimate the thickness composition of the flakes in suspension: we found that overall the percentage of single-layers graphene amounts to ~ 30% and ~ 40% for NMP/arachidic acid and NMP/1-phenyloctane dispersion, respectively. The rest of the material is composed by thin flakes (<10 layers), probably mostly re-aggregated MLG flakes, since AB stacking was never observed. This result is only qualitative as re-aggregation can happen after deposition of the material on the substrate. However, in first approximation, this analysis can be used for a first quantitative comparison between the quality and composition of different dispersions. In fact the results obtained by Raman are in good agreement with HR-TEM analysis (Figure 6.11.).

6.4.9 Electrical properties

To probe the electrical properties of the graphene exfoliated with and without dispersing agents, devices were prepared by drop-casting NMP dispersions onto dielectric substrates exposing pre-patterned interdigitated gold electrodes with variable channel length. Prior to the

drop cast of graphene, the SiO_2 surfaces were treated with either hexamethylsilazane (HMDS) or octadecyltrichlorosilane (OTS) in order to evaluate the impact of the surface wettability on the electrical performances. The sheet resistance, Rs was extracted from the two-terminal I-V traces after taking into account the actual inter-electrode area coverage. The channel coverage, typically within 6 and 20% of the total area, was estimated by optical microscope on each single device and the effective W was consistently employed in the sheet resistance determination. Drop-casting of solutions was employed as the deposition method because it is the closest to real ink-jet printing or roll-to-roll processes which allow mass production of large-area and low-cost electronics.

After the dispersion deposition on the test devices, a first set of measurements was recorded upon annealing samples at 45 °C for 2 days in order to get rid of residual solvent. However, the electrical characterization revealed high and inhomogeneous sheet resistance values which we ascribed to the presence of residual NMP in the film (see Figure 6.15 for details). This intuition was experimentally verified by a 100 - fold current increase upon annealing of the samples at 415°C overnight. Hence, the latter is a key step in order to gain a deep understanding on the transport properties, as the presence of residual NMP could be strongly detrimental for the conduction while not providing a reliable estimate of the electrical properties of the materials under test.

Figure 6.15a shows the lowest resistance measured in the 16 devices in every chip with different exfoliating agent and surface treatment. We found that the sheet resistance depends not only on the coverage but also on the concentration of the graphene flakes in the channel. When an OTS self-assembled monolayer was formed on silicon oxide, the drop-casted graphene solutions had greater tendency to sit on the gold electrodes resulting in a higher density of material between the electrodes when compared to the HMDS surface case, resulting in a typically lower average sheet resistance (see Table 5.1.3 for contact-angle measurements).

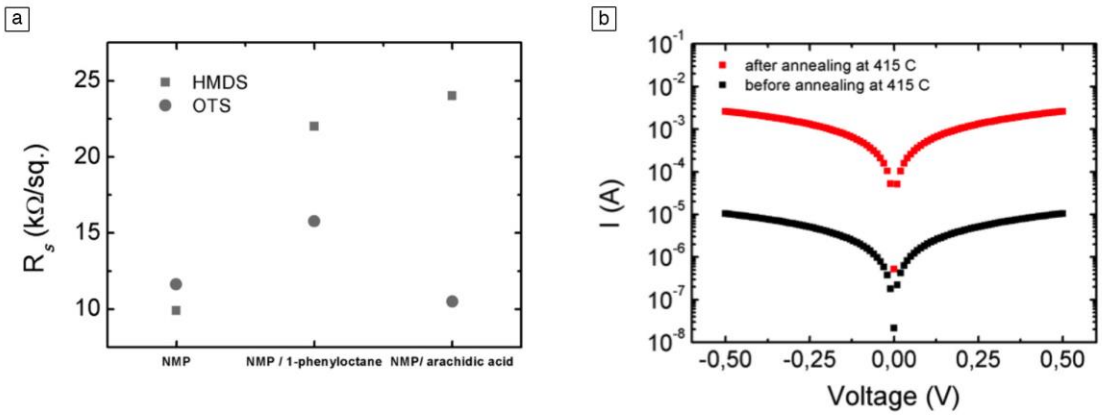

Figure 6.15. a) Comparative values of sheet resistance (R_s) for graphene with different exfoliating agents on OTS (circles) and HMDS (squares) treated substrate. Plotted values represent the lowest measured resistance in the device in every chip. The values were corrected for coverage as the actual channel width (W_{eff}) was found to be lower than the nominal channel width of the electrodes (W). b) Current-voltage curves after and before the annealing cycle at 415 °C. The curves were measured on the same device [L = 2.5 μm, W_{eff} = 800 μm, R_s was 71 kΩ after annealing at 415 °C].

Sample	SiO_2	SiO_2/HMDS	SiO_2/OTS	SiO_2/OTS after annealing @450 °C
Contact-angle [˚]	27.4 ± 0.16	33.6 ± 0.13	62.5 ± 0.18	27.6 ± 0.23

Table 5.1.3. Contact-angle data

The absolute values were found to fall in the 10 - 25 kΩ sq^{-1} range over several batches and roughly - fold larger than in common CVD - grown graphene. This behavior is somehow expected if one considers that the injected charges undergo flake-to-flake percolation in order to be collected at the other electrode. The flake-to-flake charge hopping could be clearly more detrimental for charge transport than in the case of a continuous layer with a few defects (CVD - graphene) where charges do not need to hop from a flake to another.

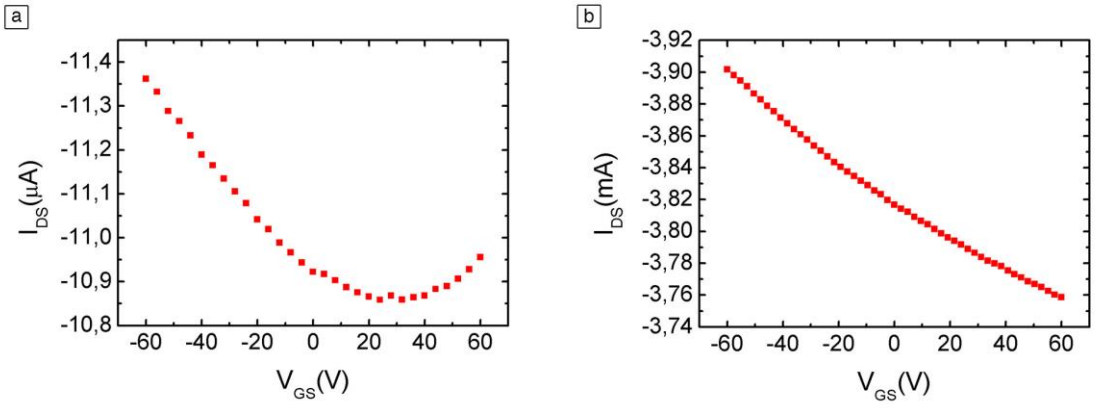

Figure 6.16. Representative transfer curves showing a marked Dirac point a) before annealing at 415 °C and b) p-type doping after annealing at 415 °C.

In addition, in order to quantify field-effect mobility the three different materials were characterized in Si-n^{++}/SiO2 test patterns with the possibility of applying an additional (gate) voltage. Before the annealing at 415°C, the FET devices showed ambipolar behavior with a clear Dirac point in the transfer curves (see Figure 6.16a). After annealing at 415°C, the graphene dispersion resulted p-doped with no clear Dirac point, which can be ascribed to reappearance of the silanol groups after the annealing of the OTS and HMDS SAMs at such high temperatures. It has been widely reported that the Si-OH groups act as efficient electron traps. In this case, the mobilities extracted from the transfer curves were found to range between 0.3 and 1 $cm^2\ V^{-1}\ s^{-1}$. (See Figure 6.17) These mobilities are in good agreement with those recently reported on devices integrating LPE-graphene deposited by means of a more cumbersome method such as Langmuir-Blodgett. The Ion/Ioff ratio was always found to be below 2, further indicating that LPE, likewise scotch-tape and CVD-grown graphene, could be best exploited to fabricate electrodes for electronics applications rather than acting as the active layer in FET devices.

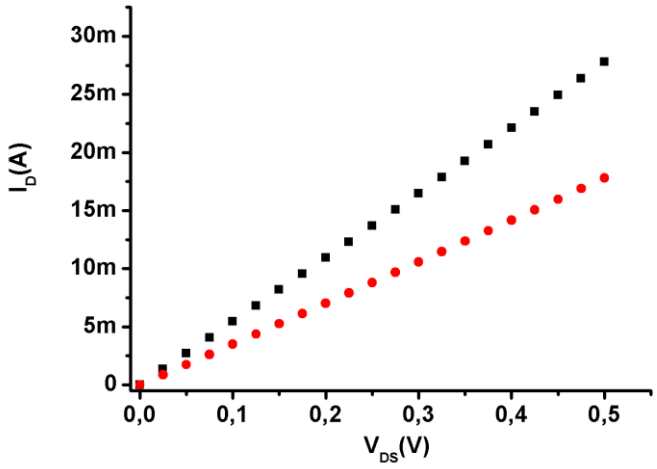

Figure 6.17. Comparative (I_D -V_{DS}) curves traced at V_{GS} = 7 V for graphene with (red circles) and without (black squares) arachidic acid used as the intercalating compound. The curves were corrected for coverage as the actual channel width, W_{eff}, was found to be lower than the channel width of the electrodes, W. These curves were recorded on devices having the same channel length (L = 2.5 μm).

6.5 Conclusion

We demonstrated that by mastering a supramolecular approach it is possible improve the yield of graphene exfoliation in an up-scalable LPE-based method to produce high-quality graphene flakes from powdered graphite. By using a molecular module possessing high affinity for the graphite surface as dispersion-stabilizing agent, high concentration dispersions of graphene were obtained. Our exfoliation protocol is effective: graphitic AB stack flakes were rarely observed by Raman spectroscopy. Notably, the latter technique revealed that the addition of the simple alkane (i) does not affect the quality and structure of graphene, as compared to the use of NMP alone, highlighting the non-invasive nature of our procedure, and (ii) leads to an increase the percentage of mono- and bilayer graphene flakes. In particular, by using 1-phenyloctane as dispersion-stabilizing agent the amount of MLG increases by ca. 10% and graphene concentration increases of 25%, with respect to graphene exfoliated in pure NMP. Conversely the addition of arachidic acid resulted in slightly lower increase of percentage of MLG and 50% increase of concentration. The LPE processed graphene dispersion was shown to be conductive ink. Our approach opens up new avenues for the technological applications of our graphene ink as low-cost electrodes and conducting nanocomposite for electronics.

6.6 References

1. M. Lotya, Y. Hernandez, P. J. King, R. J. Smith, V. Nicolosi, L. S. Karlsson, F. M. Blighe, S. De, Z. M. Wang, I. T. McGovern, G. S. Duesberg and J. N. Coleman, *J. Am. Chem. Soc.*, 2009, **131**, 3611-3620.
2. A. A. Green and M. C. Hersam, *Nano Lett*, 2009, **9**, 4031-40310.
3. X. H. An, T. J. Simmons, R. Shah, C. Wolfe, K. M. Lewis, M. Washington, S. K. Nayak, S. Talapatra and S. Kar, *Nano Lett*, 2010, **10**, 4295-4301.
4. X. Y. Zhang, A. C. Coleman, N. Katsonis, W. R. Browne, B. J. van Wees and B. L. Feringa, *Chem Commun*, 2010, **46**, 7539-7541.
5. A. Schlierf, H. Yang, E. Gebremedhn, E. Treossi, L. Ortolani, L. Chen, A. Minoia, V. Morandi, P. Samorì, C. Casiraghi, D. Beljonne and V. Palermo, *Nanoscale*, 2013, **5**, 4205-42110.
6. H. Yang, Y. Hernandez, A. Schlierf, A. Felten, A. Eckmann, S. Johal, P. Louette, J. J. Pireaux, X. Feng, K. Müllen, V. Palermo and C. Casiraghi, *Carbon*, 2013, **53**, 357-365.
7. S. Sampath, A. N. Basuray, K. J. Hartlieb, T. Aytun, S. I. Stupp and J. F. Stoddart, *Adv. Mater.*, 2013, **25**, 2740–2745.
8. A. B. Bourlinos, V. Georgakilas, R. Zboril, T. A. Steriotis, A. K. Stubos and C. Trapalis, *Solid State Commun.*, 2009, **149**, 2172-21710.
9. F. Liu, J. Y. Choi and T. S. Seo, *Chem Commun*, 2010, **46**, 2844-28410.
10. L. L. Chua, J. Zaumseil, J. F. Chang, E. C. W. Ou, P. K. H. Ho, H. Sirringhaus and R. H. Friend, *Nature*, 2005, **434**, 194-199.
11. Y. T. Liang and M. C. Hersam, *J Am Chem Soc*, 2010, **132**, 17661-17663.
12. L. Xu, J.-W. McGraw, F. Gao, M. Grundy, Z. Ye, Z. Gu and J. L. Shepherd, *J. Phys. Chem. C*, 2013, **117**, 10730-10742.
13. S. De Feyter and F. C. De Schryver, *Chem. Soc. Rev.*, 2003, **32**, 139-150.
14. A. Ciesielski, C.-A. Palma, M. Bonini and P. Samorì, *Adv. Mater.*, 2010, **22**, 3506-3520.
15. K. S. Mali, J. Adisoejoso, E. Ghijsens, I. De Cat and S. De Feyter, *Accounts Chem Res*, 2012, **45**, 1309-1320.
16. A. Ciesielski and P. Samorì, *Nanoscale*, 2011, **3**, 1397-1410.
17. J. P. Rabe and S. Buchholz, *Science*, 1991, **253**, 424-427.
18. M. Hibino, A. Sumi, H. Tsuchiya and I. Hatta, *J. Phys. Chem. B*, 1998, **102**, 4544-4547.
19. L. K. Thomas, A. Kühnle, S. Rode, U. Beginn and M. Reichling, *J. Phys. Chem. C*, 2010, **114**, 18919-18924.
20. A. C. Ferrari, J. C. Meyer, V. Scardaci, C. Casiraghi, M. Lazzeri, F. Mauri, S. Piscanec, D. Jiang, K. S. Novoselov, S. Roth and A. K. Geim, *Phys. Rev. Lett.*, 2006, **97**.
21. C. Casiraghi, in *Spectroscopic Properties of Inorganic and Organometallic Compounds: Techniques, Materials and Applications, Volume 43*, The Royal Society of Chemistry, 2012, vol. 43, pp. 29-510.
22. M. Lazzeri, S. Piscanec, F. Mauri, A. C. Ferrari and J. Robertson, *Phys. Rev. B*, 2006, **73**.

23. C. Casiraghi, A. Hartschuh, H. Qian, S. Piscanec, C. Georgi, A. Fasoli, K. S. Novoselov, D. M. Basko and A. C. Ferrari, *Nano Lett.*, 2009, **9**, 1433-1441.
24. A. Eckmann, A. Felten, I. Verzhbitskiy, R. Davey and C. Casiraghi, *Phys. Rev. B*, 2013, **88**, 035426-035437.

Chapter 7 Unraveling the role of functional groups

7.1 Introduction

To promote the exfoliation of graphite in the sonication process, organic molecules can be used, in particular molecules having a high energy of adsorption on the graphene surface. These so-called surface-stabilizing agents should exhibit higher adsorption energy than the one of the solvent interacting with graphene. In fact, the solvent dictates the choice of surfactants. For example exfoliation in water is not possible due to the hydrophobic nature of the graphene sheets and its high surface tension, but by adding charged molecules as pyrenes, linear chain surfactants or polymers exfoliation could be performed. However, the use of water is not recommended for certain types of applications in opto-electronics like field-effect transistors. Therefore, organic solvents have been tested in the presence of surface-stabilizing agents. Recently, it has been shown that LPE of graphene in NMP can be assisted by the use of porphyrins [1], lignin molecules derivatives [2], salt derivatives [3] and polymeric systems. Despite the increasing interest in the use of surfactants during the LPE of graphite in organic solvent, fundamental research is still required to get a full understanding over the role of the molecules during the LPE process and as stabilizers once the sheets have been exfoliated, ultimately identifying the best molecule(s) to promote the LPE process.

7.2 Scope

Here we show that the quantity and the quality of defect-free, few layer thick graphene dispersions in NMP can be increased by addition of a long linear alkane decorated with four different functions, i.e. amine, alcohol, carboxylic acid and alkyl. In particular, we explore the role of these functional groups by focusing our attention on four docosane derivatives: docosane, docosan-1-amine, docosanoic acid and docosanol (Scheme 7.1). Since these molecules possess a long aliphatic chain, they will have tendency to adsorb to the graphite/graphene surface forming tightly packed crystalline lamellar structures. These molecules, except docosane, are equipped with functions known to form hydrogen-bonded dimers in a majority of organic solvents, which results in the formation of stable supramolecular structure on graphite surface. Such a comparative study will make it possible to cast further light onto the role of thermodynamics of self-assembly on graphene as a route to promote it exfoliation in liquid media.

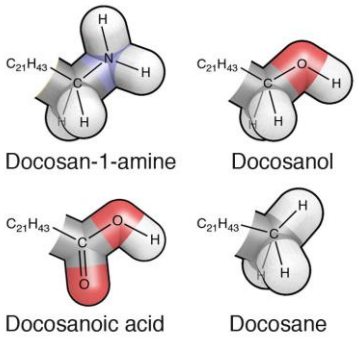

Scheme 7.1. Chemical structures of investigated heneicosane derivatives.

7.3 Experimental

7.3.1 Materials

N-methyl-2-pyrrolidinone (NMP - product number (p.n.) 332461), was purchased from Sigma-Aldrich and used as solvent for the exfoliation. Graphite powder (p.n. 332461) was also acquired from Sigma-Aldrich and used without further treatment. docosanoïc acid (p.n. 216941), docosanol (p.n. 169102), docosane (p.n. 43942) were purchased from Sigma-Aldrich and used as surface stabilizing agent. 1-phenyloctane (p.n. 113190) purchased from Sigma-Aldrich and highly oriented pyrolitic graphite (HOPG, grade ZYH) was used for scanning tunneling microscopy measurements. All chemicals were used as received, i.e. without purification.

7.3.2 Synthesis of docosan-1-amine

The compound was prepared in 77% yield over three steps from 1-docosanol according to a modification of the procedure of Sugandhi and coworkers. [5-6]

7.3.3 Preparation of graphene

Graphite flakes were sonicated for 6 h at 50 ± 2 °C (100 W) in the chosen solvents, keeping the graphite weight percent constant, i.e. 1 wt %. The temperature was kept constant to 50 °C by using a thermal controller and a cooling coil during sonication. Since the ratio between graphite powder and the solvent was kept constant, different masses of graphite flakes have been used. To remove the large numbers of macroscopic aggregates of graphite, centrifugation (Eppendorf 5804, rotor F-34-6-38, 30 min at 10 000 rpm) was performed. 3 mL of graphene dispersions were pipetted for each molecules, and a homogeneous dark phase was obtained.

7.3.4 Characterizations

The amount of exfoliated graphene was measured on a Cubis Ultramicro-Balance MSA2.7S-000DM using a membrane holder. The filters were weighted 5 times before and after the filtration process in order to average the mass of graphene. Dispersions were first transferred in 10 mm path length quartz cuvette and analyzed by means of UV-vis-IR absorption spectroscopy using a Jasco V670 spectrophotometer equipped with a Peltier thermostated cell holder at 20 ± 0.05°C.

A mother solution of each molecule in Scheme 1 was dissolved in chloroform and diluted with 1-phenyloctane to give 20 mM solutions for docosanoic acid and docosanol, and 50 mM solution for docosane and docosan-1-anime. Solutions were heat over night at 80 °C to better dissolve the molecules. STM imaging was carried out in constant height mode without turning off the feedback loop, to avoid tip crashes. 2D pattern formation was achieved by applying 4 µL of a warm solution onto freshly cleaved HOPG. The STM images were recorded at room temperature once a negligible thermal drift was achieved.

7.4 Results and discussion

7.4.1 Scanning tunnelling microscopy

To fully understand the effect of the head group attached at the end of the docosane chain on the molecular self-assembly on graphite, we used STM at the solid-liquid interface to investigate the physisorbed monolayers. This comparative study was performed by applying a drop of a 20 mM solution of each derivative in 1-phenyloctane onto freshly cleaved HOPG. Because of its high dielectric constant, the NMP solvent employed for LPE process cannot be used to perform STM measurements. The molecules were all found to pack forming lamellar crystalline patterns (Figure 7.1), use characteristic parameters are reported in Table 7.1.

C22 derivative	Chemical formula	*a* (nm)	*b* (nm)	*α*	A_{uc} (nm^2)	n_{uc}	A_{mol}
CH₃	$C_{21}H_{43}$-CH_3	0.4 ± 0.1	3.1 ± 0.1	(90 ± 2)°	1.2 ± 0.2	1	1.2 ± 0.2
NH₂	$C_{21}H_{43}$-CH_2NH_2	0.4 ± 0.1	10.1 ± 0.1	(86 ± 2)°	1.2 ± 0.2	2	1.3 ± 0.2
COOH	$C_{21}H_{43}$-COOH	0.9 ± 0.1	3.1 ± 0.1	(88 ± 2)°	2.8 ± 0.2	2	1.4 ± 0.1
OH	$C_{21}H_{43}$-CH_2OH	0.4 ± 0.1	10.0 ± 0.1	(88 ± 2)°	2.4 ± 0.2	2	1.2 ± 0.2

Table 7.1. Unit cell parameters of investigated carboxylic acids at the solid–liquid interface, **a* and *b* are the vector lengths and *α* the angle between those vectors; A_{uc} is the unit cell area, n_{uc} the number of molecules in the unit cell and A_{mol} (= A_{uc}/n_{uc}) is the area occupied by single molecules within the unit cell.

Initially we investigated the self-assembly of docosane. Figure 7.1a shows that it forms a monocrystalline lamellar structure at the graphite-solution interface. The interaction between CH_3 groups belonging to adjacent lamellae is of van der Waals type. The molecules are oriented 90° with respect to the main lamellar axis, they are physisorbed flat on the surface and do not exhibit interdigitation between molecules belonging to contiguous lamellae.

A similar packing has been also observed for docosan-1-amine (Fig. 7.1c), consisting of lamellar architectures with molecular lying flat on graphite and oriented at 90° from the lamella main axis. Also in this case, no interdigitation between molecules belonging to adjacent lamellae has been observed. The NH_2 groups exposed in the α-position interact via weak hydrogen bonds with analogue groups exposed on molecules belonging to the contiguous lamella.

Docosanoic acid also self-assembles flat on the graphite surface forming monocrystalline lamellar motifs exhibiting 90° between the molecule and lamella main axis (Figure 7.1e). The molecules forms H-bonded dimers, which are interdigitated between adjacent lamellae, in accordance with previous observations on carboxylic acids.

Docosanol physisorbed flat on HOPG forming lamellae, but in this case the OH groups (forming weak H-bonds between molecules belonging to adjacent lamellae) dictates the 60° between the molecule and lamella main axis as a result of the geometry of the non-covalent interaction (Figure 7.1g).

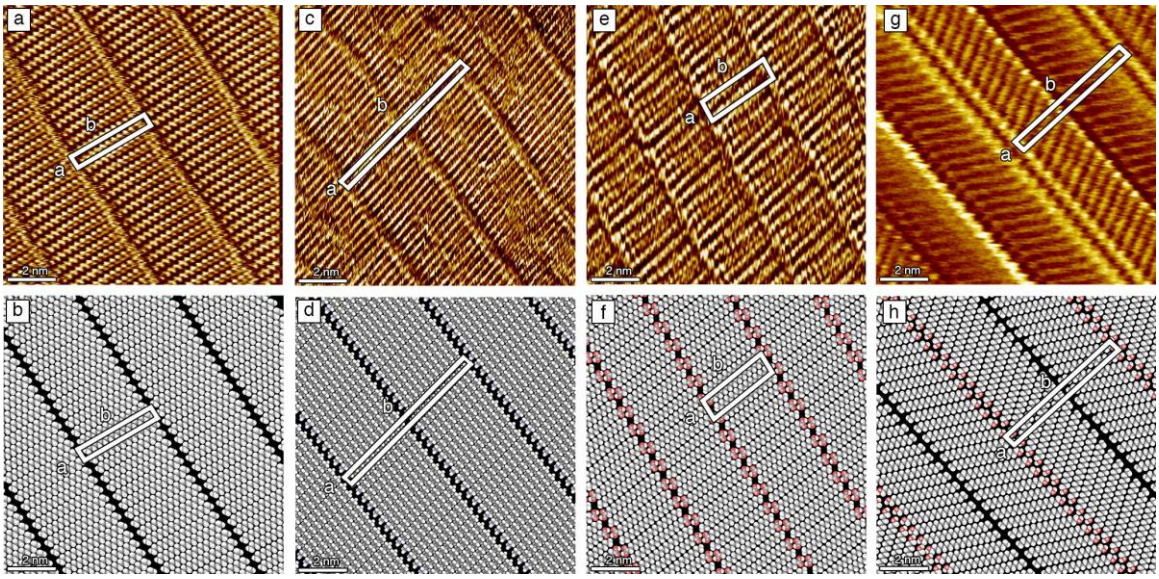

Figure 7.1. STM current images of monocrystalline lamellar structures, as well as proposed molecular packing models, obtained from (a-b) ***docosane***, (c-d) ***docosan-1-amine***, (e-f) ***docosanoic acid*** and (g-h) ***docosanol***. Tunneling parameters: average tunneling current (I_t) = 20 pA, tip bias voltage (V_t) = 350 mV.

The unit cells parameters reported in Table 7.1 are in good agreement with previous reports.[7-8] Interestingly, the self-assembled monolayers of all these derivatives with different functions can be also formed at the CVD graphene/solution interface, showing poorly resolved 2D patterns. One reason for the poor resolution is the fact that CVD graphene grown on copper were used, and the surface of these samples is not perfectly flat which is a required condition for a good molecular resolution.

7.4.2 Liquid-phase exfoliation

In order to test the ability of these four molecules to increase the yield of exfoliation if graphene, we have prepared dispersions by adding graphite powder in NMP and sonication in ultrasound bath in the presence of the four molecules in Scheme 1 as dispersion-stabilizing agents. These four dispersions have been compared to the blank experiment, i.e. graphene without dispersion-stabilizing agents. The theoretical number of molecules needed to cover the entire surface on graphene was calculated by knowing the area of graphite occupied by each molecules type (as revealed by STM). Also the initial graphite powder was

hypothetically considered as a single sheet on which molecules can adsorb on both phase. The number of molecules needed to form densely packed monolayers on graphene would be higher than the real surface of graphite powder; different percentages of molecules were therefore tried (2.5%, 5%, 7.5 %, 10%, 15% and 20%). After sonication and centrifugation step, homogeneous dark dispersions were obtained and characterized by UV-vis-IR absorption spectroscopy (see Figure 7.3.).

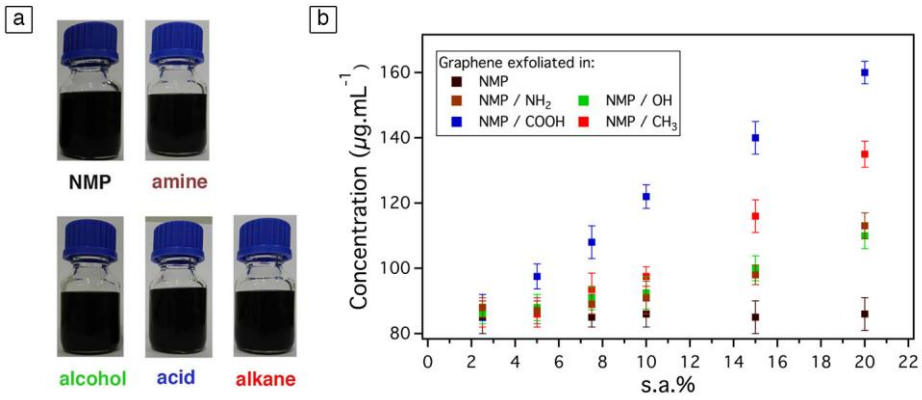

Figure 7.2. a) Photographs of graphene dispersions prepared by exfoliation of graphite flakes in NMP, in the presence/absence of surfactant molecules at 20 s.a. %; b) Average concentration of graphene dispersions after the filtration process. The error bars correspond to the different values obtained in 10 independent experiments.

In order to quantify the amount of graphene present in the dispersions, a mixture of graphene dispersion and chloroform was annealed up to 50 °C for 30 min and filtered through PTFE membrane (pore size 100 nm). The remaining solvent and C21 derivative molecules were washed three times with diethyl ether and chloroform. Careful measurements of the filtered mass gave the final concentration of graphene in dispersions.

By analyzing 10 independent experiments, we found that when exfoliation is performed in the absence of dispersion-stabilizing agents (called blank experiment), comparable concentrations of graphene were observed with NMP (86 ±10 μg mL^{-1}). The graphene-dispersed concentrations reported in this work are in good agreement with those previously reported using the same experimental set-up.

Then, we extended our LPE studies by using heneicosane derivatives as dispersion-stabilizing agents (Scheme 7.1). Interestingly, we found that the concentration of graphene prepared in

NMP in the presence of these molecules increases almost linearly with the number of *ad-hoc* molecules (s.a.%) and the highest concentrations were found at 20 s.a.%. Noteworthy, the most significant increase in graphene concentration is obtained by using docosanoic acid molecules, where it amounts to 160 μg mL^{-1}. This latter corresponds to nearly 100% increase in the yield of exfoliation, when compared to samples prepared in pure NMP (86 μg mL^{-1}). Surprisingly, the use of docosane molecules leads to 135 μg mL^{-1} of graphene, which is more concentrated than exfoliation with docosanol and docosan-1-amine molecules (109 μg mL^{-1} and 112 μg mL^{-1} respectively). These results demonstrate that the use of carboxylic acids as dispersion-stabilizing agents leads to a significant increase in the yield of exfoliation.

7.4.3 UV-Vis-IR spectroscopy

All dispersions were also characterized by UV–vis–IR absorption spectroscopy. The spectra are as expected being featureless in the visible – IR region. Each of these dispersions was diluted a number of times and the absorption spectra recorded. The absorbance (660 nm) divided by cell length is plotted versus concentration. A Lambert – Beer behavior was observed for all samples (See Figure 7.3).

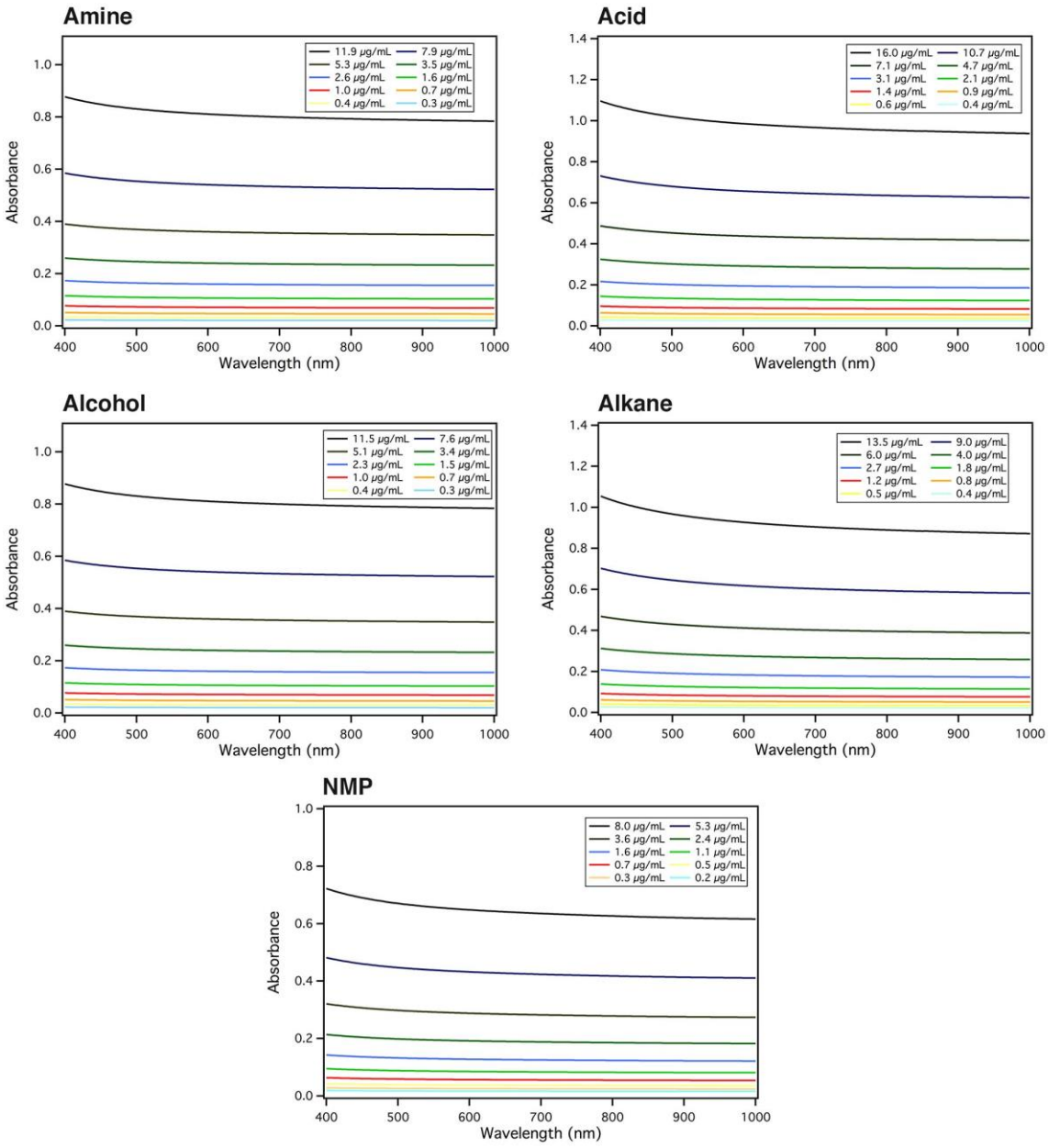

Figure 7.3. UV–Vis spectra of graphene dispersion in NMP in the presence/absence of dispersing-stabilizing agents at different concentrations for 20 s.a. %.

7.4.4 HR-TEM

HR-TEM was exploited to gain qualitative information and many relevant details such as the percentage of single-layer graphene (SLG) flakes, the lateral size of the flakes and the presence/absence of defects. In particular the analysis of the folded edges of the graphene sheets was used to estimate the number of layers composing the flakes. First, we focused our attention on dispersion prepared in NMP in the absence of the dispersion-stabilizing agents. The TEM micrographs revealed that the majority of dispersions are composed by a large fraction of bilayer graphene sheets folded over themselves, with lateral sizes < 0.8 μm, as typically observed for LPE graphene. We mainly focused our attention on the characterization of graphene dispersion exfoliated with 20 s.a.% of molecules. In terms of the lateral size of LPE graphene, no major differences were observed between the blank sample and graphene exfoliated in the presence of the different docosane molecules, with a majority of flakes having a size of 200 nm. Moreover, the HR-TEM analysis allowed us to define the number of layers of the graphene sheets, which is estimated ranging between 1 – 3 layers for docosan-1-amine, docosanoic acid and docosane, and between 2 – 4 layers for docosanol. The statistical analyses of the graphene sheet thickness and lateral flake size are reported in Figures 7.4a and 7.4c, respectively.

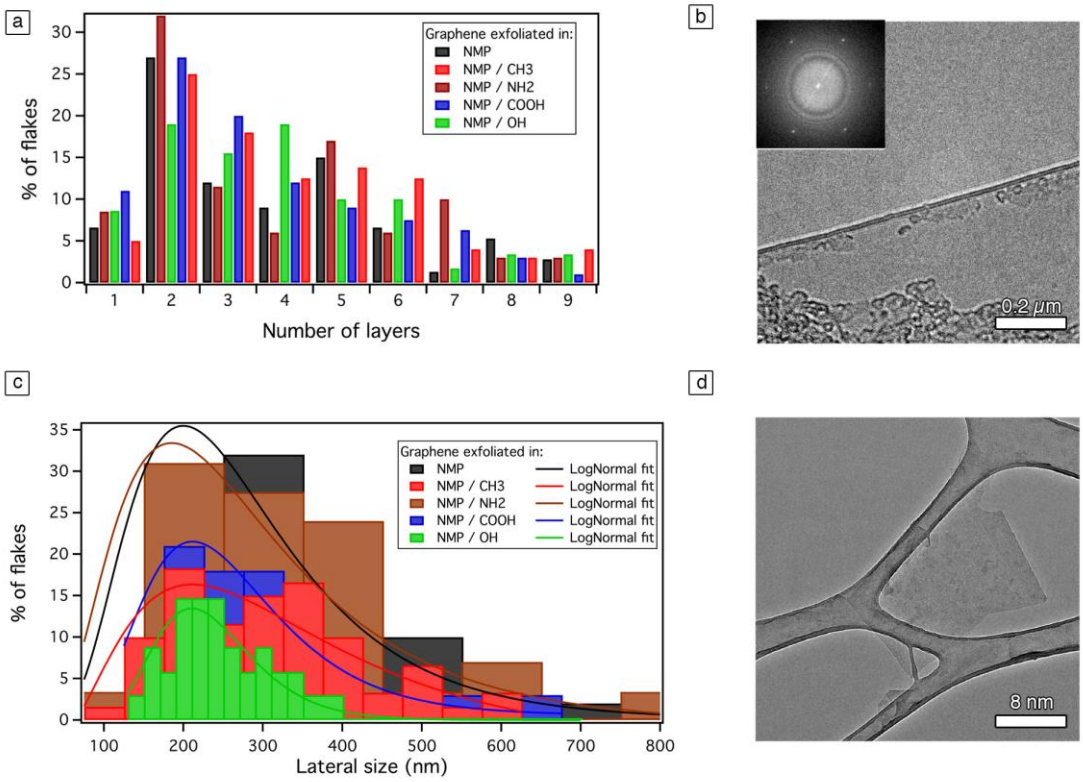

Figure 7.4. Statistical analyses of HR-TEM results of graphene exfoliated in pure NMP and in NMP in the presence of *docosane, docosan-1-amine, docosanoic acid* and *docosanol* molecules. (a) Histogram of the distribution of the flake thickness. (b) HR-TEM micrograph of the edge of a monolayer and elative fast Fourier transform (FFT), showing the typical hexagonal pattern from graphene/graphite lattice at 0.21 nm. (c) Histogram of the lateral flake size distribution. The fitting of the distribution has been obtained with a LogNormal distribution. (d) TEM micrograph of a monolayer.

7.5 Conclusion

In conclusion, we have demonstrated that by mastering the self-assembly of *ad-hoc* molecules on the graphene surfaces, in a process operating under thermodynamic control, it is possible to improve the yield of exfoliation of graphite in liquid media. This finding was attained by unraveling the interplay of molecule-graphene, molecule-molecule, solvent-substrate and solvent-molecule interactions. We used equally long linear alkanes as dispersion-stabilizing agents during the liquid phase exfoliation of graphene, and we found a dependence of the yield of exfoliation on type of head group exposed at the end of the alkane chain. In our comparative study, simple yet chemically representative head groups have been chosen

including methyl, carboxylic acid, amine and alcohol. Our investigation revealed that the yield of exfoliation (i) scales with the strength of the H-bond formed between the head groups, and (ii) increase linearly with the s.a.%. The most effective exfoliation was obtained with docosanoic acid molecules at 20 s.a.% in NMP, with a concentration of exfoliated graphene of 160 μg mL^{-1} that corresponds to a nearly 100% increase in exfoliation yield when compared to samples prepared in pure NMP (85 μg mL^{-1}). Furthermore, a remarkable increase of single-layer graphene (SLG) flakes was observed in some cases with TEM

7.6 References

1. J. Malig, A. W. I. Stephenson, P. Wagner, G. G. Wallace, D. L. Officer and D. M. Guldi, *Chem Commun*, 2012, **48**, 8745-8747.
2. W. Liu, R. Zhou, D. Zhou, G. Ding, J. M. Soah, C. Y. Yue and X. Lu, *Carbon*, 2015, **83**, 188-197.
3. C. Yeona, S. J. Yuna, K. S. Lee and J. W. Lim, *Carbon*, 2015, **83**, 136-143.
4. S. Haar, A. Ciesielski, J. Clough, H. F. Yang, R. Mazzaro, F. Richard, S. Conti, N. Merstorf, M. Cecchini, V. Morandi, C. Casiraghi and P. Samorì, *Small*, 2015, **11**, 1691–1702.
5. E. W. Sugandhi, R. V. Macri, A. A. Williams, B. L. Kite, C. Slebodnick, J. O. Falkinham, A. R. Esker and R. D. Gandour, *J Med Chem*, 2007, **50**, 1645-1650.
6. W. Q. Lin, X. M. Zhang, H. Ze, J. Yi, L. Z. Gong and A. Q. Mi, *Synthetic Commun*, 2002, **32**, 3279-3284.
7. L. Giancarlo, D. Cyr, K. Muyskens and G. W. Flynn, *Langmuir*, 1998, **14**, 1465-1471.
8. M. Hibino, A. Sumi, H. Tsuchiya and I. Hatta, *J Phys Chem B*, 1998, **102**, 4544-4547.
9. T. Yang, S. Berber, J. F. Liu, G. P. Miller and D. Tomanek, *J Chem Phys*, 2008, **128**.

.

Chapter 8 Unraveling the role of the length of fatty acids

8.1 Introduction

As the potential applications of graphene multiply, being able to produce defect-free graphene in large quantities in up-scalable ways is becoming more and more important. While small-molecule assisted graphite LPE has been widely investigated in water, only a few examples have been reported so far on the use *ad hoc* molecules in organic media [1-4]. In recent years, it has been shown that graphene dispersions can be prepared in NMP with the aid of nonionic porphyrin molecules [5], modified polyethyleneglycol [6], and oligothiophene-terminated polyethyleneglycol [7], and more recently with the use of polymeric systems [8, 9]. However, the fundamental yet extremely important question of what makes a molecule a good candidate to promote the LPE of graphite remains open.

Self-assembly of molecular building blocks at the solid-liquid interface relies on a subtle interplay between molecule–molecule, molecule–substrate, molecule–solvent, and solvent–substrate interactions leading to the targeted 2D nanopatterns [10]. The use of small organic molecules such as dispersion-stabilizing agents is expected to promote the exfoliation of graphite when the chosen molecules have a strong affinity for the basal graphitic planes and stronger than that of the solvent molecules interacting with graphene. A good starting point can be the use of alkanes which are known to exhibit a high affinity for the surface of graphite/graphene [11]. In this framework, it has been very recently demonstrated that arachidic acid can be successfully exploited to promote the exfoliation of graphene in NMP [12]. Such a finding opened the question on the optimal design of the fatty acid to assist the exfoliation, for

example on the role of the length of aliphatic side chain. In fact, surfactants stabilize exfoliated graphene in water and organic solvents, where the ζ potential of the surfactant-coated graphene nanosheets controls the dispersed concentration [13].

8.2 Scope

Here we show that both the quantity and the quality of defect-free, few layer thick graphene dispersions in four different solvents, i.e. N-Methyl-2-pyrrolidone (NMP), *ortho*-dichlorobenzene (*o*-DCB), 1,2,4-trichlorobenzene (TCB) and N,N-Dimethylformamide (DMF) can be increased by the addition of linear alkanes exposing a carboxylic acid head group. In particular, we explore the role of the length of the alkane chain by focusing our attention on five linear modules, i.e. hexanoic acid (***C6***), lauric acid (***C12***), stearic acid (***C18***), lignoceric acid (***C24***) and melissic acid (***C30***) (Scheme 8.1), whose different adsorption energies on graphene and marked tendency to form tightly packed crystalline self-assembled monolayers on such a surface are expected to play a major role during the LPE process. Alkanes and in particular carboxylic acids are one of the first molecules visualized with the sub-molecular resolution at the graphite–liquid interface by STM [5]. Among different α-functionalized alkanes, those equipped with carboxylic acid head group are of particular interest as they are known to form hydrogen-bonded dimers in majority of organic solvents, which results in the formation of extremely stable supramolecular structure on graphite surface. Scanning tunneling microscopy [7-9] at the solid-liquid interface using highly-oriented pyrolitic graphite as a model substrate was performed to test both the affinity and the self-assembly behavior of the various carboxylic-acid derivatives on graphene. Finally, the quality of the exfoliated graphene was quantitatively investigated by means of high-resolution transmission electron microscopy and Raman spectroscopy. Noteworthy, while many other groups focused their attention on LPE process using rather random molecular building blocks as surfactants/dispersion-stabilizers, none of them reported systematic studies in which the choice of molecules and their role during LPE is well explained. A comparative analysis like the one presented here is extremely important to gain a deeper understanding on the role of

dispersion-stabilizing molecules in the LPE of graphite, which can potentially result in shortening and simplifying the production of graphene for technological applications.

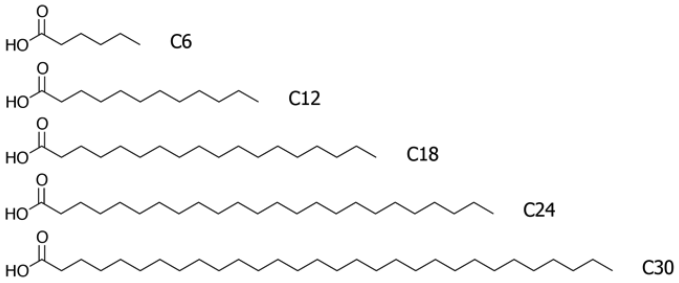

Scheme 8.1. Chemical structures of investigated carboxylic acid derivatives.

8.3 Experimental

8.3.1 Material

In a typical exfoliation process, N-methyl-2-pyrrolidinone (NMP - product number (p.n.) 332461), N,N-dimethylformamide (DMF, p.n. 33120), ortho-dichlorobenzene (o-DCB, p.n. 240664) and 1,2,4-trichlorobenzene (TCB, p.n. 256412) were purchased from Sigma-Aldrich and used as solvent for the exfoliation. Graphite powder (p.n. 332461) was also acquired from Sigma-Aldrich and used without further treatment. Hexanoic acid (p.n. 153745), lauric acid (p.n. L556), stearic acid (p.n. S4751), lignoceric acid (p.n. L6641) and melissic acid (p.n. 134805) were purchased from Sigma-Aldrich and used as surface stabilizer. 1-phenyloctane (p.n. 113190) purchased from Sigma-Aldrich and highly oriented pyrolitic graphite (HOPG, grade ZYH) was used for scanning tunneling microscopy measurements. All chemicals were used as received, i.e. without purification.

8.3.2 Preparation of graphene

In order to obtain graphene dispersions, graphite flakes were sonicated for 6 h at 40 ± 2°C (100 W) in the chosen solvents, keeping the graphite weight percent constant, i.e. 1 wt%. Since the ratio between graphite powder and the solvent was kept constant, different masses of graphite flakes have been used. Sonication of graphite powder led to grey liquid consisting of a homogeneous phase and large numbers of macroscopic aggregates. As previously reported, these aggregates can be removed by centrifugation (Eppendorf 5804, rotor F-34-6-38, 60 min at 8000 rpm), yielding a homogeneous dark dispersion.

8.3.3 Characterizations

XPS analyses were carried out on a Thermo Scientific K-Alpha X-ray photoelectron spectrometer with a basic chamber pressure of ~10^{-8} mbar and an Al anode as the X-ray source (x-ray radiation of 1486 eV). Spot sizes of 400 µm were used and pass energies of 200.00 eV for survey scans and 50.00 eV for high-resolution scans were used. 150 µL of dispersions were spin coated on Au substrate for 1 minutes at 1000 rpm and substrates were annealed for 1 day at 100°C in a oven under vacuum.

A mother solution of each carboxylic acid in Scheme 1 was dissolved in chloroform and diluted with 1-phenyloctane to give 20 mM solution. STM imaging was carried out in constant height mode without turning off the feedback loop, to avoid tip crashes. Monolayer pattern formation was achieved by applying 4 µL of a warm solution onto freshly cleaved HOPG. The STM images were recorded at room temperature once a negligible thermal drift was achieved.

8.4 Results and Discussion

8.4.1 Scanning tunneling microscopy

To achieve a full understanding of the self-assembly at the solid–liquid interface of the five carboxylic acids in Scheme 1, we performed a sub-molecularly resolved STM study of physisorbed monolayers on graphite. This comparative study was carried out by applying a drop of a 20 mM solution of each carboxylic acid in 1-phenyloctane onto freshly cleaved HOPG. Given that the solvent used for STM experiments has to be apolar (dielectric constant, ε = 2–4) and have a low vapor pressure, STM measurements cannot be performed by using the solvent commonly employed during liquid-phase exfoliation process, e.g. NMP has a dielectric constant of 31, thus 1-phenyloctane was chosen as a solvent. From the crystalline pattern obtained for each self-assembled monolayer on HOPG, the unit cell parameters, i.e. the length of the vectors *a* and *b*, the angle between the vector α, the unit cell area (A_{uc}), the number of molecules in the unit cell (n_{uc}), and the area occupied by a single molecule in the unit cell (A_{mol}, with $A_{mol} = A_{uc}/n_{uc}$), are given in table 8.1.

Acid derivative	Chemical formula	*a* (nm)	*b* (nm)	*α*	A_{uc} (nm^2)	n_{uc}	A_{mol}
C12	$CH_3(CH_2)_{10}COOH$	0.95 ± 0.2	1.81 ± 0.2	(90 ± 2)°	1.72 ± 0.24	2	0.86 ± 0.14
C18	$CH_3(CH_2)_{16}COOH$	0.94 ± 0.2	2.61 ± 0.2	(88 ± 2)°	2.45 ± 0.23	2	1.23 ± 0.09
C24	$CH_3(CH_2)_{22}COOH$	0.95 ± 0.2	3.36 ± 0.2	(90 ± 2)°	3.19 ± 0.22	2	1.59 ± 0.07
C30	$CH_3(CH_2)_{28}COOH$	0.95 ± 0.2	4.15 ± 0.2	(92 ± 2)°	3.94 ± 0.22	2	1.97 ± 0.05

Table 8.1. Unit cell parameters of investigated carboxylic acids at the solid–liquid interface. **a* and *b* are the vector lengths and *α* the angle between those vectors; A_{uc} is the unit cell area, n_{uc} the number of molecules in the unit cell and A_{mol} (= A_{uc}/n_{uc}) is the area occupied by single molecules within the unit cell.

Initially we investigated the self-assembly of hexanoic acid (***C6***) molecules, and as expected, ***C6*** molecules have not been found to form ordered monolayer at the HOPG-solution interface. Noteworthy, since the affinity of hexanoic acid to graphite surface is relatively low, this molecule (liquid) is commonly used as a solvent in STM measurements [11-15].

The STM current image in Figure 8.1a shows a monocrystalline lamellar structure of lauric acid (***C12***) molecules self-assembled on HOPG surface. In this 2D crystal, ***C12*** molecules are physisorbed flat on the surface adopting in-plane *zig-zag* conformation and forms H-bonded dimers, which are interdigitated between adjacent lamellae. Carboxylic acids exposing longer aliphatic chains showed similar self-assembly behaviors at the graphite-solution interface. Regardless of the length of the chain the observed monolayers of ***C18*** (Figure 8.1c), ***C24*** (Figure 8.1e), ***C30*** (Figure 8.1g), exhibit an akin motif consisting of lamellar structures, with molecules adopting in-plane *zig-zag* conformation and forming H-bonded dimers, which are interdigitated between adjacent lamellae. Furthermore, the comparison of the unit cell parameters of the various self-assembled monolayers (Table 8.1) reveals that the only difference between these architectures is the value of the *b* vector, which affects the area occupied by a single acid molecule (A_{mol}). Interestingly, the difference between A_{mol}***C12*** and A_{mol}***C18*** matches the difference between A_{mol}***C18*** and A_{mol}***C24***, as well as A_{mol}***C24*** and A_{mol}***C30***, being 0.37 nm^2, consistent with the area occupied by the additional molecular fragment, i.e. a hexane moiety, whose van der Walls surface area projection on graphite amounts to 0.35 nm^2. The unit cells parameters reported in Table 1 are in good agreement with previous report.[60] Interestingly, the self-assembled monolayers of carboxylic acids can be also formed and studied at the CVD graphene/solution interface,[7] showing 2D patterns having the exact unit cell parameters as those observed on HOPG/solution interface.

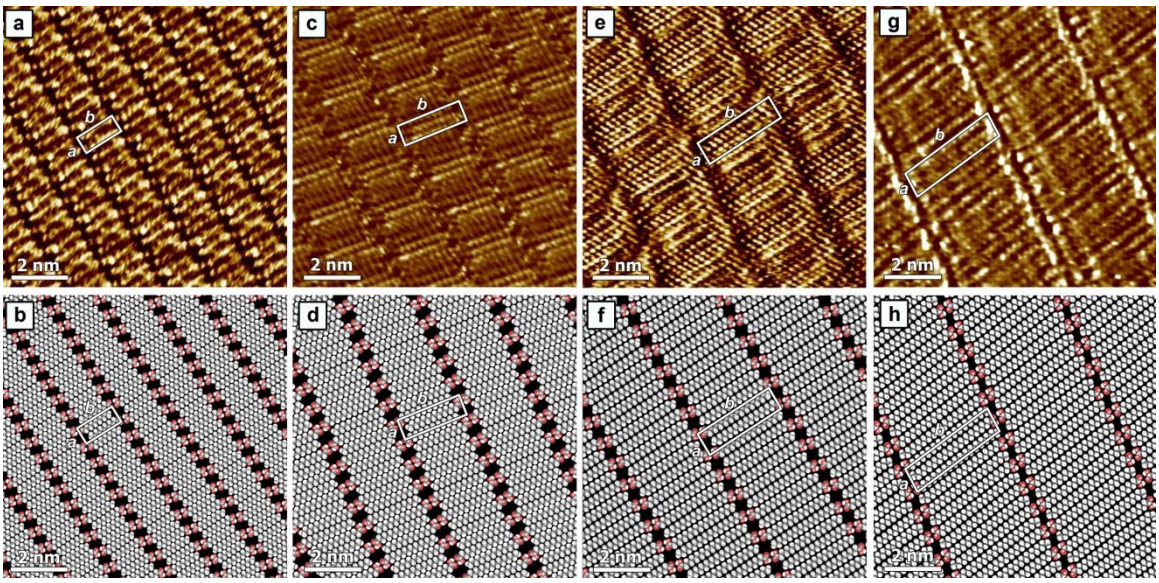

Figure 8.1. STM current images of monocrystalline lamellar structures, as well as proposed molecular packing models, obtained from (a-b) ***C12***, (c-d) ***C18***, (e-f) ***C24*** and (g-h) ***C30.*** Tunneling parameters: average tunneling current (I_t) = 20 pA, tip bias voltage (V_t) = 350 mV.

8.4.2 Liquid-phase exfoliation

To test the capability of the carboxylic acids to increase the graphene exfoliation yield, we prepared dispersions by adding graphite powder in four solvents, i.e. NMP, *o*-DCB, TCB and DMF, and sonication in ultrasound bath (6 hours) in the presence of dispersion-stabilizing agents, i.e. the five carboxylic acids in Scheme 8.1. Graphene dispersions prepared in such a way have been compared with the blank experiments, i.e. dispersion prepared in the absence of additional molecules. By considering the initial graphite powder as a single graphene sheet, and knowing the area of graphite occupied by each acid molecule type (as revealed by STM) we calculated the theoretical number of molecules needed to form densely packed monolayers on graphene [52]. Given that the calculated quantity of the molecules would be higher than the real surface of graphite in the form of powder, we have used only 20% of molecules needed to cover the entire graphene surface. Sonication of all samples led to grey liquids consisting of a homogeneous phase and large numbers of macroscopic aggregates, i.e. unexfoliated graphitic material. As previously reported [1], these aggregates can be removed by centrifugation, yielding homogeneous dark dispersions (see Figure 8.2.), which were characterized by different technics.

To quantify the concentration of graphene after centrifugation, a mixture of graphene dispersion and chloroform was first heated up to 50 °C for 30 min and then passed through polytetrafluoroethylene membrane filters (pore size 100 nm). The remaining solvent and acid molecules were washed several times with diethyl ether and $CHCl_3$. Careful measurements of the filtered mass were performed on a microbalance (Sartorius MSA2.75) to give the concentrations of graphene. The presence of adsorbed molecules on the graphene sheets may affect the mass measurements and ultimately the exfoliation yields. Thus, heating was necessary to completely remove, i.e. desorb, the acid molecules from graphene. Careful measurements of the filtered mass provided the concentration of the dispersed phases after centrifugation (see Figure 8.2).

By analyzing 15 independent experiments, we found that when exfoliation is performed in the absence of dispersion-stabilizing agents (called blank experiment) comparable concentrations of graphene were observed with NMP (86 ± 10 μg mL^{-1}) and *o*-DCB (98 ± 9 μg mL^{-1}), whereas lower concentrations were obtained when TCB (64 ± 7 μg mL^{-1}) and DMF (47 ± 7 μg mL^{-1}) were used. It is worth noting that these values of graphene concentration cannot be directly compared with the results reported by other research groups. In fact, benchmarking the values of graphene concentration is one of the biggest issues in the community, since the final concentration of graphene and lateral flake size differ significantly from one group to another. This can be simply explained by the fact that different experimental conditions, such as initial graphite concentration, solvent volume, sonication power and temperature, are (with a few exceptions) commonly omitted or not discussed. In any case, the graphene-dispersed concentrations reported in this work are in good agreement with those previously reported using the same experimental set-up [6, 15].

Finally, we extended our LPE studies by using carboxylic acids as dispersion-stabilizing agents (Scheme 8.1). Interestingly, we found that the concentration of graphene prepared in NMP, *o*-DCB and TCB increases almost linearly with the length of the aliphatic chain (Figure 8.1b), except for the data points at highest alkane length. Surprisingly, the use of acid molecules (regardless of their length) has no major influence on the concentration of dispersions prepared in DMF, although the quality of dispersion improves (see below). In contrast to the case of blank experiments, the highest concentrations of graphene obtained in acid-assisted LPE were obtained in NMP. Consistently, NMP is the most widely used organic exfoliation medium, not only for its well-matched surface tension and Hansen solubility parameters but also because it provides the exfoliated graphene with excellent stability; therefore it is not surprising that the highest gain in concentration upon addition of carboxylic acid molecules was observed using this solvent. Noteworthy, The most significant increase in graphene concentration was obtained by using ***C30*** molecules, where it amounts to 240 μg mL^{-1}. This latter corresponds to nearly 200% increase in the yield of exfoliation, when compared to samples prepared in pure NMP (85 μg mL^{-1}). In the case of the chlorinated solvents, i.e. *o*-DCB and TCB, the highest increase in the yield of exfoliation was monitored when ***C24*** molecules were used, and amounts to ca. 50% and ca. 90% increase, in case *o*-DCB and TCB, respectively. Surprisingly, an enormous drop in the exfoliation yield was observed

when using the ***C30*** molecules. This is explained by the marked tendency of long fatty acids to form gel-like dispersions in chlorinated solvents at room temperature [62]. Despite these two particular cases, a linear correlation between the concentration of exfoliated graphene and the length of the carboxylic acid is evident in all solvents (see Figure 8.2). These results demonstrate that the use of carboxylic acids as dispersion-stabilizing agents leads to a significant increase in the yield of exfoliation. Although the formation of spatially extended, ordered, and stable self-assembled monolayers of fatty acids on graphene sheets during the sonication process is unlikely, the presence of the acid molecules unambiguously leads to an increased yield of exfoliation, proving that molecule-molecule as well as molecule-graphene interactions play necessarily a major role during LPE process.

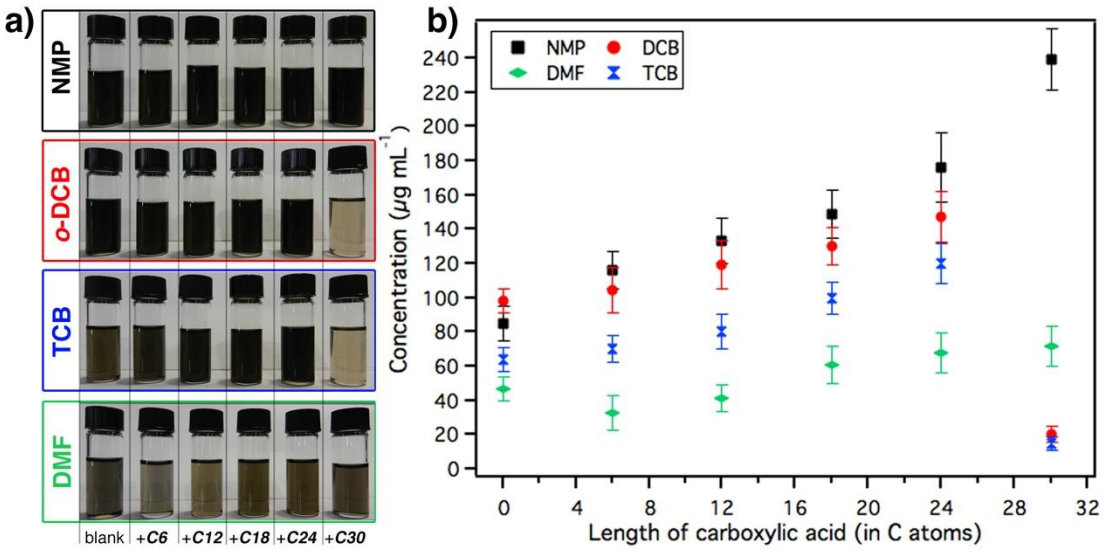

Figure 8.2. a) Photographs of graphene dispersions prepared by exfoliation of graphite flakes in NMP, *o*-DCB, TCB and DMF, in the presence/absence of carboxylic acid molecules; b) Average concentration of graphene dispersions after the filtration process. The error bars correspond to the different values obtained in 15 independent experiments.

8.4.3 UV-Vis-IR spectroscopy

Graphene dispersions were characterized by UV–vis–IR absorption spectroscopy. As expected, the spectra are featureless in the visible – IR region. Each of these dispersions in

NMP, i.e. graphene, graphene with C6 to C30 was diluted a number of times and the absorption spectra recorded (Figure 8.3).

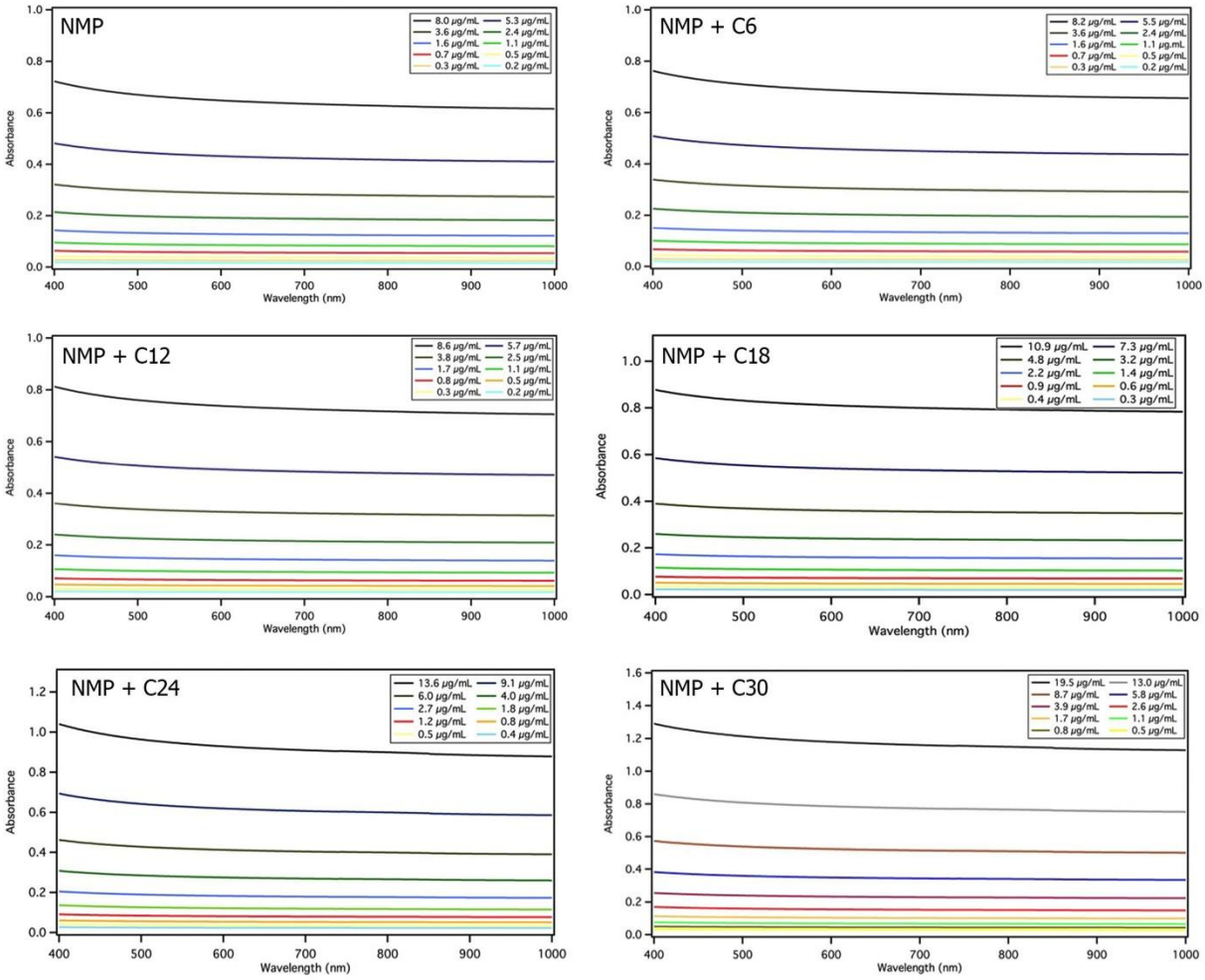

Figure 8.3. UV–Vis spectra of graphene dispersion in NMP in the presence/absence of C6 to C30 at different concentrations.

The absorbance (660 nm) divided by cell length is plotted versus concentration (Figure 8.4). A Lambert – Beer behavior was observed for all samples, with extracted values of the regression from the linear fitting amounting to 0.988 for all samples.

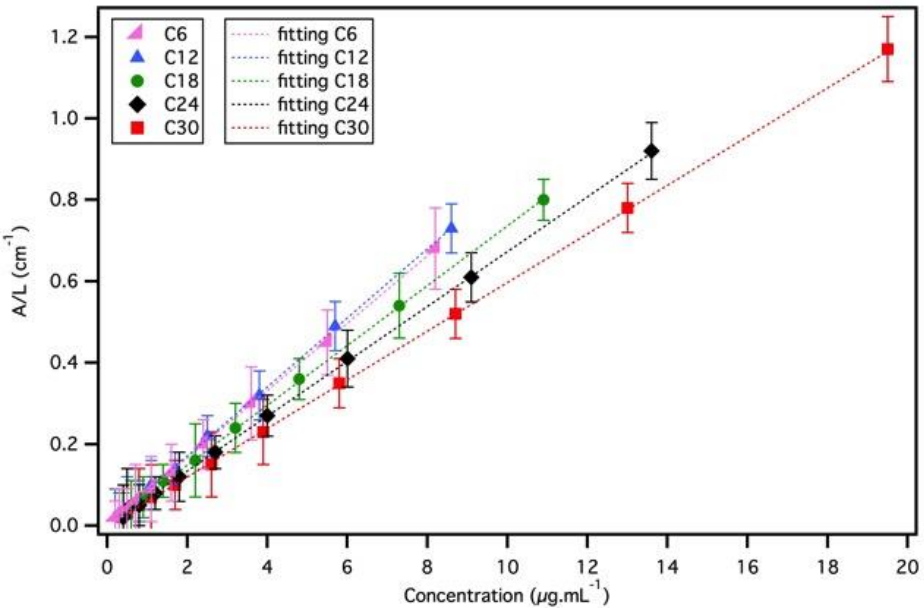

Figure 8.4. Optical absorbance (λ = 660 nm) divided by cell length (A/L) as a function of concentration showing Lambert–Beer behavior of all dispersions.

Graphene dispersions in o-DCB, TCB and DMF were also characterized by UV–vis–IR absorption spectroscopy (Figure 8.5). As expected, the spectra are featureless in the visible – IR region

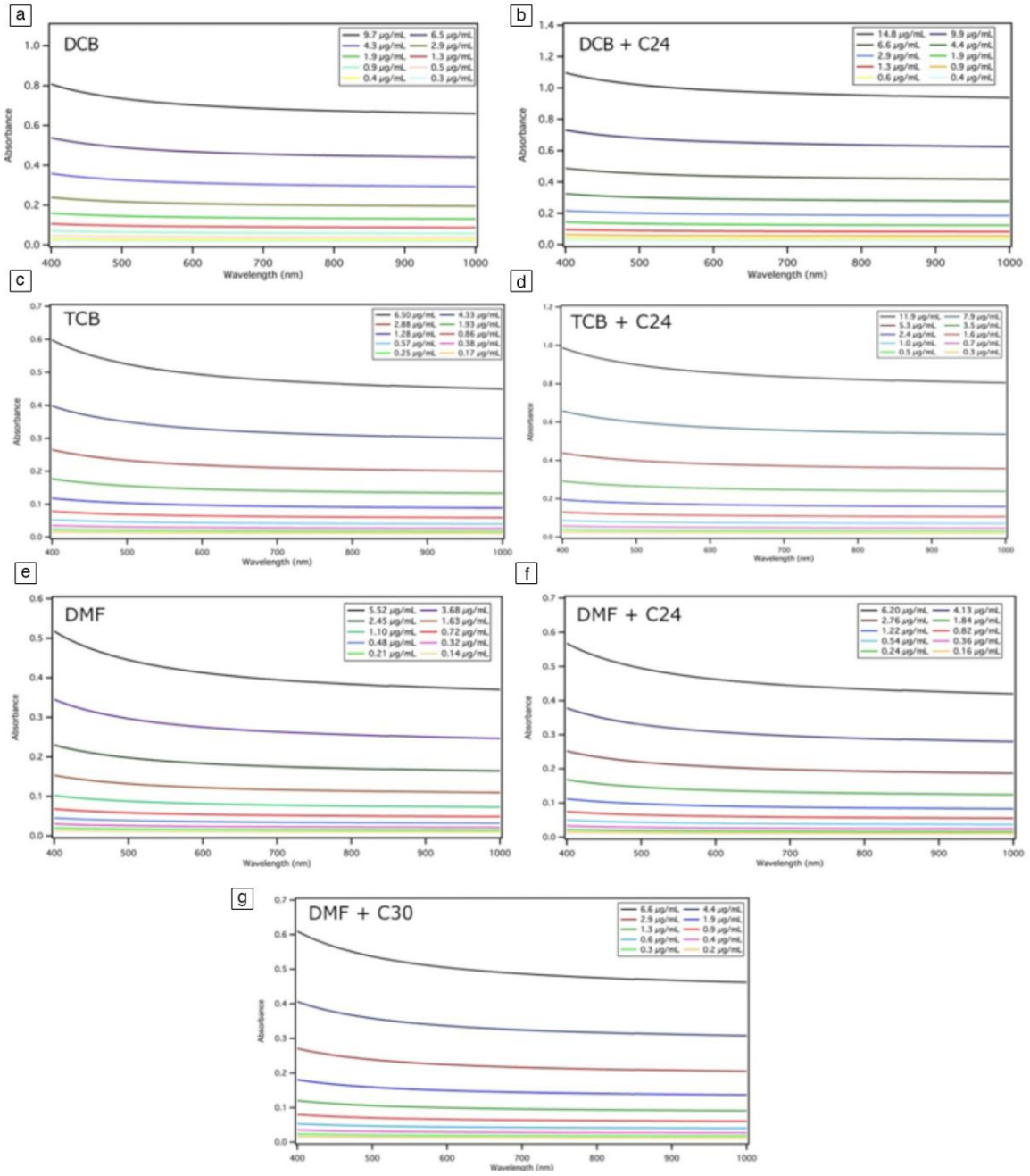

Figure 8.5. UV–Vis spectra of graphene dispersion a) in DCB, b) in DCB with C24, c) in TCB, d) in TCB with C24, e) in DMF, f) in DMF with C24 and g) in DMF with C30 at different concentrations.

The absorbance (660 nm) divided by cell length is plotted versus concentration (Figure 8.6). A Lambert – Beer behavior was observed for all samples, with extracted values of the regression from the linear fitting amounting to 0.988 for all samples.

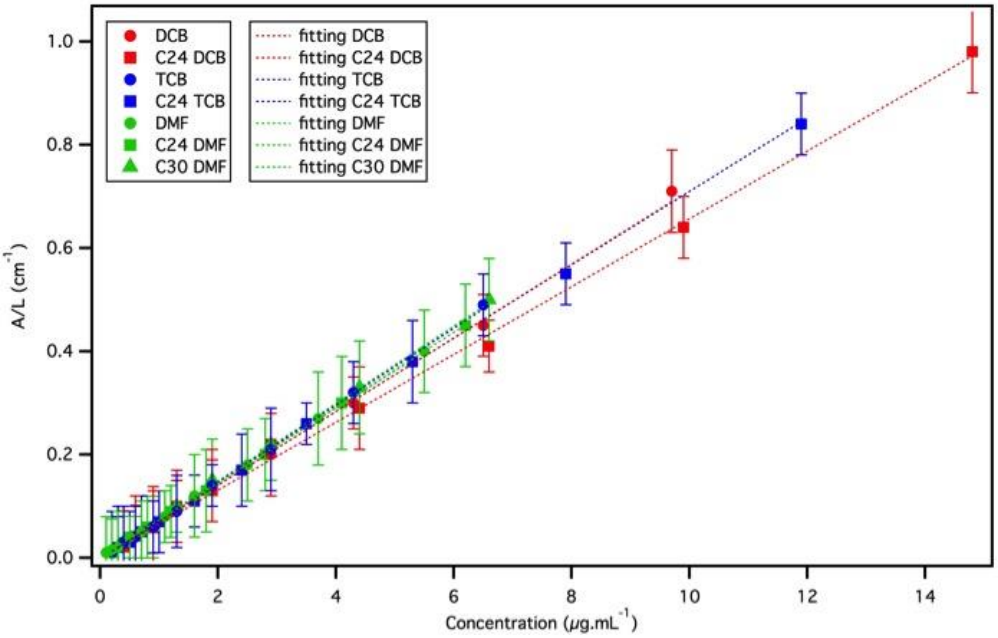

Figure 8.6. Optical absorbance (λ = 660 nm) divided by cell length (A/L) as a function of concentration showing Lambert–Beer behavior of all dispersions.

8.4.4 HR-TEM

In order to fully characterize the exfoliated graphitic material, both qualitative and quantitative information are reported. While quantitative information can be assessed simply by providing the yield of exfoliation expressed in terms of concentration (in μg mL^{-1}), the qualitative analysis provides more relevant details such as the percentage of single-layer graphene (SLG) flakes, the lateral size of the flakes and the presence/absence of defects. Currently, the only method for the identification of the number of graphene layers in material produced by LPE is based on High Resolution Transmission Electron Microscopy (HR-TEM) [2]. Together with the

information coming from electron diffraction patterns, in HR-TEM the number of layers can be directly counted by analyzing the edges [17].

8.4.4.1 Dispersions in NMP

First, we focused our attention on dispersion prepared in NMP in the absence and/or the presence of fatty acids as dispersion-stabilizing agents. The TEM micrographs reveal that the majority of dispersions are composed by a large fraction of monolayer graphene sheets folded over themselves, with lateral sizes < 1 μm, as typically observed for LPE graphene. The analysis of the folded edges of the graphene sheets provides estimates of the number of layers composing the flakes (Figure 8.7a). In terms of the thickness of LPE graphene, no major differences were observed between the blank sample and graphene exfoliated in the presence of ***C18***, ***C24*** and ***C30*** molecules, where the percentage of mono- and bi-layer thick flakes amounts to 16 ± 1 % and 20 ± 1 %, respectively. Surprisingly, the use of ***C6*** and ***C12*** molecules as dispersion-stabilizing agents resulted in a drastic decrease of the dispersions quality, in which mono- and bi-layer flakes were not observed. Based on such observation we decided to omit the dispersions prepared in the presence of these shorter acids in the further investigation by TEM. Moreover, the TEM analysis allowed us to define the average lateral size of the graphene sheets, which is estimated to be 224 ± 50 nm, 405 ± 28 nm, 279 ± 21 nm and 247 ± 20 nm, for graphene exfoliated in NMP and NMP/***C18***, NMP/***C24*** and NMP/***C30***, respectively. The statistical analyses of the graphene sheet thickness and lateral flake size are reported in Figure 8.7a and 8.7b respectively.

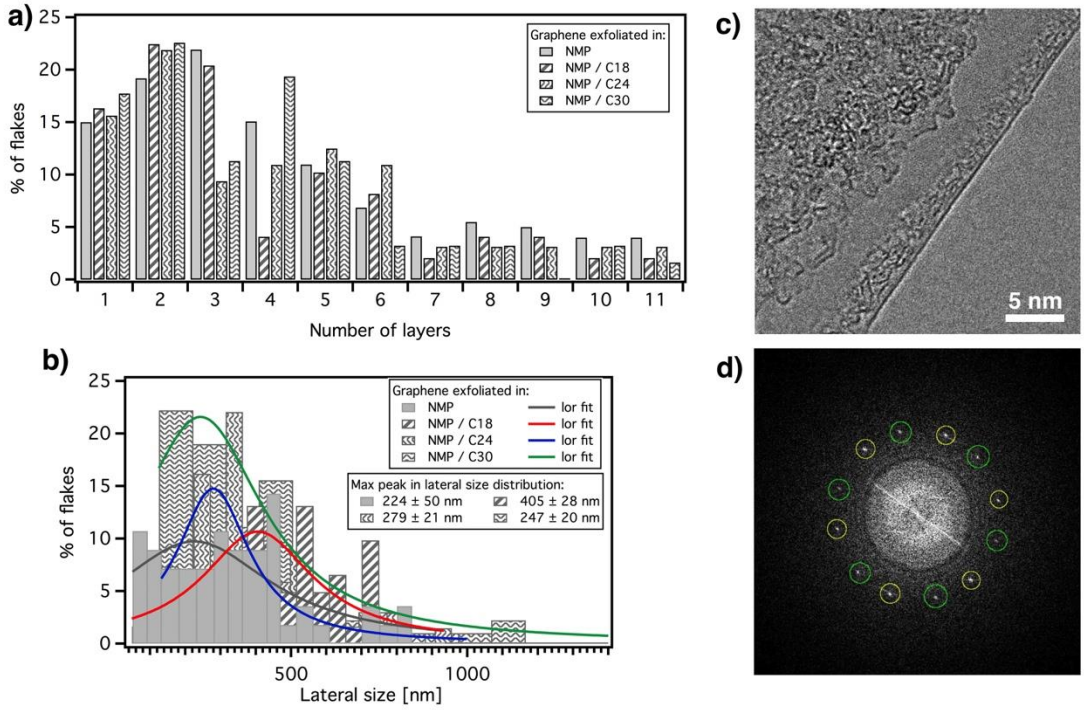

Figure 8.7. Statistical analyses of HR-TEM results of graphene exfoliated in pure NMP and in NMP in the presence of ***C18***, ***C24*** and ***C30*** molecules. (a) Histogram of the distribution of the flake thickness, data fitted with Lorentzian function (best fit among the other functions). (b) Histogram of the lateral flake size distribution. The fitting of the distribution has been obtained with a Lorentzian distribution. (c) HREM micrograph of a monolayer folding, and (d) relative Fast Fourier Transform (FFT), showing the typical hexagonal pattern from graphene/graphite lattice at 0.21 nm (yellow circles), and a twisted one correspondent to the folded layer (green circles).

8.4.4.2 Dispersions in o-DCB, TCB and DMF

We now focus our attention on the samples prepared in the three other solvents, i.e. those prepared in pure *o*-DCB, TCB and DMF, as well as on dispersions of the highest concentration prepared in the presence of acid molecules, namely *o*-DCB/***C24***, TCB/***C24*** and DMF/***C24*** and DMF/***C30***. As previously described, the use of ***C30*** molecules during LPE in chlorinated solvents, does not allow for a successful exfoliation of graphite, as reflected by the low concentration of produced graphene inks (Figure 8.2).

Similarly to the NMP samples, the TEM micrographs recorded on the samples prepared in *o*-DCB revealed that the majority of dispersions are composed by a large fraction of mono- and bilayer graphene sheets, typically folded over themselves. In terms of thickness composition, in contrast to the case of NMP dispersions, the use of ***C24*** molecules resulted in a notable

decrease of monolayer thick flakes from 26% (blank) to 13% (Figure 8.8a). Interestingly, while the percentage of monolayer graphene flakes strongly decreases, we observed a rather surprising increase in the lateral size of the flakes (Figure 8.8b), from ca. 200 nm (blank) to 440 nm.

TEM analysis of the dispersions produced in TCB revealed that the poor quality of the samples (only 3% of MLG – Figure 8.8d) can be sufficiently improved by the use of ***C24*** molecules, where the percentage of single-layer graphene (SLG) flakes amounts to 18%. However, in this case no difference in lateral flakes size was observed. Through the "blank" samples prepared in pure DMF are of the lowest quality, in terms of concentration and stability (precipitation after several days), we found that the use of acid molecules, i.e. ***C24*** and ***C30***, allows production of dispersions, which are stable over several weeks. Furthermore, if compared to blank experiment, the aid of ***C24*** and ***C30*** molecules results in 8% and 16% increase of SLG respectively.

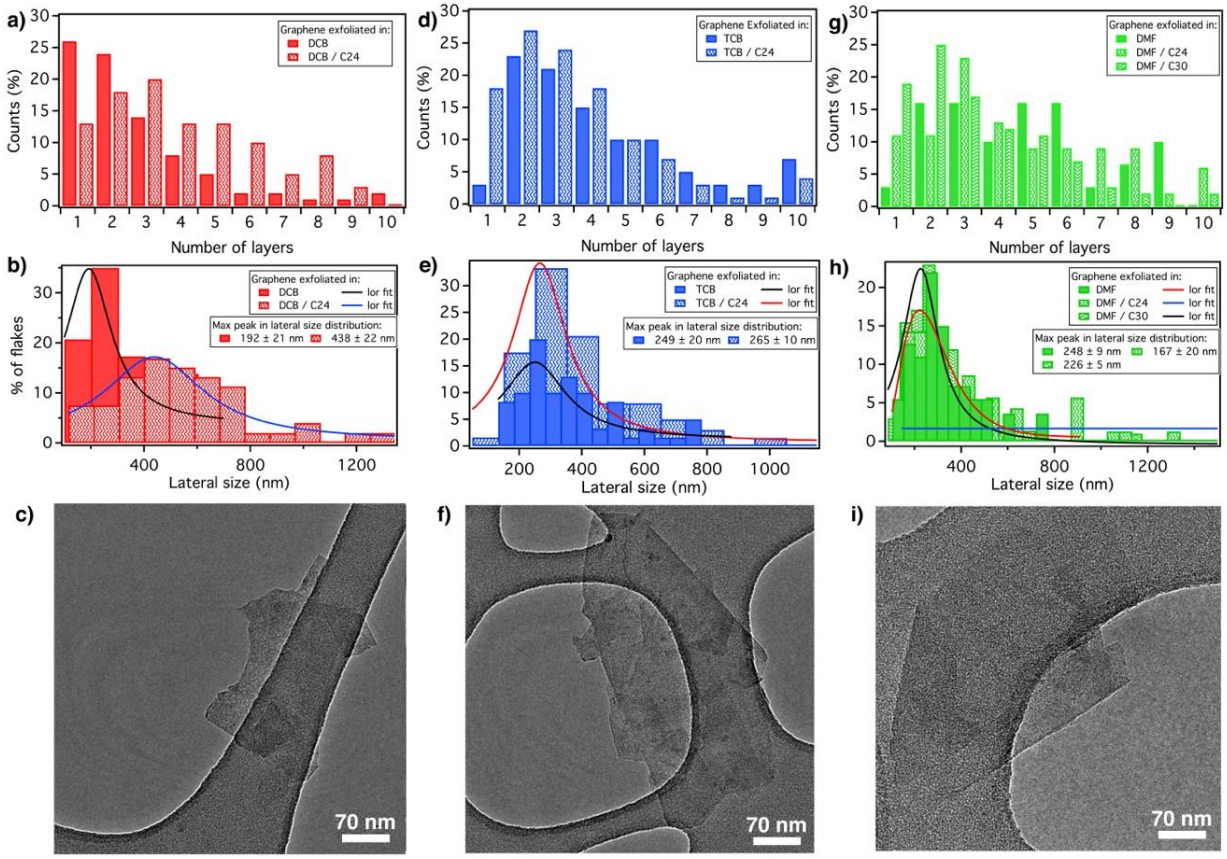

Figure 8.8. (a-h) Statistical analyses of TEM and HR-TEM results of graphene dispersions in pure (a) *o*-DCB, (d) TCB, and (g) DMF, as well as in the presence of ***C24*** (*o*-DCB, TCB, DMF) and ***C30*** molecules (DMF). Histograms of the lateral flake size distribution of graphene flakes prepared in (b) *o*-DCB, (e) TCB, and (h) DMF. The fitting of the distribution has been obtained with a Lorentzian distribution. (c, f, i) TEM micrographs of folded monolayer graphene flakes prepared from dispersions in (c) *o*-DCB/***C24***, (f) TCB, and (i) DMF/***C24***.

8.4.5 Raman spectroscopy

The results obtained by TEM are confirmed by Raman spectroscopy. Although the Raman analysis is more qualitative, it has been shown that this technique is sensitive to the changes in thickness composition under different experimental conditions [8, 9, 12]. Figure 8.9a shows the representative Raman spectrum of the blank sample as compared to the spectrum of the graphene suspension obtained with the ***C30*** molecule.

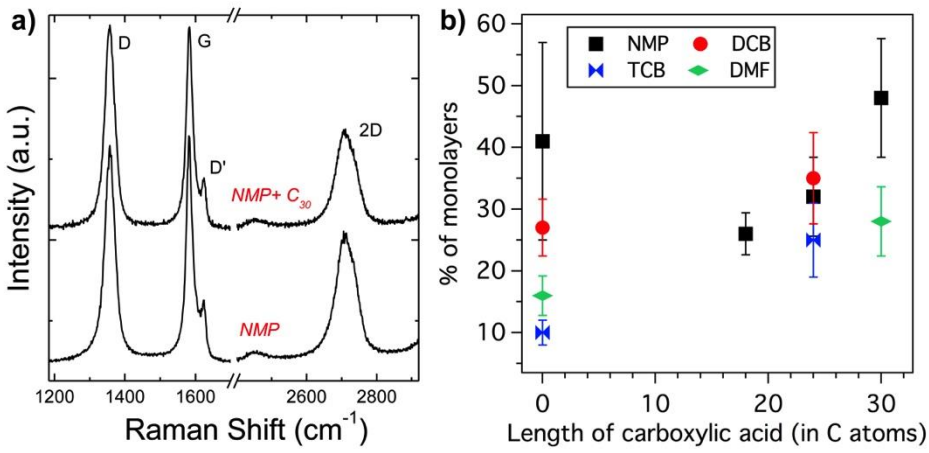

Figure 8.9. (a) Typical Raman spectrum of single-layer graphene produced in NMP and in NMP with the ***C30*** molecules. The 2D peak is in both cases highly symmetric. I(D)/I(G) is also comparable. (b) Percentage of single-layer graphene derived by the 2D peak shape analysis as a function of the length of the carboxylic acid molecules. The highest percentage is observed with the addition of the ***C24*** and ***C30*** molecules, but this strongly depends on the solvent used. Strong improvements are observed for the poorest solvents, such as DCB and DMF.

The D peak is typical of LPE graphene [31] and it is activated by the edges, being the flakes smaller than the laser spot size (Figure 8.7 and 8.8). Figure 8.9b shows the single-layer percentage as derived from the 2D peak shape analysis as a function of the carboxylic acid length. The addition of carboxylic acids to NMP increases the relative percentage of single layers from 41% to about 48%. However, the increase in single-layer concentration is not directly proportional to the length of the carboxylic acid, as also observed by TEM (Figure 8.7b). The highest concentration is obtained with the addition of the ***C30*** molecules, while ***C18*** and ***C24*** molecules give single-layers concentrations comparable with NMP alone. A drastic decrease in graphene concentration is observed for the ***C12*** and ***C6*** molecules, in relatively good agreement with TEM (Figure 8.7). Note that I(D)/I(G) does not show any strong change for the dispersions obtained with NMP alone and NMP with the ***C30*** molecules, showing that the quality and the size of the flakes are comparable (at least within the Raman resolution), which is consistent with the TEM results (Figure 8.7). By and large, Raman spectroscopy shows a slight increase in the graphene concentration when the ***C30*** molecules are used; in contrast, no improvement or even a decrease in concentration of single-layers is observed when the other carboxylic acid molecules are used.

Figure 8.2 shows that NMP gives higher concentration of graphene, while TCB and DMF are poor solvents for exfoliation of graphite. *o*-DCB gives intermediate results. However, NMP seems to give a slightly higher I(D)/I(G) compared to the other solvents. HR-TEM analysis shows that the addition of carboxylic acids strongly improves exfoliation, in particular when ***C24*** and/or ***C30*** molecules are used (Figure 8.7 and 8.8). The highest increase is observed for the poorest solvents such as TCB and DMF. The Raman analysis confirms these results: the percentage of single layers increases from 10% to 25% when the ***C24*** molecules are added to TCB, and from 16% to 28% when the ***C30*** molecules are added to DMF. Strong changes in I(D)/IG) are not observed after addition of carboxylic acids, indicating that the ***C24*** and ***C30*** molecules do not produce defects. The thickness composition analysis shows that the addition of the ***C24*** and ***C30*** molecules reduces the amounts of thick graphite (called >5 [AB] in Table 8.2) by increasing the amount of thin layers and single-layers (Figure 8.8b). Ultimately, this confirms that the use of carboxylic acids improves the exfoliation of graphite even in poor solvents.

	I(D)/I(G)	>5 [AB]
NMP	0.6 – 1.0	3%
NMP + C30	0.6 – 1.5	0%
o-DCB	0.4 – 0.8	23%
o-DCB + C24	0.3 – 0.5	6%
TCB	0.4 – 0.8	41%
TCB + C24	0.8 – 1.2	12%
DMF	0.4 – 0.8	0%
DMF + C30	0.4 – 0.8	0%

Table 8.2. Table showing the I(D)/I(G) and the percentage of thick graphitic (*i.e.* with AB stacking configuration) flakes. The addition of the ***C24*** and ***C30*** molecules reduces significantly the amounts of thick graphitic flakes.

8.4.6 X-ray photoelectron characterization

We used XPS to analyze graphene + ***C24*** dispersions in *o*-DCB or NMP before and after washing the ***C24*** molecules. (See Figure 3.5.10)

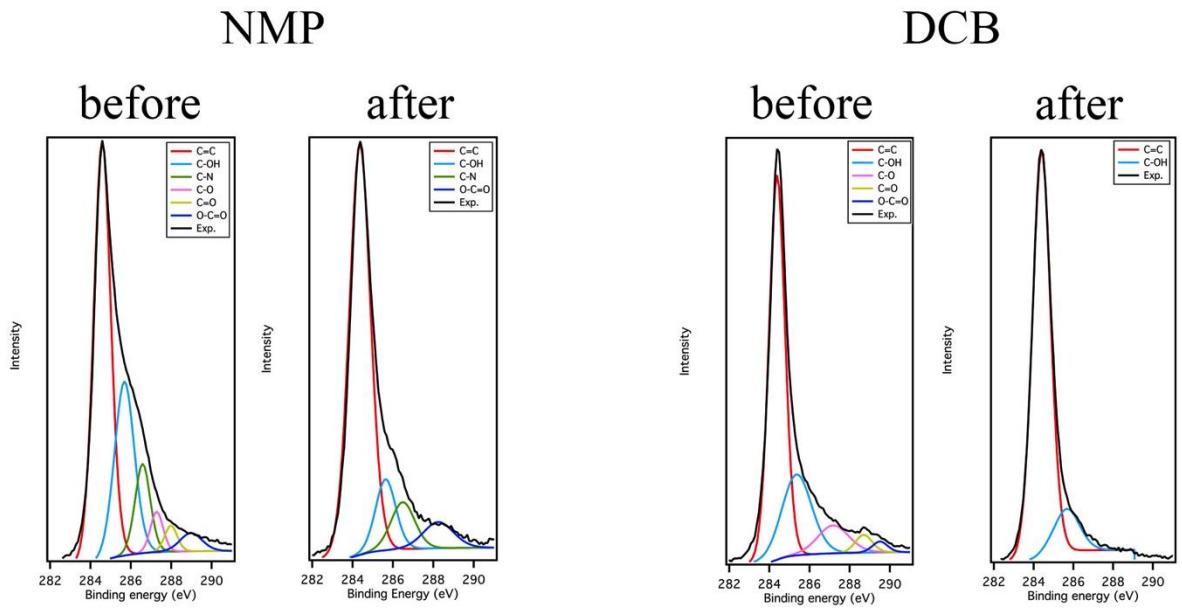

Figure 8.10. High-resolution C1s spectra of graphene exfoliated in the presence ***C24*** a) in NMP, b) in NMP after washing step, c) in *o*-DCB and d) in *o*-DCB after washing step. Experimental data are shown as black line, and the individual deconvolved components as colored lines.

The high-resolution C1s XPS spectrum of the graphene + ***C24*** sheets from NMP dispersions showed a sharp peak at 284.3 eV that corresponded to C-C bonds of carbon atoms in a conjugated honeycomb lattice. Peaks at 285.7, 287.4, 287.9 and 289.2 eV could be attributed to different C-O bonding configurations due the presence of ***C24*** molecules and NMP residues. Also the peak at 2810.6 eV can be assign to C-N bonds coming also from NMP. After the washing step, the intensities of all of the related oxygen peaks were significantly decreased in the sample, indicating that the ***C24*** molecules were removed. Also the C-N peak is present in a lower intensity corresponding to 4% of NMP molecules. The high-resolution C1s XPS spectrum of the graphene + ***C24*** sheets from DCB dispersions showed a sharp peak at 284.2 eV corresponding to delocalized π conjugation from the sp^2 atomic structure of graphite. Peaks at 285.6, 287.3, 287.8 and 289.1 eV could be attributed to different C-O

bonding configurations due the presence of ***C24*** molecules. After the washing step, the related oxygen peaks are not present, indicating that the ***C24*** molecules were removed.

8.5 Conclusion

We have demonstrated that by mastering a supramolecular approach it is possible to enhance the yield of graphite exfoliation in an up-scalable molecule assisted LPE-based method to produce high-quality graphene flakes from powdered graphite. To attain a fundamental understanding over the role of molecule-graphene interaction on the yield of graphene LPE, we have carried out a comparative study by using as prototypical dispersion-stabilizing agent fatty acids with increasing the length of the aliphatic chain. Simple washing step allowed us to completely remove the molecules used during LPE process. Careful analysis revealed a significant increase in the yield of exfoliation with the length of the aliphatic chain. In particular, the most effective exfoliation was obtained with ***C30*** molecules in NMP as a solvent, with a concentration of exfoliated graphene of 240 μg mL^{-1} that corresponds to a nearly 200% increase in exfoliation yield when compared to samples prepared in pure NMP (85 μg mL^{-1}). In the case of the chlorinated solvents, i.e. *o*-DCB and TCB, the most effective exfoliation was observed using the ***C24*** molecules, which produced ca. 50% and ca. 90% increase in the exfoliation yield with *o*-DCB and TCB, respectively. Furthermore, a remarkable increase of single-layer graphene (SLG) flakes was observed in some cases. TEM analysis of dispersions produced in TCB and DMF revealed that the poor quality of the samples (only 3% of SLG) is sufficiently improved by the use of ***C24*** (TCB) and/or ***C30*** (DMF) molecules, which results in a 16% increase of SLG respectively. The Raman analysis fully supports the TEM results. The observed dependence of the exfoliation yield with the length of the aliphatic chain has been interpreted by means of a straightforward yet effective thermodynamic model of molecular self-assembly on graphene. Our analysis shows that the shorter the aliphatic chain, the larger the (translational and rotational) entropic cost of forming a 2D self-assembled monolayer will be. These results suggest that a model based on molecular mechanics for the energetics and a statistical mechanic treatment of entropy, could be used to predict the efficiency of supramolecular building blocks as graphene dispersion-stabilizing

agents and eventually guide the chemical design of the next generation of exfoliators. Our simple yet efficient supramolecular approach to leverage the graphene production in a liquid media, relying on basic molecular modules, is generally applicable to create stable and highly concentrated graphene-inks. The attachment of functional units to the end of the alkane chains can pave the way towards the generation of graphene-based multifunctional nanocomposites.

8.6 References

1. S. Vadukumpully, J. Paul and S. Valiyaveettil, *Carbon*, 2009, **47**, 3288-3294.
2. J. Geng, B. S. Kong, S. B. Yang and H. T. Jung, *Chem Commun*, 2010, **46**, 5091-5093.
3. Y. T. Liang and M. C. Hersam, *J Am Chem Soc*, 2010, **132**, 17661-17663.
4. M. S. Kang, K. T. Kim, J. U. Lee and W. H. Jo, *J Mater Chem C*, 2013, **1**, 1870-1875.50.
5. L. Xu, J.-W. McGraw, F. Gao, M. Grundy, Z. Ye, Z. Gu and J. L. Shepherd, *J. Phys. Chem. C*, 2013, **117**, 10730-10742.
6. J. P. Rabe and S. Buchholz, *Science*, 1991, **253**, 424-427.
7. A. Ciesielski, H. Haar, M. El Gemayel, H. Yang, J. Clough, G. Melinte, M. Gobbi, E. Orgiu, M. V. Nardi, G. Ligorio, V. Palermo, N. Koch, O. Ersen, C. Casiraghi and P. Samorì, *Angew Chem Int Edit*, 2014, DOI: 10.1002/anie.2014026910.
8. A. Ciesielski, C.-A. Palma, M. Bonini and P. Samorì, *Adv. Mater.*, 2010, **22**, 3506-3520.
9. R. Gutzler, L. Cardenas and F. Rosei, *Chem. Sci.*, 2011, **2**, 2290-2300.
10. K. S. Mali, J. Adisoejoso, E. Ghijsens, I. De Cat and S. De Feyter, *Accounts Chem Res*, 2012, **45**, 1309-1320.
11. S. De Feyter and F. C. De Schryver, *Chem. Soc. Rev.*, 2003, **32**, 139-150.
12. B. J. Gyarfas, B. Wiggins, M. Zosel and K. W. Hipps, *Langmuir*, 2005, **21**, 919-923.
13. M. Lackinger, S. Griessl, W. A. Heckl, M. Hietschold and G. W. Flynn, *Langmuir*, 2005, **21**, 4984-4988.
14. L. Kampschulte, M. Lackinger, A. K. Maier, R. S. K. Kishore, S. Griessl, M. Schmittel and W. M. Heckl, *J. Phys. Chem. B*, 2006, **110**, 10829-108310.
15. M. Hibino, A. Sumi, H. Tsuchiya and I. Hatta, *J. Phys. Chem. B*, 1998, **102**, 4544-4547.
16. M. El Gemayel, S. Haar, F. Liscio, A. Schlierf, G. Melinte, S. Milita, O. Ersen, A. Ciesielski, V. Palermo and P. Samorì, *Adv. Mater.*, 2014, DOI: 10.1002/adma.201400895.
17. R. G. Weiss and P. Terech, *Molecular gels - materials with self-assembled fibrillar networks*, Springer, Dordrecht, 20010.
18. A. C. Ferrari, J. C. Meyer, V. Scardaci, C. Casiraghi, M. Lazzeri, F. Mauri, S. Piscanec, D. Jiang, K. S. Novoselov, S. Roth and A. K. Geim, *Phys Rev Lett*, 2006, **97**, 187401.

Chapter 9 Enhancing LPE upon addition of *n*-octylbenzene

9.1 Introduction

More recently, it has been reported that the use of small organic molecules acting as dispersion-stabilizing agents can promote the exfoliation of graphite when the chosen molecules have a strong affinity for the basal graphitic planes, being these interactions also stronger than those between the solvent molecules and graphene [1-3]. Indeed suitably designed molecules, possessing adsorption energy on graphene larger than the adsorption of solvent-molecules, are able to form highly ordered physisorbed monolayers on the graphene surface. In this framework, it has been recently demonstrated that the addition of simple linear alkanes of different length terminated by a carboxylic-acid head group during the LPE process increases not only the exfoliation yield but also the percentage of graphene monolayers [4]. Nevertheless, molecule-assisted LPE in organic solvents, and in particular when the molecules contain aliphatic tails, is limited by the fact that a maximum amount of molecules added during LPE cannot exceed 25 s.a. %, which can lead to the gelation of graphite/molecule dispersions [5].

9.2 Scope

To overcome this issue, in this part we extended our study to the use of molecules which at room temperature exist as a liquid, and we investigate the effect of their addition on the LPE process performed in two different commonly used solvents, i.e. NMP and *ortho*-dichlorobenzene. In particular, we focus our attention on *n*-octylbenzene (NOTBZ) as dispersion-stabilizing agent due to its total miscibility in the selected solvents and its known capacity to promote the exfoliation yield of graphene [1]. In this framework, it has been very recently demonstrated that NOTBZ molecules can be successfully exploited to promote the exfoliation of graphene in NMP. Here we explore the effect of the presence of different volume ratios of NOTBZ in either NMP or *o*-DCB during the LPE process on the quality and quantity of produced graphene flakes. We describe also a new deposition technique used for fabrication of uniform graphene films deposited from solution on flat solid surfaces. The set-up includes an integrated heating system to guarantee the fast evaporation of the solvent. More importantly, the as-obtained graphene film shows low sheet resistance and high optical transparency.

9.3 Experimental

9.3.1 Materials

N-methyl-2-pyrrolidinone (NMP - product number *p.n.* 332461), *ortho*-dichlorobenzene (*o*-DCB, *p.n.* 240664), N,N-dimethylformamide (DMF, p.n. 33120) and 1,2,4-trichlorobenzene (TCB, p.n. 256412) were purchased from Sigma-Aldrich and used as solvent for the exfoliation. *N*-octylbenzene (NOTBZ, *p.n.* 113190) and graphite powder (*p.n.* 332461) were also acquired from Sigma-Aldrich and used without further treatment.

9.3.2 Preparation of graphene

Graphite flakes were sonicated for 6 h at 40 ± 2°C (600 W) in four different solvents, i.e. NMP, *o*-DCB, DMF and TCB. Since NOTBZ is a liquid at room temperature, we decided to fix the total volume of the mixture at 10 mL. For each solvent, we varied the amount of the added molecules and fix the amount of graphite powder. The latter was changed for each of the solvents used. Sonication of graphite powder led to grey liquid consisting of a homogeneous phase and large numbers of macroscopic aggregates. As previously reported [29], these aggregates can be removed by centrifugation (Eppendorf 5804, rotor F-34-6-38, 30 min at 10 000 rpm), yielding to a homogeneous dark dispersion.

9.3.3 Characterizations

Atomic Force Microscopy (AFM) characterization was carried out by using a Veeco Dimension 3100, running with a Nanoscope IV controller. The analysis of AFM images and the extraction of the topographical profiles, for measuring the thickness of the different films, were done using Gwyddion.

XPS analyses were carried out on a Thermo Scientific K-alpha X-ray photoelectron spectrometer with a basic chamber pressure of ~10^{-8} mbar and Al anode as the X-ray source (x-ray radiation of 1486 eV). Spot sizes of 400 µm were used and pass energies of 200 eV for survey scans and 50.00 eV for high-resolutions scans were used. 150 µL of dispersions were spin coated on Au substrate for 1 minute at 1000 rpm and substrates were annealed for 1 day at 100 °C in an oven under vacuum.

9.3.4 Graphene thin film and sheet resistance measurements

Prior to use, quartz substrates were washed by applying 2 cycles of acetone and isopropanol and cleaned by UV ozone treatment. 70 µL of the as-prepared graphene dispersions in *o*-DCB

or NMP were deposed on freshly cleaned quartz substrate using our spin-controlled drop-casting set-up. A custom high torque step motor, with 1.8°/step and 200 step/revolution was used. We explored different parameters, i.e. rotation angle (from 0 to 35 steps), speed (from 1 to 35 step/s) and temperature (from 20 to 80 °C). The best condition giving a homogeneous film was by setting the rotating angle and speed at 22 steps and 11 steps/s respectively while heating at 50 °C. One deposition corresponds to one cycle of drop-casting 70 µL of graphene dispersion, 30 minutes of rotation and 180 min of post annealing at 100°C under vacuum. The numbers of deposition were varied between 1 and 9. Sheet resistances were measured with a four probes Jandel (RM3000) platform. The analysis of AFM images and the extraction of the topographical profiles, for measuring the thickness of the different films, were done using Gwyddion

9.4 Results and discussions

9.4.1 Liquid-phase exfoliation

In order to cast light onto the role of the addition of NOTBZ in the graphene liquid-phase exfoliation, we first prepared dispersions by adding graphite powder in four different solvents most commonly employed for LPE, i.e. NMP, *o*-DCB, DMF and TCB. Sonication has been applied for 6 h in an ultrasonic bath at 600 watts. Different volumes of NOTBZ were added to NMP and *o*-DCB dispersions. Sonication of all samples yielded grey liquids consisting of a homogeneous phase and large numbers of macroscopic aggregates. To remove the unexfoliated graphitic material, centrifugation at 10 000 rpm for 30 min was carried out, and the obtained homogeneous dark dispersions (see Figure 9.1a and 9.1b) were characterized by different technics. To quantify the concentration of graphene after centrifugation, graphene dispersion was mixed with chloroform and heated up to 50°C for 30 min and then passed through polytetrafluoroethylene membrane filters (pore size 100 nm). The remaining solvent and NOTBZ molecules were washed several times with diethyl ether and $CHCl_3$. As previously reported [38], the presence of adsorbed molecules on the graphene sheets may affect

the mass measurements and ultimately the exfoliation yields. Careful measurements of the filtered mass provided the concentration of the dispersed phases after centrifugation

9.4.1.1 NMP and o-DCB dispersions in the presence/absence of NOTBZ

The LPE studies started by analysing the result of do independent blank experiments performed using pure NMP and *o*-DCB. The average concentration of graphene amounted to 85 ± 5 μg mL^{-1} for NMP, and 100 ± 6 μg mL^{-1} for *o*-DCB as portrayed in Figure 9.1c and 9.1d, respectively. These results are in a good agreement with those previously reported [1, 3] using the same experimental set-up. It is worth noting that in general the concentration of graphene in LPE process is influenced by the centrifugation speed, sonication power, temperature and time, amount and type of initial graphite, as well as the volume of the solvent.

We have then extended our LPE studies to the use of NOTBZ as dispersion-stabilizing agent. At room temperature and ambient pressure, NOTBZ is a liquid which is perfectly miscible with NMP and *o*-DCB. Among the four solvents used, upon addition of NOTBZ at specific percentage, we found that the concentration of graphene was more pronounced in NMP and *o*-DCB, and the highest yield was obtained for NMP as displayed in Figure 9.1c and 9.1d. This result is in contrast with the blank experiments. Noteworthy, the most relevant increase in graphene concentration amounting to 250 μg mL^{-1} was reached upon addition to the NMP dispersion of 15 volume % of NOTBZ.

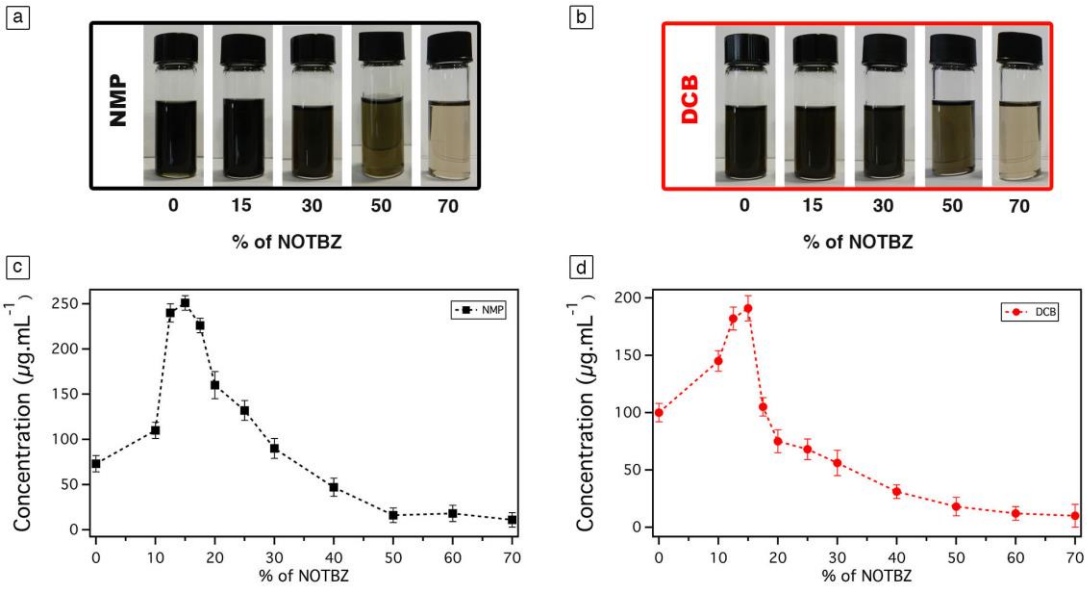

Figure 9.1. Photographs of graphene dispersions prepared by exfoliation of graphite flakes in a) NMP and b) *o*-DCB, at different percentage of NOTBZ volume. Average concentration of graphene dispersions after the filtration process at different percentage of NOTBZ volume in c) NMP and d) *o*-DCB. The error bars correspond to the standard deviation on the average values obtained through 10 independent experiments.

In the case of *o*-DCB, the maximum of graphene concentration is 190 µg mL^{-1} and is also observed upon addition of 15 volume % of NOTBZ. These concentrations correspond to an approximate increase of the exfoliation yield by 230 % for NMP and 100 % for *o*-DCB as compared to the blank experiments. It is worth noting that 15 volume % corresponds to a surface of graphene fully covered by NOTBZ molecules as detailed in Figure 9.3 and reported elsewhere [38]. Interestingly, the exfoliation at 100 volume % of NOTBZ, i.e. in pure NOTBZ, resulted in dramatic decrease of the exfoliation yield. In fact, no graphene was exfoliated, as revealed by TEM analysis. The exfoliation was successfull only when the amount of NOTBZ is below 40 %. This phenomenon can be expained by the fact that NOTBZ itself is a bad solvent for liquid-phase exfoliation. While, recent reports have demonstrated that solvents with surface tensions of ca. 40 mJ m^{-2}, e.g. NMP, *o*-DCB, are the best candidates for carying out LPE experiments, the relatively low surface tension of NOTBZ (ca. 30 mJ m^{-2}) and notably high increase of the LPE yieds in the case of NMP-NOTBZ and *o*-DCB-NOTBZ provided unambigous evidence that NOTBZ molecules can act as dispersion-stabilizing agent.

9.4.1.2 DMF and TCB dispersions in the presence/absence of NOTBZ

The average concentration of graphene amounted to 50 ± 5 μg mL^{-1} for TCB, and 60 ± 6 μg mL^{-1} for DMF as portrayed in Figure 9.2b. During the exfoliation of graphene in the presence of NOTBZ molecules, the concentration of graphene slighly increase in both solvents. Surprisingly, at the same percentage, i.e. 15%, the concentration of graphene in each of the solvents even TCB and DMF is also the highest.

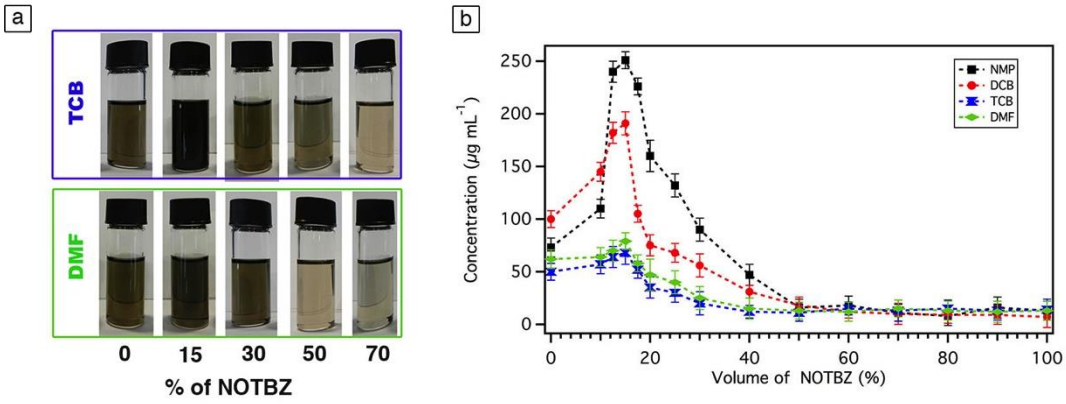

Figure 9.2. a) Photographs of graphene dispersions prepared by exfoliation of graphite flakes in TCB and DMF at different NOTBZ volume percentage, b) average concentration of graphene dispersions after the filtration process. The error bars correspond to the standard deviation on the average values obtained through 10 independent experiments.

9.4.2 Surface area

Typically NOTBZ does not form any ordered monolayers at the HOPG/graphene surface at room temperature and ambient pressure. Nevertheless, theoretical assumption of NOTBZ packing motif on graphene has been used for calculation the coverage areas. The area occupied by single molecule amounts to A= (5.92± 0.9) nm^2. The areas A occupied by single dispersion-stabilizing molecules, as well as area of graphene unit cell ($G_{unit\ cell}$ = (0.052± 0.004) nm^2) estimated by theoretical assumption can be used for calculating the mass and number of dispersion-stabilizing molecules needed to cover accessible graphene area. Noteworthy, in our calculations graphite powder has been considered as a single (rectangular)

graphene sheet. We found a correlation between the best ratio, i.e. 15 % and the surface area coverage. Interestingly, only 100 % of graphene coverage gives the highest exfoliation yield and for all the solvents we tested (Figure 9.3).

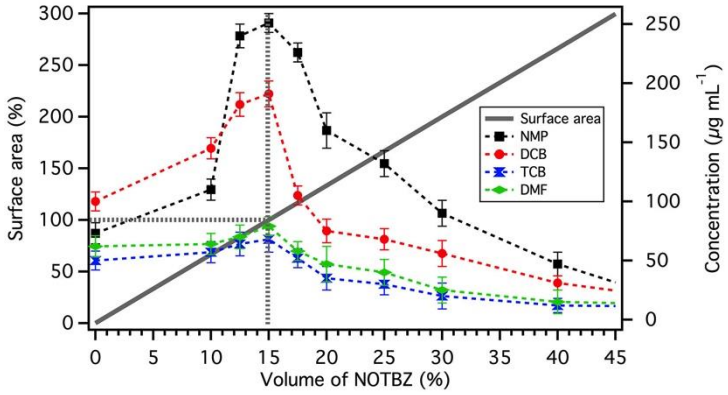

Figure 9.3. Correlation between surface area and volume percentage for all dispersions.

9.4.3 HR-TEM

In order to characterize the exfoliated graphene sheets, qualitative analysis providing more relevant details such as the percentage of single-layer graphene (SLG) flakes, the lateral size of the flakes and the presence/absence of defects is needed. Currently, the most relable method for the identification of the number of graphene layers in material produced by LPE is based on High-Resolution Transmission Electron Microscopy. Typically, the analysis of the folded edges of the graphene sheets provides estimates of the number of layers composing the flakes. Moreover, from the TEM analysis, the average lateral size of the graphene sheets can be defined.

First, we discuss dispersions prepared in NMP in the absence and/or the presence of NOTBZ molecules at the highest concentration obtained, i.e. the 15 %. The TEM micrographs reveal that the majority of dispersions in NMP are composed of a large fraction of monolayer 15 % and bilayer 18 % graphene sheets folded over themselves with lateral size smaller then 500 nm. In the presence of NOTBZ, graphene flakes were found mainly in a monolayer 35 % and

in a bilayer 28 % form (Figure 9.4c). Also, the majority of flakes were found to be smaller than 200 nm (Figure 9.4a). Figures 9.4b and 9.4d show HRTEM images of monolayered graphene.

We then focused our attention on the samples prepared in *o*-DCB in the presence and/or absence of NOTBZ as dispersion-stabilizing agent at the highest concentration obtained, i.e. the 15 %. The TEM micrographs reveal that the majority of dispersions in *o*-DCB are composed of a large fraction of monolayer 25 % and bilayer 22 % graphene sheets folded over themselves with lateral size smaller than 500 nm (Figure 9.4a). In the presence of NOTBZ, 25 % of graphene flakes were found mainly in a monolayered form and 24 % in a bilayered one. Additionnaly, the majority of flakes were found to be smaller than 500 nm.

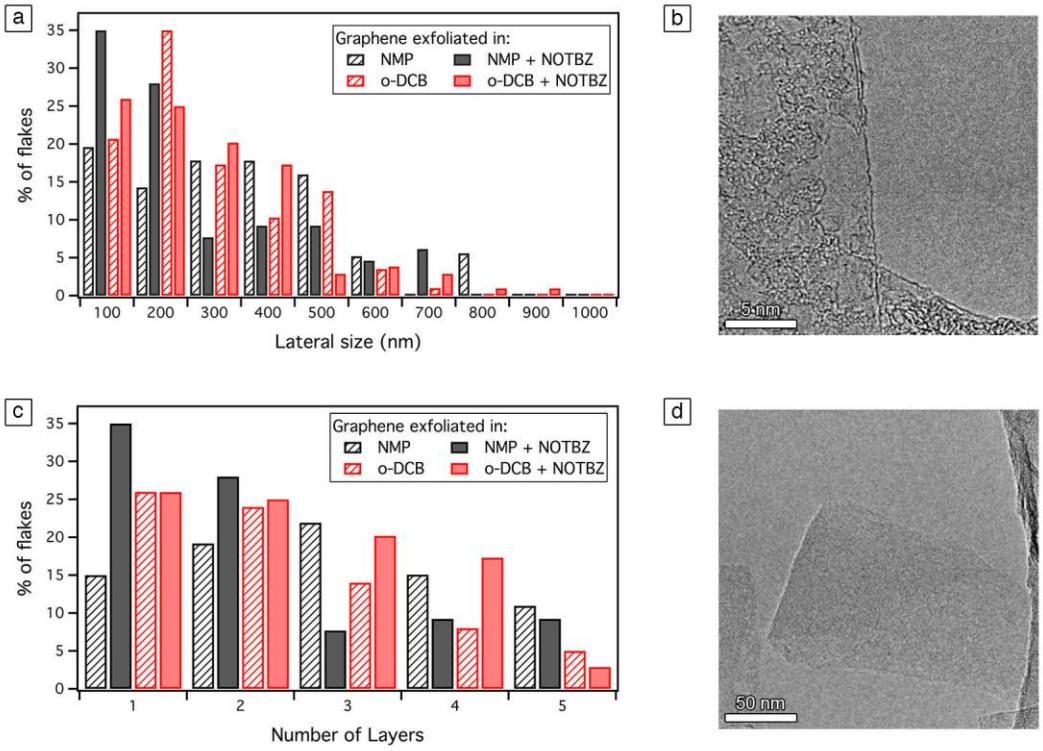

Figure 9.4. Statistical analyses of HR-TEM results of graphene exfoliated in pure NMP and *o*-DCB in the presence of NOTBZ molecules. a) Histogram of the lateral flake size distribution, b) HRTEM micrograph of a monolayer, c) Histogram of the distribution of the flake thickness, and d) TEM micrograph of a monolayer.

Also DMF and TCB dispersions were subject to TEM analysis. By analyzing hundreds of TEM micrographs, we were able to make statistic on the number of layers and the size of graphene sheets as shown in Figure 9.5. Exfoliation in the presence of NOTBZ in the four solvents leaded to a majority of mono and bi-layer flakes with more than 50 % of the total graphene flakes. More than 25 % of the total flakes are present in a monolayer form. But the size of the exfoliated graphene sheets is comprised between 100 and 400 nm. For DMF and TCB, the majority of graphene flakes have a lateral size larger than 200 nm.

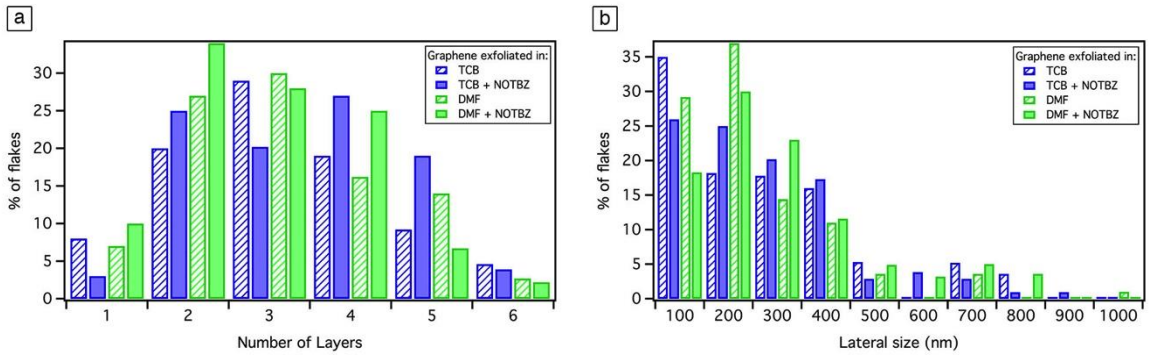

Figure 9.5. Statistical analyses of TEM and HR-TEM results of graphene dispersions exfoliated in the presence of NOTBZ in NMP, o-DCB, DMF and TCB. a) Histograms of the number of layer distribution of graphene flakes and b) histograms of the lateral size flakes size distribution of graphene flakes.

9.4.4 Raman spectroscopy

To complement the characterization result by HR-TEM, Raman spectroscopy was used. In fact, Raman analysis is more qualitative and it has been shown that this technique is sensitive to the changes in thickness composition under different experimental conditions. It has been revealed that Raman spectroscopy offers a simple and fast analysis of graphene sheet thickness with the evolution of 2D peak shape [5, 7]. However, due to the effect of the solvent, edge effects and strain and doping caused during exfoliation, the Raman spectrum of LPE graphene is more difficult to analyze compared to the spectrum of mechanically exfoliated

graphene. Therefore, the analysis is only quantitative and must be used in combination with HR-TEM results.

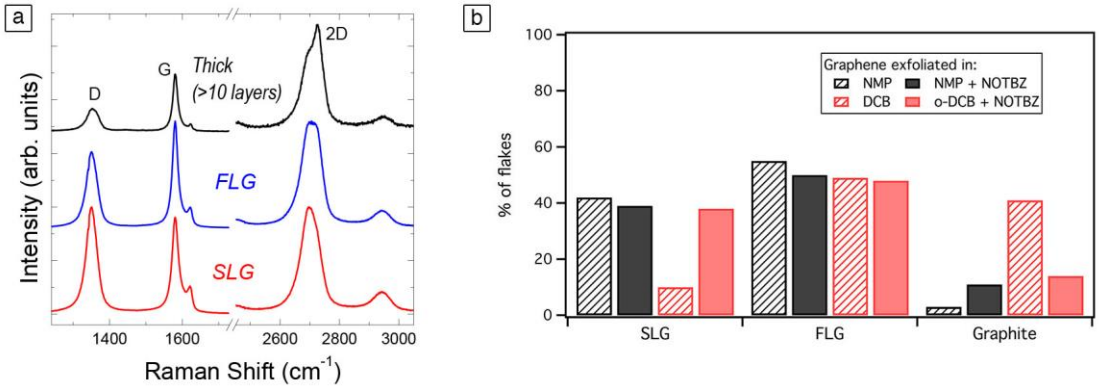

Figure 9.6. a) Typical Raman spectra observed for dispersions obtained by adding NOTBZ. b) Statistical analysis, based on Raman spectroscopy, on the thickness distribution of the flakes in NMP and DCB before and after addition of NOTBZ

Figure 9.6a shows the typical Raman spectra of LPE graphene obtained by adding NOTBZ to NMP and *o*-DCB solvents. Based on the shape of the 2D peak, we can distinguish between single-layer (SLG), few-layers graphene (FLG) and graphite (>10 layers). Statistical analysis shows that upon addition of NOTBZ to NMP and *o*-DCB, the percentage of SLG strongly increases for *o*-DCB, while it stays constant for NMP (Figure 9.6b). Therefore, based on Raman spectroscopy, NOTBZ seems to have a bigger effect on *o*-DCB than NMP. Figure 9.6 shows that the increase of single-layer concentration observed for *o*-DCB is related to a decrease in the percentage of thick layers, showing that NOTBZ is an effective exfoliation agent in *o*-DCB.

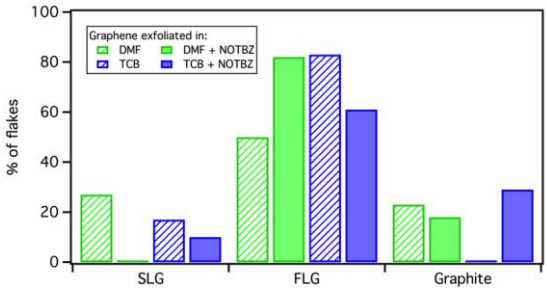

Figure 9.7. Statistical analysis, based on Raman spectroscopy, on the thickness distribution of the flakes in DMF and TCB before and after adding NOTBZ.

Note that all the spectra show a D peak, which is typical for LPE graphene [4]. We did not observe any particular difference in the intensity ratio between the D peak and G peak, I(D)/I(G), which indicates that NOTBZ does not introduce any structural defect in graphene when added either in NMP or *o*-DCB (Table 9.2).

Statistical analysis shows that upon addition of NOTBZ to DMF and TCB, the percentage of SLG strongly decreases for DMF, while it stays almost constant for TCB. Figure 9.7 shows that the majority of flakes are observed as few layers graphene flakes. Also the concentration of thick layers graphene increase for DMF in the presence of NOTBZ whereas for TCB is the opposite.

	% of flakes	**I(D)/I(G)**	**% of flakes**	**I(D)/I(G)**	**% of flakes**	**I(D)/I(G)**
	SLG		**FLG**		**Graphite**	
NMP+NOTBZ	38.9	0.6-1.9	50	0.3-1.8	11.1	0.3-0.6
***o*-DCB+NOTBZ**	38	0.6-1.7	48	0.2-1.3	14	0.2-0.7
DMF+NOTBZ	0	NA	82	0.3-1.2	18.4	0.2-0.5
TCB+NOTBZ	10.2	0.6-0.7	61	0.3-0.9	28.6	0.2-0.4

Table 9.2. Comparative table of the % of flakes and ratio I(D)/I(G) for the four solvents in the presence of NOTBZ molecules.

Noteworthy, the thickness analysis based on Raman spectroscopy is only quantitative and must be used in combination with HR-TEM results. Commonly, the results based on TEM are more reliable for liquid-phase exfoliated graphene, and the determination of number of layers based on Raman spectra is more suitable for graphene prepared by micromechanical

exfoliation and CVD methods. Therefore, the small discrepancy in the flake thickness analysis between the Raman and TEM is not surprising.

9.4.5 XPS characterization

We used XPS to analyze graphene + NOTBZ in NMP before and after washing the NOTBZ. The high-resolution C1s XPS spectrum in figure 9.8a of the graphene sheets from NMP dispersions showed a sharp peak at 284.3 eV that corresponded to C-C bonds of carbon atoms in a conjugated honeycomb lattice. Figure 9.8b represents the high-resolution C1s XPS spectrum of graphene + NOTBZ showed a larger peak at 284.6 eV corresponding to delocalized π conjugation from the sp^2 atomic structure of graphite. Also this peak exhibits a larger behavior as the C-C bond from NOTBZ is also contributed. After the washing step, the peak at 284.4 eV became sharp again (Figure 9.8c) and confirmed the removal of NOTBZ. The same behavior is observed for each of the four solvents.

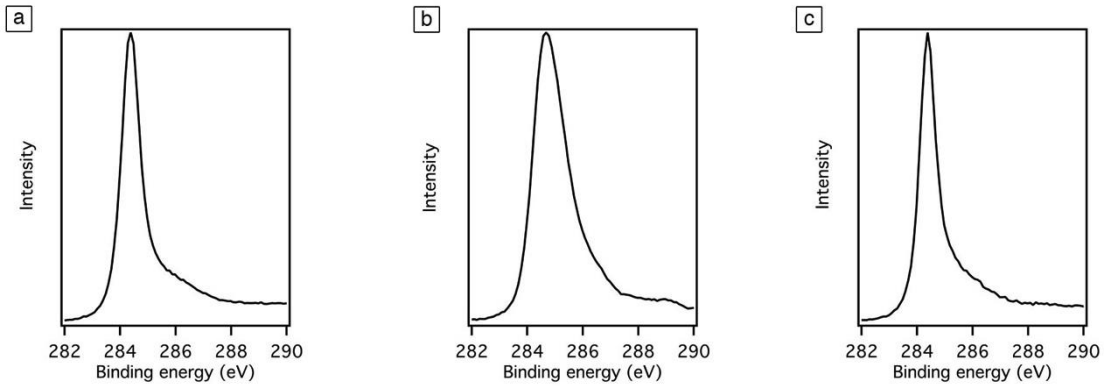

Figure 9.8. High-resolution C1s spectra of a) graphene exfoliated in NMP, b) graphene exfoliated in the presence of NOTBZ in NMP and c) graphene exfoliated in the presence of NOTBZ in NMP after washing the NOTBZ molecules.

9.4.6 Graphene thin film

Despite the increase of the exfoliation yield and the successful production of mono and few layers thick graphene sheets, the deposition of these graphene dispersions on commonly used substrates (mainly SiO_2 and quartz) to form uniform films for applications in electronics remains a challenge. The solvents used for LPE have high boiling points, which results in a re-aggregation problem particularly when drop-casting method is used. Moreover, spin-coating of such dispersions is very challenging because as a results of the poor wetting, only few graphene sheets remains on the surface of the substrate, making it an unsuitable technique to form uniform films of graphene. Another well-known phenomenon observed when a drop of graphene dispersion is drying on a surface, is the coffee-ring effect [8-10]. Some graphene flakes accumulate at the drop periphery, yielding a characteristic ring shape pattern.

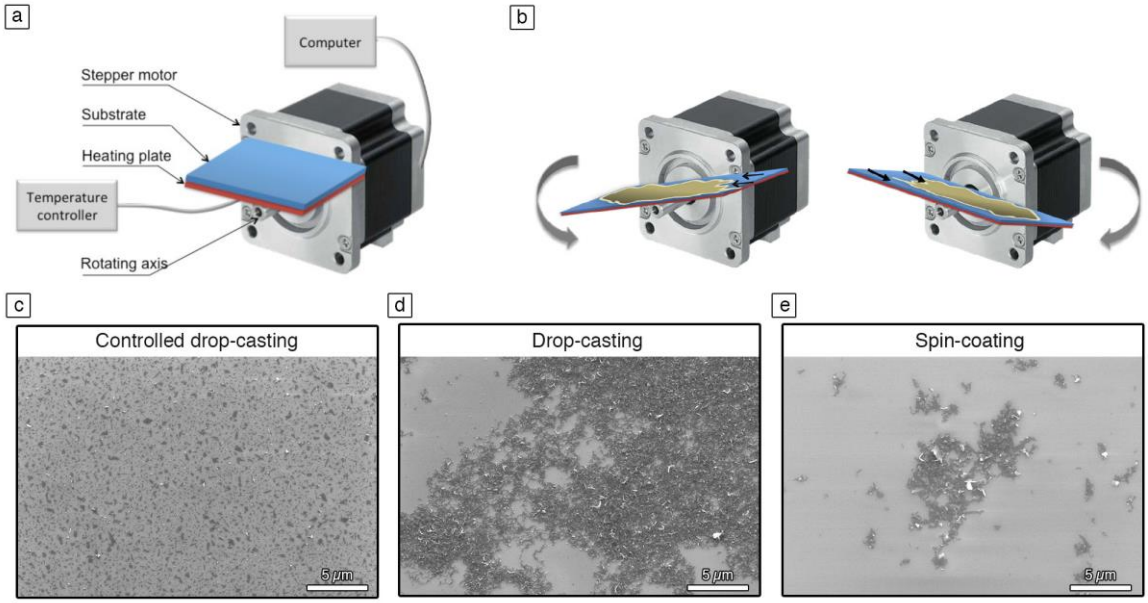

Figure 9.9. a) Schematic scheme of the developed technique for depositing graphene dispersions. b) Operating principle of the technique showing a rotation of the axis in a counterclockwise direction (image on the left) and a clockwise direction (image on the right). SEM images of graphene film prepared by c) spin-controlled drop-casting (using the set-up in a), d) drop-casting, and e) spin-coating.

Consequently, we thought of controlling the deposition from solution by devising a new simple technique, called spin-controlled drop-casting. It consists of a stepper motor featuring a rotating axis controlled by custom software as shown in Figure 9.9a. The substrate is connected to a heating plate fixed on the axis. First the drop is deposited at a zero angle, i.e. when the substrate is in its planar configuration. Then the x-axis is rotated back and forth in counterclockwise (Figure 9.9b left) and clockwise directions (Figure 9.9b right) by the stepper motor at controlled speed and angles configured by the software. These movements accompanied by the underneath heating of the substrate allow to avoid the coffee ring-effect and obtain a complete evaporation of the solvent. Interestingly, a uniform film with more dispersed and less aggregated sheets is obtained (see Figure 9.9c) unlike the normal casting method (see Figure 9.9d) or spin coating (see Figure 9.9e). Moreover, this new method allows the fabrication of graphene films fully covering the substrate on a scale of 100 μm^2 (see Figure 9.10).

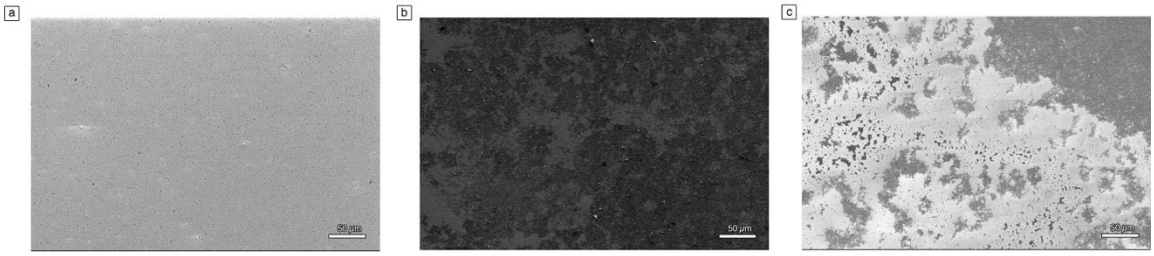

Figure 9.10. Large-scale SEM images of graphene film for N=1 prepared by a) spin-controlled drop-casting, b) drop-casting, and c) spin-coating.

AFM and SEM were used in order to investigate the change of morphology of these films, when different numbers of deposition (*n*) are applied. The graphene sheets are forming islands (as observed in Figure 9.9c) with a height up to 24 ± 4 nm (Figure 9.11).

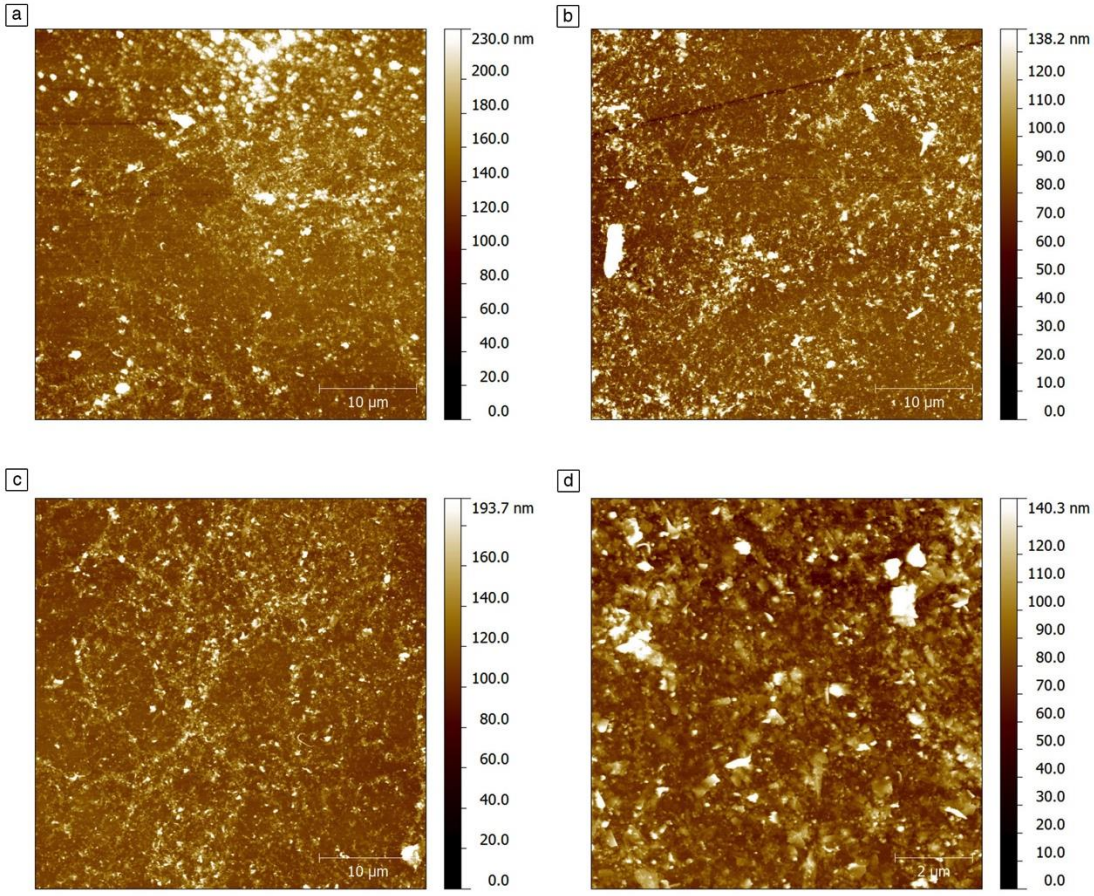

Figure 9.11. AFM images of graphene film prepared by spin-controlled drop-casting for a) N=3, b) N=5, c) N=7 and d) N=9 from NMP + NOTBZ dispersion.

The subsequent depositions of multiple dispersion drops allow increasing the surface coverage of the film, while the thickness of the films remains constant at 24 nm. Noteworthy, as many as nine depositions (n = 9) is needed in order to form a film with more than 95% of surface coverage. A correlation between the coverage and the number of deposition has been extracted from AFM analysis (Figure 9.12).

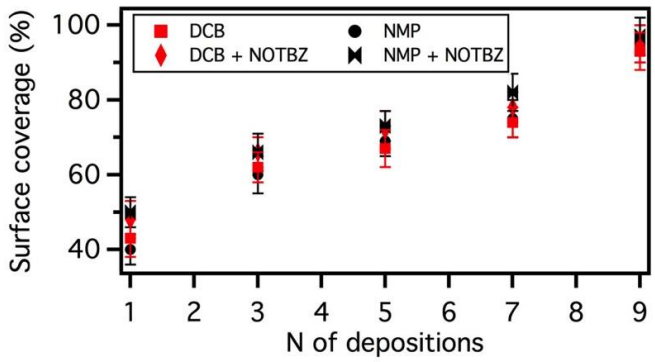

Figure 9.12. Estimation of the surface coverage

Optical transmittance and electrical resistance of graphene films are two important characteristics for many opto-electronic applications requiring transparent electrodes. Therefore, benefiting of the advantages offered by our developed set-up, we prepared on quartz substrates conductive graphene films from graphene dispersions in *o*-DCB or NMP in the presence and absence of NOTBZ molecules. The preparation mechanism is depicted in Figure 9.9. Prior to deposed graphene dispersions, quartz substrate were ozone treated in order to clean the surface. UV–Vis spectroscopy was used to measure the optical transmittance versus the number of deposition as shown in Figure 9.13a. In the visible range, graphene films prepared in *o*-DCB or NMP, with and without NOTBZ molecules, show transmittance of ~ 93 % at 550 nm for the first deposition (n = 1) regardless the type of solvent or the presence or absence of NOTBZ. In all cases and as expected, the transmittance decreases when the number of deposition or the surface coverage increases. For n = 9, where the sample is uniform with coverage exceeding 95%, the transmittance at 550 nm is lowered as compared to a single deposition and it decreases from ~93 to 72 %.

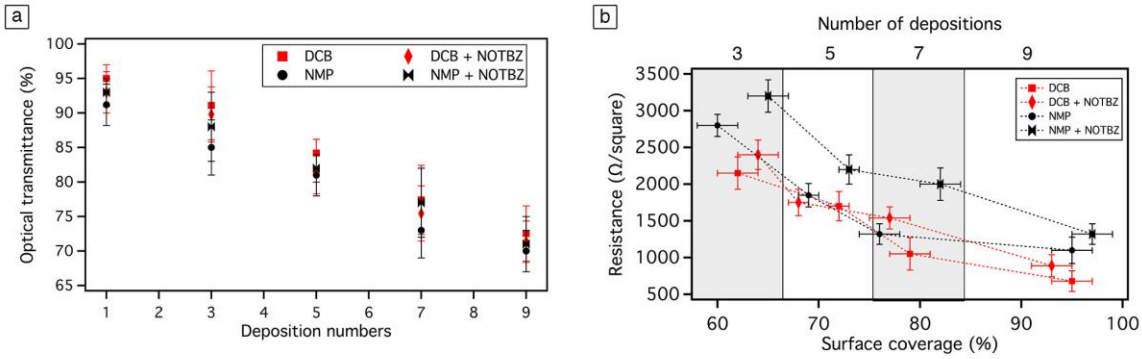

Figure 9.13. a) The optical transmittance at λ=550 nm, and b) the sheet resistance of graphene film versus number of deposition. The error bars correspond to the standard deviation on the average values obtained by performing 6 independent measurements.

The measured sheet resistances of the 24 nm thick graphene film led to very high values for films prepared from only three depositions (see Figure 9.13b). This is mainly due to the fact that these sheets are not perfectly overlapped. Average resistance values were in the range of 2500 to 1000 Ω/square for graphene prepared from *o*-DCB, and were higher in the case of NMP (3200 to 2200 Ω/square) and in the presence of NOTBZ because of the low conductivity of the molecule. However, if more depositions are performed, the film resistance decreases (see Figure 9.13b) due to the better physical interconnection among adjacent graphene sheets and the increased surface coverage. The presence of the added molecules, because of their electrically insulating nature, results in higher resistances as well. Our best sample (graphene from *o*-DCB only) shows a surface coverage close to 100 % for 9 depositions with 72 % of transmittance and 680 Ω/square. With a surface coverage amounting 100 %, the thickness of the graphene film times the sheet resistance value expressed in Ω/square is equal to the volume resistivity in Ω m of the graphene film. In our case the volume resistivity is as low as 1.6×10^{-5} Ω m. Also our sheet resistances and transparency are very close to those reported for graphene deposed by casting-dropping graphene/acetone suspension onto a polystyrene glass ride (~ 1000 Ω/square, 80 % at 550 nm) [10], or electro-chemically exfoliated graphene treated with HNO_3 (~ 400 Ω/square and 73 % at 550 nm) [11] but still far from CVD-graphene doped with HNO_3 (~ 30 Ω/square and 90 % at 550 nm) [12].

9.5 Conclusions

We have demonstrated that it is possible to enhance the yield of graphite exfoliation by mastering a molecule-assisted LPE-based approach to produce high-quality graphene flakes from bulk graphite. To attain a fundamental understanding of the role of molecule-graphene interaction on the yield of graphene LPE, we have carried out a comparative study by using NOTBZ as dispersion-stabilizing agent upon increasing the volume ratio of NOTBZ in two organic solvents, i.e. NMP and *o*-DCB. Careful analysis revealed a significant increase in the yield of exfoliation with the volume percentage of NOTBZ until a maximum. In particular, the most effective exfoliation was obtained with 15 volume % of NOTBZ in NMP as a solvent, with a concentration of exfoliated graphene of 250 μg mL^{-1} corresponding nearly to 230 % increase in exfoliation yield when compared to samples prepared in pure NMP (85 μg mL^{-1}). In the case of o-DCB, the most effective exfoliation was observed using also 15 volume % of NOTBZ, which led to ca. 100% increase in the exfoliation yield. Furthermore, a remarkable increase of single-layer graphene (SLG) flakes was observed in some cases. Careful investigation made it possible to correlate the 15 % NOTBZ volume to 100 % of surface area estimated which was found to be accurate for all studied solvents. TEM analysis of dispersions produced in NMP revealed that the quantity of SLG is improved by 100 % when using NOTBZ molecules. In the case of *o*-DCB, the quantity of SLG was found amounting 25 % even after addition of NOTBZ molecules, although a qualitative Raman analysis showed an opposite trend between NMP and *o*-DCB after adding NOTBZ. Graphene ink produced with our approach was deposed uniformly on SiO_2 or quartz substrate by using a new deposition technique relying on a spin-controlled drop casting. These graphene films exhibit sheet resistance as low as 1 kΩ/square and transparency of 70 % at 550 nm. By controlling the number of depositions and the concentration of graphene dispersions, film resistance and transparency can be tuned. Our approach opens up new avenues for the technological applications of graphene ink as low-cost electrodes and conducting nanocomposite for electronics.

9.6 References

1. A. Ciesielski, S. Haar, M. El Gemayel, H. F. Yang, J. Clough, G. Melinte, M. Gobbi, E. Orgiu, M. V. Nardi, G. Ligorio, V. Palermo, N. Koch, O. Ersen, C. Casiraghi and P. Samori, *Angew Chem Int Edit*, 2014, **53**, 10355-10361.
2. H. Yang, F. Withers, E. Gebremedhn, E. Lewis, L. Britnell, A. Felten, V. Palermo, S. Haigh, D. Beljonne and C. Casiraghi, *2D Materials*, 2014.
3. H. Yang, Y. Hernandez, A. Schlierf, A. Felten, A. Eckmann, S. Johal, P. Louette, J. J. Pireaux, X. Feng, K. Muellen, V. Palermo and C. Casiraghi, *Carbon*, 2013, **53**, 357-365.
4. A. Schlierf, H. F. Yang, E. Gebremedhn, E. Treossi, L. Ortolani, L. P. Chen, A. Minoia, V. Morandi, P. Samori, C. Casiraghi, D. Beljonne and V. Palermo, *Nanoscale*, 2013, **5**, 4205-42110.
5. S. Haar, A. Ciesielski, J. Clough, H. F. Yang, R. Mazzaro, F. Richard, S. Conti, N. Merstorf, M. Cecchini, V. Morandi, C. Casiraghi and P. Samorì, *Small*, 2015, **11**, 1691–1702.
6. C. Casiraghi, *Raman spectroscopy of graphene*, 2012.
44. A. C. Ferrari, J. C. Meyer, V. Scardaci, C. Casiraghi, M. Lazzeri, F. Mauri, S. Piscanec, D. Jiang, K. S. Novoselov, S. Roth and A. K. Geim, *Phys Rev Lett*, 2006, **97**.
7. P. Z. Sun, R. Z. Ma, K. L. Wang, M. L. Zhong, J. Q. Wei, D. H. Wu, T. Sasaki and H. W. Zhu, *Nanotechnology*, 2013, **24**.
8. P. J. Yunker, T. Still, M. A. Lohr and A. G. Yodh, *Nature*, 2011, **476**, 308-311.
9. C. J. Shih, A. Vijayaraghavan, R. Krishnan, R. Sharma, J. H. Han, M. H. Ham, Z. Jin, S. C. Lin, G. L. C. Paulus, N. F. Reuel, Q. H. Wang, D. Blankschtein and M. S. Strano, *Nat Nanotechnol*, 2011, **6**, 439-445.
10. G. Shi, A. Michelmore, J. Jin, L. H. Li, Y. Chen, L. Z. Wang, H. Yu, G. Wallace, S. Gambhir, S. M. Zhu, P. Hojati-Talemi and J. Ma, *J Mater Chem A*, 2014, **2**, 20382-20392.
11. K. Parvez, R. J. Li, S. R. Puniredd, Y. Hernandez, F. Hinkel, S. H. Wang, X. L. Feng and K. Mullen, *Acs Nano*, 2013, **7**, 3598-36010.
12. S. Bae, H. Kim, Y. Lee, X. F. Xu, J. S. Park, Y. Zheng, J. Balakrishnan, T. Lei, H. R. Kim, Y. I. Song, Y. J. Kim, K. S. Kim, B. Ozyilmaz, J. H. Ahn, B. H. Hong and S. Iijima, *Nat Nanotechnol*, 2010, **5**, 574-578.

Chapter 10 Light enhanced LPE and photoswitching current in graphene-composite

10.1 Introduction

Small organic molecules such as surfactants or dispersion-stabilizing agents, can promote the exfoliation of graphite into graphene,[1, 2] in particular when such a molecules have higher adsorption energies on the basal plane of graphene, than those involved in solvent-graphene interaction.[3, 4]

Photochromic molecules, and in particular azobenzene-based molecules either physisorbed directly[5, 6] or trough pyrene anchoring groups[7] on the graphene surface or even when graphene is adsorbed on an azobenzene self-assembled monolayer [8] can result in reversible modulation of the electronic properties of the 2D material. Nonetheless, the use of additional responsive functions exposed on a suitably designed molecule to assist the LPE of graphene into functional inks is still unexplored. This approach could lead to the production of functional hybrid materials and nanocomposites in a one-pot process.

10.2 Scope

Here we combine photochromic systems and LPE graphene exploiting the properties of these materials. We focus on 4-(decyloxy)azobenzene molecules and demonstrate that their use has two major advantages: first, the quantity of graphene dispersions in *N*-methyl-2-pyrrolidone (NMP) can be enhanced by exploiting the photoisomerization of azobenzene molecules during exfoliation process. Second, the isomerization of azobenzenes from *trans* to *cis* form and *vice versa*, when physisorbed in-between adjacent graphene flakes, leads to a reversible modulation of the inter-flake distance on the sub-Ångström scale. This is reflected in a light-response of the electrical properties of the hybrid material.

10.3 Materials

10.3.1 Materials

Graphite flakes (Sigma-Aldrich, Product Nr. 332461), 4-(decyloxy)azobenzene (Sigma-Aldrich, Product Nr. S931950) and *N*-methyl-2-pyrrolidone (NMP, Product Nr. 270458) were purchased from Sigma-Aldrich.

10.3.2 Preparation of graphene

Graphene dispersions have been prepared by adding graphite powder (100 mg) in NMP (10 mL), and tip-sonication (Labsonic M, Platinum tip, diameter 2 mm) for 3 hours either in dark or under UV light irradiation using a portable laboratory UV lamp (8 W, 365 nm, 0.34 mW cm^{-2}, Herolab GmbH), at two different temperatures, namely 20 and 40 °C in glass vials (Pyrex), in the presence of azobenzene molecules (5.5 mg). (See Figure 10.1) Subsequently, the dispersions were allowed to settle for 15 min and 90 vol.% of the dispersions were decanted and centrifuged (Eppendorf, centrifuge 5804) for 1 hour at 10.000 rpm. From the

centrifuged dispersions 70 vol.% were pipetted off the top for characterization and sample preparation. To quantify the concentration of graphene after centrifugation, the dispersions were passed through polytetrafluoroethylene (PTFE) membrane filters (pore size 100 nm). Measurements of the filtered mass were performed on a microbalance (Sartorius MSA2.75)

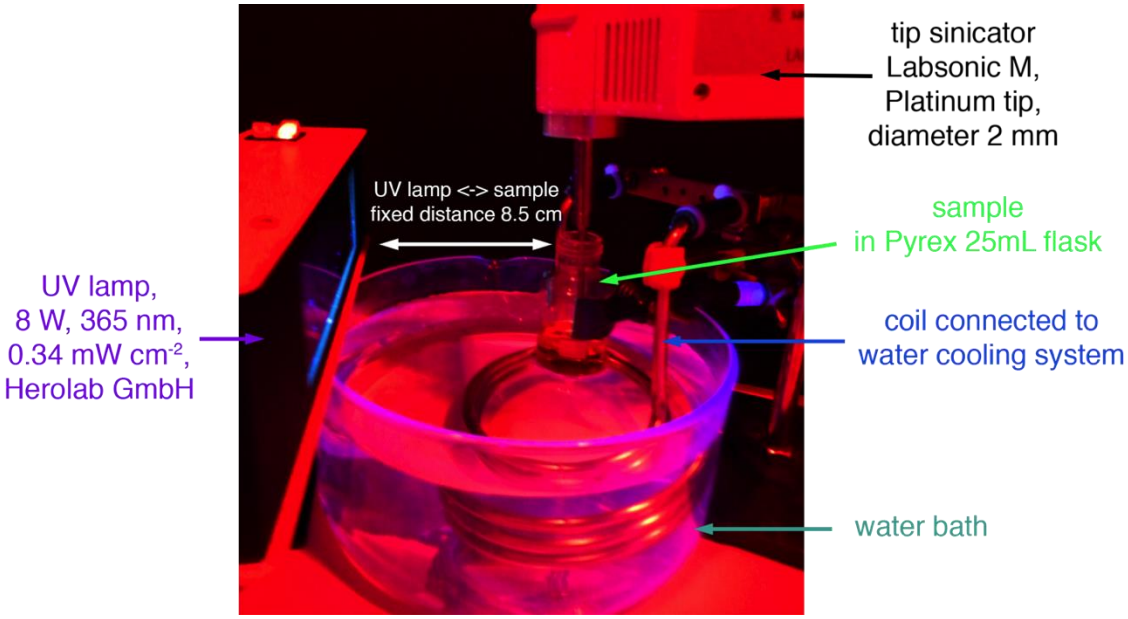

Figure 10.1. Photograph of experimental set-up

10.3.3 Device fabrication

For the device fabrication, n^{++}Si substrates with a thermally grown SiO_2 layer (230 nm) and pre-patterned interdigitated gold source and drain electrodes (IPMS Fraunhofer) with different channel length (L = 2.5, 5, 10, 20 μm) and constant channel width (W = 10 mm) were used. The substrates were cleaned prior to the device fabrication in an ultrasonic bath (FB 15047, Fisher Scientific) of acetone and isopropanol, 15 min in each solvent, and treated 5 min (+ 30 min incubation) with a UV surface decontamination system (PSD-UV, Novascan) to improve wetting of the solvent. The graphene dispersions (50 □L) were drop-cast on the cleaned substrates and dried for 48h in vacuum at 30°C.

10.3.4 Characterizations

The electrical characterization was carried out in inert atmosphere (glovebox) with an electrometer (Keithley 2636A) interfaced with LabTracer^{TM} software. For the light induced switch, a Polychrome V monochromator (Till Photonics) was used as UV light (350 nm, 5.64 mW/cm^{-2}) and visible light source (450 nm, 4.83 mWcm^{-2}). For the Raman experiments, graphene dispersions were drop-cast onto pre-cleaned n^{++}Si substrates with a thermally grown SiO_2 layer (300 nm) and dried for 48h. Raman spectra were collected with a Renishaw InVia spectrometer at 457, 514.5 and 633 nm. The excitation power was kept below 1 mW to avoid effects of local heating. The scattered light was collected with a 100x objective. HR-TEM was out with a FEI Tecnai F20 TEM/STEM equipped with a Schottky emitter and operated at a 120 keV primary beam energy. SEM images were recorded with a Quanta FEG 250 from FEI.

The thickness of the hybrid films was determined with an Alpha-Step IQ Surface Profiler from KLA Tencor. XPS analyses were carried out on a Thermo Scientific K-Alpha X-ray photoelectron spectrometer with a basic chamber pressure of ~10^{-8} mbar and an Al anode as the X-ray source (X-ray radiation of 1486 eV). Spot sizes of 400 μm were used and pass energies of 200.00 eV for survey scans and 50.00 eV for high-resolution scans were used. 150 μL of dispersions were spin coated on Au substrate for 1 minute at 1000 rpm and substrates were annealed for 1 day at 100°C in a oven under vacuum. Samples for XRD diffraction analysis were prepared by precipitating graphene and/or graphene/azobenzene by adding water:ethanol (1:1, *vol*:*vol*) into NMP dispersions. Collected precipitate was dried under vacuum for 24h. The powder X-ray diffraction (XRD) patterns of all the samples were obtained using a Bruker AXS D2 Phaser (LYNXEYE detector) with Ni-filtrated Cu-Kα radiation (λ = 1.5406 Å) with 1 mm of air-scattering slit, 0.1 mm equatorial slit. Samples were deposited on the surface of single crystal Si wafer (cut of (911)). XRD patterns were collected with degree step of 0.016° and time step increments of 10 sec/step from 8 to 80°.

10.4 Results and discussions

10.4.1 Liquid-phase exfoliation

To test the capability of the alkyl-substituted azobenzenes to increase the yield of graphene exfoliation and to exploit the photochromic nature of such molecules when interacting with graphene, vials containing NMP, graphite powder and azobenzene molecules underwent 3 hours of tip sonication. Such process was carried out either in dark or under UV light irradiation using a portable laboratory UV lamp, at two different temperatures, i.e. 20 °C and 40 °C. Subsequently, the dispersions were allowed to settle for 15 min and 90 vol% of the dispersions, were decanted and centrifuged for 1 hour at 10 000 rpm. Graphene dispersions prepared in such a way have been compared with control samples, i.e. dispersion prepared in the absence of azobenzene molecules, both in dark and irradiated at 365 nm at either 20 °C or 40 °C.

To quantify the concentration of graphene after centrifugation, a mixture of graphene dispersion and 2-propanol (IPA) was first heated up to 50 °C for 30 min and then passed through polytetrafluoroethylene (PTFE) membrane filters. The remaining solvent and azobenzene molecules were washed several times with diethyl ether and IPA. Careful measurements of the filtered mass were performed on a microbalance to infer the concentrations of graphene (see Figure 10.2b). The presence of adsorbed molecules on the graphene sheets may affect the mass measurements and ultimately the exfoliation yields. Thus, the heating step was necessary to completely remove, i.e. desorb, the azobenzene molecules from graphene, as proven with X-ray photoelectron characterization (XPS).

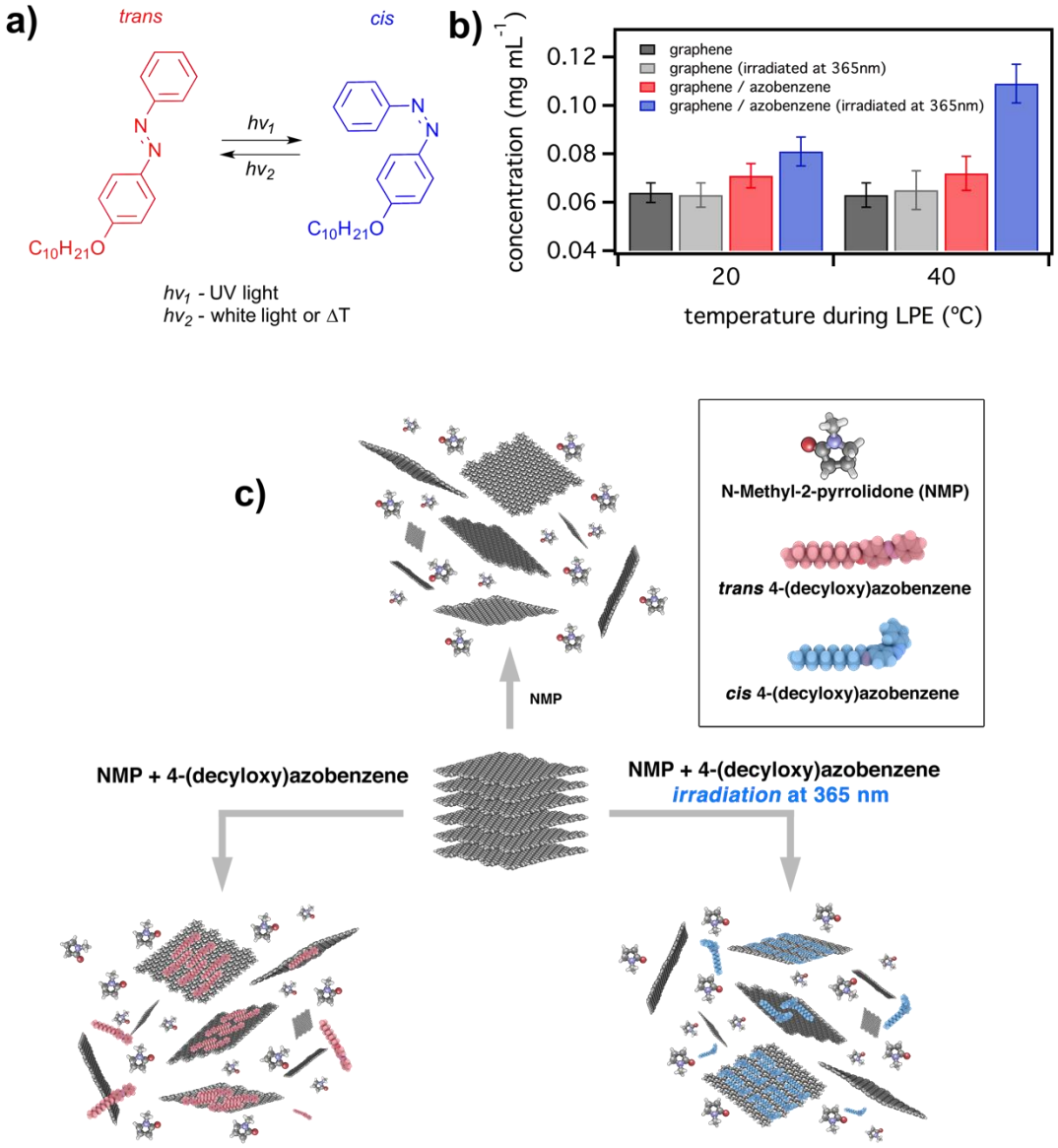

Figure 10.2. Azobenzenes, light-assisted graphene's LPE process in the presence of azobenzene and yield of exfoliation. a) Chemical structure of 4-(decyloxy)azobenzene and reversible *trans-cis* photoisomerization under UV and visible light. b) Average concentration of graphene dispersions after the filtration process. The error bars reflect a statistical analysis on 20 independent experiments. c) Schematic representation of LPE process under different experimental conditions: in NMP (reference experiment), in NMP with azobenzene molecules in dark and under UV-vis irradiation.

By analysing the results of 20 independent experiments, we found that when exfoliation is performed in the absence of azobenzene molecules (control experiments), comparable concentrations of graphene were observed when dispersions were kept at 20 °C (64 ± 5 μg mL^{-1}) or heated at 40 °C (62 ± 6 μg mL^{-1}). Moreover, the irradiation of such dispersions at 365 nm did not affect the quantities of produced material, neither at 20 °C nor at 40 °C (63 ± 6 μg mL^{-1} and 63 ± 8 μg mL^{-1}, respectively).

It is worth noting that these values of graphene concentration cannot be directly compared with the results reported by other research groups. In fact, benchmarking the values of graphene concentration is one of the hottest issues in the community, since the final concentration of graphene and lateral flake size differ significantly from one group to another. This can be simply explained by the fact that different, subtle experimental conditions, such as initial graphite concentration, solvent volume, sonication power and temperature, are (with a few exceptions) commonly omitted or not discussed. Furthermore, concentration of dispersions prepared by tip-sonication cannot be compared with those made by bath-sonication, because the different density as well as the power of ultrasounds highly affects the exfoliation yields.[9] While the majority of graphene dispersions reported in literature are produced by bath-sonication, in order to exploit the photochromic nature of azobenzene molecules, we used tip-sonicator, which allowed us to *in-situ* irradiate the dispersions with ultra-violet light continuously during LPE process.

LPE exploiting alkoxy-substituted azobenzene as dispersion-stabilizing agents can occur according to different scenarios depending on the isomeric form of the photochromic molecule (Figure 10.2c). We found that the presence of azobenzene molecules has no major influence on the concentration of dispersions prepared in dark, which amounts to 71 ± 5 μg mL^{-1} and 72 ± 7 μg mL^{-1} at 20 °C and 40 °C, respectively. As previously reported, the use of small organic molecules, and in particular those based on aromatic cores,[2] and alkyl functionalization[3, 4] can promote the exfoliation of graphite into graphene. Therefore, even a minor increase of graphene concentration (6-9 μg mL^{-1}) upon addition of a relatively small amount of azobenzene molecules (5 wt%), highlights the importance played by the molecules during the LPE.

In contrast to the case of the experiments performed in dark, irradiation with UV light at 365 nm of dispersions during LPE process resulted in a remarkable increase of the graphene concentration. In particular, substantial enhancement in graphene concentration was obtained at 20 °C, amounting to 81 ± 5 μg mL^{-1}, which corresponds to a nearly 30% increase in the yield of exfoliation, when compared to blank samples (63 μg mL^{-1}). Yet, the most significant increase in graphene concentration was obtained by irradiating graphene/azobenzene dispersions heated at 40 °C, amounting to 110 ± 8 μg mL^{-1}, which corresponds to a 75% increase in the yield of exfoliation. These results demonstrate that the addition of azobenzene molecules during LPE leads to a significant increase in the yield of exfoliation only in samples containing azobenzenes being irradiated at 365 nm. Therefore, the increase in graphene concentration can be attributed directly to *trans*-to-*cis* photoisomerization. Moreover, notable temperature dependence on the LPE yields was observed, which may be due to differences in molecule-graphene interactions at 20 and 40 °C, as well as different kinetics of *trans*-to-*cis* photoisomerization process.

10.4.2 *Trans*-to-*cis* photoisomerization and *cis*-to-*trans* relaxation

The transition from the thermodynamically stable *trans* to the metastable *cis* form can be induced by irradiation with UV light, and takes place on the picoseconds timescale,[10, 11] whereas the *cis*-to-*trans* isomerization is typically triggered by light or heat. The latter can also be activated by the use of ultrasound-induced mechanical force. Although, it has been considered that mechanoisomerization of azobenzene typically results in the cleavage of the N=N *azo* bond,[12] recent theoretical calculations[13] and experimental results[14] have challenged this view.

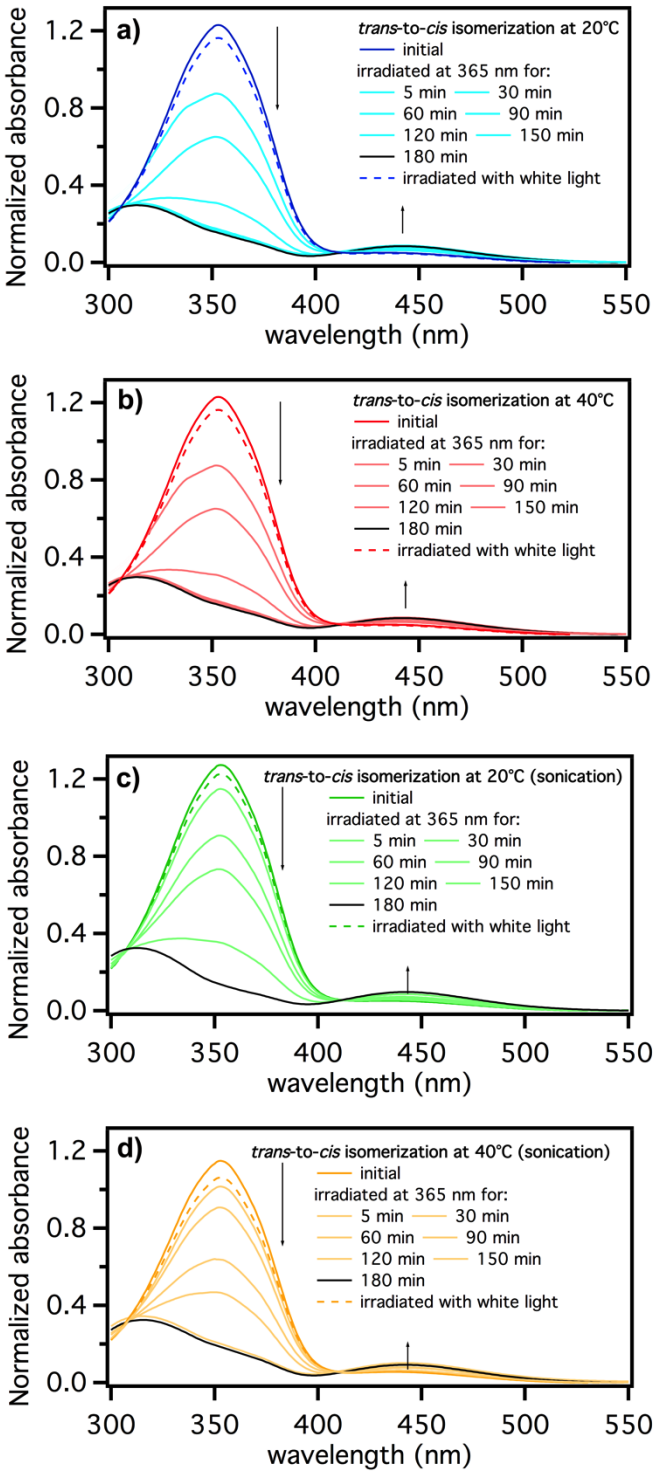

Figure 10.3. UV-vis spectra of the *trans*-to-*cis* isomerization of 4-(decyloxy)azobenzene in NMP showing disappearance of the 353 nm band and increase of 442 nm band upon irradiation with UV-light (λ = 365 nm) for 3h under different experimental conditions: a) 20 °C, b) 40 °C, c) 20 °C / sonicated and d) 40 °C / sonicated.

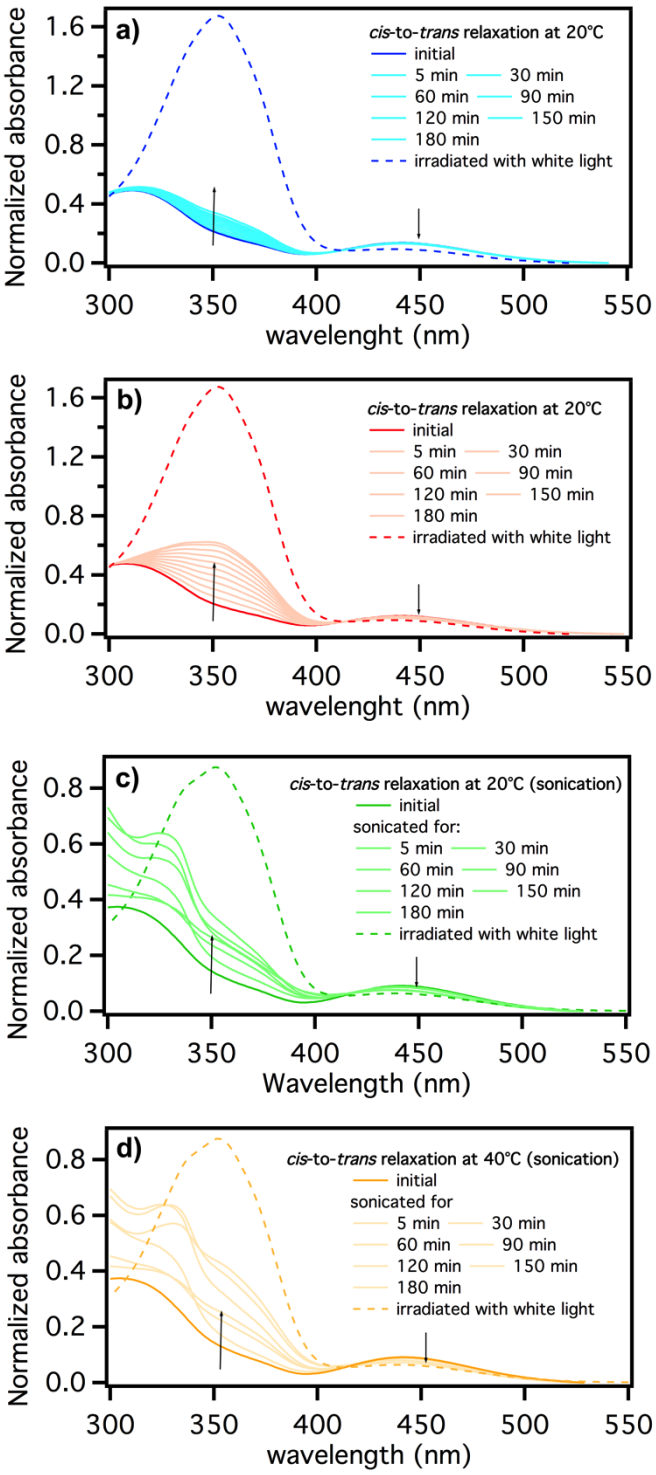

Figure 10.4. UV-vis spectra the *cis*-to-*trans* relaxation of *cis*-4-(decyloxy)azobenzene in NMP showing disappearance of the 442 nm band and increase of that at 353 nm as a function of time (samples kept in dark and sonicated) under different experimental conditions: a) 20 °C, b) 40 °C, c) 20 °C and d) 40 °C.

To gain a quantitative understanding of the photoisomerization of azobenzene, we performed a simple yet insightful kinetic analysis of both *trans*-to-*cis* and *cis*-to-*trans* isomerization. The UV-vis spectra of azobenzene dissolved in NMP (Figure 10.5a, black line) shows an absorption maxima at 353 nm, arising from the π–π* transition, and a peak at 442 nm arising from the n–π* transition. The UV-vis spectra of the above solution when irradiated with UV light at λ = 365 nm showed a dramatic reduction of the band at 353 nm, and an increase in absorbance of the 442 nm (n–π* transition) peak, which is a characteristic feature attributed to the photoisomerization from *trans* to *cis* (Figure 10.5a, red line). The photostationary state can be reversibly converted back to the *trans* isomer upon irradiation at λ = 450 nm. The conversion is more than 95% back to the thermodynamically stable *trans*-azobenzene (Figure 10.5a, black dashed line).

To probe *cis*-to-*trans* isomerization of the azobenzene molecules, under the experimental conditions corresponding to those used during the LPE process, i.e. at 20 °C and 40 °C, in the presence of ultrasound-induced mechanical forces, a stock solution of azobenzene in NMP (110.2 mM) was prepared, and then exposed to UV light at λ = 365 nm and sonicated for 3 hours. Every 30 min (except a first measurement after 5 min) 0.2 mL of UV irradiated solution was transferred (in the dark) into a quartz cuvette, diluted 10 times with NMP, and the optical absorption spectrum was recorded (shown in Figure 10.3 and 10.4). Lastly, to ensure stability of the *azo* bond during the sonication, a solution sonicated for 3 hours was exposed to white light and an absorption spectrum was recorded. Similar procedure was applied for blank experiments, i.e. in the absence of ultrasound-induced mechanical forces.

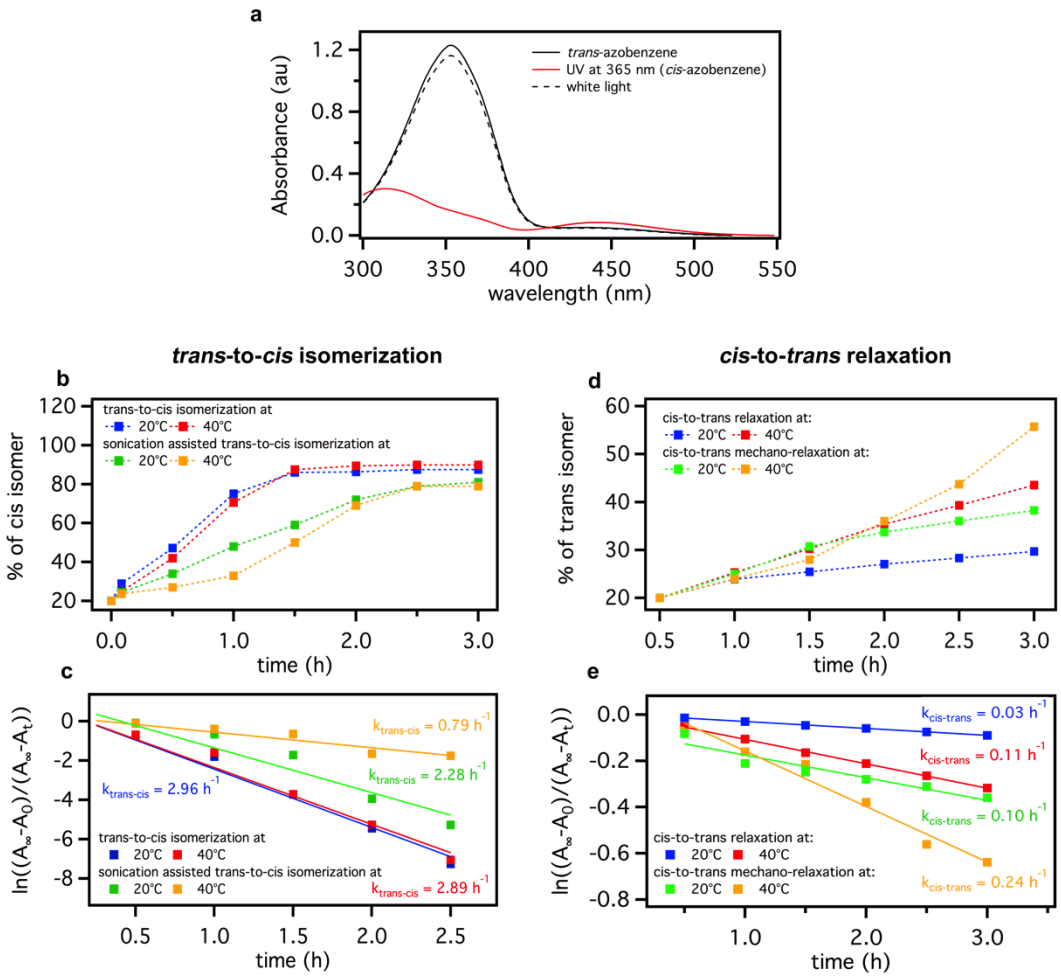

Figure 10.5. Spectroscopic characterization of *trans*-to-*cis* isomerization and *cis*-to-*trans* relaxation. a) UV-vis spectra of 4-(decyloxy)azobenzene in NMP (1.62 mM) showing the disappearance of the 353 nm band and an increase of the 442 nm band upon irradiation with UV-light (λ = 365 nm). The solid black line corresponds to the parent *trans*-azobenzene spectrum, the red line represents typical spectrum of solution irradiated with UV-light (*cis*-azobenzene), the black dashed line – *cis*-azobenzene irradiated with visible light (thus re-transformed in *trans*-azobenzene), b) Difference in percentage of conversion from *trans* to *cis* isomer as a function of UV irradiation time at 20 and 40 °C, c) First-order kinetic plots and rate constants ($k_{trans-cis}$) for the *trans*-to-*cis* isomerization of at 20 and 40 °C, d) Difference in percentage of conversion from *cis* to *trans* isomer as a function of time at 20 and 40 °C, e) First-order kinetic plots and rate constants ($k_{cis-trans}$) for *cis*-to-*trans* relaxation of at 20 and 40 °C. b-e) Blank samples, i.e. samples prepared without sonication: blue (20 °C) and red (40 °C); sonicated samples: green (20 °C) orange (40 °C).

Analysis of the absorption and ^{1}H-NMR spectra (see Figure 10.6) acquired at different experimental conditions allowed us to quantify the percentage of conversion from *trans*- to *cis*-azobenzene, as well as the rate constants for *trans*-to-*cis* isomerization. Moreover, the

NMR results show that the molecules do not suffer from poor stability when sonicated, i.e. the decyloxychains are not being chopped of from the azobenzene core.

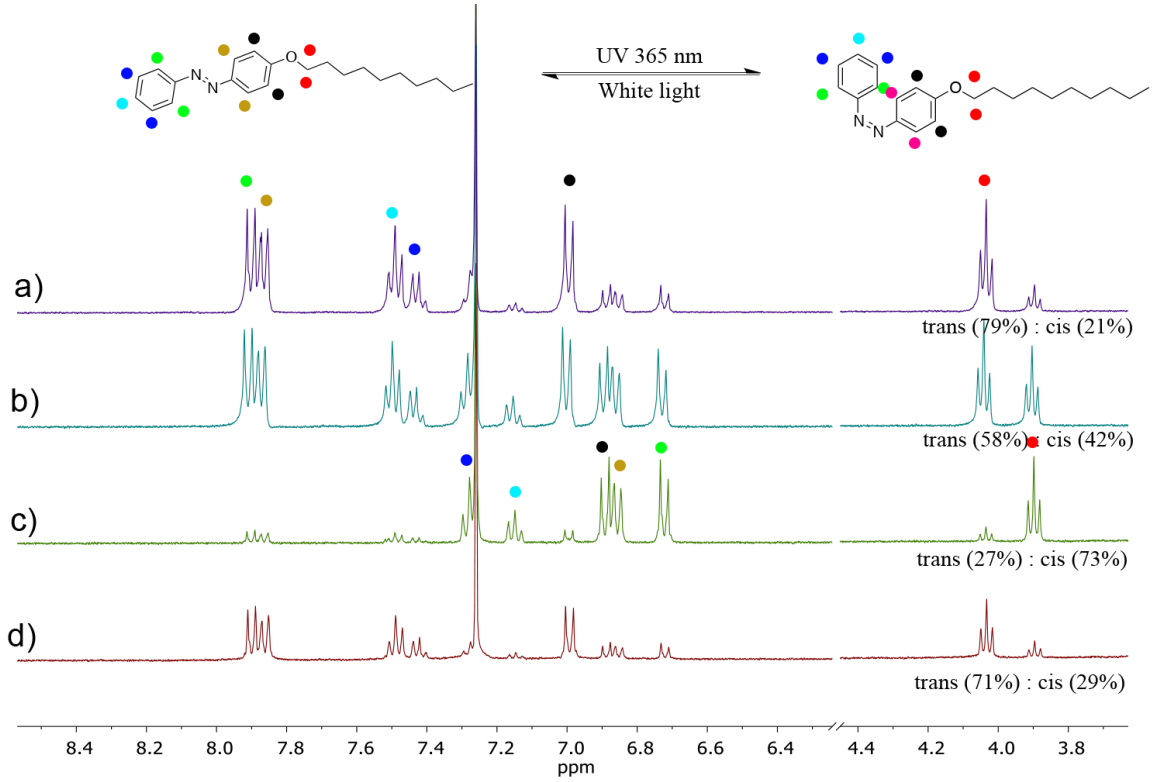

Figure 10.6 ^{1}H-NMR spectra of 4-(decyloxy)azobenzene in NMP:$CDCl_3$ (1:30 *vol:vol*, 1.6 mM): a) initial spectrum consisting of 79 and 21% of the *trans* and *cis* species respectively; b) spectrum of the solution irradiated for 1 h at 365nm consisting of 58 and 42% of the *trans* and *cis* species respectively, c) spectrum of the solution irradiated for 2.5 h at 365nm consisting of 27 and 73% of the *trans* and *cis* species respectively, d) spectrum of the solution (c) irradiated with white light consisting of 71 and 29% of the *trans* and *cis* species respectively.

The slow kinetics of the *trans*-to-*cis* isomerization of azobenzene molecules in the present case can be explained by the fact that both spectroscopic experiments and LPE process, are carried out under unusual conditions, including low power of UV-light (0.34 mW cm^{-2}). Significantly different time (30 min) between blank and sonicated samples, are needed for converting all molecules from *trans*- to *cis*-isomer, as clearly shown in Figure 10.2b. Previous studies on the *trans*-to-*cis* isomerization of azobenzene in the presence of UV light showed that the reaction follows first-order kinetics and the rate constant *k* for the process can be obtained from Eq. 10.1,[14, 15]

$$\ln \frac{(A_\infty - A_t)}{(A_\infty - A_0)} = -kt \qquad (Eq. 10.1)$$

where A_0, A_t, and A_∞ are the absorbances before irradiation, at irradiation time *t*, and after irradiation for prolonged time (ca. 6h). Applying Eq. 1, the isomerization constant $k_{trans\text{-}cis}$ for azobenzenes isomerized at 20 °C was found to be similar to the $k_{trans\text{-}cis}$ for azobenzenes isomerized at 40 °C, and amounts to 2.96 h^{-1} and 2.89 h^{-1}, respectively. Significantly different $k_{trans\text{-}cis}$ were observed for the samples exposed to ultrasound-induced mechanical forces, i.e. 2.28 h^{-1} and 0.79 h^{-1} for dispersions prepared at 20 and 40 °C, respectively. To ensure the stability of the *azo* bond during the sonication, the two samples were exposed to white light and the absorption spectra were recorded. The absorption at λ = 365 nm in both cases was found to be consistent with the *trans*-azobenzene spectra in both cases, which clearly indicates that the molecules, and in particular the *azo* bond, are stable during the sonication at various temperatures.

Because of the slow kinetics of the *trans*-to-*cis* isomerization, attributed to the UV light power and to the experimental conditions, we decided to shed light into competing processes promoting the *cis*-to-*trans* isomerization. Noteworthy, since the *trans*-to-*cis* isomerization and the LPE processes were performed under UV light, the possible *cis*-to-*trans* back conversion can be considered being promoted by thermal- or mechano-thermal relaxation, in the case of experiment performed in the absence or presence of ultrasound-induced forces, respectively.

To probe both thermal- and mechano-thermal isomerisation of azobenzene molecules, four solutions (110.2 mM) were prepared in NMP and the UV-vis spectra were recorded. The solutions were then irradiated with UV light (λ = 365 nm) for 3 hours to photoisomerize the azobenzene from its *trans* to *cis* configuration (see Figure 10.4. for absorbance spectra). The solutions were then kept for 3 hours at 20 °C and/or 40 °C, in the presence and/or absence of ultrasound-induced mechanical forces. Every 30 min 0.2 mL of solution was transferred (in dark) into quartz cuvette and diluted 10 times with NMP and absorption spectra was recorded. As expected, because of the lack of the white light during the 3 hours of the relaxation process, azobenzene molecules did not convert fully from their *cis* to *trans*-isomer. Noteworthy, notable dependency/sensitivity of/to the experimental conditions was monitored.

As shown in Figure 2c, the percentage of *cis*-to-*trans* conversion in the blank samples (without sonication) at 20 and 40 °C, amounts to 8.6 % and 27.6 %, respectively. In contrast, the ultrasound-induced conversion was found to be much higher, i.e. 29.8 % and 51.2 %, for samples kept at 20 and 40 °C, respectively. Similarly to the *trans*-to-*cis* isomerization, *cis*-to-*trans* relaxation of azobenzenes follows first order kinetics and the rate constant *k* for the process can be obtained from Eq. 10.1. The thermal-relaxation constant $k_{cis\text{-}trans}$ for azobenzenes kept at 20 °C was found to be lower than the $k_{cis\text{-}trans}$ for azobenzenes relaxed at 40 °C, i.e. 0.03 h^{-1} and 0.11 h^{-1}, respectively (Fig. 5.d). Notably different $k_{cis\text{-}trans}$ were observed for the samples exposed to ultrasound-induced mechanical forces, i.e. 0.10 h^{-1} and 0.24 h^{-1} for dispersions kept at 20 and 40 °C, respectively.

The above results indicate that the *trans*-to-*cis* isomerisation of azobenzene molecules strongly depends on the experimental conditions. In particular, the *trans*-to-*cis* conversion is strongly hindered by the ultrasound-induced mechanical forces, which most likely cause the occurrence of the competing *cis*-to-*trans* isomerisation. Furthermore, comparison of $k_{trans\text{-}cis}$ as well as $k_{cis\text{-}trans}$ of processes taking place at 20 and 40 °C, reveals that at higher temperature the process is more dynamic. As a result, the highest concentration of graphene obtained at 40 °C (110 μg mL^{-1}) can be attributed to the dynamic conformational *trans*-to-*cis* and *cis*-to-*trans* changes of azobenzene molecules triggered simultaneously by the competing effect activated by UV light, temperature and ultrasounds.

10.4.3 HR-TEM

In order to fully characterize the exfoliated graphitic material, both qualitative and quantitative information are required. While quantitative insights can be assessed by providing the yield of exfoliation expressed in terms of concentration (in μg mL^{-1}), the qualitative analysis must give more relevant details such as the percentage of single-layer graphene (SLG) and multi-layer graphene (MLG) flakes, the lateral size of the flakes and the presence/absence of defects. Currently, the best methods for the identification of the number of graphene layers in material produced by LPE are based on High Resolution - Transmission Electron Microscopy (HR-

TEM) and on Raman statistical analysis. Together with the information coming from electron diffraction patterns, in HR-TEM the number of layers can be directly counted by analysing the edges. (See Figure 10.7)

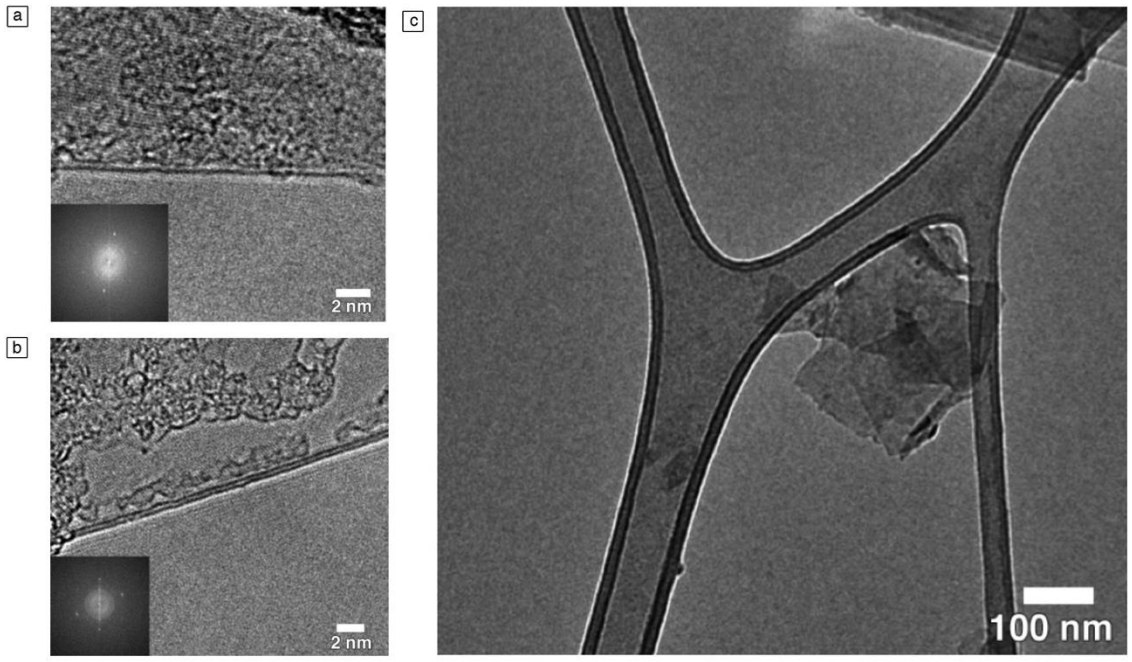

Figure 10.7. High Resolution image of a) azobenzene-exfoliated graphene double-layer. The corresponding FFT is shown in the inset, b) azobenzene-exfoliated graphene double-layer. The corresponding FFT is shown in the inset and c) low magnification TEM image of an azobenzene-exfoliated graphene flake.

We focussed our attention on the graphene samples exfoliated at 40 °C in the presence of azobenzene molecules while irradiating with UV-light (highest concentration), and compared them to those exfoliated in pure NMP at 40 °C under UV-irradiation (in absence of azobenzene). TEM samples were prepared by drop casting the graphene dispersions on standard Quantifoil holey carbon copper grid, followed by solvent evaporation at 150 °C for 10 min. The TEM micrographs revealed folded SLG, with lateral sizes below 1 µm, as typically observed for LPEG.[2] The statistical analyses of the graphene sheet thickness and the lateral flake size are reported in Figure 10.8a and 10.8b, respectively.

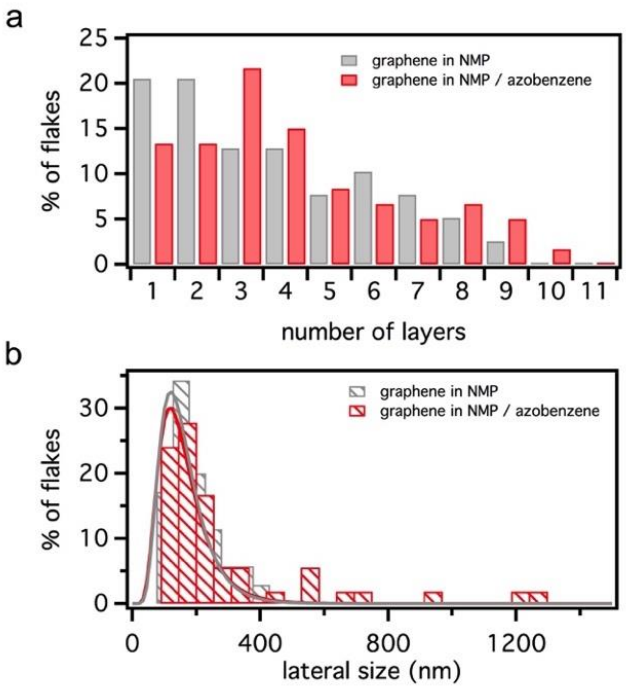

Figure 10.8. a) Histogram of the distribution of the flake thickness based on statistical analyses of HR-TEM results of graphene exfoliated in NMP (grey) and in NMP/azobenzene (red), b) Histogram of the lateral flake size distribution. The fitting of the distribution has been obtained with a lognormal distribution.

10.4.4 Raman spectroscopy

Raman spectroscopy was carried out on the same set of samples in order to characterize the quality of graphitic material. Figure 10.9a plots a typical Raman spectrum of our azobenzene-exfoliated graphene flake measured at 514.5 nm.

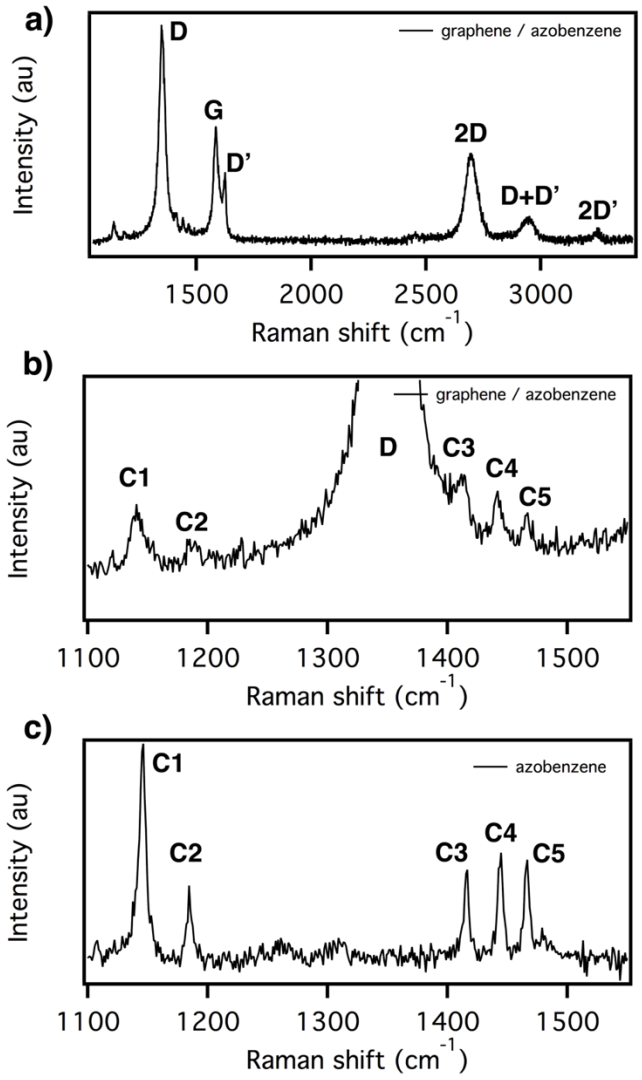

Figure 10.9. a) Raman spectrum of azobenzene-exfoliated flake. b) Zoom around the D peak region showing the Raman peaks due to the azobenzene molecules, C1-C5. c) Raman spectrum of pure azobenzene powder.

The Raman spectrum of graphite and multilayer graphene (MLG) consists of two fundamentally different sets of peaks. Those, such as D, G and 2D, present also in SLG, and due to in-plane vibrations,[16, 17] and others, such as the shear (C) modes[18] and the layer breathing modes (LBM),[19] due to the relative motions of the planes themselves, either perpendicular or parallel to their normal. The G peak corresponds to the high frequency E_{2g} phonon at Γ. The D peak is due to the breathing modes of six-atom rings and requires a defect for its activation.[20] It comes from TO phonons around the Brillouin Zone (BZ) edge K,[20] is

active by double resonance (DR),[21] and is strongly dispersive with excitation energy due to a Kohn Anomaly (KA) at K.[22] connecting two points belonging to the same cone around K or K'. This gives the so-called D' peak. The 2D peak is the D peak overtone. The 2D' peak is the D' overtone. Since 2D and 2D' originate from a process where momentum conservation is satisfied by two phonons with opposite wave vectors, no defects are required for their activation, and are thus always present.[23] The 2D peak is composed of a single lorentzian in SLG, whereas it splits in several components as N increases, reflecting the evolution of the electronic band structure.[23]

10.4.5 XPS characterization

We used XPS to analyse graphene/azobenzene dispersions in NMP before and after washing the azobenzene molecules. The high-resolution C1s XPS spectrum shows a sharp peak at 284.4 eV that corresponded to C=C bonds in a conjugated honeycomb lattice (Figure 10.10a). Peak at 285.7 eV and 285.1 eV could be attributed to different C-O and C-C bonding configurations respectively.[4] Also the peak at 2810.4 eV can be assign to C-N bonds coming also from NMP. The C1s XPS spectrum of the azobenzene molecules provides a major peak at 285.1 eV and a minor one at 287.0 eV. These two peaks can be attributed to C-C and C-N bonding configurations respectively. The C1s spectrum of graphene/azobenzene dispersions exhibits four peaks including a sharp at 284.3 eV, assigned to delocalized π conjugation from the sp^2 atomic structure of graphite. A peak at 284.9 is attributed to C-C due to the presence of azobenzene molecules. Also minor peaks at 285.7 eV and 287.1 eV corresponding to C-O and C-N bond are present and can be assigned to the trace of NMP residues and azobenzene molecules. After washing, the intensities of all C-N and C-C peaks significantly decrease, until reaching the same intensities as pristine graphene, indicating removal of azobenzene molecules.

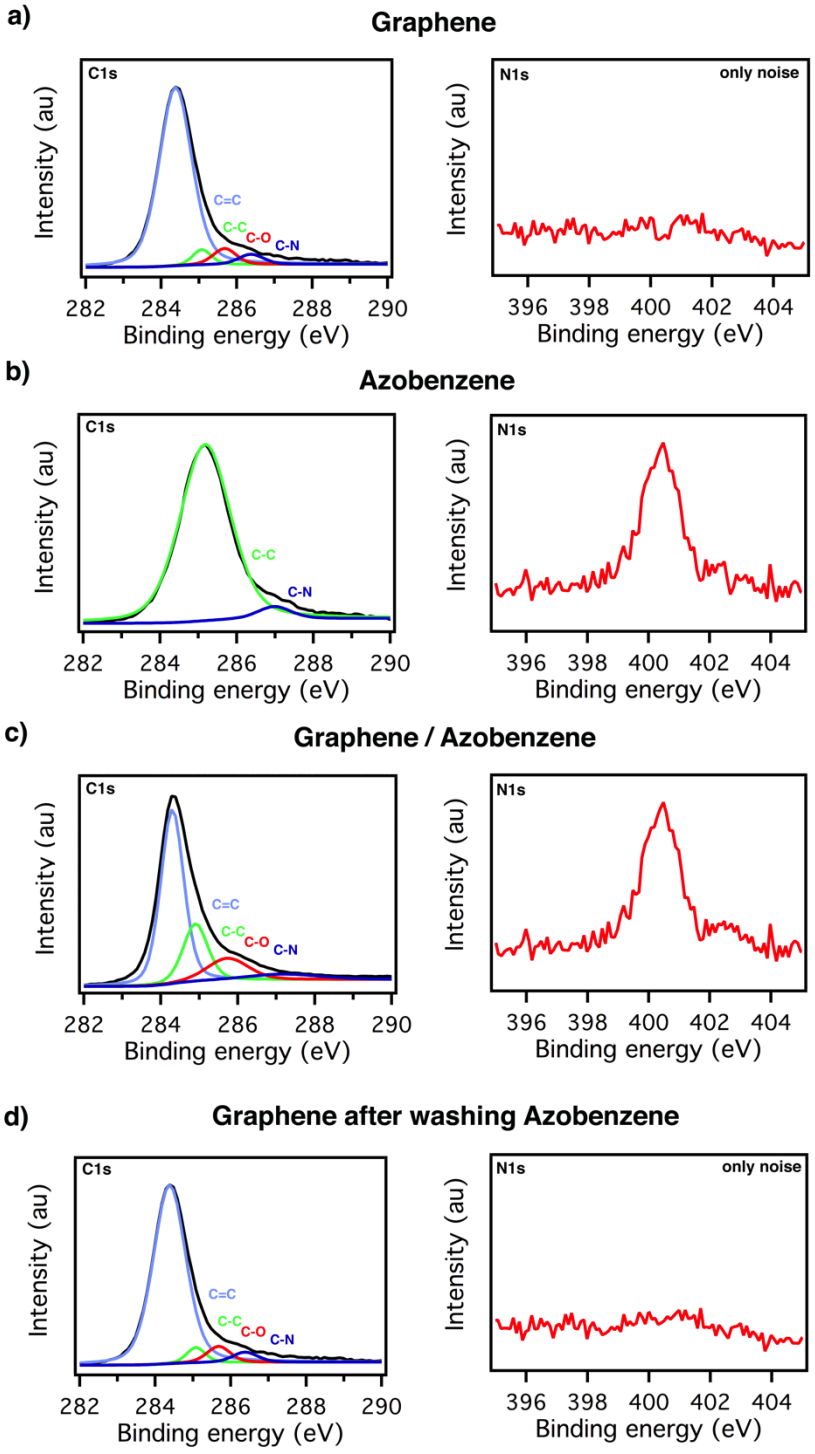

Figure 10.10. High-resolution C1s and N1s spectra of graphene exfoliated in NMP of a), azobenzene b), graphene exfoliated in NMP at 40 C in the presence of azobenzene molecules, c) and after washing step and d) Experimental data are shown as black line, and the individual deconvolved components as colour lines.

The high-resolution N1s XPS spectrum of the graphene doesn't show any nitrogen signal (Figure 10.10a). A peak at 400.4 eV corresponds to azobenzene molecules (Figure 10.10b). The same peak is observed in the spectrum of graphene/azobenzene (Figure 10.10c), but it is absent after the removal of molecules following the washing step (Figure 10.10d).

10.4.6 X-Ray analysis of graphene-azobenzene hybrid materials

Powder X-ray diffraction was further used to characterize the structure of the graphene-azobenzene hybrid powder and compared to control samples, i.e. powders composed of graphene without *ad hoc* azobenzene molecules (see *Methods* for sample preparation). Similarly to graphite, the powder prepared from LPE graphene displays a typical sharp peak at 210.7^{o}, corresponding to an interlayer spacing of ~ 0.33 nm (see Figure 10.11a). To validate the hypothesis that the insertion of a *trans*-/*cis*- azobenzene molecules sandwiched between two graphene layers could result in different spacing between adjacent graphene sheets, we extended our XRD analysis to powders prepared from graphene/*trans*-azobenzene and graphene/*cis*-azobenzene hybrid materials. The XRD pattern of these powders (see Figure 10.11b and 10.11c) shows newly arise peaks at 2θ =12.3° ($d_{spacing}$ ~0.72 nm) and 9.9° ($d_{spacing}$ ~0.89 nm), for the material containing *trans*- and *cis*-azobenzene molecules, respectively. Figures 10.11d and 10.11f show simulated (using modelled sandwich structures) XRD patterns for graphene/*trans*-azobenzene and graphene/*cis*-azobenzene, respectively. Such experimental evidence confirms the presence of *trans* and/or *cis* azobenzenes sandwiched between two graphene sheets.

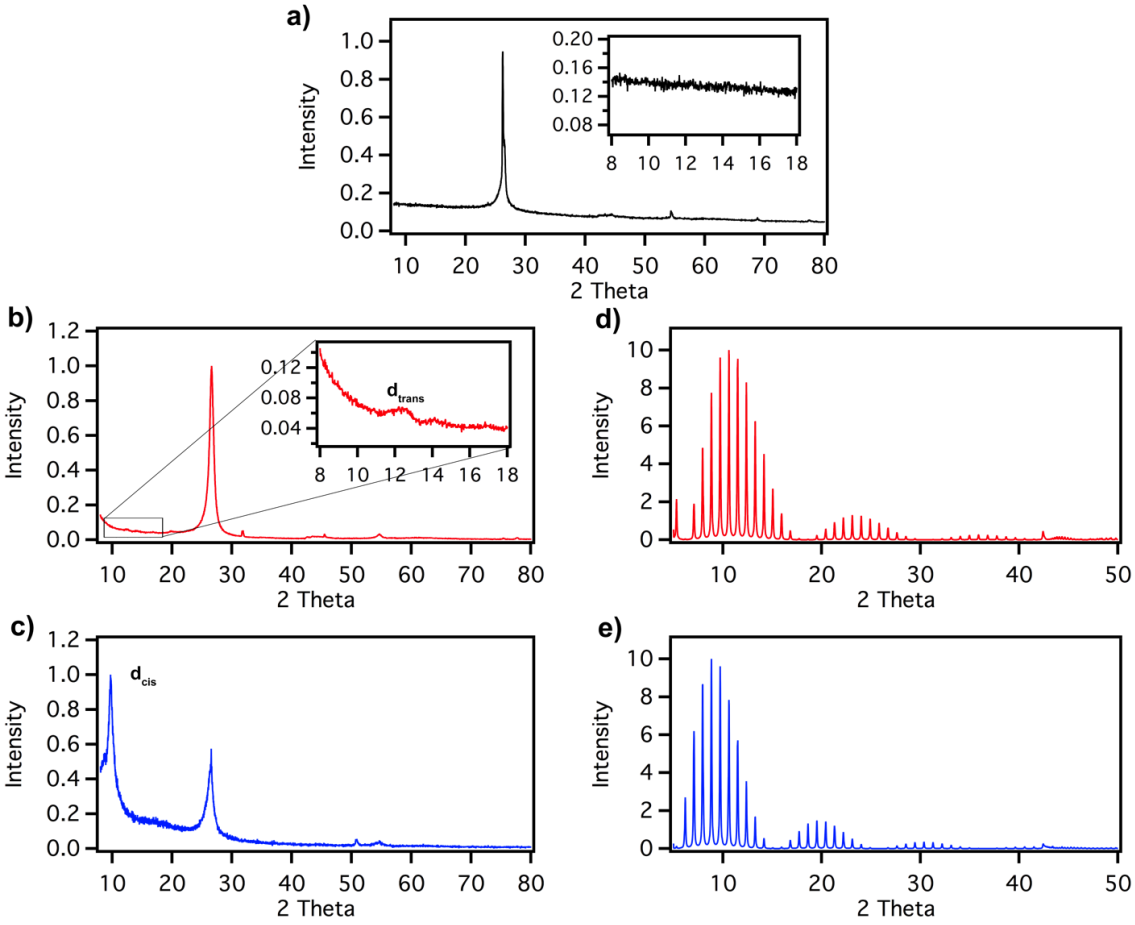

Figure 10.11. XRD patterns of graphene of a) hybrid material composed of graphene/*trans*-azobenzene, b) and graphene/*cis*-azobenzene, c) Simulated XRD patterns of calculated structures of *trans*-, d) and *cis*-azobenzene and e) intercalating graphene sheets.

10.4.7 Electrical characterization of graphene-azobenzene hybrid materials

In order to probe electrical properties of graphene-azobenzene hybrid and in particular to explore potential light-responsive nature of the material, we drop-cast a ~100 nm thick graphene-azobenzene film from NMP dispersions on cleaned $n^{++}Si/SiO_2$ substrates exposing pre-patterned interdigitated gold electrodes (channel length = 10 □m), and performed electrical characterization by measuring the charge transport properties of the film. Typical *I-V* curve exhibit a non-linear resistive behaviour, as shown in Figure 10.12a.

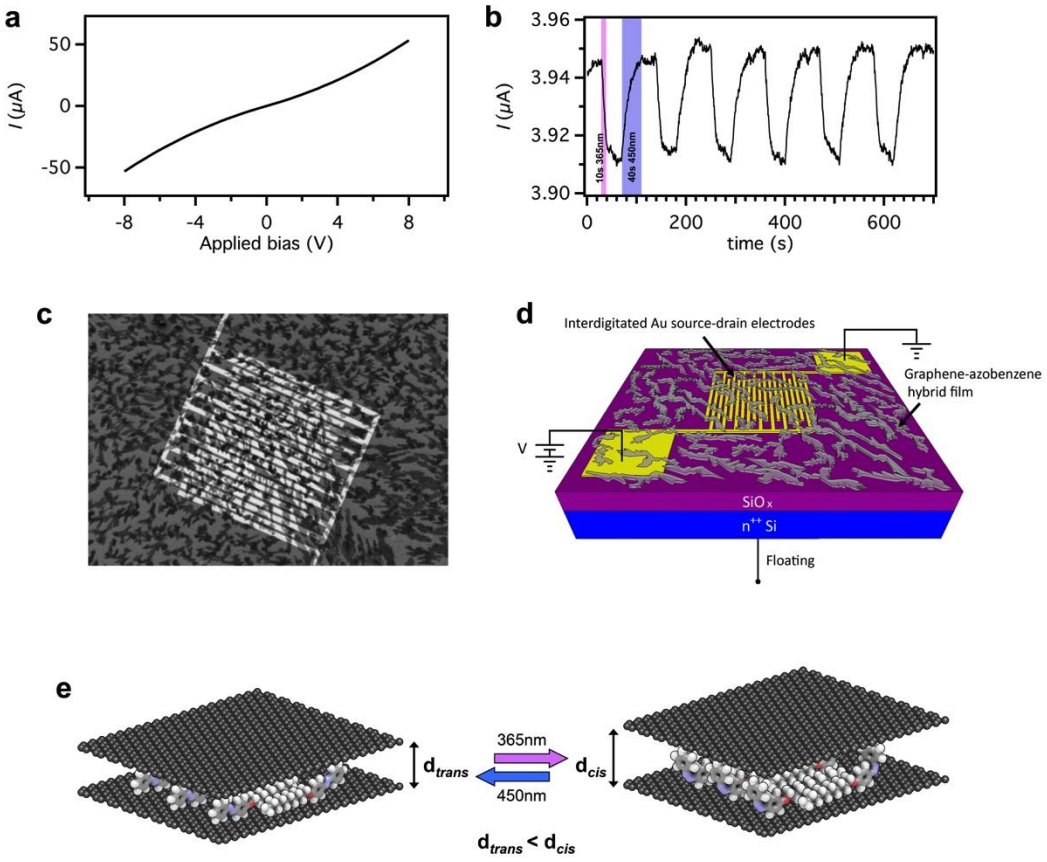

Figure 10.12. a) I-V characteristics, b) Optical modulation of device current response illustrated for a static bias and dynamic alternative UV and visible light irradiation (channel length between Au electrodes is 10 μm), c) SEM image of interdigitated Au electrodes covered with a graphene-azobenzene hybrid film, d) Scheme of the two-terminal device configuration, e) mechanism which occurs in thin graphene-azobenzene hybrid films under UV and visible light irradiation cycles.

Noteworthy, the conductivity of the graphene-azobenzene hybrid material is lower compared to pure graphene films (Figure 10.13), which is due to the introduction of the poorly conducting azobenzene layer. Remarkably, modulation of the current in a two terminal device comprising a graphene-azobenzene hybrid film was observed upon cycles of UV and visible light irradiation (Figure 10.12b), when a constant bias of 1 V was applied between the two electrodes. One cycle consisted of 10 sec UV-light (365 nm), 1 min rest in dark followed by 40 sec visible light (450 nm) irradiation. Under UV-light exposure (pink background) a prompt decrease in the current was monitored which reversibly increased to about the initial value under visible light irradiation (violet background) over various cycles. Noteworthy, no fatigue was observed during 6 cycles of photoisomerization. Conversely, the electrical

characteristics of devices incorporating graphene exfoliated in pure NMP showed no response to light stimuli (Figure 10.13).

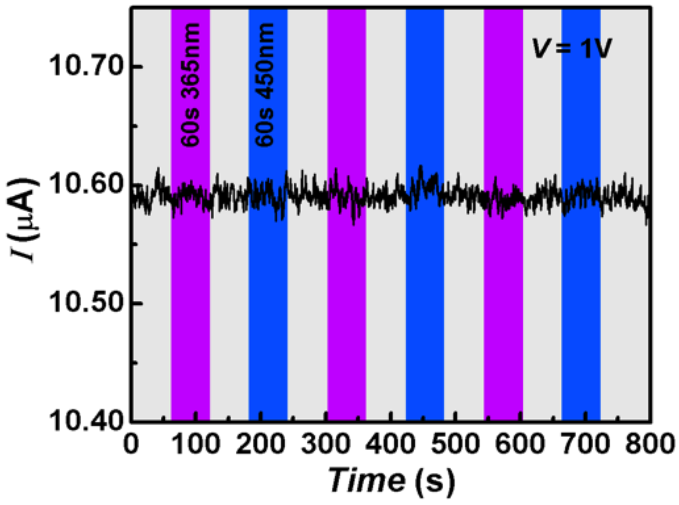

Figure 10.13. Optical modulation of device current response illustrated for a static bias and dynamic alternative UV and visible light irradiation cycles (channel length between Au electrodes is 10 μm).

Figure 10.12c portrays the interdigitated Au electrodes homogeneously covered with a thin film of graphene-azobenzene material as observed by SEM. It indicates that the electrodes are well connected with the hybrid material. A scheme of the two-terminal device configuration is depicted in Figure 10.12d.

In the azobenzene-graphene hybrid film, the molecules are physisorbed on top and in between the graphene sheets. When the photoisomerization is triggered by UV-light, the azobenzene molecules undergo conformational change from the *trans* to the *cis* form, a process that is accompanied by an increase in the graphene inter-sheet distance, thereby hindering the charge transport between the sheets, resulting in lower conductivity of the hybrid film. Significantly, the conductivity of the hybrid material can be fully restored by irradiating it with the visible light, which highlights the reversibility of the process and occurrence of the back *cis*-to-*trans* photoisomerization.

10.4.8 Spectrophotometrical analysis of hybrid material film

As a further proof for the reversible isomerisation we carried our spectrophotometrical analysis of drop casted grapheme-azobenzene hybrid films on quartz slides using a Jasco V-670 spectrophotometer. Samples were prepared by drop casting the graphene-azobenzene dispersion on a quartz substrate and drying the substrate for 48 h at 30 °C in vacuum.

The absorbance band of azobenzene at 365 nm typically decreases upon UV light irradiation when the photochromes isomerizes to the *cis* form and a new band arises at 450 nm. This behaviour is reversible when the molecules switch back to the *trans* isomer upon visible light excitation. Figure 10.14a shows a typical UV-Vis spectrum of a graphene-azobenzene hybrid on quartz. The absorbance bands of azobenzene at 365 and 450 nm in graphene-azobenzene hybrid reversibly change upon UV and visible light (VL) irradiation cycles (30s for each wavelength) as for Figures 10.14b and 10.14c. This shows the repeated *trans-cis* conformational changes of the photochromes in the hybrid film.

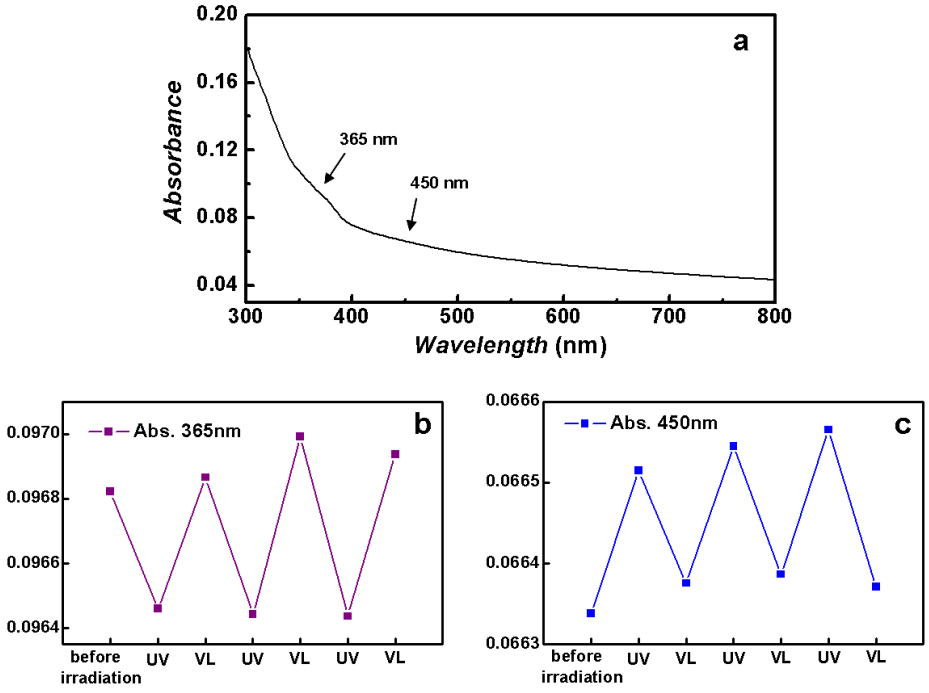

Figure 10.14. a) UV-Vis spectrum of a graphene-azobenzene hybrid film. Absorbance at b) 365 nm and c) 450 nm under repeated light irradiation cycles.

10.5 Conclusions

We demonstrated that photochromic molecules can act as photo addressable surfactant and dispersion-stabilizing agents to enhance the yield of exfoliation in an upscalable molecule assisted LPE-based method. The simultaneous use of UV-light irradiation promoting the *trans*-to-*cis* isomerization as well as thermal annealing at 40 °C and mechanical forces generated by sonic bath, both favouring *cis*-to-*trans* isomerization, we can generate mechanical motions in the azobenzene intercalated between adjacent graphene flakes, ultimately promoting the exfoliation in liquid media. The most effective exfoliation was obtained with azobenzene molecules irradiated with UV-light in NMP at 40 °C, with a concentration of exfoliated graphene of 110 μg mL^{-1} that corresponds to a nearly 80% increase in exfoliation yield when compared to pure NMP (63 μg mL^{-1}). By applying such a hybrid component into Au pre-patterned SiO_2 substrates, light responsive thin hybrid films, formed in a one-step co-deposition process can be realized, whose conductivity can be reversibly modulated by making use of *trans-cis* photoisomerization of the azobenzenes. As cost effective printing techniques such as ink-jet printing towards flexible graphene electronics gain pace, more complex device designs and architectures could be envisaged, e.g. miniaturization of electronic circuits and multilayer devices can be realized. The hybrid system presented, combining the unique electrical characteristics of graphene with the stimuli-responsive nature of azobenzene, holds great potential as key component for future applications as optically controllable memory switching elements for light-assisted programming and high-sensitive photo-sensors.

10.6 References

1. Y. Hernandez, V. Nicolosi, M. Lotya, F. M. Blighe, Z. Y. Sun, S. De, I. T. McGovern, B. Holland, M. Byrne, Y. K. Gun'ko, J. J. Boland, P. Niraj, G. Duesberg, S. Krishnamurthy, R. Goodhue, J. Hutchison, V. Scardaci, A. C. Ferrari and J. N. Coleman, *Nat. Nanotechnol.*, 2008, **3**, 563-568.
2. A. Ciesielski and P. Samorì, *Chem. Soc. Rev.*, 2014, **43**, 381-398.
3. A. Ciesielski, S. Haar, M. El Gemayel, E. Orgiu, H. Yang, S. Johal, O. Ersen, C. Casiraghi and P. Samorì, *Angew. Chem. Int. Ed.*, 2014, **53**, 10355–10361.
4. S. Haar, A. Ciesielski, J. Clough, H. Yang, R. Mazzaro, F. Richard, S. Conti, N. Merstorf, M. Cecchini, V. Morandi, C. Casiraghi and P. Samorì, *Small*, 2014, **11**, 1691–1702.
5. N. Peimyoo, J. W. Li, J. Z. Shang, X. N. Shen, C. Y. Qiu, L. H. Xie, W. Huang and T. Yu, *Acs Nano*, 2012, **6**, 8878-88810.
6. S. Seo, M. Min, S. M. Lee and H. Lee, *Nat. Commun.*, 2013, **4**.
7. M. Kim, N. S. Safron, C. H. Huang, M. S. Arnold and P. Gopalan, *Nano Lett.*, 2012, **12**, 182-187.
8. E. Margapoti, P. Strobel, M. M. Asmar, M. Seifert, J. Li, M. Sachsenhauser, Ö. Ceylan, C.-A. Palma, J. V. Barth, J. A. Garrido, A. Cattani-Scholz, S. E. Ulloa and J. J. Finley, *Nano Lett.*, 2014, **14**, 6823-6827.
9. U. Khan, A. O'Neill, H. Porwal, P. May, K. Nawaz and J. N. Coleman, *Carbon*, 2012, **50**, 470-475.
10. J. Griffiths, *Chem. Soc. Rev.*, 1972, **1**, 481-493.
11. N. Tamai and H. Miyasaka, *Chem. Rev.*, 2000, **100**, 1875-1890.
12. J. M. Joseph, H. Destaillats, H. M. Hung and M. R. Hoffmann, *J. Phys. Chem. A*, 2000, **104**, 301-307.
13. R. Turansky, M. Konopka, N. L. Doltsinis, I. Stich and D. Marx, *Phys. Chem. Chem. Phys.*, 2010, **12**, 13922-13932.
14. S. K. Surampudi, H. R. Patel, G. Nagarjuna and D. Venkataraman, *Chem. Commun.*, 2013, **49**, 7519-7521.
15. K. H. Shin and E. J. Shin, *Bull. Korean Chem. Soc.*, 2008, **29**, 1259-1262.
30. A. C. Ferrari and J. Robertson, *Philos. Trans. R. Soc. Lond. Ser. A*, 2004, **362**, 2477-2512.
16. A. C. Ferrari, *Solid State Commun.*, 2007, **143**, 47-57.
17. P. H. Tan, W. P. Han, W. J. Zhao, Z. H. Wu, K. Chang, H. Wang, Y. F. Wang, N. Bonini, N. Marzari, N. Pugno, G. Savini, A. Lombardo and A. C. Ferrari, *Nat. Mater.*, 2012, **11**, 294-300.
18. C. H. Lui, L. M. Malard, S. Kim, G. Lantz, F. E. Laverge, R. Saito and T. F. Heinz, *Nano Lett.*, 2012, **12**, 5539-5544.
19. A. C. Ferrari and J. Robertson, *Phys. Rev. B*, 2000, **61**, 14095-14107.
20. J. Maultzsch, S. Reich and C. Thomsen, *Phys. Rev. B*, 2004, **70**.
21. S. Piscanec, M. Lazzeri, F. Mauri, A. C. Ferrari and J. Robertson, *Phys. Rev. Lett.*, 2004, **93**.

22. A. C. Ferrari, J. C. Meyer, V. Scardaci, C. Casiraghi, M. Lazzeri, F. Mauri, S. Piscanec, D. Jiang, K. S. Novoselov, S. Roth and A. K. Geim, *Phys. Rev. Lett.*, 2006, **97**, 187401-187405.

Chapter 11 Conclusions and Perspectives

11.1 Attainments

Liquid-phase exfoliation of bulk graphite is an extremely mild, versatile and potentially up-scalable approach to obtain high-quality graphene inks using equipment available in all chemistry labs. Liquid-phase exfoliation is interesting for the preparation of stable inks that can be processed in thin films and composite materials; in this regard future research is needed to control on-demand the number of layers and lateral size. In this way, we decided to focused our researches on controlling the temperature and the power of sonication during the LPE of graphite for different organic solvents. By choosing the right combination, it is possible to produce size controlled graphene from nanoflakes to GQDs. These GQDs were found to have an average diameter of 16 nm and 1-3 layers with photoluminescence properties.

To take full advantages of the structural uniqueness and exceptional properties of graphene as reinforcement in composites, harvesting well-dispersed graphene is essential. LPE in the presence of a given solvent molecule with the aid of an additional predesigned molecule as a dispersion-stabilizing agent is a relevant solution. LPE assisted by molecules leaded to an increase of the exfoliation yield. Well-chosen molecules avoid graphene re-aggregation due to van der Waals attraction between graphene surface and dispersion-stabilizing agent. We demonstrated that by mastering a supramolecular approach it is possible to improve the yield of graphene exfoliation in an up-scalable LPE-based method to produce high-quality graphene flakes from powdered graphite. Molecules possessing high affinity for the graphite surface

were tested as dispersion-stabilizing agent. In particular, two molecules were chosen: 1-phenyloctane and arachidic acid. Sonication followed by centrifugation gave graphene dispersions with their concentration increased by 25% and 50%, respectively. Also TEM revealed that the number of SLG was as high 10% for 1-phenyloctane and 5% for arachidic acid. These dispersions were shown to be conductive inks.

In order to extend our understanding, we have explored the importance of the functional groups. We focused our attention on the study of LPE of graphene in the presence of heneicosane linear alkanes terminated with different head groups, i.e. alkane, amine, carboxylic acid and alcohol. These molecules act as graphene dispersion-stabilizing agents during the exfoliation process. The efficiency of the exfoliation in terms of concentration of exfoliated graphene is found to depend on the functional head group, in particular in view of the strength of their dimerization through dipole-dipole interactions. Importantly, a high percentage of single-layer graphene flakes were revealed by high-resolution transmission electron microscopy and Raman spectroscopy analyses.

To attain a fundamental understanding of the role of molecule-graphene interaction on the yield of graphene LPE, we explored a new type of dispersion-stabilizing agent. In this way fatty acids with increasing the length of the aliphatic chain were chosen. Dispersions prepared in the presence of **C30** in NMP showed an increase of 200% in exfoliation yield when compared to samples prepared in pure NMP. In chlorinated solvents, *o*-DCB and TCB, the most effective exfoliation was obtained with **C24** molecules, which corresponded to ca. 50% and ca. 90% increase in the exfoliation yield respectively. TEM revealed that the % of SLG was increased in some case. Dispersions prepared in pure DMF and TCB presented a poor quality of flakes but the addition of molecules improved up to 16% the quantity of SLG. Raman analysis fully supports TEM results. Furthermore a linear dependence of the exfoliation yield with the length of the aliphatic chain was observed.

A deeper study on LPE-assisted by NOTBZ molecules allowed us to understand the importance of different parameters. By tuning the ratio between organic solvents such as NMP or *o*-DCB, and NOTBZ molecules, the concentration of exfoliated graphene can be enhanced by 230% as a result of the high affinity of the latter molecule for the basal plane of graphene. TEM and Raman showed high % of SLG. The LPE processed graphene dispersions

were further deposited onto solid substrates by exploiting a new deposition technique called spin-controlled drop casting, which was shown to give uniform highly conductive and transparent graphene films.

Graphene is at the center of an every growing research effort due to its combination of unique properties. We showed that the large conformational change associated with the *trans-cis* photochemical isomerization of alkyl-substituted azobenzenes can be used to improve the efficiency liquid phase exfoliation of graphite, with the photochromic molecules acting as dispersion-stabilizing agents. We also demonstrated reversible photo-modulated current in two-terminal devices based on graphene-azobenzene composites. We assigned these tuneable electrical characteristics to the intercalation of the azobenzenes between adjacent graphene layers and the resulting increase in the interlayer distance upon (photo)switching from the linear *trans*-form to the bulky *cis*-form of the photochromes.

11.2 Outlooks

The impressive increase of graphene applications using graphene dispersed in a liquid media will force scientists to produce graphene with even higher purity and in larger quantities. Despite its advantages for large-scale production, liquid phase exfoliation results in graphene sheets with uncontrolled sizes and thicknesses.

Graphene-based membranes and functional films, in particular composite membrane, extraordinary permeation properties, opening the door to ultrafast and highly-selective transport of water, gases and some specific small molecules.

Graphene can also be used as a carrier to form three-dimensional materials. Composite materials have many properties and seem to have great potential in the field of gas storage and energy. The formation of these new materials is often dependent on binding agents, which are likely covalent or non-covalent linked to graphene.

Exfoliation techniques have been extended to a wider range of other 2D materials (boron nitride, molybdenum disulfide, and even more). The availability of dispersions containing

different 2D materials opens up a range of application in composites, thin films and inks. Combining different 2D materials can leads to hybrid super-structure with enhanced properties.

Acknowledgements

That's it! It's over after spending more than three years at the laboratory. This was an exceptional stage of life and how rewarding. This was not possible without many people including my supervisor, the groups that I collaborated with, my colleagues, my friends and my family who directly or indirectly helped me and supported me with this thesis.

First I'm highly grateful to Prof. Paolo Samorì for giving me the opportunity to perform this PhD at the Nanochemistry Laboratory within his group. I would also like to thank him for his patience, guidance, continuous support and supervision. Also Corinne for the good advices and helps in whatever I was asking.

I would like to thank all my co-workers (members of the Nanochemistry laboratory) for making the past three years pleasant. Many thanks to Dr. Emanuele Orgiu, Dr. Oliver Fenwick, Dr. Sara Bonacchi, Dr. Lili Hou, Dr. Songlin Li, Dr Lei Zhang, Dr. Xiaoyan Zhang, Dr. Marco Gobbi, dr. Nicolas Weibel and Dr. Alexander Klekachev. I thank also all PhD students and master students, in particular, Matilde, Tim, Thomas, Wassima, Maria, Marco, Chiarra, Dawid, Marc-Antoine and Yoshimi…

I want to thank my nearest colleagues: Artur, Mohamed and Mirella for their support, non-scientific discussions, coffee breaks, jokes, desserts and for thousand other thinks. Life was more sunny at the lab thanks to you !! I also address special acknowledgements to Nicolas Merstorf for chatting when I needed.

I want to express my deep gratitude to all my friends, in particular Joris, Olivier and Pierre that allowed me to have a wonderful time. I also salute all my teammates from *O.S.* for unforgettable moments.

Last but not least, my family members, and more particularly my parents, Patricia and Bruno, who support me since the beginning of the road. I should thank them a hundred times for believing in me anyway. I am very grateful to Nicolas & Laurie and Elodie & Walyd for their encouragements. And of course, I want to truly acknowledge Marie, who thanks to her support, tenderness and love, helped me to tackle all difficult steps during these three years.

Finally, I dedicate all my work to my grandfather "Papi Hubert", who left us too soon. I'm more than sure that this is not the way you expected for me, but I went to the end. I hope you would have been proud.

List of publications

- A. Ciesielski, **S. Haar**, G. Paragi, Z. Kupihár, Z. Kele, S. Masiero, C. Fonseca Guerra, F. M. Bickelhaupt, G. P. Spada, L. Kovács, P. Samorì, "Supramolecular H-bonded porous networks at surfaces: exploiting primary and secondary interactions in a bi-component melamine–xanthine system", *Phys. Chem. Chem. Phys*., **2013**, 15, 12442–124410.

- A. Ciesielski, **S. Haar**, A. Bényei, G. Paragi, C. Fonseca Guerra, F. M. Bickelhaupt, S. Masiero, J. Szolomájer, P. Samorì, G. P. Spada, L. Kovács, "Self-Assembly of N3-Substituted Xanthines in the Solid State and at the Solid–Liquid Interface", *Langmuir*, **2013**, 29, 7283–7290.

- A. Ciesielski, **S. Haar**, M. El Gemayel, H. Yang, J. Clough, G. Melinte, M. Gobbi, E. Orgiu, M. V. Nardi, G. Ligorio, V. Palermo, N. Koch, O. Ersen, C. Casiraghi, P. Samorì, "Harnessing the Liquid-Phase Exfoliation of Graphene using Aliphatic Compounds: A Supramolecular Approach", *Angew. Chem. Int. Ed*., **2014**, 53, 10355–10361.

- M. El Gemayel, **S. Haar**, F. Liscio, A. Schlierf, G. Melinte, S. Milita, O. Ersen, A. Ciesielski, V. Palermo, P. Samorì, "Leveraging the ambipolar transport in polymeric field-effect transistors via blending with liquid-phase exfoliated graphene", *Adv. Mater*., **2014**, 26, 4814–4819.

- A. Ciesielski, M. El Garah, **S. Haar**, P. Kovaříček, J.-M. Lehn, P. Samorì, "Dynamic covalent chemistry of bisimines at the solid/liquid interface monitored by scanning tunnelling microscopy", *Nature Chem*., **2014**, 6, 1017–1023.

- **S. Haar**, A. Ciesielski, J. Clough, H. Yang, R. Mazzaro, F. Richard, S. Conti, N. Merstorf, M. Cecchini, V. Morandi, C. Casiraghi, P. Samorì, "A supramolecular strategy to

leverage the liquid-phase exfoliation of graphene in the presence of surfactants: unraveling the role of the length of fatty acids", *Small*, **2015**, 11, 1691–1702.

- O. Fenwick, C. Van Dyck, K. Murugavel, D. Cornil, F. Reinders, **S. Haar**, M. Mayor, J. Cornil and P. Samorì, "Modulating the charge injection in organic field-effect transistors: Fluorinated oligophenyl self-assembled monolayers for high work function electrodes", *J. Mater. Chem. C.*, **2015**, 3, 3007-3015.

- T. Mosciatti, **S. Haar**, F. Liscio, A. Cieselski, E. Orgiu and Paolo Samorì, "A novel multifunctional polymer-graphene thin-film transistor device with tunable transport regimes", *ACS Nano*, **2015**, 9, 2357–2367.

- M. El Garah, R. C. Perone, A. S. Bonilla, **S. Haar**, M. Campitiello, R. Gutierrez, G. Cuniberti, S. Masiero, A. Ciesielski and P. Samorì, "Guanosine-based hydrogen-bonded Scaffolds: G-ribbons and G-quartets Formed in the Absence of a Templating Metal Cation", *Chem. Commun.*, **2015**, 51, 11677–11680.

- M. Döbbelin, **S. Haar**, Silvio Osella, M. Bruna, A. Minoia, T. Mosciatti, F. Richard, E. A. Prasetyanto, L. De Cola, R. Mazzaro, V. Morandi, R. Lazzaroni, A. C. Ferrari, D. Beljonne, A. Ciesielski and P. Samorì, "Graphene/azobenzene nanocomposites: light enhanced liquid-phase exfoliation and photoswitching current in hybrid material", *submitted.*

- **S. Haar**, M. El Gemayel, Y. Shin, G. Melinte, O. Ersen, C. Casiraghi, A. Ciesielski and P. Samorì, "Leveraging the liquid-phase exfoliation of graphene in organic solvents with *n*-octylbenzene", *submitted*.

- **S**. **Haar**, M. El Gemayel, F. Richard, M. El Garah, G. Tregnago, F. Cacialli, F. Bonaccorso, A. Ciesielski and P. Samorì "Direct exfoliation of graphite into size controlled graphene: from nanoflakes to quantum dots", *in preparation*.

- **S**. **Haar**, A. Ciesielski, M. Bruna, J. X. Lian, J. Moran, Y. Olivier, D. Beljonne, A. C. Ferrari and P. Samorì "A supramolecular strategy to leverage the liquid-phase exfoliation of graphene in the presence of surfactants: unraveling the role of functions", *in preparation*.

Contributed talks

- GDR-I GNT 2013, Lorient: "Liquid-phase exfoliation of graphene using aliphatic intercalating compounds: A Supramolecular Approach". ***S. Haar**, A. Ciesielski, M. El Gemayel, H. Yang, J. Clough, M. Gobbi, E. Orgiu, M. V. Nardi, V. Palermo, C. Casiraghi, and P. Samorì.*

Posters

- Elec'mol 2012, Grenoble: "Self-assembly of N3-substitued xanthines in solid state and at the solid-liquid interface". *A. Ciesielski, **S. Haar**, A. Bényei, G. Paragi, C. Fonseca Guerra, F. M. Bickelhaupt, S. Masiero, J. Szolomájer, P. Samorì, G. P. Spada, and L. Kovács.*

- SUPERIOR 2013, Strasbourg: "Liquid-phase exfoliation of graphene using aliphatic intercalating compounds: A Supramolecular Approach". ***S. Haar**, A. Ciesielski, M. El Gemayel, H. Yang, J. Clough, M. Gobbi, E. Orgiu, M. V. Nardi, V. Palermo, C. Casiraghi, and P. Samorì.*

- Joint Symposium Groningen-Strasbourg 2014, ISIS: "Liquid phase exfoliation of graphene - a supramolecular approach". ***S. Haar**, A. Ciesielski, M. El Gemayel, H. Yang, J. Clough, G. Melinte, M. Gobbi, E. Orgiu, M. V. Nardi, G. Ligorio, V. Palermo, N. Koch, O. Ersen, C. Casiraghi, and P. Samorì.*

Sébastien HAAR

L'approche supramoléculaire appliquée au graphène: production d'assemblées hybrides fonctionnalisées

Résumé

Cette thèse démontre le potentiel dont dispose l'exfoliation en phase liquide du graphite dans le but d'obtenir des feuillets de graphène dispersés dans un solvant organique. Ainsi le mécanisme d'exfoliation a été étudié en profondeur, en particulier, l'influence de plusieurs paramètres (température, puissance et solvants). Le choix de ses paramètres se montre crucial dans le contrôle du procédé, et pour l'obtention des feuillets de graphène ayant une taille ciblée. Il est donc possible de fabriquer des nano-feuillets de quelques dizaines de nanomètre qui en plus possèdent des propriétés de photoluminescence.

Dans le but de comprendre le mécanisme d'exfoliation en phase liquide assistée par des molécules, une nouvelle approche a été mise au point : l'approche supramoléculaire. Cette approche se base sur l'utilisation de surfactants d'un nouveau type. En effet, les molécules sélectionnées possèdent une longue chaine alkyle. Cette chaine s'adsorbe sur la surface du graphène et permet de stabiliser les feuillets lors de l'exfoliation. L'influence de la taille de la chaine alkyle de ces molécules lors de l'exfoliation a été vérifiée. De plus, ces molécules ont été équipées de différentes fonctions supramoléculaires afin qu'elles puissent former des dimères sur la surface du graphène. L'ajout de ces molécules augmente non seulement le rendement d'exfoliation mais aussi le nombre de mono-feuillets présents dans ces dispersions. Ces dispersions présentent des propriétés conductrices lorsqu'elles sont déposées sur des substrats. Une nouvelles méthode de déposition a été mise au point afin d'améliorer et d'augmenter la conductivité mais aussi le pourcentage de transparence.

Mots clés: graphène, exfoliation en phase liquide, chimie supramoléculaire, film de graphene ultrafin

Résumé en anglais

This thesis demonstrates the potential of exfoliation of the graphite in the liquid phase in order to obtain graphene sheets dispersed in an organic solvent. Thus the exfoliation mechanism has been studied, in particular, the influence of several parameters (temperature, power and solvents). The choice of parameters is actually crucial for the control of the process, and to obtain graphene sheets having a targeted size. It is therefore possible to manufacture nano-sheets of several tens of nanometers, which in addition exhibit photoluminescence properties.

In order to understand the exfoliation mechanism in liquid phase assisted by molecules, a new approach has been developed: the supramolecular approach. This approach is based on using a new type of surfactant. Indeed, the selected molecules carry a long alkyl chain. This chain is adsorbed on the surface of graphene and can stabilize the sheets during exfoliation. The influence of the size of the alkyl chain of these molecules during exfoliation was verified. Furthermore, these molecules have been equipped with various supramolecular functions, which can form dimers on the surface of graphene. The addition of these molecules not only increases exfoliation performance but also the number of mono-layers present in these dispersions. These dispersions have conductive properties when deposited on substrates. A new deposition method was developed to enhance and increase conductivity but also the percentage of transparency.

Keywords: graphene, liquid-phase exfoliation, supramolecular chemistry, graphene thin film